

1. Report No. FHWA/TX-98/1304-3		2. Government Accession No.		3. Recipient's Catalog No.	
4. Title and Subtitle AN EXPERIMENTAL STUDY OF ELASTOMERIC BRIDGE BEARINGS WITH DESIGN RECOMMENDATIONS				5. Report Date OCTOBER 1995	
				6. Performing Organization Code	
7. Author(s) J.V. MUSCARELLA AND J.A. YURA				8. Performing Organization Report No. RESEARCH REPORT 1304-3	
9. Performing Organization Name and Address Center for Transportation Research The University of Texas at Austin 3208 Red River, Suite 200 Austin, Texas 78705-2650				10. Work Unit No. (TRAIS)	
				11. Contract or Grant No. Research Study 3-5-92/4-1304	
12. Sponsoring Agency Name and Address Texas Department of Transportation Research and Technology Transfer Office P.O. Box 5080 Austin, Texas 78763-5080				13. type of Report and Period Covered Interim	
				14. Sponsoring Agency Code	
15. Supplementary Notes Study conducted in cooperation with the U.S. Department of Transportation, Federal Highway Administration Research Study Title: <i>"Elastomeric Bearings."</i>					
16. Abstract Recent AASHTO specifications have placed a number of restrictions on the use of elastomeric bridge bearings. Elastomeric bearings with tapers built in to accommodate span end elevation differences were disallowed by the most current specifications even though no previous research into elastomeric bearing performance has included tests on tapered pads. The purpose of this study was to analyze elastomeric bearing performance on the basis of elastomer hardness, shape factor, reinforcing shim orientation, degree of taper and compressive stress level with the goal of developing a simple design procedure which standardizes as many of those parameters as possible. Particular emphasis was placed on comparing the behavior of flat and tapered bearings. Experimentation included shear, compressive, and rotational stiffness tests, shear and compression fatigue loading, long-term compressive loading, and tests to determine compressive stress limits. In many cases, bearings were intentionally loaded non-uniformly to define safe limits for bearing/girder slope mismatches. Research showed that tapered elastomeric bearings performed equally as well as flat bearings and that manufacturing tapered bearings with steel shims oriented parallel to one another offers several benefits over spacing shims radially. Additionally, bearings made from elastomers with lower hardness ratings displayed several advantages over those made from harder elastomers, particularly rotation capacity far in excess of the current AASHTO limitation. More highly reinforced bearings performed better in compression fatigue and creep tests and easily accommodated compressive stresses in excess of 6.9 MPa (1000 psi). Mismatches between the slope of the girder and the bearing taper had little effect on performance. Also, a field and laboratory investigation was performed into bearing slip and anchorage by friction. Bearings that had slipped while in service were subjected to comparable conditions in a laboratory test apparatus to study their behavior. Research showed that secretion of antiozonant waxes to the bearings' surfaces caused a dramatic lowering of the bearing's friction coefficient and resulted in slipping. Several tests were performed that established friction coefficients for natural rubber against a variety of steel and concrete surfaces. A standard design for Texas bearings is recommended. Recommended changes to the current AASHTO specification are presented.					
17. Key Words: bridges, design, behavior, bearings, elastomers, neoprene, rubber			18. Distribution Statement No restrictions. This document is available to the public through the National Technical Information Services, Springfield, Virginia 22161		
19. Security Classif. (of this report) Unclassified		20. Security Classif. (of this page) Unclassified		21. No. of Pages 192	22. Price

**AN EXPERIMENTAL STUDY OF ELASTOMERIC BRIDGE
BEARINGS WITH DESIGN RECOMMENDATIONS**

by

J.V. Muscarella and J.A. Yura

Research Report No. 1304-3

Research Project 3-5-92/4-1304

“ELASTOMERIC BEARINGS”

conducted for the

Texas Department of Transportation

in cooperation with the

**U.S. Department of Transportation
Federal Highway Administration**

by the

**CENTER FOR TRANSPORTATION RESEARCH
BUREAU OF ENGINEERING RESEARCH
THE UNIVERSITY OF TEXAS AT AUSTIN**

OCTOBER 1995

IMPLEMENTATION

This research shows that tapered elastomeric bearings of up to 6% slope should be allowed by the AASHTO Specification. The report includes proposed changes to the AASHTO Specification, which TxDOT should begin to process through for national adoption. TxDOT should continue the ban on the use of natural rubber bearing pads because of the wax that blooms to the surface of such bearings. Standard bearing designs utilizing 50 durometer material with a greater amount of steel reinforcement than is generally used are shown to give very good performance.

Prepared in cooperation with the Texas Department of Transportation and the U.S. Department of Transportation, Federal Highway Administration.

The contents of this report reflect the views of the authors, who are responsible for the facts and the accuracy of the data presented herein. The contents do not necessarily reflect the official view or policies of the Federal Highway Administration or the Texas Department of Transportation. This report does not constitute a standard, specification, or regulation.

NO INTENDED FOR CONSTRUCTION,
BIDDING, OR PERMIT PURPOSES

Joseph A. Yura, P.E. #29859

Research Supervisors

TABLE OF CONTENTS

CHAPTER 1 —	INTRODUCTION	1
1.1	BACKGROUND	1
1.2	ELASTOMERIC BEARING TERMINOLOGY	1
	Bearing Dimensions and Components	1
	Elastomer type	2
	Elastomer hardness/shear modulus	2
	Maximum shear strain	3
	Maximum compressive stress	4
	Number of reinforcing steel shims	5
	Thickness of steel shims	5
	Rotation capacity	5
	Maximum allowable mismatch between the bridge girder and the bearing	6
	Maximum taper	6
	Fatigue limits	6
	Fabrication tolerances	6
1.3	HISTORICAL PROBLEMS WITH ELASTOMERIC BEARINGS	6
	1.3.1 Bearing Slip	6
	1.3.2 Delamination	8
	1.3.3 Ozone Degradation	8
	1.3.4 Low Temperature Stiffening	8
1.4	LITERATURE REVIEW	8
	1.4.1 Early Uses: 19 th Century to 1961	9
	Pare and Keiner (1958) - Joint, State of Rhode Island and Charles A. Maguire and Associates (19)	9
	E. I. du Pont de Nemours & Co. (1959) (6)	9
	Ozell and Diniz (1959) - The University of Florida, Gainesville (18)	9
	Clark and Moultrap (1959) - Joint, Enjay Laboratories and The University of Rhode Island (5)	10
	Fairbanks (1960) - Master’s Thesis, Texas A & M University (8)	10
	1.4.2 Use with Minimum Guidance: 1961-1985	10
	Suter and Collins (1964) - University of Toronto (37)	10
	Minor and Egan (1970) - Batelle Memorial Institute (17)	10
	Stanton and Roeder (1982) - University of Washington (33)	11
	1.4.3 Explicit design procedures: 1985-Present	11
	Roeder and Stanton (1987) - University of Washington (25)	11
	Roeder and Stanton (1988) - University of Washington (24)	12
1.5	RESEARCH GOALS	12
	Quantify the “walking out” phenomenon	12
	Define Tapered Bearing Limits	12
	Develop a Tapered Bearing Design Procedure	12
1.6	RESEARCH SCOPE	13
	Application	13

	Material	13
	Shape factor	13
	Reinforcement	13
	Anchorage	13
	Environment	13
	Stability	14
1.7	LIMITATIONS OF CURRENT AASHTO SPECIFICATION	14
1.8	ORGANIZATION OF STUDY	14
1.9	SUMMARY	15
CHAPTER 2	— EXPERIMENTAL PROGRAM	17
2.1	BEARING SHEAR TEST MACHINE	17
2.1.2	Middle Platen Design.....	21
	X-Axis Leveling Mechanism.....	21
	Z-Axis Stabilization	21
2.1.3	Instrumentation/Data Acquisition.....	24
2.2	TEST SPECIMEN DESIGN AND FABRICATION	25
2.2.1	Field Study Bearings	25
	Slaughter Creek Bridge, Austin.....	25
	Valley Ridge Bridge, Dallas.....	25
2.2.2	Test Specimen Design.....	25
	Elastomer Properties	25
2.2.3	Specified Dimensions.....	26
2.2.4	Steel-Reinforcing Shims.....	26
	Number of Shims.....	26
	Steel Properties	26
	Shim Orientation	27
2.2.5	Fabrication Accuracy And Precision Of Test Specimens.....	28
	Shear Modulus/Hardness.....	28
	Wax Content.....	28
	Dimensions.....	29
	Taper	30
	Steel Shims.....	31
CHAPTER 3	— INVESTIGATION INTO BEARING SLIP	33
3.1	DEFLECTIONS UNDER VERTICAL LOAD ALONE.....	33
3.1.1	Experimental Test Program.....	34
3.1.2	Test Results	35
	Horizontal Forces	35
	Horizontal Deflections	38
	Influence of Reinforcing Shim Orientation on Horizontal Force and Displacement	40
3.1.3	Discussion of Horizontal Force and Deflection Tests	41
	Conclusions	42
3.2	BEARING SLIP INVESTIGATION	42
3.2.1	Field Studies.....	43

	Slaughter Creek Bridge, Austin.....	44
	Valley Ridge Bridge, Dallas.....	47
3.2.2	Laboratory Investigation	47
	Wax Additive	47
	Slip Tests on Slaughter Creek Natural Rubber Bearings.....	48
	Explanation of Slip Test Results	48
	Slip Tests on Valley Ridge Natural Rubber Bearings	52
	Mechanics of the “Walking Out” Phenomenon.....	52
3.2.3	Direct Friction Tests.....	54
3.2.4	Conclusions From Slip Tests.....	55
	Wax Additive	55
	“Walking out” Phenomenon.....	55
	Anchorage by Friction.....	55
CHAPTER 4	— BEARING STIFFNESS TESTS	57
4.1	SHEAR STIFFNESS/MODULUS TESTS	57
4.1.1	Test Program.....	57
4.1.2	Results of Shear Stiffness/Modulus Tests	59
	4.1.2.1 Matched Slope Tests.....	59
	Influence of Taper on Shear Modulus.....	60
	Influence of Compressive Stress on Shear Modulus	61
	Influence of Shape Factor on Shear Modulus	62
	Influence of Steel Shim Orientation on Shear Modulus.....	62
	4.1.2.2 Non-uniform Loading Tests.....	63
4.1.3	Comparison with Shear Modulus Tests on Plain Specimens.....	68
4.2	COMPRESSIVE STIFFNESS/MODULUS TESTS	68
4.2.1	Test Program.....	68
4.2.2	Results	69
	Effect of Increasing Hardness/Shear Modulus on Compressive Modulus.....	71
	Effect of Increasing Shape Factor on Compressive Modulus.....	71
	Effect of Tapering on Compressive Modulus.....	71
	Influence of Reinforcing Shim Orientation on Compressive Modulus and Deformation	74
4.2.3	Experimental versus Calculated Values	74
4.3	ROTATIONAL STIFFNESS TESTS	76
4.3.1	Test Program.....	76
4.3.2	Test Results	77
	Influence of Hardness/Shear Modulus on Rotation Capacity/Stiffness	81
	Influence of Shape Factor on Rotational Behavior.....	82
	Effect of Tapering on Rotational Behavior	82
	Effect of Reinforcing Shim Orientation on Rotational Behavior.....	84
4.3.3	Summary of Rotational Behavior Tests.....	84
4.4	DISCUSSION OF STIFFNESS TEST RESULTS.....	88
	Shear Modulus/Stiffness Tests.....	88
	Compressive Modulus/Stiffness Tests	89

	Rotational Stiffness Tests	89
	Common Factors	89
CHAPTER 5 —	COMPRESSIVE CREEP BEHAVIOR	91
5.1	TEST PROGRAM.....	91
	Logarithmic Prediction.....	92
	Southwell Plot Prediction	93
5.2	TEST RESULTS	93
	Analysis of Creep Deformations.....	93
	Influence of Shape Factor on Compressive Creep Behavior	94
	Influence of Hardness on Compressive Creep Behavior	95
	Influence of Taper on Compressive Creep Behavior.....	95
5.3	DISCUSSION OF CREEP TEST RESULTS	96
	Design Implications.....	97
CHAPTER 6 —	FATIGUE TESTS	99
6.1	SHEAR FATIGUE TESTS	99
6.1.1	Test Program.....	99
6.1.2	Test Results	100
	Fatigue damage	100
	Loss of Shear Stiffness	101
6.2	COMPRESSION FATIGUE TESTS	103
6.2.1	Test Program.....	103
6.2.2	Test Results	104
	Fatigue Damage.....	104
	Loss of Compressive Stiffness	105
6.3	DISCUSSION OF FATIGUE TESTS.....	106
	Shear Fatigue	106
	Compression Fatigue	106
	Common Factors	107
CHAPTER 7 —	DETERMINATION OF FAILURE STRESSES	109
7.1	COMPRESSION FAILURE TESTS.....	109
7.1.1	Test Program.....	109
7.1.2	Test Results	110
	Unreinforced Bearings	110
	Reinforced Bearings.....	112
	Comparison of Experimental and Theoretical Results	113
7.2	SHEAR FAILURE TEST.....	115
7.2.1	Test Procedure.....	116
7.2.2	Test Results	116
7.3	DISCUSSION OF FAILURE TESTS	117
	Compression Failure.....	117
	Shear Failure	117
CHAPTER 8 —	CONCLUSIONS AND RECOMMENDATION	119
8.1	CONCLUSIONS	119
8.1.1	Bearing Slip.....	119

	Antiozonant Additives.....	119
	Contact Surfaces.....	119
8.1.2	Common Design Considerations	119
	Shear Modulus Determination.....	119
	Manufacturing Precision and Accuracy.....	120
	Elastomer Hardness.....	120
	Shape Factor.....	121
	Compressive Stress	121
	Rotation Capacity.....	121
	Steel Shims.....	122
	Cover Layers	122
8.1.3	Design of Tapered Bearings.....	122
	Maximum Taper.....	122
	Slope Mismatch.....	122
	Compressive Deformations	123
	Horizontal Deflections	123
	Orientation of Steel Shims.....	123
8.2	RECOMMENDATIONS.....	124
8.2.1	Recommendations to Preclude Bearing Slip	124
8.2.2	Recommendations Common to All Elastomeric Bearings.....	124
8.2.3	Recommendations for Tapered Bearings	127
8.3	SUGGESTED FUTURE RESEARCH.....	128
	Performance at Higher Compressive Stresses	128
	Ozone Degradation Testing.....	128
CHAPTER 9 — RECOMMENDED DESIGN PROCEDURE		129
	Standard Design Parameters	129
APPENDIX A — PROPOSED SPECIFICATION		133
APPENDIX B — DESIGN EXAMPLES USING METHOD C SPECIFICATIONS.....		145
APPENDIX C — SELECTED PROPERTIES OF NATURAL RUBBER		153
APPENDIX D — NOTATION		155
APPENDIX E — INDIVIDUAL TEST RESULTS		157
GLOSSARY		177
REFERENCES		179

LIST OF FIGURES

Figure 1- 1	Girder/bearing configurations.....	1
Figure 1- 2	Elastomeric bearing nomenclature.....	2
Figure 1- 3	Forces on elastomeric bearing during shear.....	3
Figure 1- 4	Unreinforced elastomeric pad under compressive load	4
Figure 1- 5	Reinforcement limiting bulging of the elastomeric pad.....	4
Figure 1- 6	Tensile forces on reinforcing shims from elastomer compression	5
Figure 1- 7	Rotation capacity of elastomeric bearing.....	5
Figure 1- 8	Non-uniform loading of elastomeric bearing.....	6
Figure 1- 9	Extreme examples of bearing “walking out” phenomenon	7
Figure 2- 1	Bearings being tested in the shear test machine.....	17
Figure 2- 2	Schematic of the elastomeric bearing test setup	18
Figure 2- 3	Constant compressive force system.....	19
Figure 2- 4	Steel dead weights	19
Figure 2- 5	311-kN (35-ton) screw jacks	20
Figure 2- 6	Electronic controller/motor/reduction gear system.....	20
Figure 2- 7	Middle platen detail.....	21
Figure 2- 8	Data acquisition system.....	22
Figure 2- 9	Optron with light source directed toward bearing	23
Figure 2- 10	Optron tracking a target on a bearing	23
Figure 2- 11	optron target as seen through the optron view finder.....	24
Figure 2- 12	Spacing of steel shims in tapered bearing specimens	27
Figure 2- 13	Tapered bearing with parallel steel shims.....	27
Figure 2- 14	Steel shims bent during manufacturing process.....	31
Figure 2- 15	Misoriented steel shims	31
Figure 3- 1	Bearing under girder dead weight.....	33
Figure 3- 2	Bearings shearing due to girder dead weight.....	33
Figure 3- 3	Test setup for measuring horizontal forces.....	34
Figure 3- 4	Horizontal to compressive force ratio vs. middle platen slope	35
Figure 3- 5	Actual and predicted P- Δ curves for a 57-durometer 3-shim 6% taper bearing.....	36
Figure 3- 6	Actual and predicted P-D curves for a 70-durometer 6-shim 6% taper bearing	39
Figure 3- 7	Geometry of displaced bearing.....	39!
Figure 3.8	Sliding gage for measurement of girder movement	43
Figure 3- 9	Girder expansion/contraction measurement gage	43
Figure 3- 10	Reference marks under girder.....	44
Figure 3- 11	Restraining devices to prevent bearing movement	45
Figure 3- 12	Bridge lifting system.....	45
Figure 3- 13	Steam cleaning the girders and bearing seats with degreasing agent	46
Figure 3- 14	Movement of neoprene bearing pads from June 1993 to April 1994	46
Figure 3- 15	Movement of neoprene bearing pads since April 1994	47
Figure 3- 16	Initial load-displacement curve and optron plot	49
Figure 3- 17	Load-displacement curve with bearing stationary	50
Figure 3- 18	Bearing walking out slowly	50
Figure 3- 19	Bearing walking out significantly	51
Figure 3- 20	Final load-displacement and slip curves.....	51
Figure 3- 21	Bearing under girder dead weight alone.....	52
Figure 3- 22	Forces on bearing during girder expansion.....	52
Figure 3- 23	Forces on bearing during girder contraction.....	53
Figure 3- 24	Load displacement curves from direct friction tests	56
Figure 4- 1	Concrete platens with surface accumulation.....	58

Figure 4- 2	Cleaning of concrete platens.....	58
Figure 4- 3	Shear load-displacement curve for a flat bearing.....	59
Figure 4- 4	Horizontal load vs. displacement at 100% strain.....	60
Figure 4- 5	Load-displacement curve for a tapered bearing at 50% shear strain.....	61
Figure 4- 6	Flat bearing loaded non-uniformly at low compressive stress	65
Figure 4- 7	Tapered bearing loaded non-uniformly on the thin end.....	66
Figure 4- 8	Bearing under non-uniform loading at 3.85 MPa (550 psi).....	66
Figure 4- 9	Bearing under non-uniform loading at 7.69 MPa (1100 psi).....	67
Figure 4- 10	Typical shear stress-strain curve from ASTM 4014 test.....	67
Figure 4- 11	Compressive stress-strain relationship for plain pad	69
Figure 4- 12	Flat 6 shim bearing loaded to 14 MPa (2000 psi) in compression.....	72
Figure 4- 13	apered 6 shim bearing loaded to 3.5 MPa (500 psi)	72
Figure 4- 14	Tapered 6 shim bearing loaded to 14 MPa (2000 psi).....	73
Figure 4- 15	Stress-strain curves for 70 durometer flat and tapered 3 shim bearings.....	73
Figure 4- 16	Stress-strain curves for 54 durometer flat and tapered 6 shim bearings.....	74
Figure 4- 17	Stress-strain curves for flat and tapered bearings of 55 and 70 durometer	76
Figure 4- 18	Schematic diagram of rotational stiffness test setup	77
Figure 4- 19	Rotational stiffness test instrumentation	77
Figure 4- 20	Moment-rotation curve - flat 54 Durometer 3 shim bearing at 7.69 MPa.....	78
Figure 4- 21	Moment-rotation curve - flat 69 Durometer 6 shim bearing at 3.85 MPa.....	78
Figure 4- 22	Bearing exhibiting lift-off at 3.85 MPa (550 psi)	80
Figure 4- 23	Bearing exhibiting lift-off at 7.69 MPa (1100 psi)	80
Figure 4- 24	Typical moment-rotation relationship for a tapered bearing.....	82
Figure 4- 25	Tapered bearing at lever arm lift-off.....	83
Figure 4- 26	Comparison of flat bearing designs	85
Figure 4- 27	Comparison of flat and tapered designs.....	85
Figure 5- 1	Compressive creep apparatus	91
Figure 5- 2	Standard creep relationship	92
Figure 5- 3	Logarithmic prediction of long-term creep.....	92
Figure 5- 4	Southwell plot prediction of long-term creep	93
Figure 5- 5	Comparison of total compressive deformation in 3 versus 6 shim specimens	94
Figure 6- 1	Shear fatigue apparatus.....	100
Figure 6- 2	Bearing with three reinforcing shims at 10.35 MPa (1500 psi)	101
Figure 6-3	Fretting damage on bearing surface.....	102
Figure 6-4	Bearing with six reinforcing shims at 10.35 MPa (1500 psi)	104
Figure 6- 5	Bearing with six reinforcing shims at 10.35 MPa (1500 psi)	104
Figure 7- 1	Compression failure test apparatus	110
Figure 7- 2	Unreinforced bearing under 31.0 MPa (4500 psi) compressive stress.....	111
Figure 7- 3	Stress-strain relationship for a plain pad loaded to 31.0 MPa (4500 psi)	111
Figure 7- 4	Reinforced bearing compression test stress-strain relationship	112
Figure 7- 5	Elastomer tearing/delamination	114
Figure 7- 6	Fractured reinforcing steel shims.....	114
Figure 7- 7	Specimen with steel shims yielded in shear.....	116

LIST OF TABLES

Table 1- 1	Values of Shear Modulus Based Upon Elastomer Hardness	3
Table 2- 1	As delivered hardness measurements	28
Table 2- 2	Average shear moduli as determined from testing	29
Table 2- 3	Average elastomer thickness measurements	30
Table 2- 4	As delivered bearing tapers	30
Table 3- 1	Schedule of horizontal to compressive force ratio tests	34
Table 3- 2	Influence of compressive force level on ratio of horizontal to compressive force	36
Table 3- 3	Influence of shear modulus on horizontal to compressive force ratio	36
Table 3- 4	Influence of shear modulus on horizontal to compressive force ratio	37
Table 3- 5	Average horizontal force produced by compressive force of 311 kN and 622 kN	37
Table 3- 6	Ratio of horizontal to compressive force from displacement tests	38
Table 3- 7	Comparison of actual and predicted horizontal displacements	40
Table 3- 8	Influence of steel shim orientation on horizontal force and displacement	40
Table 3- 10	Friction coefficients from slip tests	48
Table 3- 11	Coefficients of friction from direct friction tests	54
Table 4- 1	Influence of bearing taper on shear modulus	61
Table 4- 2	Influence of compressive stress on shear modulus	62
Table 4- 3	Influence of shape factor on shear modulus	62
Table 4- 4	Influence of steel shim orientation on shear modulus	62
Table 4- 5	Effect of non-uniform loading at low compressive stress	64
Table 4- 6	Influence of shape factor on shear modulus in non-uniform loading at low compressive stress	64
Table 4- 7	Effect of non-uniform loading at higher compressive stress	64
Table 4- 8	Influence of shape factor on shear modulus in non-uniform loading at high compressive stress	65
Table 4- 9	Comparison of ASTM and full-scale shear modulus tests - Manufacturer A	65
Table 4- 10	Comparison of ASTM and full-scale shear modulus tests, Manufacturers B and C	68
Table 4- 11	Compressive stiffness test results	70
Table 4- 12	Effect of increasing shape factor on compressive modulus	70
Table 4- 13	Effect of increasing shape factor on compressive modulus	70
Table 4- 14	Influence of taper on compressive stiffness	71
Table 4- 15	Influence of reinforcing shim orientation on compressive modulus and deformation	74
Table 4- 16	Experimental vs. calculated compressive modulus	75
Table 4- 17	Actual and predicted changes in compression modulus	75
Table 4- 18	Average rotational stiffnesses	79
Table 4- 19	Average rotation capacities of bearings	79
Table 4- 20	Influence of compressive stress on rotational stiffness and rotation capacity	81
Table 4- 21	Effect of increasing hardness on rotational behavior	81
Table 4- 22	Effect of increasing shape factor on rotational behavior	82
Table 4- 23	Influence of taper on rotational behavior	84
Table 4- 24	Influence of steel shim orientation on rotational behavior	84
Table 4- 25	Comparison of rotation test results and theoretical calculations	87
Table 5- 1	Two-week creep deformations	94
Table 5- 2	Influence of shape factor on long-term compressive creep behavior	94
Table 5- 3	Influence of hardness on compressive creep behavior	95
Table 5- 4	Influence of bearing taper on compressive creep behavior	95
Table 5- 5	Comparison of creep test results	96
Table 6- 1	Loss of shear stiffness due to shear fatigue loading	102
Table 6- 2	Loss of compressive stiffness due to compression fatigue loading	105

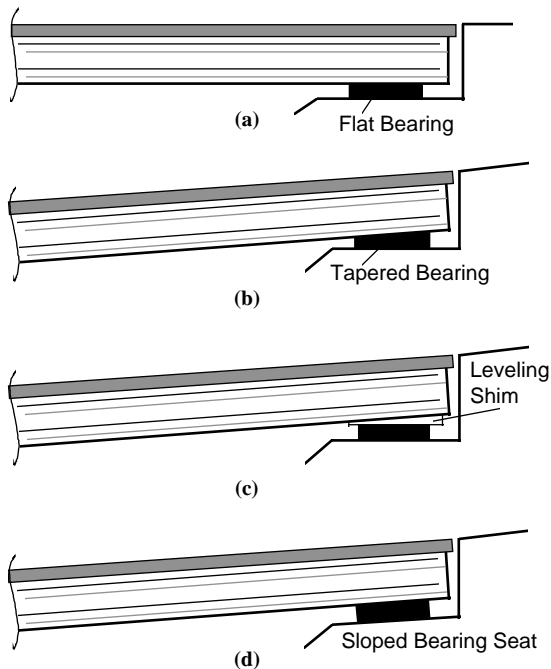
Table 6- 3	Comparison of shear fatigue test results	106
Table 7- 1	Results of reinforced bearing compression tests.....	113
Table 7- 2	Comparison of theoretical yield stresses and experimental stiffness loss stress	115
Table 9- 1	Compressive deformation for 55 durometer bearings of $S = 10$	130
Table 9- 2	Standard tapered bearing ranges.....	131

CHAPTER 1

INTRODUCTION

1.1 BACKGROUND

This report describes an experimental investigation into the behavior of elastomeric bridge bearings, the purpose of which was to develop a simple design procedure for the State of Texas Department of Transportation. Although elastomeric bridge bearings have been widely used in Texas and throughout the United States and Europe since the 1950's — the first recorded use of neoprene bearing pads in the United States was to support prestressed concrete beams in Victoria, Texas in 1957 — these types of bearings have only recently become the subject of intense investigation and regulation. The first AASHTO *Standard Specifications for Highway Bridges* to address elastomeric bearings was the 8th Edition, published in 1961 and consisted of only one page of details governing their use (30). The most recent AASHTO Specifications, the 15th Edition, based largely on research performed at the University of Washington in 1987 and 1988 (24,25), contain 26 pages of design and construction regulations and place significant restrictions on compressive stresses, shear strain, rotation, taper and fabrication tolerances (32). The overall effect of the AASHTO Specifications published during the past 10 years has been to more severely restrict the use of elastomeric bearings with each new edition. Particularly, tapered elastomeric bearings, (Figure 1.1b) which have been employed by TxDOT for a number of years and were allowed by AASHTO until 1992, were disallowed by the most current Specifications even though none of the research cited above included tests on tapered pads. This prohibition forces either modification of the concrete girder bottom flange with leveling shims (Figure 1.1c) or sloping of bearing seats with additional concrete (Figure 1.1d) to ensure that the girder bottom flange and bearing seats are parallel. Clearly, accommodating span end elevation differences with tapered elastomeric bearings is a simpler proposition than either of the alternatives. As one of the goals of this study is to recommend simplifications to the existing Specifications and design procedures wherever possible, a particular effort will be made to show that using tapered elastomeric bearings to account for girder end elevation differences is just as safe, durable, and economical as using flat bearings.



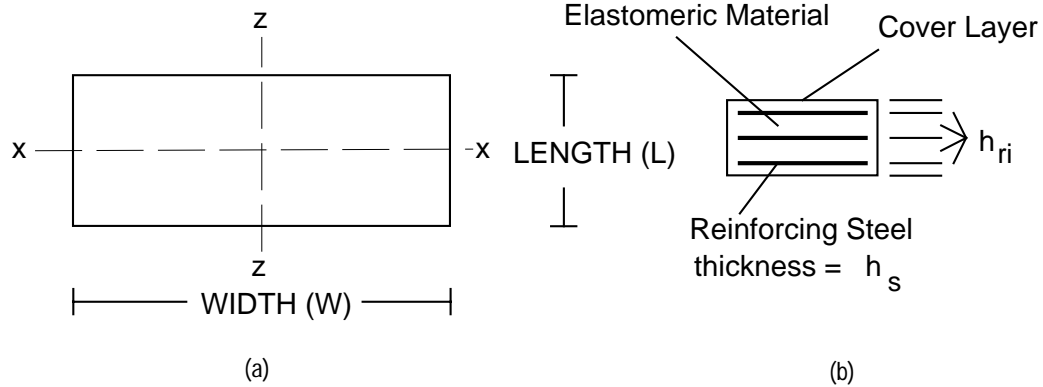
In addition to proposing acceptance criteria for use of tapered bearings, this study will examine the phenomenon of bearing slip which has been documented throughout this state as well as others, and will show that this phenomenon is neither peculiar to tapered bearings nor an inevitable consequence of tapered bearing mechanics. An analytical study employing finite element modeling was performed by Hamzeh (10) and is cited throughout this report.

1.2 ELASTOMERIC BEARING TERMINOLOGY

Bearing Dimensions and Components

Figure 1.2 shows a plan view and cross section of a typical flat elastomeric bearing with the nomenclature from the AASHTO specification (Appendix D contains a more complete notation):

Figure 1-1 Girder/bearing configurations



- Longitudinal Axis (z-axis) = Axis parallel to the longitudinal axis of the bridge girder
- Transverse Axis (x-axis) = Axis perpendicular to the longitudinal axis
- h_{ri} = Thickness of elastomer layer number i
- h_{rt} = Total elastomer thickness of the bearing = $\sum h_{ri}$
- h_s = Thickness of reinforcing steel shim
- W = Width, Gross dimension of the bearing parallel to the transverse axis
- L = Length, Gross dimension of the bearing parallel to the longitudinal axis

Figure 1-2 Elastomeric bearing nomenclature

Elastomer type

A number of elastomeric materials can be used for bearings: natural rubber; and man-made materials such as neoprene, butyl rubber, urethane, and ethylene propylene dimonomer (EPDM). Natural rubber and neoprene are by far, however, the most common compounds. Although neoprene was the first elastomeric bearing material (the 1961 AASHTO Specifications named neoprene as the only acceptable elastomeric compound) and remains the most common material in use today, natural rubber, imported mainly from Malaysia, has recently challenged neoprene's dominance in the field due to its (of late) lower cost. According to bearing manufacturers, a natural rubber bearing pad (finished product) can be provided to the user for approximately 75 percent of the cost of a neoprene pad of the same design. Thus, as long as the reservations concerning the use of natural rubber can be overcome, i.e. ozone degradation and the "walking out" phenomenon (to be discussed later), a significant reduction in the cost of elastomeric bearings can be achieved. A so-called "standard" TxDOT bearing of 228.6 mm (9 inches) in length, 558.8 mm (22 inches) in width and 63.5 mm (2.5 inches) in total height with five 2.66-mm (12-gage) steel reinforcing shims was quoted by one manufacturer as costing \$94.75 if made from neoprene and \$72.80 if made from natural rubber. Though chemically different, rubber manufacturers claim that the engineering properties of the two materials, at least as they apply to structural bearings, are the same. The literature shows that while Great Britain and Australia use natural rubber for bearing pads (38), Germany has prohibited its use and allows only neoprene (9).

Elastomer hardness/shear modulus

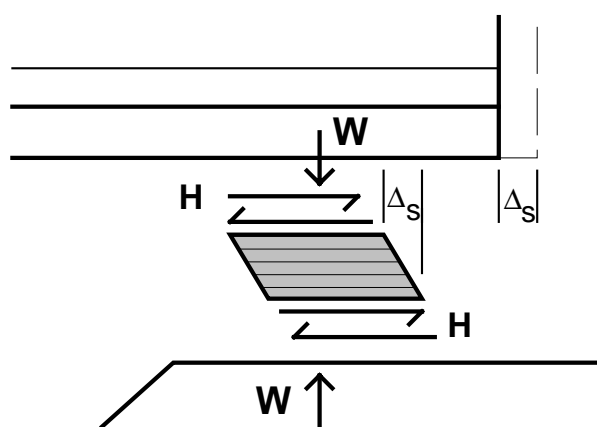
Hardness, defined as the "reversible, elastic deformation produced by a specially-shaped indenter under a specified load" (13) is most commonly measured in International Rubber Hardness Degrees (IHRD) or Shore "A" Durometer points, which are approximately the same in the ranges discussed in this study (45 to 65). The instrument used to perform this measurement is called a Durometer and gives readings to a generally accepted repeatability of ± 3 points. Although hardness can give an indication of shear modulus

Table 1- 1 Values of Shear Modulus Based Upon Elastomer Hardness

HARDNESS	45-55	55-65	65-75
Shear Modulus (MPa)	0.53-0.75	0.75-1.05	1.05-1.40
Shear Modulus (psi)	77-110	110-150	150-200

range, it cannot be used in engineering calculations. However, according to manufacturers and references, a reasonably narrow range of shear moduli (0.21-0.28 MPa, 30-40 psi) can be assumed given a specific elastomer hardness (13,15,32). Table 1.1 gives values of shear modulus at 50 percent strain based on hardness from past research (13). It should be pointed out that these shear moduli are determined through tests on unreinforced vulcanized rubber and may not reflect the actual shear modulus of an elastomeric bearing in use.

Obviously, the shear modulus of a bridge bearing is important since that property influences the shear force which can be transmitted to the girder flange and the bridge abutment. Additionally, if the shear force



produced by the bearing exceeds the static friction force between the bearing surfaces and the girder or abutment slip will occur.

Maximum shear strain

As the bridge girder goes through its thermal cycle, the bearing must shear from its original orientation by the same amount as the girder expands or contracts (See Figure 1.3). The bearings' shear deformation divided by the original elastomer thickness before compressive loading is the shear strain. The magnitude of the shear strain, γ , (Δ_s divided by h_{rt}) along with the plan area of the bearing and the shear modulus, G , determines the shear force transmitted to the girder flange and the abutment:

Figure 1- 3 Forces on elastomeric bearing during shear

$$H = \gamma G A \quad (1.1)$$

The greater the shear strain, the greater the shear force and the greater the possibility of slip. Additionally, rubber technologists recommend a limit on shear strain to keep elastomer stresses low (13). Currently, the AASHTO limit on shear strain is 50 percent of the pre-loading elastomer thickness. Thus, the magnitude of the thermal deformation dictates the total thickness of the elastomer in the bridge bearing:

$$h_{rt} = 2 \Delta_s \quad (1.2)$$

where the subscript, rt , represents the summation of the thicknesses of elastomer in all layers between steel reinforcing shims plus cover layers. (See Figure 1.2.)

Maximum compressive stress

Two factors limit the maximum compressive stress allowed on the bearing: compressive deformation and shears strains which result from compression. The first factor is the compressive deformation of the bearing, most of which results from the bulging of the elastomer under compressive load. There is actually very little volume change in elastomeric materials of lower hardness ratings but, as the hardness of the elastomer increases, the volume change of the material becomes more significant.

This tendency to bulge under compressive load can be described by a quantity known as the shape factor, S , the ratio of the loaded plan area, divided by the area free to bulge (calculated for each layer if thicknesses vary):

$$S = \frac{(L \times W)}{2h_{ri}(L + W)} \quad (1.3)$$

The actual compressive deformation of the bearing can be estimated by first calculating the compression modulus of the pad, which is a function of the shear modulus, G , the shape factor, S , and a factor, k , based upon the elastomer hardness, which takes into account the volume change of the material itself (See Appendix D for values of k based on hardness):

$$E_c = 3G(1 + 2kS^2) \quad (1.4)$$

and then using the standard relationship for calculating axial deformations in elastic materials:

$$\Delta_c = \frac{Ph_{rt}}{AE_c} \quad (1.5)$$

The second limitation on compressive stress is derived from the elastomer's ability to withstand the shear stresses created in the material itself from the bulging due to compressive load. This limitation comes from research performed by elastomer technologists rather than from engineers. The only ways to limit compressive deformation are to use an elastomer formulated for greater hardness or to increase the shape factor by bonding into the elastomer reinforcing shims of steel or other axially stiff material oriented on a plane perpendicular to the compressive load. This reduces the elastomer's ability to bulge and therefore limits the compressive deformation as shown in Figures 1.4 and 1.5. Shear stress can be reduced by increasing the shape factor as explained below.

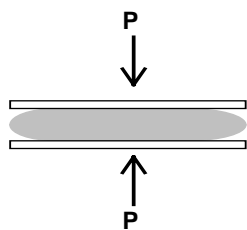


Figure 1-4 Unreinforced elastomeric pad under compressive load

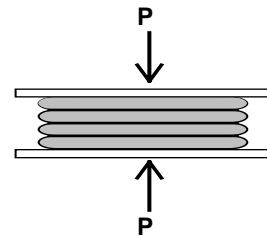


Figure 1-5 Reinforcement limiting bulging of the elastomeric pad

Number of reinforcing steel shims

While the minimum required thickness of the elastomeric material in the bearing is determined by calculating the expected expansion and contraction of the bearing from thermal and other sources, the number of reinforcing shims must be determined by the amount of axial deformation which will be allowed as well as the amount of elastomer shear stress to which the material is restricted according to current Specifications. According to AASHTO, the relationship

$$\sigma_c \leq GS \quad (1.6)$$

which dictates an increase in the bearing's shape factor at higher compressive stresses ensures that shear stresses due to compression "will not cause serious damage" (32). In a bearing of a given total elastomer thickness, the greater the number of the steel reinforcing shims, the lower the shear stresses in the elastomer and the lower the axial deformation under load. Steel shims increase cost, so the minimum number of shims that results in an acceptable design should be prescribed. In this study, bearings with 6 shims cost 10-15% more than bearings with 3 shims.

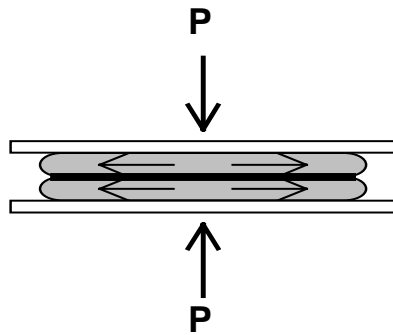


Figure 1-6 Tensile forces on reinforcing shims from elastomer compression

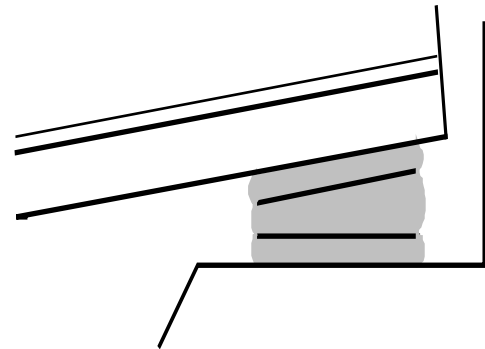


Figure 1-7 Rotation capacity of elastomeric bearing

Thickness of steel shims

The primary purpose of the reinforcing shims in the bearing is to restrict the bulging of the elastomer. Although bending stresses occur in the shims due to bearing shear, the most significant stresses are the transverse tensile stresses transferred to the steel due to elastomer bulging. Therefore, the steel need only be thick enough to withstand the tensile stresses produced under the given loading condition. Thicker shims are more costly and unnecessary.

Rotation capacity

Just as elastomeric materials deform in shear, compression, and tension, they are capable of absorbing significant rotations of the girder. This rotation capacity is a function of the axial stiffness of the bearing. When the rotation of the girder exceeds the rotation capacity of the bearing, the girder will begin to pivot on the still loaded section of the bearing and "lift-off" will occur. Existing Specifications require that this condition be controlled by placing limitations on the amount of end rotation that the bearing is allowed to accommodate so that it does not experience "lift-off" (15,25,32,33). The current AASHTO rotation limitation is discussed in Section 1.7.

Maximum allowable mismatch between the bridge girder and the bearing

Directly related to the rotation capacity of the bearing is the maximum allowable mismatch between the bridge girder and the top of the bearing. This is commonly referred to as “non-uniform loading.” If the mismatch is severe enough, the loading medium, i.e. the girder may lift off from the top of the bearing. In the case of non-uniform loading this will be a permanent condition unless the bearing is able to deform to accommodate the orientation of the load.

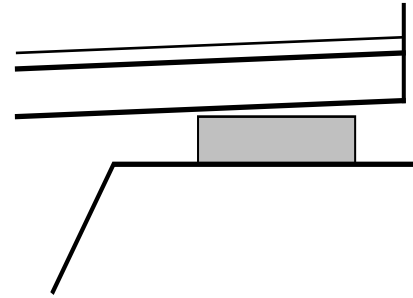


Figure 1- 8 Non-uniform loading of elastomeric bearing

Maximum taper

As bearing taper is increased to accommodate greater span end elevation differences, the forces on the bearing change. Horizontal as well as vertical displacements are produced which introduce immediate shear strains before any thermal cycle is considered. As the taper increases so does the horizontal displacement. These displacements are discussed in more detail in Chapter 3. Currently, bearings with up to 6% taper are employed, but, due to horizontal displacements, there may be need to place a restriction on the degree of taper allowed.

Fatigue limits

Bearings can undergo significant fatigue loading. In a 55-year service life, bearings may be subjected to 20,000 cycles of up to 50% shear strain and millions of cycles of compressive stress. This loading can cause delamination of the elastomer-steel bond, tearing of the elastomer and loss of axial or shear stiffness. Bearing parameters such as thickness of elastomer layers, hardness, and degree of non-uniform loading may influence the bearing’s ability to withstand fatigue loading.

Fabrication tolerances

Elastomeric bearing fabrication is not an exact science. Each bearing is individually molded from pre-vulcanized sheets of varying shapes and thicknesses. While it is assumed that the bearing as delivered has the required thickness to accommodate the shear deformations, the hardness to produce the correct shear modulus, and the correct taper to accommodate the slope of the girder, this may not be the case. Chapter 2 will show how bearings ordered for this study varied from their specifications.

1.3 HISTORICAL PROBLEMS WITH ELASTOMERIC BEARINGS

While elastomeric bearings have been used successfully for almost 50 years, there have been some instances of less than ideal performance in the past.

1.3.1 BEARING SLIP

Since 1992, the state of Texas has experienced several instances of elastomeric bridge bearings slipping (moving in rigid-body motion) along with the bridge girder rather than remaining in their original location and accommodating the bridge movement by elastomer deformation. In many instances, pads have been observed to completely “walk out” from underneath bridge girders. (See Figures 1.9a and b.) In all cases, the bearings in question were constructed of natural rubber, the spans were at least 30.48 m (100 feet) long and the bridges were subject to significant thermal expansion and contraction. Current attempts to remedy this problem include lifting the bridge end and replacing the bearings or constructing steel collars around the bearings to limit their movement. The former method is expensive, disruptive,



(a)



(b)

Figure 1-9 Extreme examples of bearing “walking out” phenomenon

potentially dangerous, and not always successful. On several occasions, bridges with bearing slip problems were lifted and the bearings were reset, only to “walk out” again. The latter method, although simple, can result in damage to the bearings when they continue to slip and come in contact with the restraints. In several such cases, bearings have become severely damaged due to the shear and bending forces to which they are subjected when they are pushed against the restraints. In extreme cases, these bearings must be replaced, resulting in the same difficulties as described above. In the investigation reported herein, only natural rubber pads have slipped. Neoprene bearing pads have not experienced this problem.

Additionally, all of the bridges where “walking out” was documented used tapered pads raising serious concern about the use of sloped natural rubber bearings.

1.3.2 DELAMINATION

Although in-service failure of well-manufactured elastomeric material itself is very rare, separation of the elastomer-steel bond—the most often cited failure mechanism—must be considered when using laminated elastomeric bearings. Delamination is a result of essentially two causes: 1) poor bond between the elastomer and the steel shim during the vulcanization process and 2) loading of the bearing to stresses beyond the capacity of even a good bond. Depending upon the degree of delamination, the bearing will lose some or all of its ability to carry compressive load without significant deformation. While this does not mean failure of the bridge, the magnitude of the additional deformation, which could easily surpass 100 to 200 percent of the original deformation, may require replacement of the pad.

1.3.3 OZONE DEGRADATION

Elastomeric materials, especially natural rubber, are susceptible to degradation from the effects of atmospheric chemicals and solar radiation (13). In the case of natural rubber, ozone attack at normal atmospheric concentrations (about 1 part per hundred million) can cause significant surface cracking within a few weeks (13). While neoprene has an intrinsic resistance to the effects of ozone, natural rubber compounds must be protected with additives known as chemical antiozonants and antiozonant waxes in order to pass the ozone resistance provisions of the AASHTO specification—no cracking when subjected to 25 parts per hundred million of ozone at 38° C (100° F) for 48 hours while strained to 20 percent elongation.

1.3.4 LOW TEMPERATURE STIFFENING

Natural rubber and neoprene both become stiffer when subjected to extremely cold environments. Tests to -30° C (24,37) have shown that exposure to temperatures below 0° Celsius will increase shear stiffness to as much as 20 times that at normal temperature (26° C). The increase in stiffness is greater at lower temperatures and longer exposures to the colder environment. This tendency can introduce an additional consideration into the calculation of forces transmitted to the bridge girder and abutment by the elastomeric bearing.

1.4 LITERATURE REVIEW

Although the reference on elastomeric bearings cite uses dating to before this century, the vast majority of the written record of their employment and research starts in the 1950's. This literature review has been divided into chronological periods based upon the state of elastomeric bearing advancement at the time. While the studies described here are all either US or Canadian, much research has been performed in Britain, France, and Germany which has been incorporated into the studies cited below.

1.4.1 EARLY USES: 19TH CENTURY TO 1961

Lindley (14) recounts the first use of rubber as a bearing material to support a viaduct in Australia in 1889. Examination of these structural bearings, which were still in use as of 1982, showed them to be fully functional but suffering from some environmental degradation to a depth of approximately one millimeter. Modern use of elastomeric materials as currently formulated dates to the late 1940's in France (20), 1955 in Great Britain (14), and 1957 in the United States (2) and Canada (16). Research from that time period was conducted primarily on plain neoprene or natural rubber pads to evaluate their shear, compressive, creep and fatigue properties. Attempts were made to correlate hardness to shear and compressive modulus. Durability of the material itself was more of a concern than the development of design provisions for the design of the bearing based upon the loading case. Although ASSHO (now AASHTO) provided an interim specification in 1958 which allowed the use of elastomeric bearings, it was very brief (8). Research conducted directly following the publication of the interim specification and successful field evaluations to this point culminated in the acceptance by AASTHO of the material as a legitimate bearing option. The Specification of 1961 (30), which was now more thorough, allowed the use of elastomeric bearing pads with very few restrictions. Significant contributions to the early knowledge base concerning elastomeric pads were made by the following researchers:

Pare and Keiner (1958) - Joint, State of Rhode Island and Charles A. Maguire and Associates (19)

Tests were performed on 152.4-mm (6-inch) by 304.8-mm (12-inch) plain neoprene pads of 12.7-mm (0.5-inch), 25.4-mm (1.0-inch), and 38.1-mm (1.5-inch). Results showed that: the shear and compressive stiffnesses of the pads were directly proportional to the durometer; compressive stress and plan shape had very little effect on the shear stiffness; compressive creep under repeated shearing was approximately 50 percent greater than under static loading; and the coefficient of friction on concrete should be taken as approximately 0.2. Although shear modulus could be determined from stiffness test results, this report, like other early studies, did not calculate shear modulus or refer to it as a design parameter. It is interesting to note that the authors suggested that girder slopes may be accommodated by ensuring that the pad selected was thick enough to deform sufficiently so that the entire bearing was deformed, rather than only a portion of it.

E. I. du Pont de Nemours & Co. (1959) (6)

The du Pont company, the manufacturer of neoprene, conducted tests on neoprene pads and developed a design for plain or reinforced bearings. Design curves for compressive deformations based upon durometer and shape factor were presented, as well as estimates of long-term compressive creep by hardness. A shear strain of 50 percent was recommended and shear moduli were given for 50, 60, and 70 durometer neoprene (0.77, 1.12, 1.50 MPa (110, 160, 215 psi) respectively). Additionally, factors were provided to modify these shear moduli for temperatures from -7° C (+20° F) to -29° C (-20° F). Again, the coefficient of friction against concrete was given as 0.2. The du Pont research was instrumental in the publication of the 1958 tentative addition to the AASHTO specification.

Ozell and Diniz (1959) - The University of Florida, Gainesville (18)

The authors conducted shear fatigue tests on 25.4-mm (1.0-inch) plain neoprene pads of various lengths and widths under compression up to 5.62 MPa (815 psi). Bearings were subjected to as many as 1,090,000 cycles of up to 45% shear strain at 120 cycles per minute. A number of failures (extensive cracking) were reported, but du Pont engineers explained this as resulting from the excessive rate of fatigue loading that would never have occurred under normal service conditions (18).

Clark and Moultrap (1959) - Joint, Enjay Laboratories and The University of Rhode Island (5)

Tests were performed on plain neoprene, butyl rubber, and chlorinated butyl rubber pads 25.4 mm (1.0 inches) thick, 152.4 mm (6 inches) long and 304.8 mm (12 inches) wide. These are the first recorded tests which evaluated elastomeric bearing pads at temperatures as low as -43° C (-45° F) and under accelerated aging (5 to 10 days at 121° C (250° F) conditions). Results showed that neoprene stiffened under low temperature conditions to a greater extent than the other two materials and that neoprene also became more brittle under accelerated aging.

Fairbanks (1960) - Master's Thesis, Texas A & M University (8)

The author conducted tests on 6.35-mm (0.25-inch), 12.7-mm (0.5-inch) and 19.1-mm (0.75-inch) thick 127 mm (5 inches) long by 190.5 mm (7.5 inches) wide neoprene pads as bearing systems for wide-flange steel sections. Although his main purpose for testing was to evaluate the effect of the bearing system on the steel beam itself, several conclusions as to the limitations of elastomeric pads could be made. When beam rotations were introduced into the system, the beam end tended to lift-off the thinner bearing pads. This did not occur when the 190.5-mm (0.75-inch) pads were used. Additionally, several instances of bearing slip were noted when pad shear strain surpassed 25 percent, leading the author to conclude that this strain was a limiting factor. However, the author did not calculate the friction coefficient at which the slip occurred. Had he done this, he would have found that slipping started at a friction coefficient of 0.3-0.35 under 2.76 MPa (400 psi) and 0.25 to 0.30 at 5.69 MPa (825 psi) which is consistent with results from the study reported herein.

1.4.2 USE WITH MINIMUM GUIDANCE: 1961-1985

During this period of research, the trend was to show that elastomeric bearings were extremely adaptable to any condition and that they were capable of accommodating a variety of end conditions and bridge movements without failure. More attention was paid to controlling the quality of the manufacturing process than restricting the use of the pads. The specification governing their use essentially did not change from its introduction in 1961 until the interim specification of 1985. Although numerous studies were conducted during this period, a few are particularly noteworthy:

Suter and Collins (1964) - University of Toronto (37)

Static and dynamic tests at normal and low temperatures were conducted on plain and reinforced pads 25.4 mm (1.0 inch) thick, 152.4 mm (6 inches) long and 304.8 mm (12 inches) wide of neoprene, natural rubber, urethane, and butyl. Reinforced pads were of neoprene only and consisted of two layers of 25.4-mm (1.0-inch) material. The study shows that all materials tested performed well in both static and fatigue tests throughout the entire range of temperatures, and that neoprene displayed more low-temperature stiffening than natural rubber (as measured by increase in durometer), as did 70-durometer material versus 60 durometer material (as measured by shear stiffness). Additionally, the laminated bearing design displayed less tendency to creep, and (according to the authors) “exhibits more desirable stress/strain properties with respect to both static and dynamic loading than a homogeneous bearing.” Also, the authors found that compressive stress has little influence on shear properties. Most significantly, the authors found that under 4.14 and 6.90 MPa (600 and 1000 psi) at -37° C (-35° F), at a ratio of shear force to compressive force of 0.4, none of the bearings slipped over their concrete contact surfaces during testing.

Minor and Egan (1970) - Batelle Memorial Institute (17)

In what was clearly the most comprehensive US study to date (NCHRP Report #109), researchers tested a wide range of neoprene, natural rubber, neoprene-dacron mix and ethylene propylene dimonomer (EPDM) specimens in lengths from 76.2 mm (3 inches) to 304.8 mm (12 inches), widths from 76.2 mm (3 inches) to 685.8 mm (27 inches) and elastomer layer thicknesses from 6.35 mm (0.25 inch) to 25.4 mm (1.0 inch). Plain and reinforced bearings having one to 18 layers were tested. Hardness ratings ranged from 50 to 70

durometer. Many of the specimens were “off the shelf” commercial bearings. That was the first study which consistently determined and referred to shear modulus rather than simply to hardness as a design parameter. Significant among the findings and recommendations were: that lower durometer material is less effected by lower temperature and creeps less than higher durometer material; that shear fatigue up to 100,000 cycles resulted in an average 6% reduction in shear modulus — more for higher durometer material — less for lower durometer material; and that AASHTO’s concern over ozone attack may be unfounded as no evidence had ever been presented that ozone effects anything but the outer surface of a bearing. Additionally, the authors compared theoretical and experimental results and developed an exponential equation for compressive deformations. No further restrictions were recommended on the use of elastomeric bearings, however the authors pointed out that quality control during the fabrication of bearings and physical testing of the finished products are of extreme importance to ascertain the actual material properties.

Stanton and Roeder (1982) - University of Washington (33)

This study dealt with NCHRP Project 10-20 (and was published as NCHRP Report 248), was not an experimental study but rather was an analysis of current practice in the US and throughout the world. Codes from Britain and Europe were analyzed and recommendations for changes to the AASHTO Specifications were made. These revisions became part of the Specifications with the publication of the interim 1985 AASHTO Specifications. Based upon the authors’ analysis of foreign codes and practice: the allowable stress for reinforced bearings was raised from 5.52 MPa (800 psi) to 6.90 MPa (1000 psi); the compressive deformation limit of 7% of the elastomer thickness was removed - no limit was stated; compressive stresses in plain bearings and cover layers of reinforced bearings were required to be multiplied by a factor (β) of 1.8 and 1.4 respectively to account for the greater stresses in the elastomer due to bulging (a method used by the British); a rotation restriction of twice the compressive deformation divided by the bearing dimension perpendicular to the axis of rotation was stipulated — also based upon a British code and common practice; a worst-case friction coefficient of 0.2 was recommended for design purposes; and the use of tapered elastomer layers was discouraged as “their behavior is not well understood.”

1.4.3 EXPLICIT DESIGN PROCEDURES: 1985-PRESENT

Based upon the work of Stanton and Roeder cited above, a second and third phase of NCHRP Project 10-20 was undertaken by the same authors. This included an extensive series of laboratory tests on elastomeric bearings of all shapes and sizes, and was reported in NCHRP Reports 298 and 325. The final result of the test program was to give a choice of two design methods, a simple restrictive one, (Method A), and another (Method B) based more on theoretical calculations which required additional testing of the elastomer so that its material properties would be well defined. The reports formed the basis of the current 1992 AASHTO specification.

Roeder and Stanton (1987) - University of Washington (25)

This research was performed on bearings of natural rubber and neoprene of many different shape factors, laminate thicknesses and layers, and plan shapes (including square, rectangular and circular). Both steel- and fiberglass-reinforced specimens were examined. Tests were conducted for shear modulus determination, compressive failure, stability limits, rotational stiffness, shear fatigue, and compression fatigue. An attempt was made to correlate experimental results with finite element analyses as well as theoretical models to determine recommended limiting values for various parameters such as shear strain, compressive stress, rotation, aspect ratio, and reinforcement thickness. As in previous research by the authors, British code limits were referred to and used as the basis for some of the recommended strain bounds. Based upon these codes and experimental results, the authors decided upon a limitation of the overall shear strain of 3.0 from all loads such that:

$$\gamma_c + \gamma_s + \gamma_r \leq 3.0 \quad (1.6)$$

where the subscripts c, s, and r, designate shear strain due to compression, direct shear, and rotation respectively. Assuming a direct shear strain of 50%, and using theoretical relationships to relate shear strain due to compression and rotation, the authors arrived at an expression governing the interaction of these two stresses in terms of compressive stress and rotation in radians. Additionally, compressive failure test results showed that two improperly manufactured specimens with non-parallel reinforcing shims failed at lower stress levels than otherwise identical specimens with uniform elastomer layers. On the basis of these test results, even though the bearings tested were flat with misoriented steel shims, all bearings with tapered elastomer layers were prohibited by AASHTO, thus effectively disallowing the use of tapered bearings.

Roeder and Stanton (1988) - University of Washington (24)

In their most recent NCHRP Report, the authors tested 101.6-mm (4-inch) square laminated bearings of neoprene and natural rubber with two 10.2-mm (0.4-inch) elastomer layers and 4.76-mm (0.1875-inch) steel shims separating them and as bonded cover plates. Tests were conducted from room temperature to as low as -45°C (-50°F). A range of durometer ratings from 50 to 65 was examined. In agreement with previous tests at low temperatures, the authors noted that natural rubber bearings stiffened (as measured by shear modulus) less than neoprene bearings of the same hardness, and that compounds of lower hardness stiffen (by the same measure) less than those of higher hardness. Also included in this report were recommended acceptance criteria that tightened the fabrication tolerance on laminated bearing layer thickness from $\pm 3.175\text{ mm}$ (0.125 inch) to $\pm 20\%$ of the design thickness. For example if the design thickness is 6.35 mm (0.25 inch), the manufacturer must fabricate the layer within 1.27 mm (± 0.05 inch).

1.5 RESEARCH GOALS

The goals of the research described here are threefold:

Quantify the “walking out” phenomenon

While many pads have been observed to slip out from under bridge girders, no quantifiable study has yet been performed which explains the reason for and the mechanics of the phenomenon. The first goal of this study is to describe this behavior in terms of the forces and environment required to initiate bearing slip and to understand the reason why bearings slip in some instances and not in others.

Define Tapered Bearing Limits

Insofar as elastomeric bearings have been in wide spread use throughout the world with great success, this study will concentrate on a comparison between bearings with the standard flat design described in the current AASHTO Specifications, and comparable tapered bearings. In all cases, specimens are fabricated so that all parameters to be studied were duplicated in both flat and tapered models, thus allowing for a direct comparison between flat and tapered bearing behavior.

Develop a Tapered Bearing Design Procedure

As a result of the extensive testing on flat and tapered bearings, the final goal of the study is to produce a simple design procedure that would specify a suitable, durable and economical tapered bearing conforming to the recommended limits on the parameters described above. This procedure takes into account the ability of elastomeric bearings to accommodate the inconsistencies of span ends, and it standardizes as many of the design parameters as possible.

1.6 RESEARCH SCOPE

Since their inception, use of elastomeric bearings has become accepted (32) as an alternative to more complicated and costly bearing designs. Currently such bearings are found in practically every shape, size, man-made elastomeric material, reinforcing and anchorage scheme imaginable. With this in mind, the scope of the research was limited to the following:

Application

Although elastomeric bearing pads are widely used in applications that require them to be extremely large in plan or very thick, the bearings tested in this program were intended to be analogous to those used in the most typical configuration for 30.48-m (100-foot) or greater prestressed girders with bottom flanges up to 609.6 mm (24 inches) in width. Some circular bearings were tested, but the standard specimen was rectangular in plan, and no attempt was made to determine differences in bearing performance based upon plan dimensions or shapes.

Material

Most of the research project was devoted to the study of natural rubber bearings with the intention of showing that this elastomeric material was a viable alternative to neoprene. Furthermore, although the lessons learned from this study can be applied to other types of elastomeric bearing pads, no attempt has been made to study the numerous variations of pads, such as random fiber reinforced pads (ROF) or butyl rubber pads.

Shape factor

Test specimens were all identical in length and width and total elastomer thickness, so the influence of these variables was not investigated. The only influence on the shape factor was the steel reinforcing scheme which was either 2, 3 or 6 steel reinforcing shims.

Reinforcement

Only reinforced bearings were examined, since many of the applications for elastomeric bearings in Texas bridges result in compressive stresses well beyond the ranges recommended for unreinforced pads. All reinforcement was internal; elastomeric material covered all steel shims except where intentionally removed for observation purposes. Additionally, only steel reinforcement was used although elastomeric bearings with fiberglass or cotton-fiber duck fabric reinforcement are currently marketed.

Anchorage

In the combined compression/shear performance portion of this study, all bearings were anchored to concrete surfaces by friction alone. No attempt was made to determine the effect upon their compression/shear behavior of gluing or otherwise bonding bearings to girder bottoms or to bearing seats. No bearings with fabricated holes to accommodate dowels were tested.

Environment

Bearings were tested at room temperature, and were not subjected to any adverse weathering conditions. Fatigue tests were conducted at frequencies that were low enough to preclude overheating the elastomeric material.

Stability

All test specimens were well within the current AASHTO limits for stability of reinforced rectangular bearings: total height less than one third the smallest of the length or width.

1.7 LIMITATIONS OF CURRENT AASHTO SPECIFICATION

The current AASHTO Specifications are restrictive in a number of ways and, as a result of these restrictions, fail to take full advantage of the versatility of reinforced elastomeric bearings.

There is no specific description in the specification of the reasoning for disallowing tapered elastomer layers except that “they cause large shear strains and bearings made from them fail prematurely because of delamination or rupture of the reinforcement” (32). This study will report test results comparing bearings with uniform and tapered elastomer layers on the basis of delamination, and fracture of reinforcing steel shims.

The magnitude of girder end rotations that elastomeric bearings are allowed to accommodate is restricted considerably under the current specification. According to the AASHTO specification, bearing rotations are allowed as follows:

$$\theta_{TL} = \frac{2\Delta_c}{L} \quad (1.7)$$

where θ is the rotation that the bearing can accommodate, Δ_c is the instantaneous compressive deformation of the bearing, and L is the dimension of the bearing parallel to the length of the girder. Given the specification’s guide for compressive deformations, a 50 durometer 228.6-mm (9-inch) x 355.6-mm (14-inch) bearing with a shape factor of eleven compressed under 7.0 MPa (1000 psi) would have an instantaneous deformation of approximately 1.27-mm (0.05-inch) and would be allowed a rotation of 0.0111 radians or a 1.11% slope. In this study, bearings with this design were intentionally subjected to rotations as much as three times that allowed by the current AASTHO Specifications.

The current Specification allows for two design methods for elastomeric bridge bearings. Under Method A, which does not require any material testing be performed by the manufacturer or user other than that called for in the fabrication criteria, compressive stress due to all loads is limited to 6.90 MPa (1000 psi) for steel reinforced bearings. If extensive testing is performed, Method B may be used which will allow for bearings to be subjected to 11.0 MPa (1600 psi) from all loads. Additionally, cover layers of reinforced bearings must be intentionally constructed thinner than internal layers due to the β - factor which is intended to limit the shear strain on that layer:

$$\sigma_{cTL} \leq \frac{GS}{\beta} \quad (1.8)$$

where G is the shear modulus of the elastomer and S is the shape factor of the bearing. The shape factor for the cover layers must be reduced by $\beta = 1.4$. As a result of this requirement, under high compressive stresses, the cover layer must be so thin as to inhibit it from accommodating the irregularities of the bearing seat. Many of the test specimens used in this study were designed to evaluate the behavior of cover layers thicker than currently allowed.

1.8 ORGANIZATION OF STUDY

This report is organized into nine chapters, five appendices, and a glossary. Chapter 1 describes the background of elastomeric bearings as well current problems associated with their use. Chapter 1 also discusses the pertinent research that has been performed in this field to date as well as the evolution of the AASHTO Specifications since 1961. Additionally, it defines the parameters that were studied in the research project and the scope of that research. Also, the limitations of the current AASHTO specification are discussed. Chapter 2 contains a description of the major test apparatus designed and constructed for this study as well as a description of the test specimens and the precision and accuracy to which they were fabricated. Chapter 3 describes the displacements produced in tapered bearings under dead load which are peculiar to them due to their geometry and gives an explanation of the investigation into bearing slip.

Chapter 4 describes the experimental program used to define of tapered bearing stiffness and gives the results of those tests. Chapter 5 gives results of compression creep tests. Chapter 6 gives the results of shear and compression fatigue tests and Chapter 7 gives the results of tests to compressive and shear failure. Chapter 8 contains the conclusions arrived at through analysis of the test results as well as recommendations for elastomeric bearing design and use. Chapter 9 is a proposed design procedure. Appendix A contains proposed specifications and Appendix B contains design examples. Appendix C is a table of elastomeric material properties, which are referred to in this study or may be of general interest to the reader. Appendix D contains a listing of the notation used in this report. Appendix E gives the results of individual tests by specimen. A glossary of terms peculiar to the study of elastomers which will aid the reader who is not familiar with this field is presented following Appendix E.

1.9 SUMMARY

The purpose of this study is to perform a rigorous examination of elastomeric bearings concentrating on tapered, natural rubber pads with the end product being a simple design procedure for proportioning elastomeric flat and tapered bearings. A strong attempt has been made to determine the performance, limitations, and tolerances of the bearings in their intended mode of employment.

CHAPTER 2

EXPERIMENTAL PROGRAM

2.1 BEARING SHEAR TEST MACHINE

As a major part of the project, a test machine, shown in Figures 2.1 and 2.2, was designed and constructed which could duplicate the dead weight and daily thermal deformation response of the bridge girder, subjecting the bearings to the same compressive and shear stresses and strains as those in service. The purpose of the test machine was to study bearing behavior under typical field conditions including those responsible for causing walking out. Pursuant to this goal, the test machine could be configured to subject bearings to both uniform and non-uniform loading, and to enable and measure bearing slip. Bearings were set in pairs between the platens as shown in Figure 2.2 and sheared under various conditions depending upon the objectives of the particular test. All major components of the apparatus were bolted so that adjustments could easily be made to accommodate the various different sizes of the bearings that were tested.

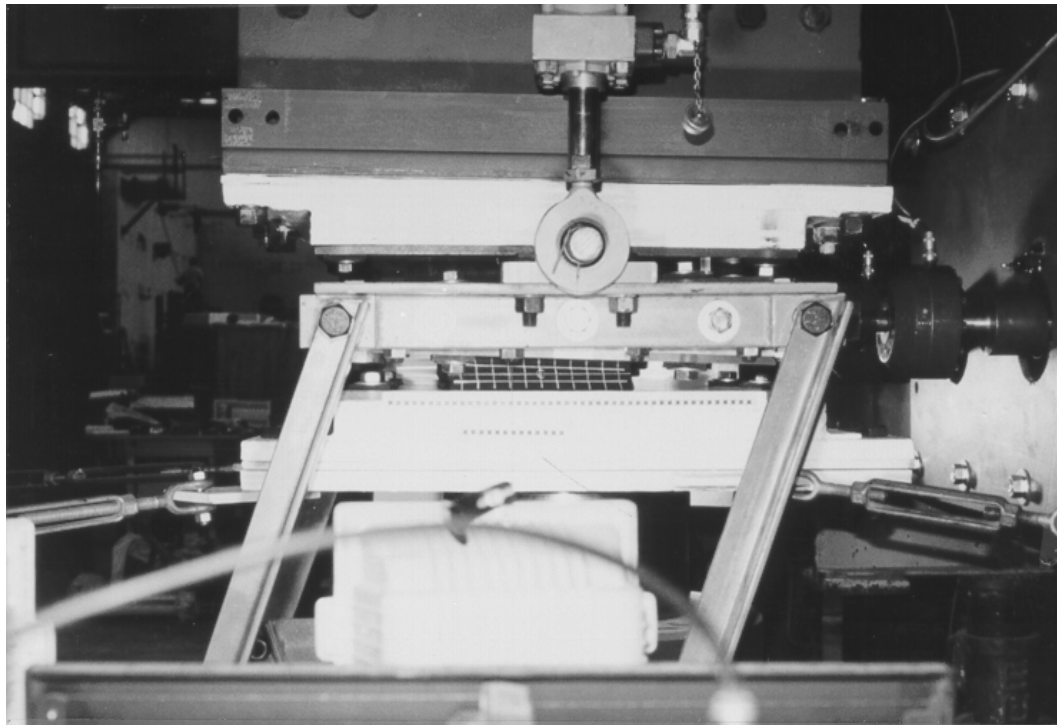
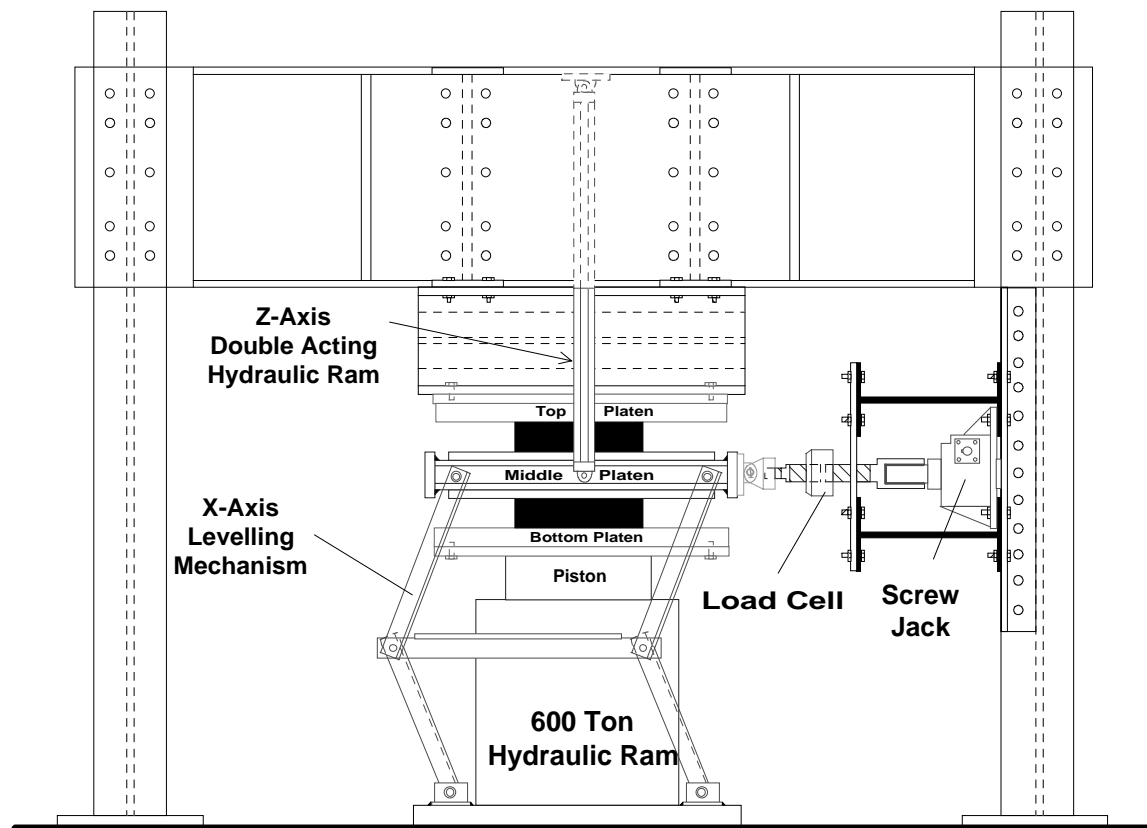


Figure 2- 1 Bearings being tested in the shear test machine



Side View of the Elastomeric Bearing Test Setup

Figure 2- 2 Schematic of the elastomeric bearing test setup

A compression force was applied by means of a 5340-kN (600-ton) hydraulic ram. To ensure that the compressive stress on the bearings remained constant during the tests (some of which lasted for several weeks), a system shown schematically in Figure 2.3 was designed to provide a constant pressure to the compression ram. Steel weights of various sizes (see Figure 2.4) were suspended from a small hydraulic piston which introduced a pressure into the hydraulic line leading to the pressure inlet side of the 5340-kN (600-ton) ram. Regardless of the movement of the bearings or the middle platen in the apparatus, the dead weight would always maintain the same pressure in the inlet line thus allowing the compression ram to provide a constant force. This was especially important due to the bearings' propensity for compressive creep during shearing. Without the system, pressure would have gradually been lost.

The expansion and contraction of the bridge was duplicated by 311-kN (35-ton) screw-type jacks as shown in Figure 2.5 which provided the force to translate the middle platen thus shearing the bearings. The jacks were driven by a 0.56-kW (0.75-HP) electric variable speed reversible motor/288:1 ratio reduction gear system that was controlled by a programmable electronic controller (See Figure 2.6) and timer. The system thus could be programmed for any magnitude of a repeatable thermal cycle. The horizontal force application system could be raised or lowered to match the level of the middle platen, which was dependent upon the thickness of the bearings being tested. See Figure 2.2.

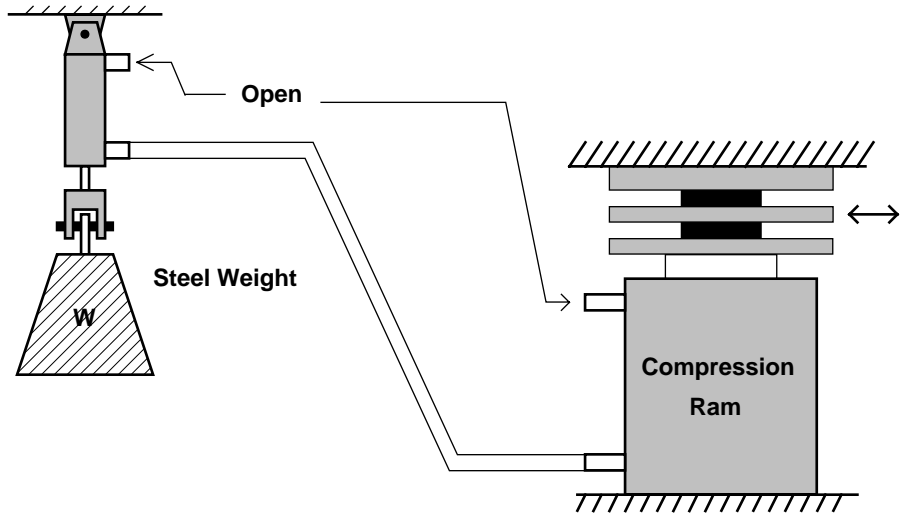


Figure 2- 3 Constant compressive force system

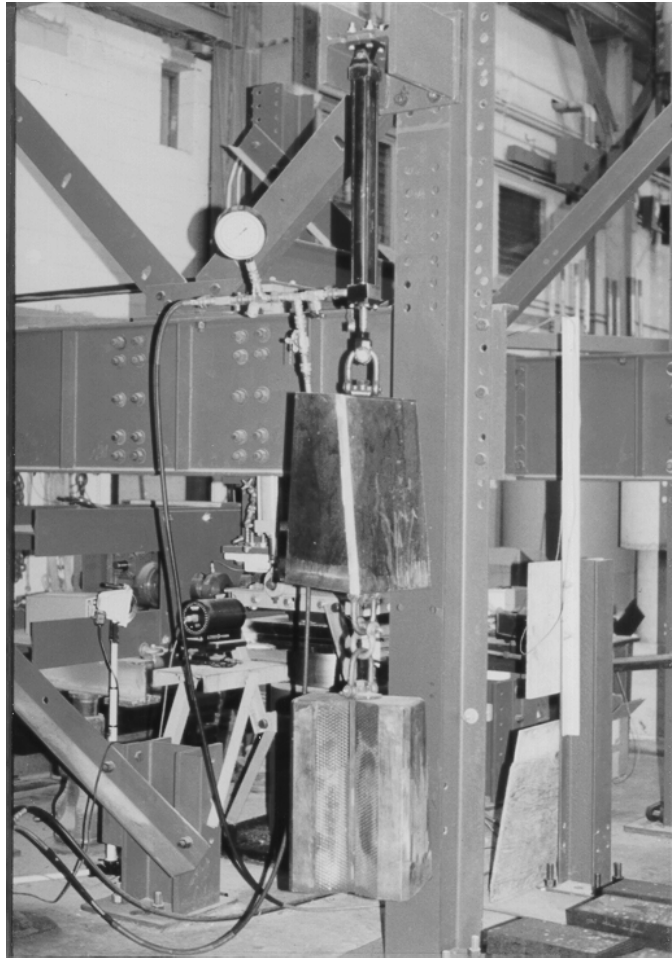


Figure 2- 4 Steel dead weights

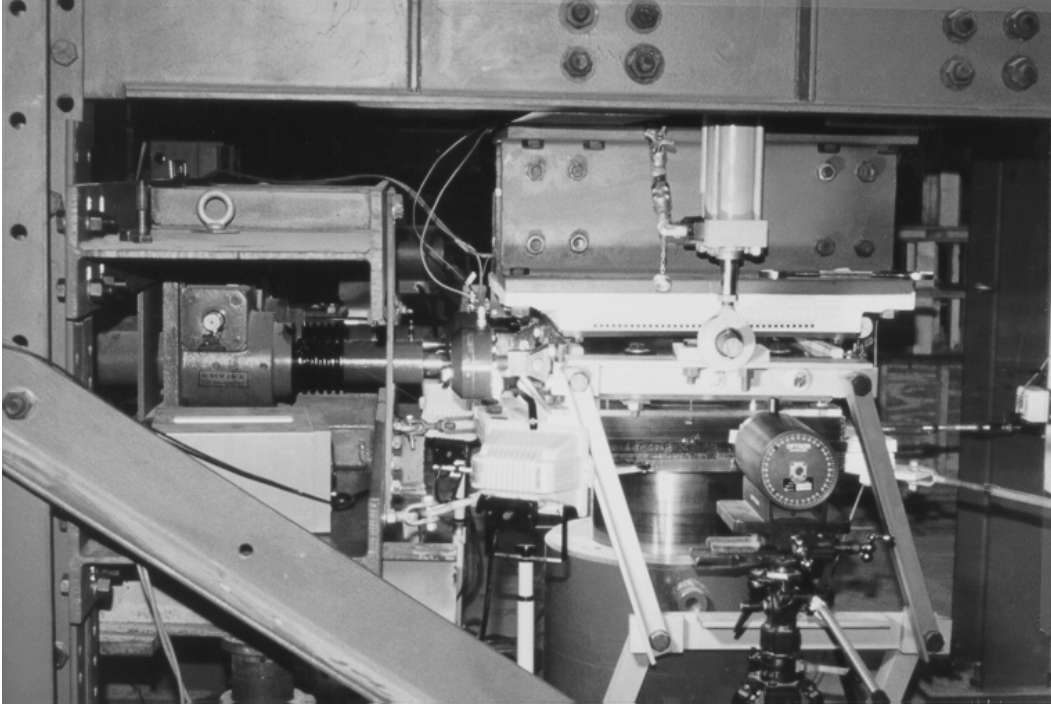


Figure 2- 5 311-kN (35-ton) screw jacks

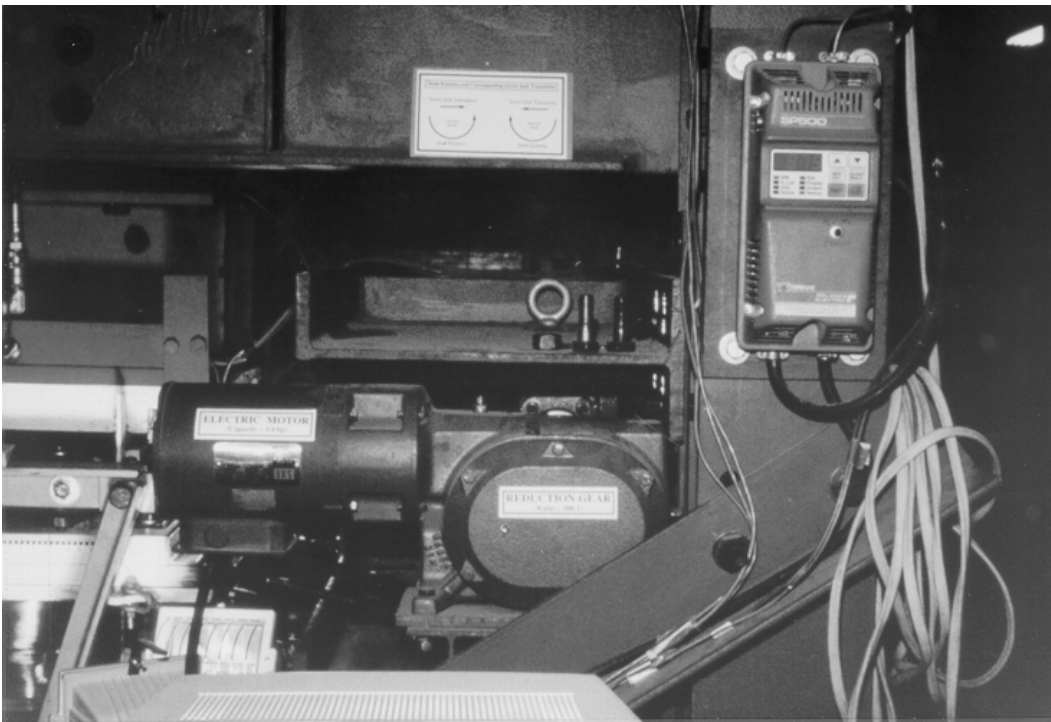


Figure 2- 6 Electronic controller/motor/reduction gear system

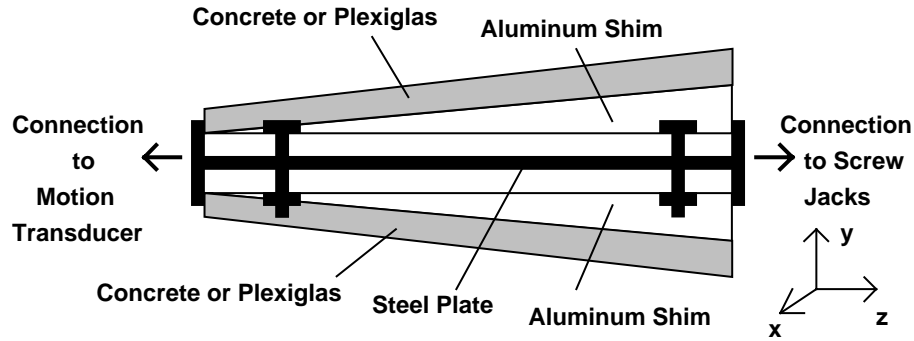


Figure 2-7 Middle platen detail

2.1.2 MIDDLE PLATEN DESIGN

Top, bottom and middle platens were removable so that various materials such as concrete, steel and Plexiglas could be used as bearing surfaces for the tests. In cases where tapered bearings were tested, aluminum plates were machined to matching slopes to accommodate the pads. These plates were designed such that the various platens could be attached to them creating a wedge-shaped middle platen as shown in Figure 2.7.

Two systems were designed to prevent the middle platen from rotating due to bearing misalignments. These systems were extremely important because any significant rotation of the middle platen might have resulted in severe damage to the screw jacks, the most expensive components of the apparatus.

X-Axis Leveling Mechanism

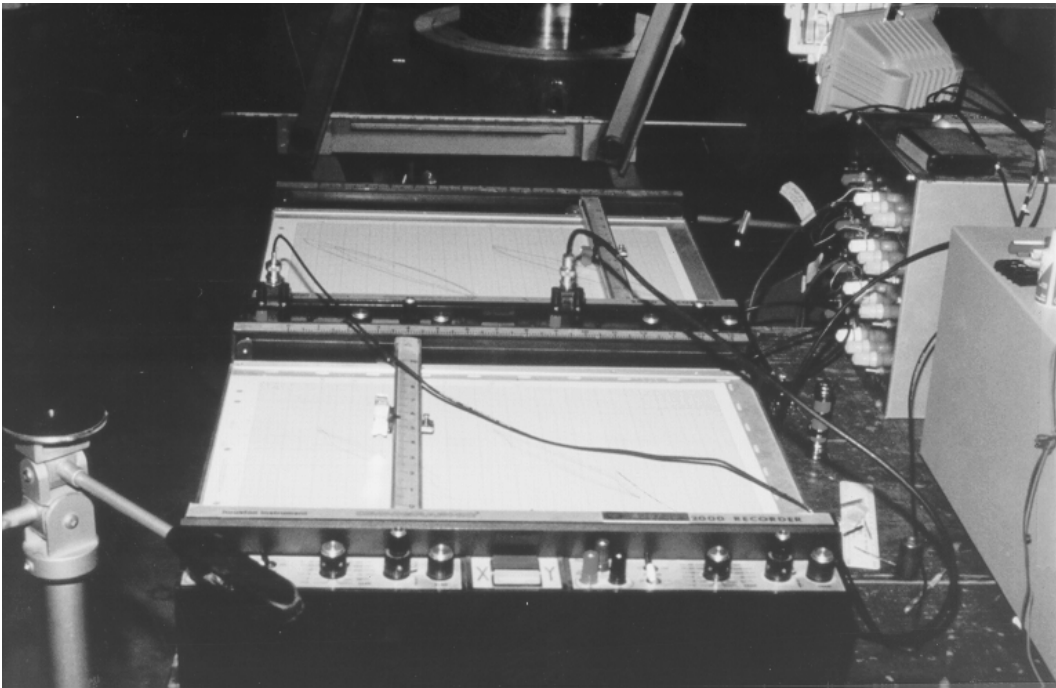
When tests to characterize bearing walking out were proposed, the possibility had to be considered that the top and bottom specimens could walk out unequally thus creating a couple which would tend to rotate the middle platen about the bearings' x-axis. Therefore, a mechanism was designed which permitted middle platen translation and elevation, but not rotation. Figure 2.2 shows the leveling mechanism as it was configured for the test program. Each joint where members of the mechanism were connected was constructed with roller bearings so that even if a couple was produced, rotation could be limited without causing additional horizontal force to be read by the load cells (other than friction in the roller bearings). The size of the members of the mechanism was determined by calculating the force that would result from the greatest possible compressive force and bearing misalignment.

Z-Axis Stabilization

In anticipation that the bearings might also slip in the direction of their x-axis, another stabilizing device was designed which again permitted translation and elevation but prevented the middle platen from rotating about the bearings' z-axis. Two double acting hydraulic rams (see Figure 2.2) were attached to the middle platen and were cross linked so that they could not extend or retract independently from one another. Because very little force was required to extend or retract the rams together, no significant additional horizontal force was read by the load cells as the middle platen translated. The rams could be prevented from extending or retracting by stopping the oil flow between them via a globe valve installed in the hydraulic line. Thus in addition to their stabilization function, they were also used to hold the middle platen in place while changing specimens.



(a)



(b)

Figure 2- 8 *Data acquisition system*

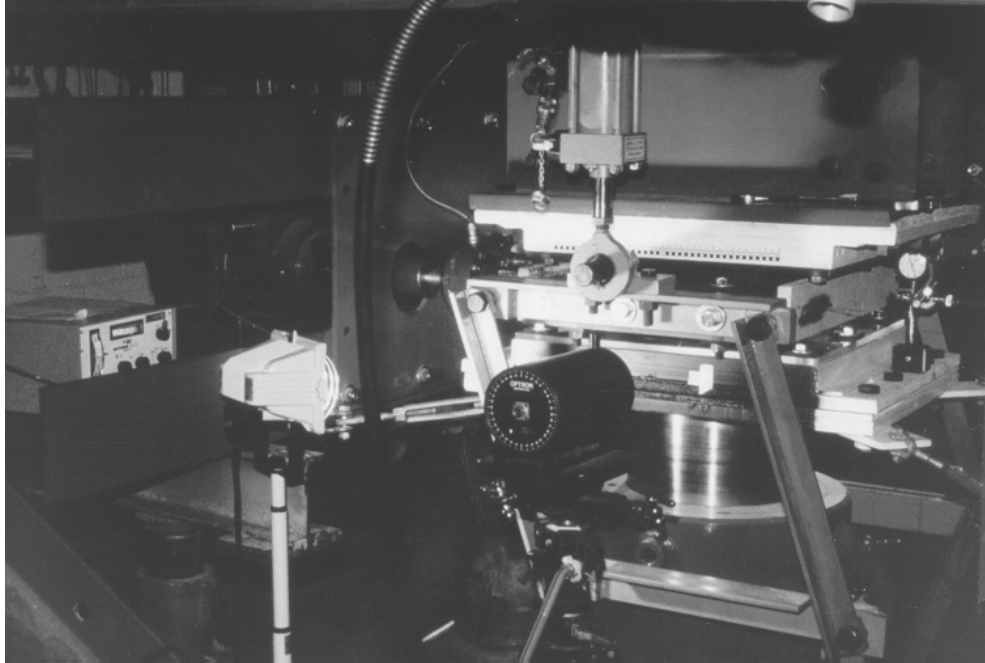


Figure 2- 9 Optron with light source directed toward bearing

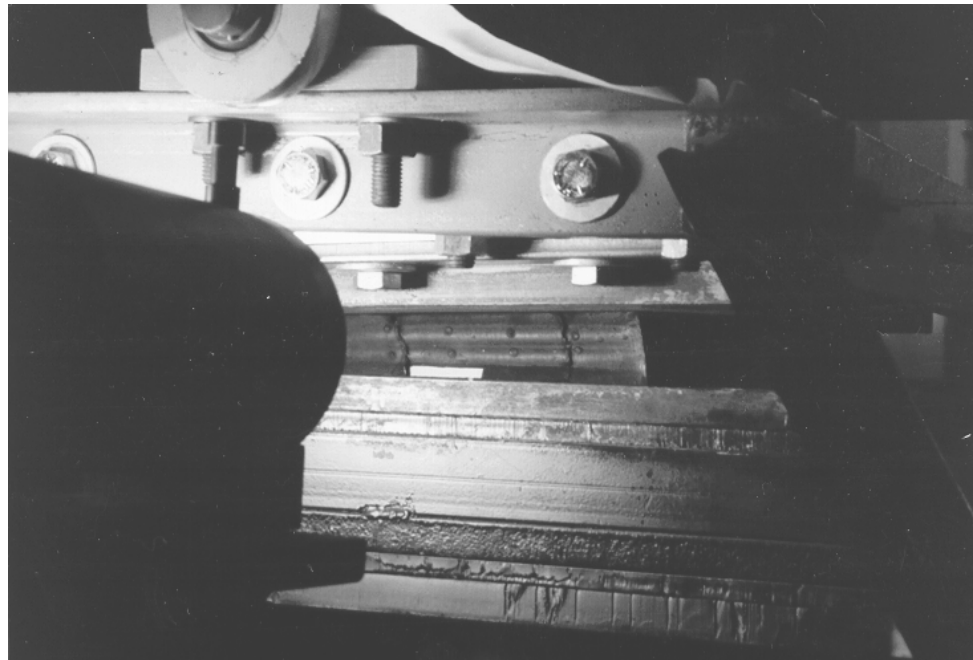


Figure 2- 10 Optron tracking a target on a bearing

2.1.3 INSTRUMENTATION/DATA ACQUISITION

Instrumentation consisted of two 222-kN (50-kip) load cells connected with fittings to the screw jack shafts and the middle platen as shown in Figure 2.1 and electronic motion transducers to measure the middle platen translation. Data acquisition was provided by personal computer with data acquisition software and plotters as shown in Figures 2.8a and b.

Bearing slip was measured by an optical instrumentation system known as an Optron, which is shown in Figure 2.9. This instrument is essentially a light meter capable of converting an increase or decrease in the light reflected from a small target on the object to be tracked (in this case a bearing—see Figure 2.10) into a voltage increase or decrease which can be sent via signal cable to a data acquisition system in the same manner as any other electronic instrument (load cells, linear potentiometers, etc.). The voltage output can be calibrated to the target movement by measuring the Optron field of view as projected onto the object to be tracked. For a target whose edge is originally located at the midpoint of the Optron's field of view, a voltage increase or decrease of 5 volts represents a movement of the object a through a distance of 50% of the projected field of view. See Figure 2.11.

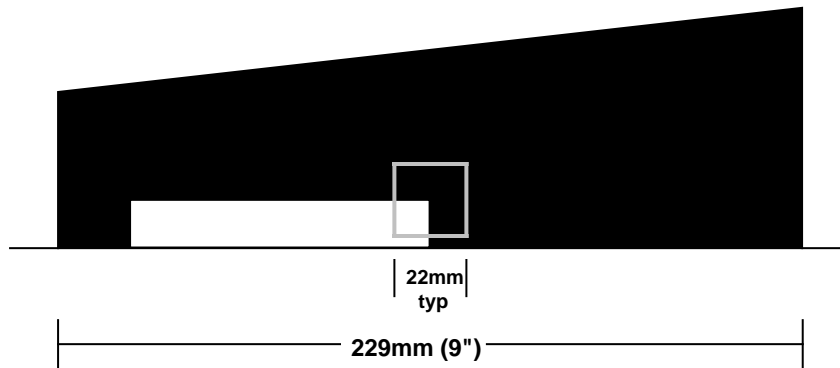


Figure 2- 11 Optron target as seen through the optron view finder

In the case shown in Figure 2.11, where the dimensions are typical of those during the tests, a movement of the bearing 11 mm in either direction would result in a voltage increase or decrease of 5 volts. The Optron is capable of continuing to track the target to 60% of the field of view in either direction before losing the signal.

2.2 TEST SPECIMEN DESIGN AND FABRICATION

2.2.1 FIELD STUDY BEARINGS

Slaughter Creek Bridge, Austin

Bearings from this bridge were made from natural rubber and were 559 mm (22") long, 229 mm (9") wide and 44.5 mm (1.75") in overall height. The bearings had two 3.18-mm (0.125") steel-reinforcing shims leaving an elastomer thickness of 38.1 mm (1.5"). The specified durometer was 70 and the durometer as measured in the laboratory after removal from service was 68. The specified taper of the pads was 3.8%. Tapers were measured after removal from service and were found to vary from 2.5% to 3.8% due to the elastomer's ability to deform to accommodate the actual slope of the individual girder which it supported.

Valley Ridge Bridge, Dallas

Bearings from this bridge were also made from natural rubber and were circular with a 384 mm (15.1") diameter and an overall height of 44.5 mm (1.75"). The bearings had two 3.18-mm (0.125") steel-reinforcing shims leaving 38.1 mm (1.5") of elastomer. The specified durometer was 60 and the durometer as measured in the laboratory after removal from service was 68. The specified taper was 2.6%. Tapers were measured after removal from service and were found to vary from 2.1% to 2.6%. In one case, where the bearing must have been improperly oriented with the girder slope, the bearing was almost perfectly flat due to the long-term effect of the non-uniform loading.

2.2.2 TEST SPECIMEN DESIGN

Test specimens were designed to provide a sharp contrast by which to evaluate the effects of varying certain parameters. Through analysis of preliminary tests performed on bearings removed from service, conclusions were reached as to which characteristics would provide the most insight into the behavior of elastomeric bridge bearings. A number of parameters were considered, but, in the interest of narrowing the scope of the study, only shear modulus, the number and orientation of steel-reinforcing shims, and the magnitude of taper were chosen as variables. Bearings were ordered from three manufacturers: "A", from whom only flat bearings were received, and "B" and "C" with whom identical orders were placed for flat and tapered bearings. Two different companies were chosen to provide the same specified bearings in order to gage the variation in performance. The two manufacturers used two different rubber suppliers for the raw material.

Elastomer Properties

In each batch of specimens from different manufacturers, two values of shear modulus were requested: 0.7 and 1.4 MPa (100 and 200 psi). Bearings were requested by shear modulus alone, not by durometer. The manufactures were free to provide any durometer they wished as long as the end shear modulus was as specified. Originally, it was planned to include specimens with shear moduli as high as 2.1 MPa (300 psi), but, on closer examination, it was apparent that bearings with such a high shear modulus were not desirable.

In fact, the highest shear modulus material routinely produced by the manufacturers is approximately 70 durometer (the maximum allowable in reinforced bearings according to the most recent AASHTO specification) which yields a shear modulus appreciably lower than 2.1 MPa (300 psi).

So that all bearings manufactured under a specific design would be as close to identical as possible, the manufacturers were instructed to produce all of the specimens from one uniform batch of elastomer compound. Cross-mixing separately prepared batches was permitted to achieve the total amounts required to produce the number of bearings ordered. It was hoped that by specifying this procedure, the shear modulus of each bearing delivered at a nominal value would be the same and that any difference in the modulus determined from the various tests would be due to the other variables such as taper, number of

steel shims, compressive stress and non-uniform loading. In addition to the bearings themselves, one plain pad of vulcanized natural rubber from each compound used to fabricate the specimens was requested so that material property tests could be conducted.

As explained earlier, waxes are added to the natural rubber compound to satisfy the ozone exposure specification. These additives contain varying percentages of paraffin and microcrystalline waxes, the former being the most aggressive in secreting and building up on the bearing surface. Due to the slipping problems associated with the paraffin based waxes, all of the specimens were requested with only microcrystalline wax to ensure that the test results would not be influenced by bearing slip.

2.2.3 SPECIFIED DIMENSIONS

All pads were ordered 229 mm (9") long and 711 mm (28") wide. The length corresponds with the majority of the bearings in service throughout the state. Bearing width is most often determined by the flange width of the girder it is supporting. The test apparatus described earlier was capable of accommodating bearings up to 559 mm (22 inches), but smaller specimens can be just as representative of bearing performance. A standard width of 356 mm (14 inches) was selected based upon the various test apparatus' ability to load the specimens to the stresses desired. For fatigue and compression failure tests, this dimension was further reduced to 229 mm (9 inches) for the same reason. Specimens were ordered in 711 mm (28 inch) widths so that they could be cut in two or three sections with identical properties.

In order to compare results with the analytical study performed by Hamzeh (10), a standard elastomer thickness of 44.5 mm (1.75 inches) was specified. Regardless of the number of reinforcing steel shims, the thickness of the elastomer was not varied. Overall bearing thickness was simply greater in bearings with more steel shims. In tapered specimens, the 44.5-mm (1.75- inch) dimension was to be taken at the mid-length of the bearing. The average total thickness of the bearings was 51.3 mm (2.02"), 52.4 mm (2.06"), and 60.4 mm (2.38") for 2, 3, and 6 shim bearings respectively.

Three degrees of bearing taper were examined: flat bearings (no taper) which would be subjected to the same tests as the tapered specimens to establish a "baseline" performance; a nominal 4% taper, and a nominal 6% taper, the maximum taper currently employed by TxDOT.

2.2.4 STEEL-REINFORCING SHIMS

Number of Shims

The number of reinforcing shims has a significant influence on the axial and rotational stiffness of the bearing. From Manufacturer "A," plain bearings (no reinforcement) and bearings with two steel-reinforcing shims were requested which, based upon a standard 229-mm x 236-mm (9" x 14") specimen, yielded shape factors of 1.57 and 4.70 respectively. From tests on those specimens, it was clear that such lightly reinforced bearings would deform excessively under the compressive stresses that were planned for the tapered bearing test program. Therefore, from Manufacturers "B" and "C," more heavily reinforced bearings were ordered. The reinforcing schedule was specified as 3 or 6 steel shims yielding shape factors of 6.26 and 10.96 respectively.

Steel Properties

The standard steel for reinforcing shims, according to all three manufacturers, is A570, Grade 40. Manufacturer B provided a Mill report which gave the results of two tensile tests showing yield strengths of 276 MPa (40.3 ksi) and 339 MPa (49.1 ksi) and ultimate strengths of 340 MPa (56.5 ksi) and 459 MPa (66.6 ksi). No independent tensile tests were performed for this study. The thickness of the reinforcing plates was determined through analysis of the tensile forces that would be produced by the hydrostatic pressure from the compression of the elastomer. (See Figure 1.6.) The maximum expected compressive

stress on the bearings was 1100 psi (7.59 MPa) and the analysis of the required steel shim thickness according to AASHTO specification 14.4.2.6 is as follows:

$$h_s \geq \frac{1.5(h_{r1} + h_{r2})\sigma_{c,TL}}{F_y} \quad (2.1)$$

where h_s is the required thickness of the steel shim, h_{r1} and h_{r2} are the thicknesses of the surrounding elastomer layers, F_y is the yield strength of the shim (assumed to be 276 MPa (40.0 ksi)), and $\sigma_{c,TL}$ is the compressive stress on the bearing. The equation includes a factor of safety of 2. Based upon this calculation, for the specimens with 3 steel shims, and elastomer layers of 11.1 mm (0.438 inches), the steel shim thickness should be a minimum of 1.02 mm (0.04 inches). Although this thickness would suffice, the manufacturers felt that shims thinner than 2.66 mm (12 gage (0.1046 inches)) would most likely deform severely during the vulcanization process. Therefore, the 12 gage thickness was used in all bearings. (Manufacturer A's bearings, which were supplied before this analysis was performed, were fabricated with 3.42-mm (0.1345" (10-gage)) shims).

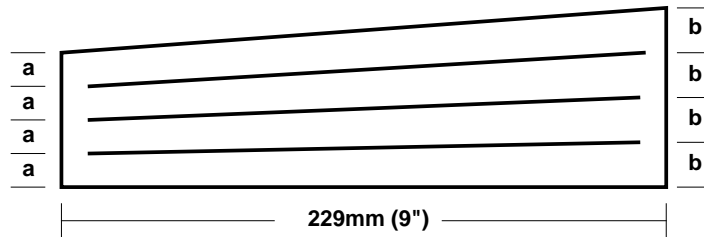


Figure 2- 12 Spacing of steel shims in tapered bearing specimens

Shim Orientation

Reinforcing shims for flat bearings were requested to be equally spaced throughout the length of the bearing. In most of the tapered specimens, the shims were to be equally spaced at each point along the length. (See Figure 2.12.)

One set of bearings with a nominal 6% taper, 3 steel shims and 0.7 MPa (100 psi) shear modulus was ordered from Manufacturer B with steel shims parallel as shown in Figure 2.13 so that the effect of varying the shim orientation could be observed. The dimension "c" is equal to dimension "a" plus 229 mm (9 inches) times the bearing taper in radians.

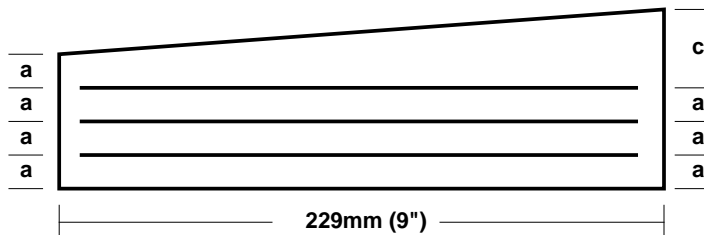


Figure 2- 13 Tapered bearing with parallel steel shims

2.2.5 FABRICATION ACCURACY AND PRECISION OF TEST SPECIMENS

As described above, a number of parameters were specified to the manufacturers. No special tolerances other than those given in the AASHTO specification however, were demanded. One of the reasons for doing this was to determine the “as manufactured” properties and dimensions of the bearings to better understand the fabrication process as well as to study first hand what the engineer specifying a certain bearing design is most likely to receive. In some cases, the manufactured product varied significantly from that which was requested. These variations are described below:

Shear Modulus/Hardness

Hardness measurements were taken with a Shore “A” Durometer on the 25.4-mm (1-inch) plain pads that were delivered with each shipment. The results of those measurements are shown in Table 2.1. The column labeled “stated” indicates the hardness that the manufacturer targeted to achieve the requested shear modulus:

Table 2-1 As delivered hardness measurements

Specified Shear Modulus MPa (psi)	Manufacturer A		Manufacturer B		Manufacturer C	
	Stated	Actual	Stated	Actual	Stated	Actual
0.7 (100)	None	65.1	55	57.0	50	53.9
1.4 (200)	None	71.3	70	68.7	60	69.5

The results of shear modulus determination tests on the reinforced bearings are discussed in greater detail in Chapter 4, but overall average shear moduli are presented in Table 2.2. Two values for shear modulus are shown, one is the modulus between zero and 25% strain (the range used in ASTM 4014) and the other is the modulus between zero and 50% strain.

Only Manufacturer B expressed concern about producing 1.4 MPa (200 psi) shear modulus material. Their order was delayed due to attempts to produce the desired modulus as determined by the test procedure specified in ASTM 4014. According to Manufacturer B, bearings of this modulus are rarely called for and their standard 70-durometer material (the highest allowed by AASHTO in reinforced bearings) would yield a shear modulus of approximately 1.03 MPa (150 psi). The manufacturer was given permission to provide their standard 70-durometer material without modification.

Wax Content

As stated earlier, the manufacturers were specifically instructed to use a microcrystalline wax. Manufacturer A complied with this instruction and produced bearings that had (according to the manufacturer) only microcrystalline wax. When delivered, absolutely no residue could be removed from the surface of these bearings. When tested, they showed no evidence of slipping over any concrete surface at shear strains up to 100%. However, after nine months, the bearings were examined again and very small quantities of wax could be removed their surfaces. Manufacturer B’s first delivery was clearly impregnated with paraffin wax as evidenced by the accumulation of waxy material on the bearing surface when delivered. The manufacturer was contacted concerning this problem and stated that the rubber supplier had been informed of the specification and had reported that the material was in compliance. Manufacturer C delivered bearings that were compounded (according to the manufacturer) exclusively with microcrystalline wax. In this case, some residue was noted and removed form the surface of the bearings, but the texture of the

Table 2- 2 Average shear moduli as determined from testing

Specified Shear Modulus MPa (psi)	Manufacturer A MPa (psi)		Manufacturer B MPa (psi)		Manufacturer C MPa (psi)	
	0-25% strain	0-50% strain	0-25% strain	0-50% strain	0-25% strain	0-50% strain
0.7 (100)	0.693 (101)	0.680 (98.6)	0.617 (89.5)	0.604 (87.5)	0.614 (89.1)	0.602 (87.3)
1.4 (200)	0.861 (125)	0.841 (122)	0.933 (135)	0.910 (132)	0.868 (126)	0.847 (123)

residue was completely different than that found on the surface of Manufacturer B’s bearings. The residue was “gritty” and did not appear to be excessive or as “waxy” as the paraffin secretion. According to the manufacturer, this type of residue is consistent with microcrystalline wax. A subsequent visit to Manufacturer A revealed that all microcrystalline waxes employed in the industry are a blend of paraffin and microcrystalline waxes and that the cost of the wax is the most reliable method of determining the percentage of microcrystalline versus paraffin, the former being much more expensive. Apparently, there are no industry standards or specifications that apply here and wax manufacturers can call any wax microcrystalline however small the percentage of that ingredient. Therefore, it is presently not possible to write a specification that would preclude having a problem caused by the wax used as an ingredient in the compounding process.

Dimensions

Almost uniformly, the bearings were delivered at 711+3 mm (28+1/8 inch) in width and 229+0 mm (9+0 inches) in length. In no cases were bearings found to be less than the specified length and width dimensions. Elastomer thickness, which was specified as 44.5 mm (1.75 inches), was reasonably consistent considering the process by which the bearings are manufactured, although there were a number of noteworthy discrepancies as described below. After specimens were cut into two or three pieces depending upon the test to be performed, the mid-length thickness was measured with calipers and recorded. The averages of these measurements are shown in Table 2.3. Although the thicknesses of individual layers were not recorded, spot checks of internal and cover layers showed that elastomer layer thicknesses varied considerably. This was especially true of the 6 shim specimens where cover layers were frequently found to be up to 2.54 mm (0.10 inches) greater than requested (6.35 mm (0.25 inches)), due to the difficulty of precisely positioning the steel shims.

According to the current AASHTO tolerances, bearings must be no less than the specified overall thickness but not greater than 6 mm (1/4 inch) over the specified overall thickness. Subtracting the thickness of the steel shims from the overall thickness, the total elastomer thickness in this case must be between 44.5 mm (1.75”) and (50.8 mm (2.0”). A number of the bearings would have failed this specification because they were less than the minimum thickness, but none would have exceeded the maximum thickness. Clearly, Manufacturer B’s second lot targeted a thicker elastomer layer but was technically still within specifications. Bearings with the same design almost always had the same measured elastomer thickness as they most likely were manufactured at the same time. There does not appear to be any inherent difficulty in manufacturing tapered bearings to the same precision as flat ones, nor does the number of reinforcing shims influence the outcome.

Table 2- 3 Average elastomer thickness measurements

Taper	Number of Shims	Manufacturer A mm (in)	Manufacturer B		Manufacturer C mm (in)
			Lot A mm (in)	Lot B mm (in)	
Flat	0	46.7 (1.84)			
	2	45.5 (1.79)			
	3		45.0 (1.77)	46.0 (1.81)	45.0 (1.77)
	6		44.5 (1.75)	46.2 (1.82)	45.0 (1.77)
4% (nom)	3		44.2 (1.74)	46.5 (1.83)	45.2 (1.78)
	6		43.4 (1.71)	46.5 (1.83)	45.0 (1.77)
6% (nom)	3		45.0 (1.77)	47.2 (1.86)	46.6 (1.83)
	6		44.5 (1.75)	46.5 (1.83)	45.2 (1.78)
Mean		46.1(1.82)	44.3 (1.74)	46.4 (1.83)	45.2 (1.78)
Standard Deviation		Too Few Samples	0.589 (0.0232)	0.585 (0.0231)	0.690 (0.0272)

Taper

Bearings with 0, 4.0, and 6.0% nominal tapers were specified from the manufacturers. The first manufacturer provided only flat (0% taper) bearings and these were delivered with to a very close tolerance. The second and third manufacturers however, were requested to provide all three degrees of taper. When the bearings were received, their actual tapers were measured with a digital inclinometer. The results of the measurements are shown in Table 2.4.

Table 2- 4 As delivered bearing tapers

Nominal Taper (%)	Manufacturer B	Manufacturer C
4.0 mean	4.54	4.08
Lot A / Lot B	4.18 / 4.89	
4.0 Standard Deviation	0.376	0.225
6.0 mean	5.68	5.84
6.0 Standard Deviation	0.214	0.150

These measured values were consistent from bearing to bearing with the same design, which would be expected, as they would have been formed in the same molds. The only noticeable discrepancy occurred with Manufacturer B, which was fabricated in two separate lots. Upon discussing the variations with the manufacturers, the reason for the discrepancy between ordered and delivered tapers was apparent. As each bearing must be individually molded, and molds must be machined for a variety of bearing designs, manufacturers standardize their tapered molds in 3-mm (1/8-inch) increments over the length of the bearing. Thus, 229-mm (9-inch) long tapered bearings are manufactured in increments of 229 mm/3.18 mm (0.125"/9") or 1.389% slopes. The tapered bearings produced according to this schedule would be: flat,

1.39%, 2.78%, 4.17%, and 5.56% which accounts for the results of the measurements as shown above. Again, Manufacturer B's second lot showed some discrepancy.

Steel Shims

Steel shim thicknesses were spot checked with calipers. In all cases, they were found to be at the specified thicknesses. The steel shim placement within the bearing however, was not generally this precise. Steel shims were found to be improperly oriented and, occasionally, actually bent (See Figures 2.14 and 2.15). While the bearing bulging pattern would, in some cases, expose the errors, in most circumstances the pattern would likely not show any obvious fault as the inconsistency is in the interior of the bearing. The incidence of improper orientation seemed to occur more frequently in tapered than in flat bearings.

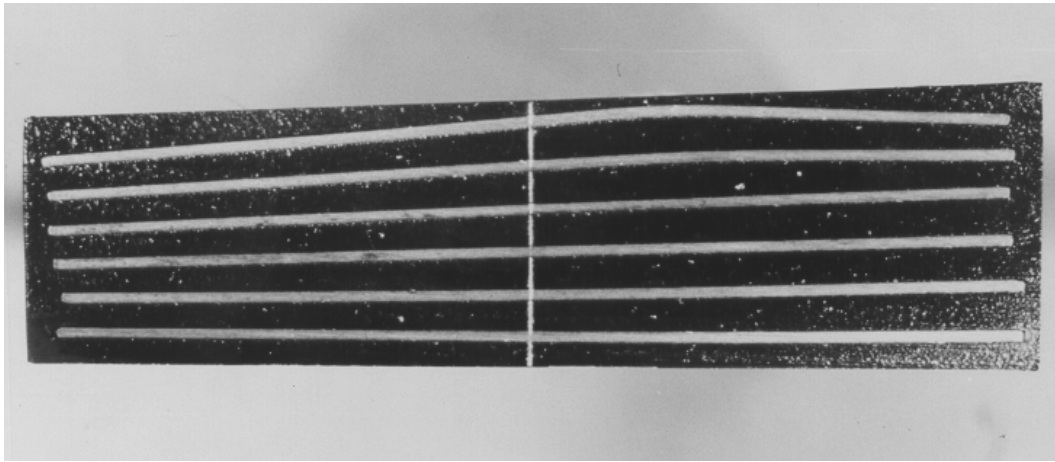


Figure 2- 14 Steel shims bent during manufacturing process

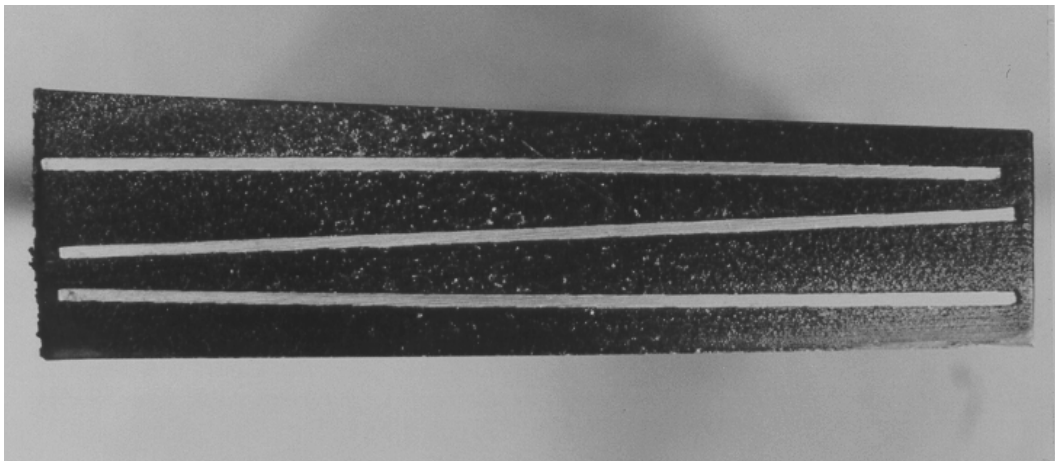


Figure 2- 15 Misoriented steel shims

CHAPTER 3

INVESTIGATION INTO BEARING SLIP

Before conducting any tests to determine slip phenomenon or tapered bearing characteristics and durability, the forces on these bearings, which are quite different than those on flat bearings, must be quantified. Experimentation showed that all bearings experience some horizontal displacement due to vertical load alone when that load is inclined as shown in Figure 3.1. This displacement must be quantified and accounted for in calculations of shear strain to ensure that the overall strain including that caused by thermal effects is kept below the design shear strain limit.

3.1 DEFLECTIONS UNDER VERTICAL LOAD ALONE

Figure 3.1 shows the forces on a bearing under the dead weight of a sloped girder. Although there is a force along the surface of the bearing in contact with the girder which must be accounted for in friction calculations, the forces **parallel** and normal to the bearing's sloped surface yield no net horizontal force. Thus, there is no shear force produced at the bottom bearing surface. Although the bearing is not subject to an external shear force under the dead weight of the girder alone, both field observations and laboratory experimentation show that the bearings experience a horizontal deflection, Δ_s , under dead load alone as illustrated in Figure 3.2.

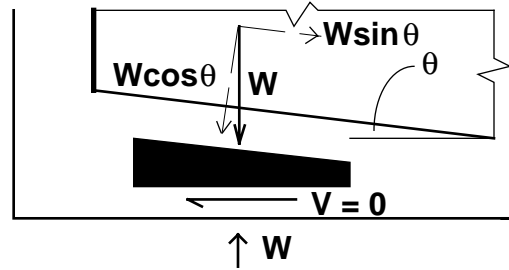


Figure 3-1 Bearing under girder dead weight

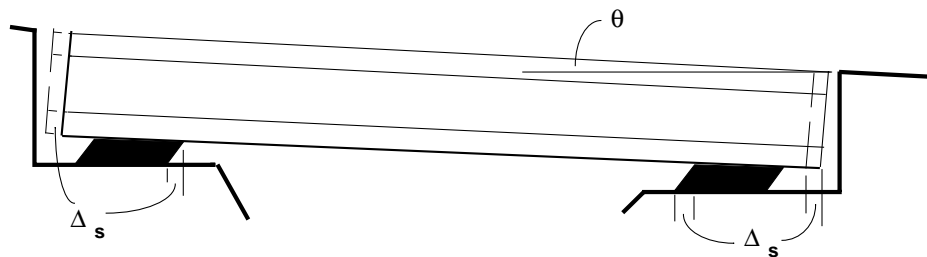
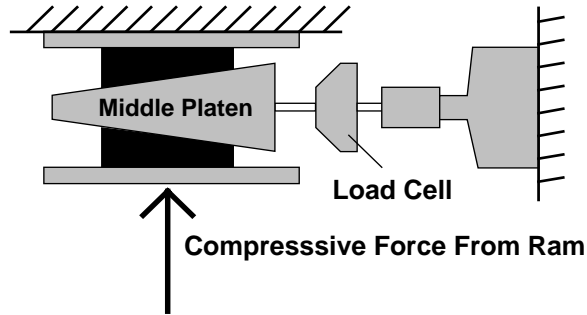


Figure 3-2 Bearings shearing due to girder dead weight

Assuming that the girder is unrestrained against horizontal movement (since typically there is an elastomeric bearing at each end of the girder), the bearings deform in shear under the dead weight and cause the entire girder to translate in the direction of the lower support. If the girder is restrained against horizontal movement, then there will be a shear force in the bearing equivalent to the force required to produce a shear displacement of Δ_s .

The magnitude of the bearing shear deformation is a very important consideration, and must be known to ensure that the displacement of the girder and the shear strain of the elastomer are within acceptable limits. In order to determine the magnitude of the expected shear deformation under dead load, a test program was developed to study the behavior of tapered bearings under pure compression. From the experimentation, the magnitude of the displacements can be estimated.



3.1.1 EXPERIMENTAL TEST PROGRAM

Figure 3-3 Test setup for measuring horizontal forces

Before each shear modulus test, the bearings were positioned in the test machine described in Chapter 2 and the compressive force (P) for that test (311 or 622 kN (70 or 140 kips)) was applied via the dead weight system. The load cells recorded the horizontal force (H) as shown in Figure 3.3. A schedule of the slopes against which the bearings were compressed is given in Table 3.1.

Table 3-1 Schedule of horizontal to compressive force ratio tests

Bearing Taper	Middle Platen Slope		
	1.5 %	3.8%	6.25%
None (Flat)	X		
4% Taper		X	X
6% Taper		X	X

From the tests on the 4% bearings against 6.25% slopes and the 6% bearings against 3.8% slopes, the influence on the horizontal force produced when a tapered bearing was compressed against a surface that did not match the taper of the bearing was determined.

To determine horizontal deflections, another series of tests were performed where tapered bearings (4% and 6%) were compressed in the test machine without the load cell connected. The bearings were free to shear and the magnitude of this shearing was recorded as was the compressive force. Given the total shear displacement, Δ_s , the shear area, A, the elastomer thickness, h_{rt} , and the shear modulus, G, of each specimen, the horizontal force, H, required to cause the recorded displacement could be calculated from the relationship $H = GA\Delta_s/h_{rt}$. The data from both series of tests were compared so that an equivalent horizontal force, H, could be determined which could be used to predict the amount of horizontal deflection in the bearing under vertical load alone.

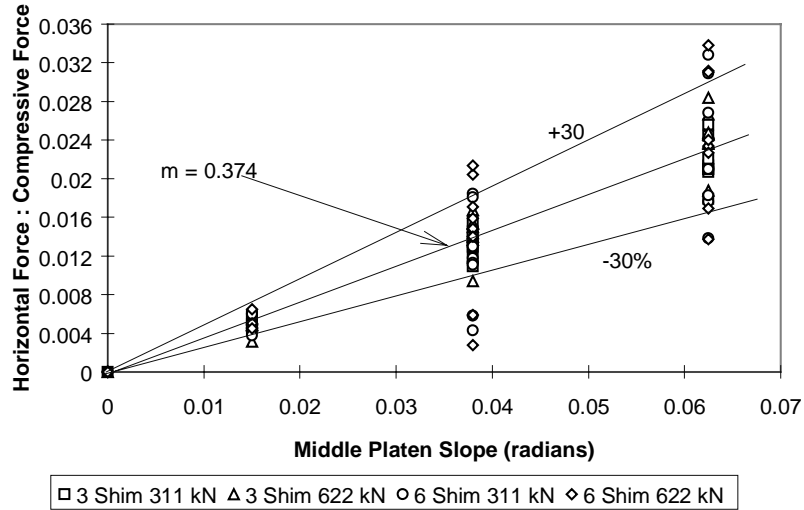


Figure 3- 4 Horizontal to compressive force ratio vs. middle platen slope

3.1.2 TEST RESULTS

Horizontal Forces

Each horizontal force recorded was divided by the applied compressive force and plotted against the slope of the middle platen used during the test. The results are shown in Figure 3.4. (Tests performed on tapered bearings fabricated with shims oriented parallel to one another are intentionally omitted). The data points are sorted by number of reinforcing shims and the compressive force. Results plotted at 1.5% are for flat bearings only; results for tapered bearings are plotted by middle platen slope not by bearing taper. A regression analysis was used to determine the slope of the line through all the points. The value of this slope was calculated at 0.374. Also, lines with slopes corresponding to a slope of $0.374 \pm 30\%$ are shown. Approximately 85% of the data points fall within these bounds. Thus it can be estimated that the ratio of the horizontal to compressive force is 0.374θ , where θ is the slope of the middle platen.

As illustrated by Figure 3.5, the ratio of horizontal to compressive force increases with increasing platen (girder) taper. Table 3.2 compares the ratio of horizontal to compressive force at the two compressive force levels at which data were taken. At each force level, the ratio is within 6% of the average — 0.374θ .

The results presented in Table 3.2 are for all tests combined. Additional comparisons can be made on the basis of a number of parameters. As described earlier, the force ratios in Figure 3.5 are plotted against the slope of the middle platen used during the test rather than against the actual bearing taper. To determine whether there was any influence on the force ratio from mismatching the platens against the bearing taper, the data were sorted according to matched and mismatched tests and is shown in Table 3.3. Table 3.3 also compares the results from tests on all 3 shim and 6 shim specimens.

Clearly, there is almost no influence on the force ratio from the number of reinforcing steel shims. Although there is a small difference between the results of matched versus mismatched tests, there is no trend, and the overall influence of a mismatch between the platen and the bearing taper appears small.

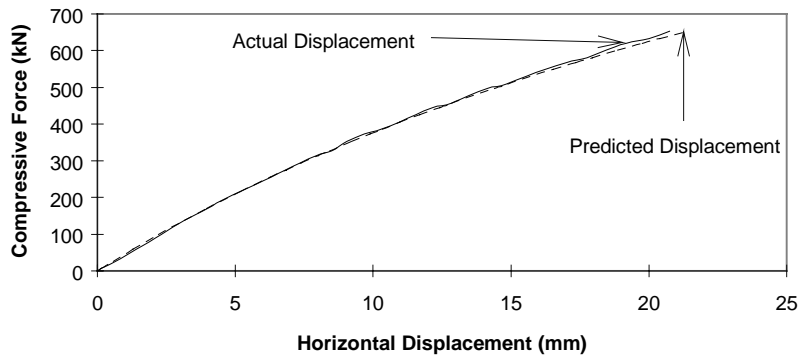


Figure 3- 5 Actual and predicted P-Δ curves for a 57-durometer 3-shim 6% taper bearing

Table 3- 2 Influence of compressive force level on ratio of horizontal to compressive force

Slope of Middle Platen, θ	Horizontal to Compressive Force Ratio $\div \theta$	
	311 kN (70 kips)	622 kN (140 kips)
0%	0	0
1.5%	0.347	0.324
3.8%	0.329	0.371
6.25%	0.356	0.392
Horizontal to Compressive Force Ratio (by regression analysis)	0.353θ	0.395θ

Table 3- 3 Influence of shear modulus on horizontal to compressive force ratio

	Horizontal to Compressive Force Ratio	
	3 Shim Bearings	6 Shim Bearings
Matched Slopes	0.366θ	0.389θ
Mismatched Slopes	0.378θ	0.362θ
All Matched plus Mismatched	0.372θ	0.376θ
Ratio Matched:Mismatched	1.03	0.93

Table 3- 4 Influence of shear modulus on horizontal to compressive force ratio

Actual Shear Modulus MPa (psi)	Ratio of Actual to Specified Shear Modulus		Ratio of Horizontal to Compressive Force	
	Mfr B	Mfr C	Manufacturer B	Manufacturer C
0.602 (87.3)		0.873		0.415 θ
0.603 (87.5)	0.875		0.275 θ	
0.848 (123)		0.615		0.448 θ
0.924 (134)	0.660		0.358 θ	

Thus it may be concluded that the horizontal force produced by the dead weight of the girder is a function of the girder slope rather than the slope of the bearing.

Because two manufacturers provided bearings fabricated to the same specifications, additional comparisons can be made on the basis of the manufacturer and the shear modulus. Table 3.4 shows the horizontal to compressive force ratios that were calculated for each manufacturer’s specimens sorted by actual shear modulus.

Manufacturer C’s bearings produced a higher horizontal force when compressed than did Manufacturer B’s. Although the overall average force ratio is higher for the higher shear modulus material, Manufacturer C’s lower shear modulus specimens produced a higher ratio than did Manufacturer B’s higher shear modulus specimens. There is no obvious explanation for this behavior other than that each manufacturer used a different rubber supplier and that, although the hardness ratings and actual shear moduli were very close, other properties of the material itself may have some influence upon the transmission of forces through the bearing.

Finally, a comparison may be made to observe the overall accuracy of assuming that a force ratio of 0.374 θ can be used to estimate the horizontal force produced when an average bearing is compressed. Table 3.5 compares the average of all recorded horizontal forces to the value predicted by 0.374 θ .

From Table 3.5, it appears that assuming the horizontal force to be equal to 0.374 θ times the girder dead weight yields a reasonable estimate of the force which will actually be produced.

Table 3- 5 Average horizontal force produced by compressive force of 311 kN and 622 kN

Slope of Middle Platen	Horizontal Force Actual ÷ Predicted P = 311 kN (70 kips)	Horizontal Force Actual ÷ Predicted P = 622 kN (140 kips)
1.5%	0.925	0.867
3.8%	0.877	0.994
6.25%	0.950	1.05

Table 3- 6 Ratio of horizontal to compressive force from displacement tests

Slope of Middle Platen	Ratio of Horizontal to Compressive Force	
	P = 311 kN (70 kips)	P = 622 kN (140 kips)
0%	0	0
3.8%	0.455 θ	0.492 θ
6.25%	0.466 θ	0.488 θ

Horizontal Deflections

With the relationship between compressive and horizontal forces now known, it should be a simple matter to determine the shear deformation of a bearing of a given shear modulus, area, and elastomer thickness. From the results of the horizontal deflection tests, the magnitude of the equivalent horizontal force required to cause that deflection was calculated by using the relationship $H = GA\Delta/h_{rt}$, where Δ is the measured horizontal displacement. The ratio of the calculated horizontal force (H) to the applied compressive force (P) was then determined. Table 3.6 gives the ratio of the equivalent horizontal force to compressive force at 311 and 622 kN (70 and 140 kips). In these tests, only tapered specimens were used and no mismatched tests were performed.

These ratios are clearly greater than those presented in Table 3.2 (the calculated slope is 0.471 vs. 0.374) which indicates that the bearings sheared more than they would have been expected to when subjected to a horizontal force of 0.374 θP . Visual observation of the bearings in compression and analyzing the plot of the compressive force-horizontal displacement relationship showed the movement of the middle platen caused the compressive load to become eccentric. As a result a P- Δ effect is introduced due to the bearing's displacement. Reference 25 gives an equation derived by Gent for the critical buckling load for reinforced bearings that are free to translate but not to rotate:

$$P_{cr} = \frac{\phi GA_s}{2} \left\{ \sqrt{1 + \frac{4EIf_r}{GA_s} \left(\frac{\pi}{\phi h_{rt}} \right)^2} - 1 \right\} \quad (3.1)$$

where:

ϕ = total bearing thickness (including steel) divided by total elastomer thickness, h_{rt}

A_s = shear area of the bearing

f_r = ending stiffness coefficient = $1.0 + 0.575 S^2$

E = $3G$

The recorded displacements were assumed to be magnified displacements based upon the critical buckling load for each bearing. From the displacement magnification relationship

$$\Delta_{total} = \frac{\Delta_{initial}}{1 - \frac{P}{P_{cr}}} \quad (3.2)$$

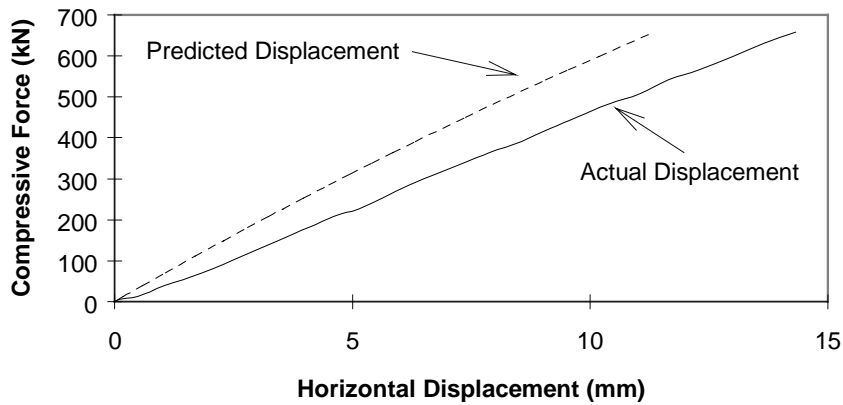
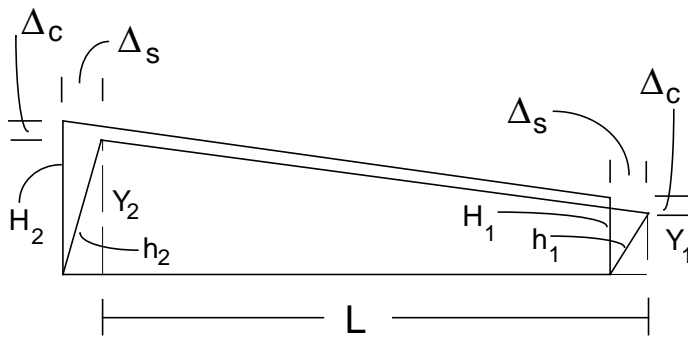


Figure 3-6 Actual and predicted P-D curves for a 70-durometer 6-shim 6% taper bearing



where:

- Δ_c = The total vertical deflection of the bearing due to compression and sidesway (same on both ends of the bearing)
= δ_c , the vertical deflection due to compression + δ_s , the vertical deflection due to sway
- $H_{1,2}$ = Original height of each end of the bearing
- $h_{1,2}$ = Original height of each end of the bearing minus δ_c .
- $Y_{1,2}$ = The original height of each end of the bearing minus δ_c and δ_s .
- Δ_s = The horizontal deflection of the bearing (same on both ends)

Figure 3-7 Geometry of displaced bearing

an initial displacement produced by $H=0.374 \theta P$ magnified by Equation 3.2. The results of all tests sorted by taper, number of steel shims, manufacturer and specified shear modulus are given in Table 3.7. The value given is the average of the ratios of the actual displacement recorded to the total displacement predicted at 311 and 622 kN (70 and 140 kips).

Although the results show much scatter, especially for the 6 shim specimens, the average of all of the tests is 1.005, which appears to indicate that the basic method is correct. Based upon the calculations of the

the values of the initial displacements were calculated and then the equivalent horizontal force required to cause them was calculated as before. Figures 3.5 and 3.6 show typical compressive force - horizontal displacement (P- Δ) curves from tests on 3 and 6 shim bearings compared to the predicted P- Δ relationships based upon $\Delta_{\text{initial}} = 0.374\theta P_{\text{Rt}}/GA$ and Δ_{total} as determined by Equation 3.2.

While the predicted P- Δ curve for the 3 shim bearing is almost exact, the predicted P- Δ relationship for the 6 shim bearing yields approximately a 30% error. In most cases, the predictions for 3 shim bearings were within $\pm 15\%$ of the actual displacements but the predictions for 6 shim bearings were only within approximately $\pm 50\%$. Overall however, the average of all of the tests yields reasonable agreement between recorded displacements and those predicted by

Table 3- 7 Comparison of actual and predicted horizontal displacements

	Specified Shear Modulus	Displacements Actual ÷ Predicted			
		4% Bearings		6% Bearings	
		3 Shim	6 Shim	3 Shim	6 Shim
Manufacturer B	0.7 MPa (100 psi)	0.60	0.25	0.99	0.76
	1.4 MPa (200 psi)	0.90	0.69	1.14	0.83
Manufacturer C	0.7 MPa (100 psi)	1.01	1.47	1.03	1.46
	1.4 MPa (200 psi)	1.17	1.50	0.94	1.32
Average		0.92	0.98	1.03	1.09

Table 3- 8 Ratio of horizontal to compressive force considering P-Δ effect

Slope of Middle Platen	311 kN (70 kips)	622 kN (140 kips)
0%	0	0
3.8%	0.0138	0.0132
6.25%	0.0258	0.0236

horizontal force required to produce the initial displacements, new horizontal to compressive force ratios were determined. The results are given in Table 3.8.

When these points are plotted versus taper, the best fit regression line has a slope of 0.392 which is much closer to the original value of 0.374 based upon the recorded horizontal forces when the bearings were restrained from moving. Because the primary interest is to determine horizontal deflections, and for simplicity of calculations, a horizontal to compressive force ratio of 0.4 θ would appear to be a reasonable factor to use to estimate the initial horizontal deflection of a bearing when compressed under a sloped girder. The total deflection can be determined by magnifying the initial deflection to take into account P-Δ effects.

Influence of Reinforcing Shim Orientation on Horizontal Force and Displacement

During the course of the displacement tests, it was noted that some bearings of similar slope and shear modulus sheared to different magnitudes. Upon closer examination, it was observed that the steel reinforcing shims of some bearings were less perfectly radially spaced than others. The best example of the influence of steel shim orientation on deflection and equivalent horizontal force is given by comparing the behavior of the bearings with radially spaced reinforcing shims to those with reinforcing shims oriented parallel to one another. Table 3.9 gives the recorded horizontal forces and displacements from the tests

Table 3- 9 Influence of steel shim orientation on horizontal force and displacement

	Horizontal Force - kN (kips)		Horizontal Displacement - mm (in)	
	P = 311 kN	P = 622 kN	P = 311 kN	P = 622 kN
Radial Shims	6.81 (1.53)	15.3 (3.43)	7.87 (0.310)	19.2 (0.754)
Parallel Shims	5.07 (1.14)	10.4 (2.33)	4.75 (0.187)	11.4 (0.450)
Ratio Parallel:Radial	0.75	0.68	0.60	0.60
Value Predicted by H=0.4 θ P	7.79 (1.75)	15.6 (3.50)	7.32 (0.288) not magnified	14.6 (0.575) not magnified

performed on the nominal 6% taper, 3 steel shim, 0.7 MPa (100 psi) shear modulus specimens at compressive force levels of 311 and 622 kN (70 and 140 kips).

From the results of these tests, it appears that orienting the reinforcing shims parallel to one another will reduce substantially, but not eliminate the horizontal force and deflection. Subsequent chapters will describe the influence of steel shim orientation upon other behavior such as shear, compressive and rotational stiffness.

3.1.3 DISCUSSION OF HORIZONTAL FORCE AND DEFLECTION TESTS

Although the horizontal displacement of the bearings cannot be explained in terms of external forces acting upon them, an explanation can be offered that the bearings displace due to their dissymmetry. In tapered bearing designs, the steel shims are generally radially spaced creating a system with a greater axial stiffness on the thin end and a lesser axial stiffness on the thick end. If the bearing were free to rotate under the vertical load, the thick end would compress more than the thin end. However, bearings supporting a bridge girder cannot rotate to reach equilibrium but can translate to do so. The magnitude of the horizontal translation is directly proportional to the magnitude of the difference in stiffness between the thin end and the thick end. Figure 3.7 shows the geometric relationships describing the movement.

From Figure 3.7 it is shown that

$$(h_n)^2 = (\Delta_s)^2 + (Y_n)^2 \quad (3.3)$$

where $h_n = H_n - \delta_{cn}$ and $Y_n = H_n - \delta_{cn} - \delta_{sn}$. Substituting into equation 3.3 and rearranging:

$$(\Delta_s)^2 = (H_n - \delta_{cn} - \delta_{sn})^2 - (H_n - \delta_{cn})^2 \quad (3.4)$$

Expanding and simplifying:

$$\Delta_s^2 = \delta_{sn} (2H_n - 2\delta_{cn} - \delta_{sn}) \quad (3.5)$$

The vertical displacements of the two ends of the bearing can be expressed as:

$$\delta_{c1} + \delta_{s1} = \delta_{c2} + \delta_{s2} \quad (3.6)$$

where the additional vertical displacement due to sway added to the original vertical displacements due to compression result in equal vertical displacements on both ends of the bearing, which must be the case. Because the horizontal displacement of both ends of the bearing must be equal, equations in the form of Equation 3.5 can be written for each side of the bearing and set equal to one another yielding:

$$\delta_{s2} (2H_2 - 2\delta_{c2} - \delta_{s2}) = \delta_{s1} (2H_1 - 2\delta_{c1} - \delta_{s1}) \quad (3.7)$$

Using values for H_1 and H_2 and δ_{c1} and δ_{c2} in the ranges measured for bearings used in this study, ($H_2 = 57.2$ mm (2.25 in), $H_1 = 47.8$ mm (1.88 in), $\delta_{c2} = 2.54$ to 2.67 mm (0.100 to 0.105 in), $\delta_{c1} = 2.29$ to 2.41 mm (0.09 to 0.095 in) where δ_{c2} and δ_{c1} are based upon the stiffnesses of the two ends of the bearing), the values for δ_{s1} and δ_{s2} can be determined from Equations 3.6 and 3.7 which can be used in Equation 3.5 to determine a predicted horizontal displacement. In the ranges given above, the horizontal displacements ranged from 8.07 to 11.4 mm (0.318 to 0.447 in) for the lower and greater differences in compressive deflection for the two ends respectively. These predicted values are comparable to those recorded in experiments on bearings free to translate horizontally 2.62 to 10.6 mm (0.103 to 0.416 in). From these calculations, the predicted horizontal displacement increases with increasing relative difference in vertical displacement due to compression of the thin end versus the thick end of the bearing.

Conclusions

Compressing a bearing pad under the dead weight of a girder sloped at an angle θ will cause a tapered bearing to displace in the direction of its thin end and a flat bearing to displace in the direction of its more compressed end. If the girder is unrestrained, as is the normal practice, the magnitude of the horizontal deflection can be estimated by assuming an equivalent horizontal force H approximately equal to $0.4\theta P$, where P is the compressive force, which will result in an initial deflection of Hh_{rt}/GA . The bearing's critical buckling load must be calculated according to Equation 3.1 and the calculated initial deflection must be magnified according to Equation 3.2 to determine the final deflection. Because each bearing is individually fabricated, there are distinct differences from bearing to bearing which cause the magnitude of the displacement to differ greatly even when all design parameters such as shear modulus, taper, and shape factor are the same. Therefore the horizontal deflection can only be estimated within $\pm 30\%$. From the experimentation, the greatest influences upon the magnitude of the horizontal force produced or the horizontal deflection recorded are the orientation of the reinforcing shims and the degree of the slope of the applied compressive load.

Although the majority of the bearings tested in this study were tapered, the results showed very clearly that a flat bearing loaded by a girder on a slope will also displace horizontally. Since the current AASHTO Specification allows the use of flat bearings when the girder is sloped up to 1%, horizontal deflections should be a consideration. From the results of the tests presented in this chapter, it can be predicted that the magnitude of the horizontal displacement will be less if a flat or tapered bearing with steel shims oriented parallel to one another or is used rather than using a tapered bearing with radially spaced shims. Orienting the reinforcing steel shims in a tapered bearing parallel to one another can reduce the horizontal deflection by 30-40% as shown in Table 3.9. Although for this shim orientation, there may be additional horizontal deflection due to second order effects, the total horizontal deflection is less than that predicted by $H=0.4\theta P$.

Therefore, the deflection predicted by $H=0.4\theta P$ can be regarded as a maximum to be expected and there is no utility in calculating a critical buckling load and magnifying the expected deflection if parallel shims are employed.

A reasonable assumption as to the horizontal deflection expected can also be made by the method described earlier in this section. As long as the dimensions of the bearing's cross section and the reinforcing scheme is known, an estimate can be made of the vertical deflection due to compression and the relationships given in Equations 3.5, 3.6 and 3.7 used to calculate a predicted horizontal displacement for the bearing.

3.2 BEARING SLIP INVESTIGATION

To investigate the bearing "walking out" phenomenon, a test program was developed with the purpose of characterizing the friction coefficient of rubber on a number of surfaces and duplicating in the laboratory the daily thermal expansion and contraction of the concrete bridge girder at various amplitudes. Additionally, several field studies of bridges throughout the state of Texas were conducted to record the actual magnitudes of the thermal cycles as well their effect upon the movement of the associated bridge bearings. Two of those studies are described below. Slip tests were performed on the bearings that were removed from service on these two bridges.

3.2.1 FIELD STUDIES

As part of the research, bridges were instrumented and observed over a period of three years. Gages as shown in Figures 3.8 and 3.9 were attached to measure the maximum movement of the girder end where the bearings in question were located. Reference marks as shown in Figure 3.10 were established on the bottom of the girders to measure actual bearing movement, which was determined by taking a tape measure distance from the reference mark to the edge of the bearing.

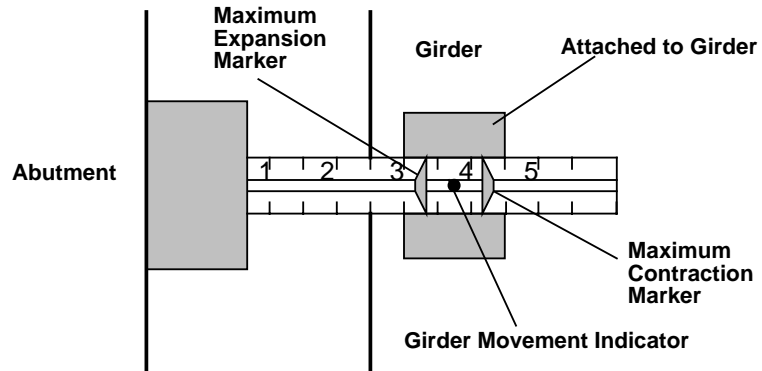


Figure 3- 8 Sliding gage for measurement of girder movement



Figure 3- 9 Girder expansion/contraction measurement gage

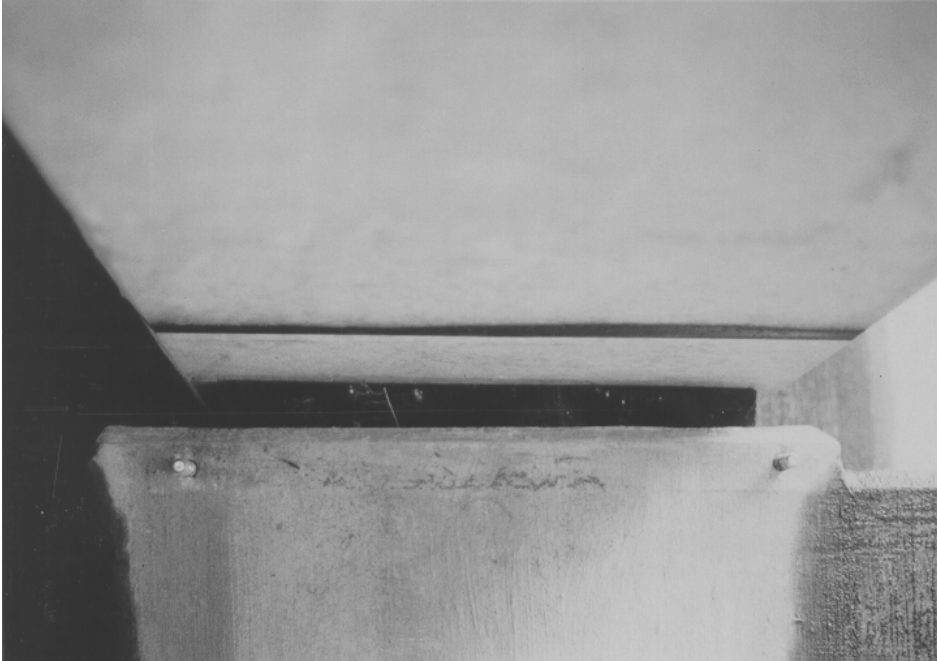


Figure 3- 10 Reference marks under girder

Slaughter Creek Bridge, Austin

The Slaughter Creek Bridge is a 109.7-m (360-ft) bridge that carries the west (southbound) frontage road for IH-35 over Slaughter Creek in south Austin. The bridge is divided into three approximately 36.6-m (120-ft) spans and each end span is comprised of six prestressed concrete girders approximately 1.22 m (4 ft) in depth. The deck is continuous over the three spans. Each girder has a reaction of approximately 400 kN (90 kips). Originally, this bridge was constructed with new, nominal 70 durometer (68 durometer measured) natural rubber bearings pads which were installed as normally done under the girders. The bearings were 228 mm x 559 mm x 44.5 mm (9"x22"x1.75") with two steel shims of 3.18 mm (0.125 in) each yielding a 38.1-mm (1.50-in) elastomer thickness. Within a few months, the bearings had "walked out" significantly at the north abutment. When slipping was discovered, a restraining device as shown in Figure 3.11 was installed around these bearings to preclude walking out.

The six bearings on the south abutment were left unrestrained so that they could be studied over a period of three years to describe their movement due to thermal cycle of the bridge. The expansion/contraction of the girders was measured to be between 6.35 mm (0.25 in) and 12.7 mm (0.50 in) depending upon the time of year. As part of this research project, the south end of the bridge was lifted with hydraulic jacks as shown in Figure 3.12, the bearings were reset at their original locations and their movement charted over a period of six months. In October 1992, the bearings were reset again, and their movement again charted. In November 1992, the original rubber bearings were removed from the bridge and replaced with neoprene bearings of the same length and width but with an overall thickness of 50.8 mm (2.0 in) and four 3.18-mm (0.125-in) steel shims for a total elastomer thickness of 38.1 mm (1.50 in) as before. These bearings seemed to perform as required until June 1993 at which time they also were observed to begin walking out. The movement of these bearings was charted for almost one year until April 1994 (See Figure 3.14) when the bridge was lifted for a final time, the bearings were removed (See Figure 3.12), the bearings, bearing



Figure 3- 11 Restraining devices to prevent bearing movement

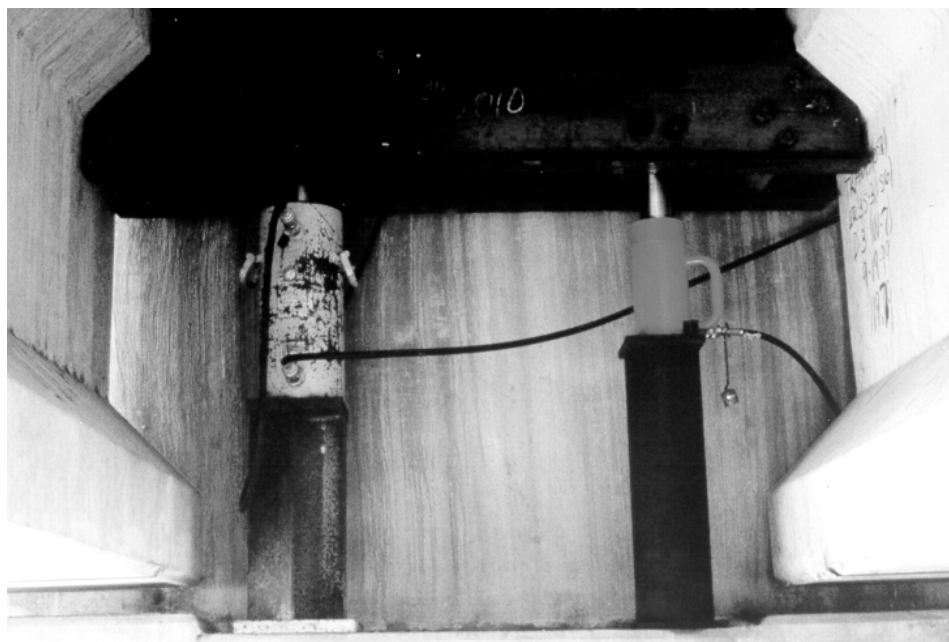


Figure 3- 12 Bridge lifting system



Figure 3- 13 Steam cleaning the girders and bearing seats with degreasing agent

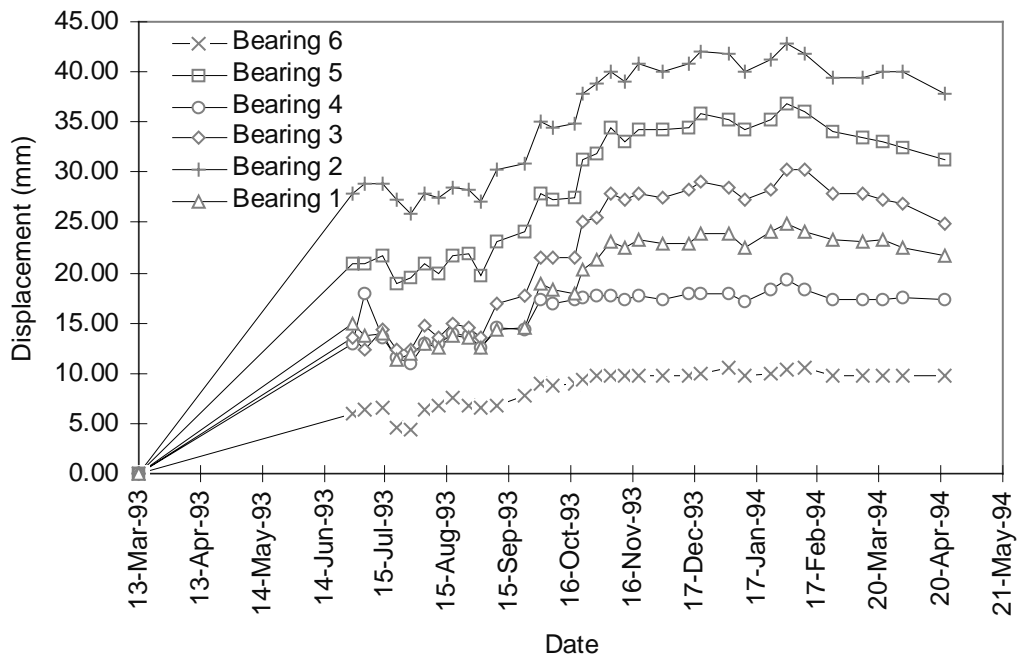


Figure 3- 14 Movement of neoprene bearing pads from June 1993 to April 1994

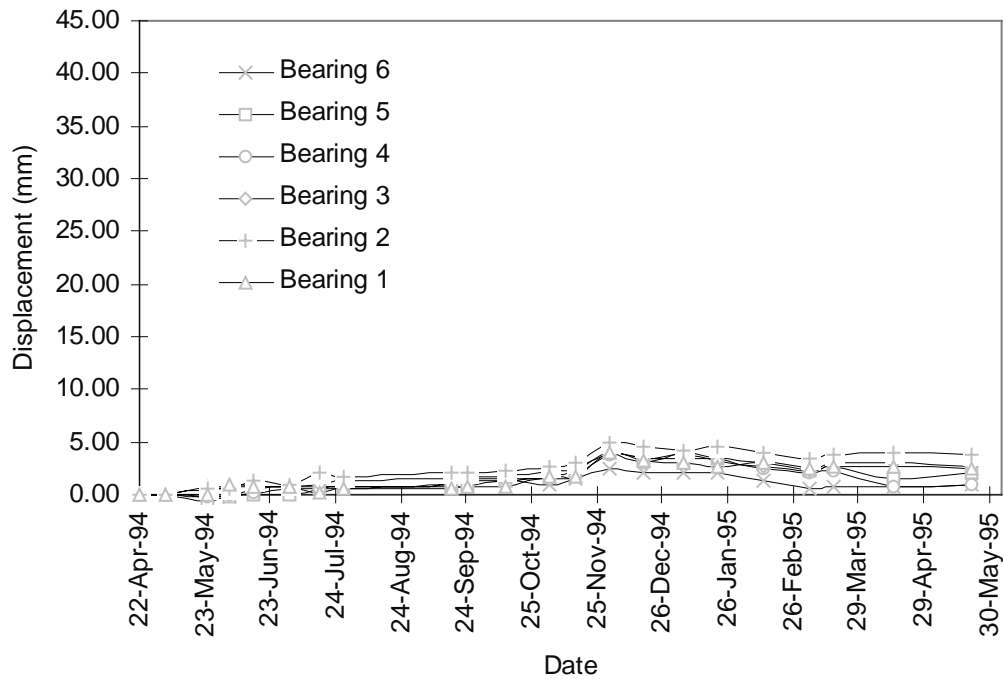


Figure 3- 15 Movement of neoprene bearing pads since April 1994

seats, and the girders were cleaned of all residue (See Figure 3.13), and the bearings were reset. No significant movement has been noted since May 1994. (See Figure 3.15)

Valley Ridge Bridge, Dallas

In addition to charting the bearing movement at the Slaughter Creek Bridge in Austin, the Valley Ridge Bridge over IH-35 in Dallas was also monitored for a period of three years albeit not as closely as was the Austin bridge. This investigation was nonetheless enlightening as only half of the original natural rubber bearings that walked out (See Figure 1.9) were replaced with neoprene pads. As part of the replacement procedure, the girders and bearing seats where the neoprene pads were installed were cleaned but those left with natural rubber pads were not. The natural rubber pads were, however, reset when the neoprene pads were installed. Over the course of the charting period, the natural rubber pads were noted to slip as significantly as before, but the neoprene pads maintained their original locations and simply sheared as intended. This observation is significant in that it shows that the bearing walking out phenomenon should be regarded as a function of the bearing itself rather than of the bridge.

3.2.2 LABORATORY INVESTIGATION

Wax Additive

As stated in section 1.3.3, natural rubber is susceptible to attack from atmospheric ozone. Several ingredients are added to the raw rubber during the compounding process to preclude this degradation and to ensure that the vulcanate can pass the ozone exposure test required by the ASTM specification. One of those ingredients is antiozonant wax of any number of variants. This wax migrates to the surface of the rubber part and blocks the penetration of ozone into the exposed faces of the material. Unfortunately, in

the case of natural rubber bearing pads, the effect of this wax migration is to coat the entire bearing surface with a viscous (liquid exhibiting flow under shear stress) material. While it was reasonably clear that this wax could be the cause of the walking out phenomenon, a laboratory investigation to quantify the effect of the waxy bearing surface was undertaken and is described below. Pursuant to this goal, natural rubber bearings, which had been removed from the Slaughter Creek and Valley Ridge bridges, were tested on concrete and Plexiglas surfaces to determine the circumstances required to initiate the walking out phenomenon. The purpose of the Plexiglas surfaces was to provide a medium for the rapid deposit and accumulation of the wax that had coated the bearing surfaces.

Slip Tests on Slaughter Creek Natural Rubber Bearings

The bearings that are described in Section 3.1.1 were tested against Plexiglas and then concrete surfaces. During tests on Plexiglas surfaces, the thermal cycle controller was set to subject the bearings to a small shear strain then to gradually increase the shear strain until the bearing showed a tendency to walk out or accumulate slip in one direction. Once this occurred the magnitude of the shear cycle was decreased to just below the determined threshold and gradually brought back up to the same magnitude that resulted in uncontrolled slip to determine the repeatability of the phenomenon. The test was performed at 2.76 and 5.17 MPa (400 and 750 psi) compressive stress to observe the influence of compressive stress on slip. The horizontal force required to initiate uncontrolled slipping was divided by the compressive force used during the test to determine a friction coefficient ($\mu = H/N$). The Optron, described in Chapter 2, was used to track the displacement of a target on the bottom bearing in the apparatus. The results of the tests shown in Table 3.10, indicate that the wax build up on the surface of the bearings has a clear effect upon the friction coefficient of the bearing against the Plexiglas. Additionally, the results are consistent with published research (28) on the friction properties of elastomers and results from direct friction tests in this study (See section 3.2.3) which show that as the compressive stress increase, the friction coefficient decreases. From the load-displacement curves and the plot of bearing movement (Optron output) versus middle platen displacement, the phenomenon can be shown to occur very abruptly as soon as the shear strain in the bearing causes the shear force to exceed the friction force.

Table 3- 10 Friction coefficients from slip tests

σ_c MPa (psi)	Plexiglas Platen Surface		Concrete Surface Clean Bearing
	Bearing With Wax	Clean Bearing	
2.76 (400)	0.104	0.132	0.297
5.17 (750)	0.054	0.079	0.201

Explanation of Slip Test Results

Figure 3.16 shows the load-displacement curve (bottom) and Optron output versus platen displacement (top) from the start of the test. The bearings were subjected simultaneously to a 2.76 MPa (400 psi) compressive stress and a shear strain cycle of 18.6% in either direction. Although the Optron plot shows a target movement from the start of the test, the bearing is not actually slipping until much later. What the Optron is detecting at this point is the cover layer of elastomer shearing, not rigid body motion. This shearing is observed in all Optron plots even when the bearing shows no sign of slipping during the cycle. (See Figure 3.17.) The Optron plot shows that the bearings actually began to slip when they sheared approximately 4 mm (0.157 in), a shear strain 10.5%. The load-displacement relationship shows that at

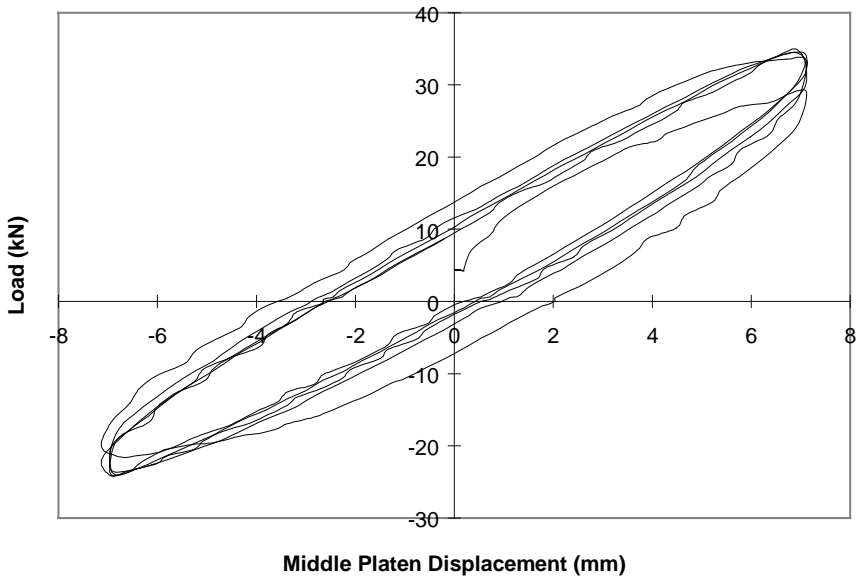
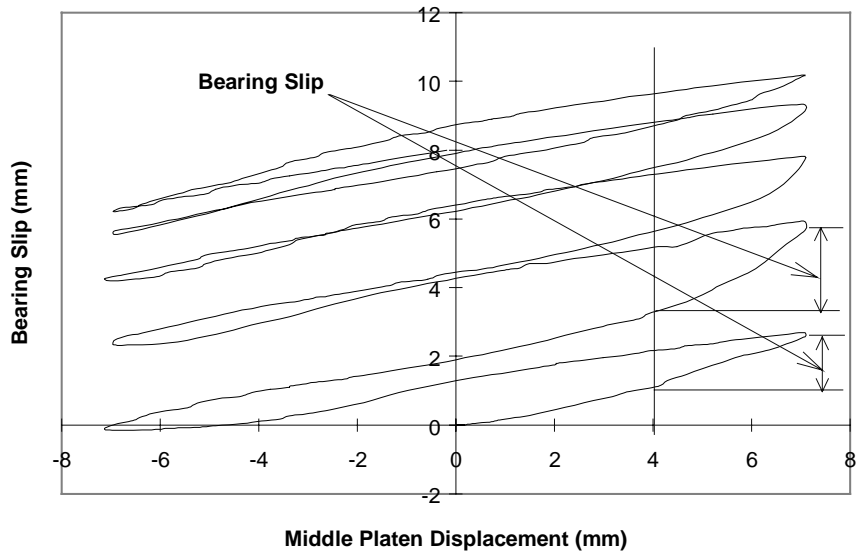


Figure 3- 16 Initial load-displacement curve and optron plot

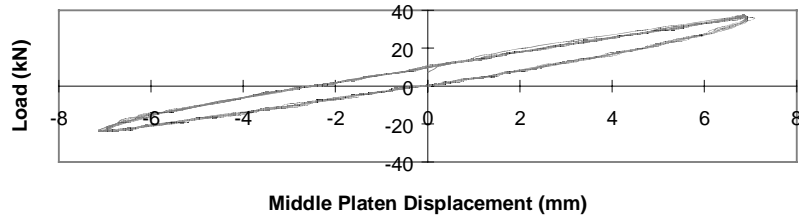
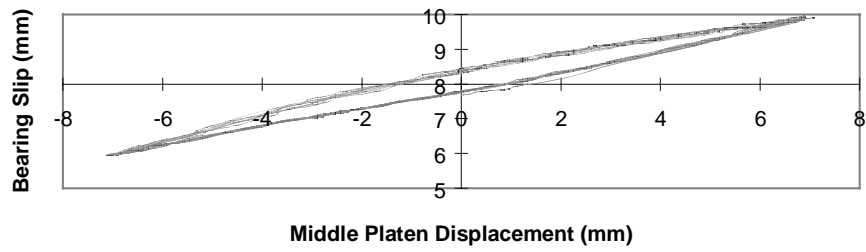


Figure 3-17 Load-displacement curve with bearing stationary

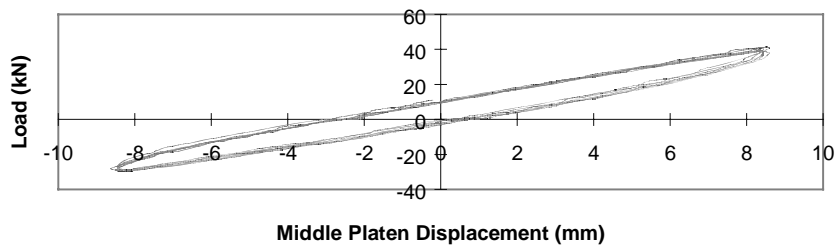
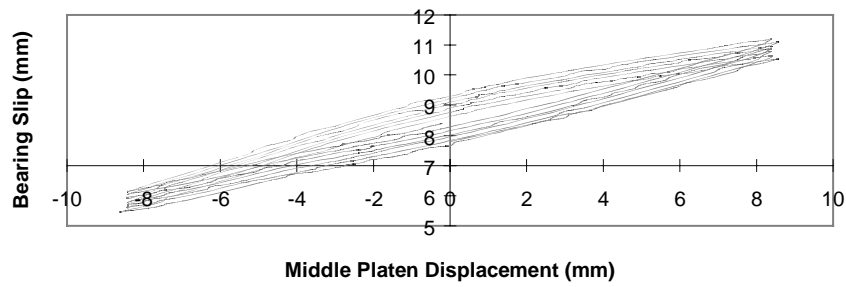


Figure 3-18 Bearing walking out slowly

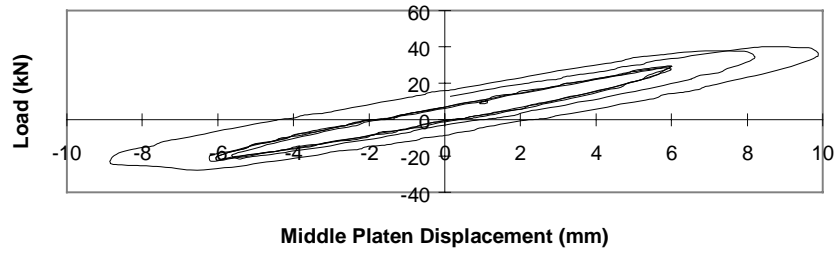
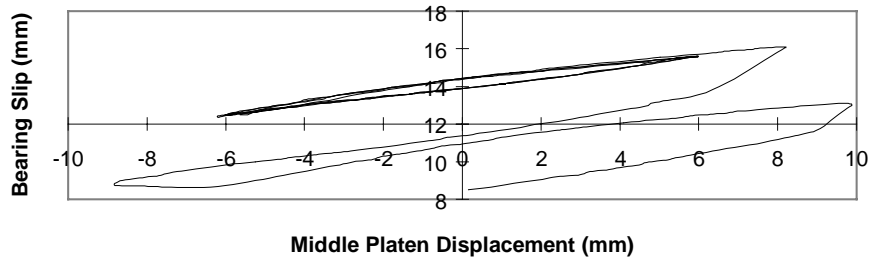


Figure 3-19 Bearing walking out significantly

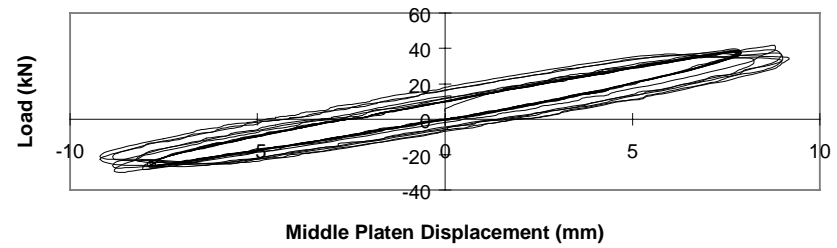
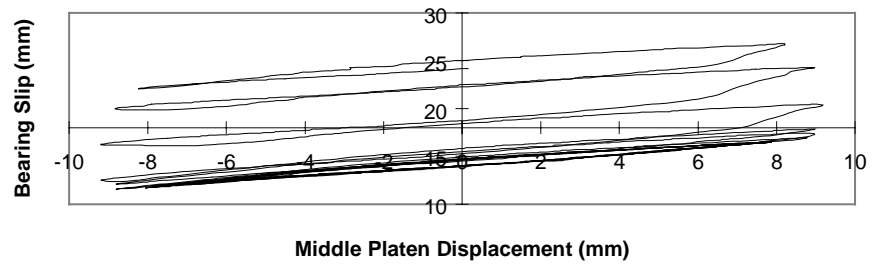


Figure 3-20 Final load-displacement and slip curves

that same point (4 mm) the curve flattens out signifying that the middle platen is displacing without resulting in any additional load to the system. Therefore, the bearing is no longer undergoing additional shear strain as the platen moves. The Optron plot shows that the edge of the target, which is located at the centerline of the bearing length, has moved approximately 2 mm after each cycle from its position at the start of the cycle.

After five cycles at 18.6% strain, the bearing reached an equilibrium position and remained in place for a number of additional cycles. (See Figure 3.17.) At this point, the thermal cycle was increased to 23.5% strain and the bearings began a steady slip of 0.1 mm per cycle as shown in Figure 3.18. The thermal cycle was then increased to 26.0% strain and the bearings began uncontrolled slipping as shown in Figure 3.19. The thermal cycle was decreased back to 23.5% strain, but slip continued. Finally, the strain was reduced to 15.6% and the bearings stabilized once more, also shown in Figure 3.19. A number of cycles were run at 15.6%, 18.2%, and 20.8% strain with no net slip occurring. The strain was increased to 24.0% as shown in Figure 3.20 and uncontrolled slip commenced again. The test was terminated with the conclusion that any strain greater than 20.8% would result in the bearings slowly walking out. At greater strains the phenomenon would occur much more dramatically. The same tests were repeated at 5.24 MPa (750 psi) where the bearings were found to begin walking out at strains over 13.0%. The Plexiglas platens and the same bearings were thoroughly cleaned of wax and the test repeated. During these tests, the walking out threshold strain was 31.3% and 26.0% at 2.76 MPa (400 psi) and 5.17 MPa (750 psi) respectively. Finally, the same clean bearings were tested against cleaned, smooth concrete surfaces. In these tests, walking out did not occur. Strains of 75% and 65% were reached at 2.76 MPa (400 psi) and 5.17 MPa (750 psi) respectively before the load displacement curves showed any signs of nonlinearity.

Slip Tests on Valley Ridge Natural Rubber Bearings

In addition to the Slaughter Creek rectangular bearing tests described above, circular natural rubber bearings from the Valley Ridge Bridge in Dallas were tested in the apparatus against smooth concrete surfaces at a compressive pressure of 3.12 MPa (446 psi). The bearings were nominal 60 durometer hardness (68 durometer measured), 384 mm (15.1 in) in diameter and 45.0 mm (1.77 in) in overall thickness (38.1 mm (1.50 in) of rubber and two 3.18-mm (0.125-in) steel shims) with a 2.6% taper. The surface of the bearings was obviously saturated with wax when delivered to the laboratory. The load-displacement curve started to show slipping had begun at a strain of 25.5% which translated to a friction coefficient of 0.107 comparing very closely to that of the waxy Slaughter Creek bearings at similar compressive stress on Plexiglas. Walking out occurred readily at a strain of 40% but the bearing stabilized with some slipping back and forth but no walking out at a strain of 33.9%. After five cycles at 40% strain, the bearings had walked out 8.54 mm (0.336 in).

Mechanics of the “Walking Out” Phenomenon

From the load-displacement and bearing slip plots, the mechanics of the walking out phenomenon for tapered bearings can be deduced. As explained earlier, the dead weight of the girder causes the bearing to shear somewhat as shown in Figure 3.21.

As the girder (in the case of these tests, the middle platen) expands, a horizontal force, H, is produced as a result of the bearing shearing as shown in Figure 3.22.

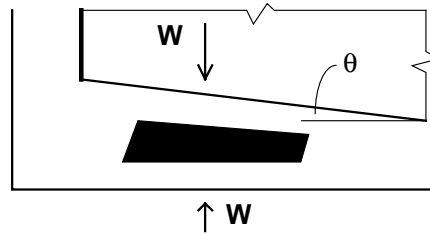


Figure 3- 21 Bearing under girder dead weight alone

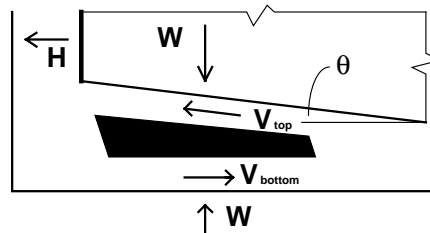


Figure 3- 22 Forces on bearing during girder expansion

The force on the bottom of the bearing, V_{bottom} , is equal to H .

$$V_{\text{bottom}} = H \quad (3.8)$$

and the ratio of the horizontal to normal force on the bottom of the bearing is as shown below:

$$\frac{H}{W} \quad (3.9)$$

The force on the top of the bearing, V_{top} , is as shown below:

$$V_{\text{top}} = H \cos \theta - W \sin \theta \quad (3.10)$$

Which, for small values of θ , reduces to:

$$V_{\text{top}} = H - W\theta \quad (3.11)$$

The force normal to the top of the bearing, N , is also a function of the shear force, H , and the girder weight, W :

$$N = W \cos \theta + H \sin \theta \quad (3.12)$$

Which reduces to:

$$N = W + H\theta \quad (3.13)$$

For the typical girder slopes and horizontal forces under consideration, the magnitude of $H\theta$ is much less than the magnitude of W making the ratio of horizontal to normal force on the top of the bearing as follows:

$$\frac{H - W\theta}{W} \quad (3.14)$$

Therefore it is clear that the ratio of the horizontal to normal forces on the bottom of the bearing will exceed that required to overcome static friction before the forces on the bearing top will. The load-displacement plot becomes flat at this point and the Optron shows the bottom face of the bearing slipping along the bottom platen. When the girder contracts however, the forces are quite different. See Figure 3.23.

As the girder contracts, the same horizontal force, H , is again produced as a result of the bearing shearing. The force on the bottom of the bearing, V_{bottom} , is again equal to H but now acts in the opposite direction as before, and the ratio of horizontal to normal force is as shown:

$$\frac{H}{W} \quad (3.15)$$

The force on the top of the bearing has also changed and is as shown below:

$$V_{\text{top}} = H \cos \theta + W \sin \theta \quad (3.16)$$

Which reduces to:

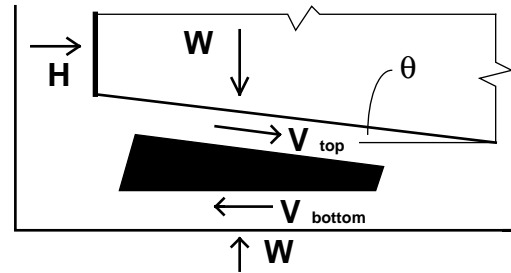


Figure 3- 23 Forces on bearing during girder contraction

$$V_{\text{top}} = H + W\theta \quad (3.17)$$

The force normal to the top of the bearing, N , is now:

$$N = W \cos \theta - H \sin \theta \quad (3.18)$$

Which reduces to:

$$N = W - H\theta \quad (3.19)$$

Once again, $H\theta$ is very small compared to W making the ratio of horizontal to normal force on the top of the bearing as follows:

$$\frac{H + W\theta}{W} \quad (3.20)$$

In this case, however, it is clear that the ratio of the horizontal to normal forces on the top of the bearing will exceed that required to overcome static friction before the forces on the bottom of the bearing will. The load-displacement plot again becomes flat and so does the Optron plot, signifying that the bottom of the bearing is stationary and that the middle platen (girder) is slipping over the top of the bearing. After repeating this cycle numerous times, the bearing will “walk out” from its original position under the girder.

3.2.3 DIRECT FRICTION TESTS

Because of the difficulty in ascertaining the exact friction coefficient of clean bearings against concrete surfaces, a series of direct friction tests was performed using the shear test machine. Two 229-mm (9-inch) by 355-mm (14-inch) natural rubber bearings of 68 durometer, 44.5-mm (1.75-inch) elastomer thickness with two 3.18-mm (0.125-inch) steel shims were bonded to the top and bottom platen with epoxy cement. A compressive force was applied and the middle platen was displaced at a constant speed of 1.6 mm (0.063 inches) per minute until the applied shear force exceeded the friction force of the bearings against various surfaces. The coefficient of friction for each test was determined by dividing the maximum horizontal force recorded by the compressive force for that test ($\mu = H_{\text{max}}/N$). Tests were conducted at compressive stresses of 3.79 and 5.86 MPa (550 and 850 psi). Results of the tests are presented in Table 3.11.

The friction coefficient for rubber against rough concrete is listed as a minimum as the bearings were beginning to debond from the epoxy and no slipping had yet occurred. The decrease in the friction coefficient of rubber against mill scale steel was large because much of the mill scale was worn off during the friction test at 3.79 MPa (550 psi). In all cases, although the friction coefficient was lower at the higher compressive stress level, the magnitude of the horizontal force required to initiate slip was greater. Load displacement curves are shown in Figure 3.24.

3.2.4 CONCLUSIONS FROM SLIP TESTS

From years of field observations conducted as part of this study as well as the laboratory investigations described above, several conclusions can be formed as to the causes of bearing slip and the sufficiency of anchorage by friction alone.

Table 3- 11 Coefficients of friction from direct friction tests

σ_c MPa (psi)	Concrete Finish		Steel	
	Glossy	Rough	Sanded Smooth	Mill Scale
3.79 (550)	0.297	0.474 (min)	0.339	0.415
5.86 (850)	0.229	NA	0.288	0.308

Wax Additive

The wax additive used by manufacturers in an attempt to ensure that natural rubber can meet the ASTM ozone resistance specification causes a viscous (liquid exhibiting flow under shear stress) coating to accumulate on the surface of the bearings, which significantly lowers their coefficient of friction against the girder and bearing seat. In the absence of this coating, the same bearings behave as designed and exhibit no tendency to slip under expected service conditions. In fact, bearings made from any elastomer can exhibit the same behavior if they are compounded with antiozonant waxes. One manufacturer contacted during this study stated that it is the practice of some fabricators to add antiozonant waxes to neoprene compounds despite their inherent ozone resistance. If neoprene is specified to preclude the slipping problem, it must be made clear to the manufacturer that antiozonant wax shall not be used.

“Walking out” Phenomenon

There is nothing mysterious about this phenomenon and it has nothing to do with natural rubber itself. It occurs when the horizontal force on the bearing exceeds the coefficient of friction between the bearing and the surfaces against which it is in contact. There is a threshold strain below which the phenomenon does not occur which is the reason why bearings can be observed to behave perfectly for a number of months but then dramatically slip several inches in just a few days. The reason why the bearing actually walks out is a due to the girder slope and the extremely waxy bearing surface. Without the wax, walking out does not happen. This is also shown through analytical studies performed by Hamzeh (10), which included finite element modeling of bearing movements considering viscosity. That study concluded that walking out would not occur under normal circumstances (without wax). There is also no reason to conclude that this phenomenon must be peculiar to tapered bearings. From the mechanics of the process, it is shown that as long as the girder is sloped (by current specifications, flat bearings can be employed when the bridge is sloped up to 0.01 radians), the forces can develop such that a flat pad with wax coated surfaces would walk out.

Anchorage by Friction

A conservative friction coefficient to use for all surfaces is 0.2. This has been shown not only in this study but in numerous others as referenced in Chapter 1. From the tests reported in this study, glossy concrete surfaces are apt to come close to this limit and therefore must be avoided. As long as the designer checks that the expected horizontal forces are less than 20% of the girder dead load, sufficient anchorage by friction will be provided to preclude bearings from slipping under normal conditions. Roughened concrete surfaces as normally provided for bearing seats will perform exceptionally well.

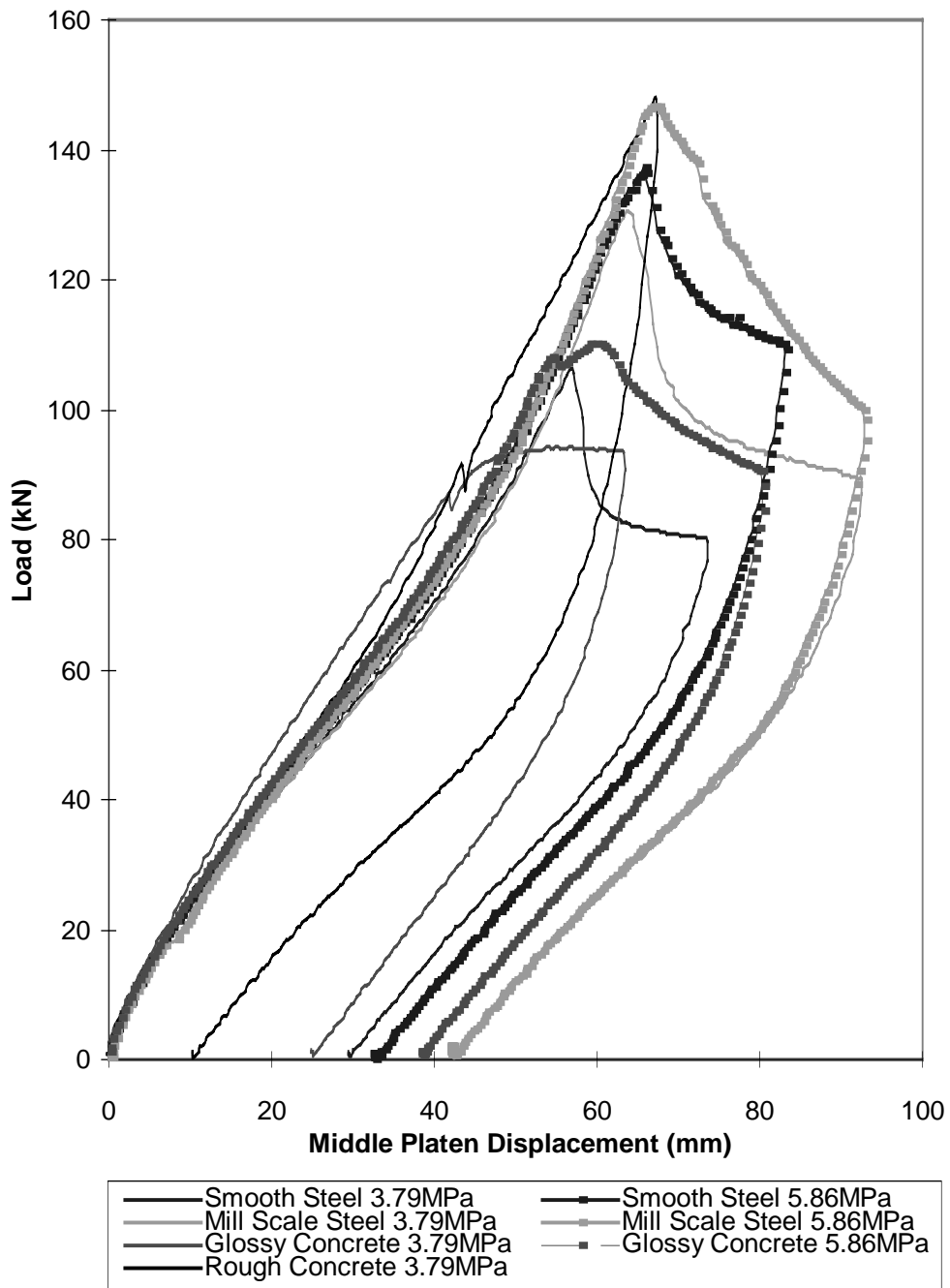


Figure 3- 24 Load displacement curves from direct friction tests

CHAPTER 4

BEARING STIFFNESS TESTS

The purpose of these tests was to determine the shear, compression and rotational stiffnesses of the various designs and to evaluate the relative merits of those designs based upon test results. Additionally, comparisons are made to theoretical stiffness calculations.

4.1 SHEAR STIFFNESS/MODULUS TESTS

Over 100 shear stiffness tests were performed on the specimens ordered for this study using the apparatus described in Chapter 2. Each bearing design was tested at nominal compressive stresses of 3.85 MPa (550 psi) and 7.69 MPa (1100 psi) with the apparatus configured to match the bearing taper as precisely as possible and also under intentionally mismatched slope conditions to simulate non-uniform loading. The actual tapers of the aluminum plates described in section 2.1.2 were 3.8% and 6.25% versus the average tapers of the specimens, which were 4.17% and 5.5%. The reason for this discrepancy was that one set of plates (3.8%) was already on hand from an earlier series of tests and approximated the requested taper of 4.17% closely enough and the other set of plates (6.25%) was machined based upon the taper requested from the manufacturers - 6.25%. The upper and lower platens of the test machine were parallel to within a 0.25% slope ensuring that, for matched slope tests, there would never be more than a 1% mismatch. The bottom and top platen bearing contact surfaces were wood trowel finished concrete to simulate the bearing seat and the middle platen contact surfaces were steel trowel finished concrete to simulate the girder bottom. In both cases, any surface paste that would result in a “glossy” finish was removed after curing. Because the bearings were clearly delivered with wax on their surfaces, each specimen was thoroughly degreased with a steam cleaner before being set in the test frame. Even though this was done, some residue accumulated on the concrete platens as shown in Figure 4.1. Although this accumulation was not actually chemically tested, water would bead up on the surface unless the substance was washed off. Therefore, after every four tests on the concrete surfaces, each platen was removed from the apparatus and thoroughly degreased with a steam cleaner and chemical degreasing agents as shown in Figure 4.2.

4.1.1 TEST PROGRAM

In the matched slope tests, the shear modulus of the bearings was determined under conditions that were as ideal as possible so that the true modulus of the material delivered by the manufactures could be compared to the requested modulus. The test apparatus was configured so that the bearing tapers were matched within 1%. The bearing pairs were centered over the middle of the compressive ram piston and the required compressive force was applied with the middle platen disconnected from the horizontal load cells. The middle platen and load cells were then reconnected, the compressive force removed and then reapplied so that the load cells could record the horizontal load applied to the bearings as a result of the compressive force (as described in Chapter 3). The test apparatus was set to strain the bearings through 50% shear or 22.2 mm (0.875 inches) in approximately 14 minutes, a rate of 1.6 mm (0.0633 inches) per minute. At the point of 50% strain, the timer reversed the motor and the bearings were sheared to 50% strain in the other direction. The Optron, described in Chapter 2, was also used for each test to evaluate the slip tendency of the specimen. After subjecting the bearings to four cycles at 50% strain, the amplitude of the cycles was increased to 100% strain or 44.5 mm (1.75 inches) for two cycles. The slope of the load displacement curve on the fourth 50% strain cycle from the zero middle platen displacement point to the 50% strain point was used to determine the shear stiffness. The displacement of a bearing centerline reference mark with respect to a reference mark on the platen was recorded at 50% and 100% strain in either direction.

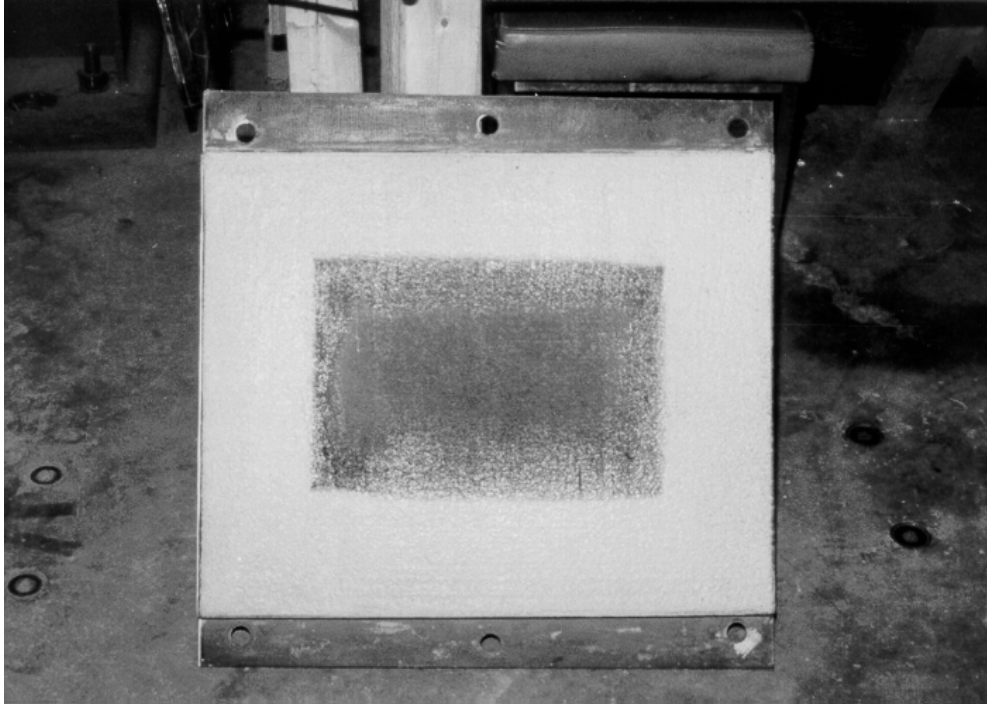


Figure 4- 1 Concrete platens with surface accumulation



Figure 4- 2 Cleaning of concrete platens

Additionally, during a second set of tests on the same set of bearings, the specimens were intentionally “mismatched” with the platens to obtain a 1.5 to 2.0% mismatch. In tests on flat bearings, a specially machined aluminum shim with a slope of 1.5% was employed to simulate non-uniform loading on a standard flat specimen. Nominal 6% slope bearings were tested against 3.8% slope platens and the nominal 4% bearings were tested against the 6.25% slope platens. The Optron was used in each test to determine bearing slip, if any. The shear stiffness was determined in the same manner as described above, as was the displacement of the reference marks on the bearing with regard to the reference marks on the platens.

4.1.2 RESULTS OF SHEAR STIFFNESS/MODULUS TESTS

4.1.2.1 Matched Slope Tests

A typical horizontal load-displacement relationship for a 57 durometer, flat, 6 steel shim bearing at 50% strain, under 3.85 MPa (550 psi) is shown in Figure 4.3.

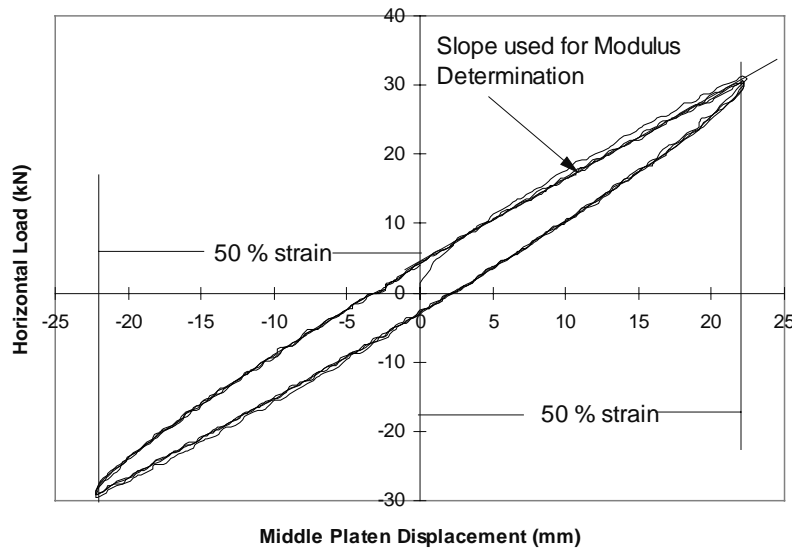


Figure 4- 3 Shear load-displacement curve for a flat bearing

The slope of the load-displacement relationship calculated between zero and +50% strain is 1.174 kN/mm (6.7 kips/in) and the shear modulus based on a 44.5-mm (1.75-inch) elastomer thickness and a 0.0814m² (126 in²) area is calculated at 0.652 MPa (93.21 psi) by using Equation 4.1:

$$G = \frac{Hh_{rt}}{A\Delta_s} \tag{4.1}$$

The same calculation made for zero strain to -50% strain yields a stiffness of 1.170 kN/mm (6.68 kips/in) and a shear modulus of 0.639 MPa(92.8 psi) which shows good agreement. When the shear strain is increased to 100% as shown in Figure 4.4, the stiffness calculation shows a decrease which is not due to slipping (note the linearity) but is a well-documented phenomenon of elastomer properties, lower shear modulus at greater strains (13). (The last cycle at 50% strain is also shown in Figure 4.4 so that a comparison may be made). From zero to

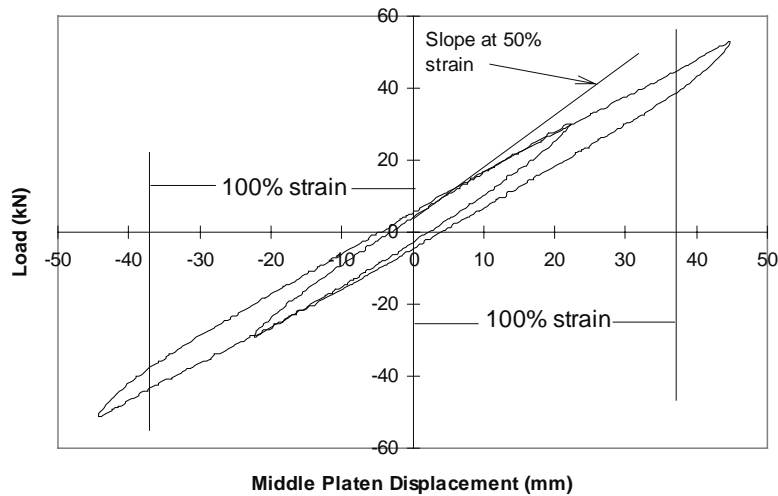


Figure 4- 4 Horizontal load vs. displacement at 100% strain

+100% strain, the stiffness is 1.04 kN/mm (5.94 kips/in) and the shear modulus is 0.572 MPa (83.0 psi). From zero to -100% strain the stiffness is 1.03 kN/mm (5.88 kips/in) and the shear modulus is 0.566 MPa (82.2 psi). Results of these tests were compiled to provide a comparison of the influence of the following variables on the computed shear modulus:

- Taper
- Number of Steel Shims (Shape Factor)
- Orientation of Steel Shims
- Compressive Stress

Influence of Taper on Shear Modulus

The key aspect of this study was to compare tapered and flat bearings. Assuming that the manufacturers were successful in fabricating all bearings uniformly, differences in shear modulus calculations for flat and tapered specimens should be a function of only that parameter and not shape factor, shear modulus or steel shim orientation. Figure 4.5 shows the load-displacement curve for a 57 durometer, 6% taper bearing with 6 reinforcing shims at 50% strain under 3.85 MPa (550 psi) compressive stress. Although there is an initial horizontal force of 5.40 kN (1.21 kips) due to the taper of the bearing, (as explained in Chapter 3) when the bearing is sheared the same amount of force is required to move it through 50% strain in either direction (H+ = H-). The shear stiffness for this bearing in the +50% strain range was 1.198 kN/mm (6.840 kips/in) and in the -50% strain range it was 1.196 kN/mm (6.824 kips/in), a 0.2% difference. The shear modulus, calculated on the basis of the elastomer thickness at mid-length was 0.655 MPa (95.0 psi) which compares very closely (0.652 MPa (93.2 psi)) to the previous flat bearing example. The only difference between the two bearings is the taper.

Table 4.1 shows the results of shear modulus calculations for flat and tapered bearings by nominal hardness. The values reported include an average four shear modulus tests — both 3 and 6 reinforcing steel shim specimens tested at both compressive stress levels — so that the greatest possible sample could be obtained.

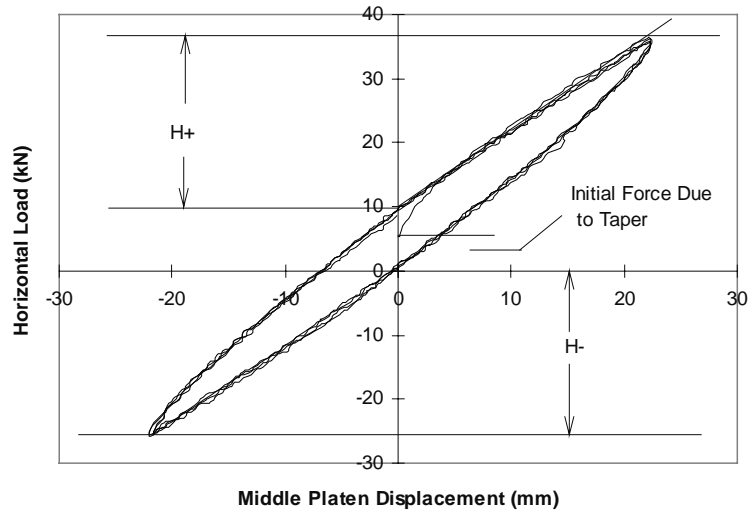


Figure 4- 5 Load-displacement curve for a tapered bearing at 50% shear strain

Table 4- 1 Influence of bearing taper on shear modulus

Measured Hardness	Specified Shear Modulus MPa (psi)	Shear Modulus Flat Specimens MPa (psi)	4 % Nominal Taper Percent Change from Flat	6 % Nominal Taper Percent Change from Flat
54	0.7 (100)	0.610 (87.2)	+1.9	+1.6
57	0.7 (100)	0.608 (86.9)	-5.1	-0.2
70	1.4 (200)	0.832 (119.0)	+5.5	+0.3
69	1.4 (200)	0.977 (139.8)	-9.6	-7.3

Typically, the shear moduli determined for bearings of the same hardness and shape factor fall within a range of $\pm 5\%$ from their average. Therefore, the results presented above show no significant deviation from the flat specimens other than at 70 durometer, which has no obvious explanation.

Influence of Compressive Stress on Shear Modulus

Each specimen was tested at both 3.85 and 7.69 MPa (550 and 1100 psi) to study the effect of compressive stress on shear modulus. Table 4.2 shows the average results of tests performed with matched slopes at the two stress levels.

As shown above, the higher durometer specimens seemed to decrease in calculated shear modulus less than the lower durometer specimens. The average drop of all hardnesses is 5.75% compared to an average reduction of 3% found by Hamzeh in the finite element study. The phenomenon is explained by Porter and Meinecke (20) as only an apparent drop in shear modulus with increasing compressive stress. When they factored in the internal shear force produced in the rubber due to compressive loading, the resulting shear modulus was identical at varying compressive stress levels. In bridges however, the magnitude of the horizontal forces transferred to the bridge by shearing the bearings is of interest and this quantity is shown to decrease slightly with increasing compressive stress. Lindley (13) also shows that application of a compressive force will decrease the shear stiffness of the material.

Table 4- 2 *Influence of compressive stress on shear modulus*

Measured Hardness	3.85 MPa (550 psi) Shear Modulus MPa (psi)	7.69 MPa (1100 psi) Shear Modulus MPa (psi)	Percent Change
54	0.634 (90.68)	0.587 (83.88)	-7.5
57	0.632 (90.42)	0.592 (84.64)	-6.4
70	0.875 (125.13)	0.843 (120.53)	-3.7
69	0.948 (135.61)	0.897 (128.30)	-5.4

Influence of Shape Factor on Shear Modulus

Table 4.3 shows the results of shear modulus calculations for 3 and 6 shim bearings (shape factors of 6.26 and 10.96 respectively) of all tapers and compressive stresses averaged within hardness categories. Although the available literature claims that the shear modulus is a function of the elastomer thickness alone, the results of the tests for this study show a difference in shear modulus based upon reinforcement.

Table 4- 3 *Influence of shape factor on shear modulus*

Measured Hardness	3 Shims S = 6.26 MPa (psi)	6 Shims S = 10.96 MPa (psi)	Percent Change 6 shim/3 shim
54	0.605 (86.5)	0.618 (88.5)	+2.3
57	0.585 (83.6)	0.639 (91.4)	+9.3
70	0.813 (116.2)	0.885 (126.5)	+8.8
69	0.892 (127.5)	0.954 (136.4)	+7.0

It appears reasonably consistent that increasing the number of steel shims in a bearing will increase the shear stiffness. The overall average 6.9% increase in shear modulus in bearings with 6 steel shims is consistent with the finite element study (10), which shows the increase to be 5%.

Influence of Steel Shim Orientation on Shear Modulus

Two sets of specimens as described in section 2.2.4 were compared on the basis of steel shim orientation (parallel vs. radial) with all other parameters the same. Results are shown in Table 4.4.

Table 4- 4 *Influence of steel shim orientation on shear modulus*

Compressive Stress MPa (psi)	Parallel Shim Modulus MPa (psi)	Radial Shim Modulus MPa (psi)
3.85 (550)	0.609 (88.03)	0.607 (86.86)
7.69 (1100)	0.574 (83.31)	0.567 (81.04)

If the results from the tests at both compressive stress levels are averaged, the difference between the shear moduli for the two designs is approximately 2%. Given that any two shear moduli tests on the same specimen at the same compressive stress have varied by as much as 3%, it probably can be assumed that shim orientation has little effect on shear modulus. Additionally, the two specimens were produced by the manufacturer from batches compounded with the same formula 5 months apart, which shows the repeatability of the compounding

procedure. Although this only represents one set of tests, analytical studies by Hamzeh (10) come to the same conclusion.

4.1.2.2 Non-uniform Loading Tests

Results of these tests were intended to provide a basis for comparison of the effects of non-uniform loading on the various bearing designs. Comparisons of shear modulus calculations for mismatched slope tests were made to tests on the same bearings at matching slopes. As stated earlier, flat bearings were tested against 1.5% slopes, 4% bearings against 6.25% slopes, and 6% bearings against 3.8% slopes. This procedure allowed for additional comparisons to be made on the basis of how the mismatch was imposed as well as simply between uniformly and non-uniformly loaded specimens. Table 4.6 shows the results of non-uniform loading at 3.85 MPa (550 psi):

Overall, the effect of non-uniform loading is to lower the calculated shear modulus by 6.2% over that calculated at matched slope conditions. Compressing the thick end of the 6% bearings more than the thin end has less of an effect than compressing the flat bearings more on either end or the 4% bearings on the thin end. Figures 4.6 and 4.7 show how non-uniform loading on flat and 4% bearings results in a lesser loaded area than does uniform loading. (Note how a slip of paper is inserted between the top of the bearing and the middle platen. Vertical lines are spaced 20 mm apart). The reason for the lower shear modulus calculation is illustrated by the relationship

$$\mathbf{H = GA\gamma} \quad \mathbf{(4.2)}$$

where G is the actual shear modulus of the material, A is the loaded area (which is smaller when bearings are loaded non-uniformly) and γ is the shear strain (which is the same in all tests). Because the area, A is smaller, and G and γ are the same, the force required to shear the specimen is lower. When this lower value of V is used to determine the shear modulus by the relationship

$$\mathbf{G = \frac{V}{A\gamma}} \quad \mathbf{(4.3)}$$

but the area, A is assumed to still be the total plan area, the shear modulus, G appears to decrease. When the results of the tests are sorted by number of steel reinforcing shims (shape factor), the influence of axial stiffness becomes clear and is shown in Table 4.6.

Clearly, the more axially stiff bearings (more steel shims) have more difficulty in accommodating the non-uniform loading at lower compressive stresses than do the less axially stiff specimens.

It was shown in Table 4.5 that the overall effect of non-uniform loading at 3.85 MPa (550 psi) was to lower the calculated shear modulus by 6.2 percent. When the compressive stress is increased to 7.69 MPa (1100psi) more of the bearings' plan area is in contact with the girder requiring more force to shear the bearing through the same strain. Table 4.7 shows the percentage change in calculated shear moduli at 7.69 MPa (1100 psi) from matched to mismatched conditions. Values in parentheses are the results from tests at 3.85 MPa (550psi) so that a comparison can be made.

The overall average decrease in shear modulus at the higher compressive stress level is only 2%, which is inconsequential. Table 4.8 shows that even the more axially stiff bearings show a lesser decrease in shear modulus under the higher compressive stress due to the higher compressive stress resulting in a greater loaded area. Figures 4.8 and 4.9 show the same bearing under non-uniform loading at low and high compressive stress. Note the decrease in separation between the bearing and the girder (the paper does not penetrate as far) at the higher stress level.

Table 4- 5 *Effect of non-uniform loading at low compressive stress*

Measured Hardness	Percent Change from Shear Modulus at Matched Slopes			
	Flat Bearings	4% Nominal Taper	6% Nominal Taper	Overall
54	-2.2	-12.2	+2.5	-4.0
57	-5.1	-9.3	-5.8	-6.7
70	-7.7	-18.5	+2.2	-8.0
69	-10.9	-1.5	-6.3	-6.2
Average	-6.5	-10.4	-1.9	-6.2

Table 4- 6 *Influence of shape factor on shear modulus in non-uniform loading at low compressive stress*

Measured Hardness	Percent Change in Shear Modulus from Matched Slope	
	3 Steel Shims S = 6.26	6 Steel Shims S = 10.96
54	-1.5	-8.7
57	-4.8	-7.1
70	-6.5	-9.6
69	-3.5	-9.1
Average	-4.1	-8.6

Table 4- 7 *Effect of non-uniform loading at higher compressive stress*

Measured Hardness	Percent Change From Shear Modulus at Matched Slopes			
	Flat Bearings	4% Nominal Taper	6% Nominal Taper	Overall
54	+1.5 (-2.2)*	-6.4 (-12.2)	+2.6 (+2.5)	-0.6 (-4.0)
57	-4.2 (-5.1)	-7.7 (-9.3)	-0.8 (-5.8)	-4.2 (-6.7)
70	-3.5 (-7.7)	-8.0 (-18.5)	+3.5 (+2.2)	-2.7 (-8.0)
69	+0.6 (-1.5)	-1.3 (-1.5)	-0.7 (-6.3)	-0.5 (-6.2)

*values in parentheses are for lower compressive stress

Table 4- 8 *Influence of shape factor on shear modulus in non-uniform loading at high compressive stress*

Measured Hardness	Percent Change in Shear Modulus from Matched Slope Tests	
	3 steel shims (S = 6.26)	6 steel shims (S = 10.96)
54	-0.7 (-1.5)*	-0.8 (-8.7)
57	-4.1 (-4.8)	-3.3 (-7.1)
70	-2.2 (-6.5)	-3.3 (-9.6)
69	+1.7 (-3.5)	-4.0 (-9.1)

* values in parentheses are for lower compressive stress

Table 4- 9 *Comparison of ASTM and full-scale shear modulus tests - Manufacturer A*

Nominal Shear Modulus MPa (psi)	Shear Modulus MPa (psi)		
	50.8x50.8x12.7 mm (2"x2"x0.5")	101.6x101.6x25.4 mm (4"x4"x1")	Full-Scale Specimens (0 to 50% strain)
0.7 (100)	0.891 (127.5)	0.825 (118)	0.6808 (98.6)
1.4 (200)	1.29 (184.5)	1.13 (162)	0.841 (122)

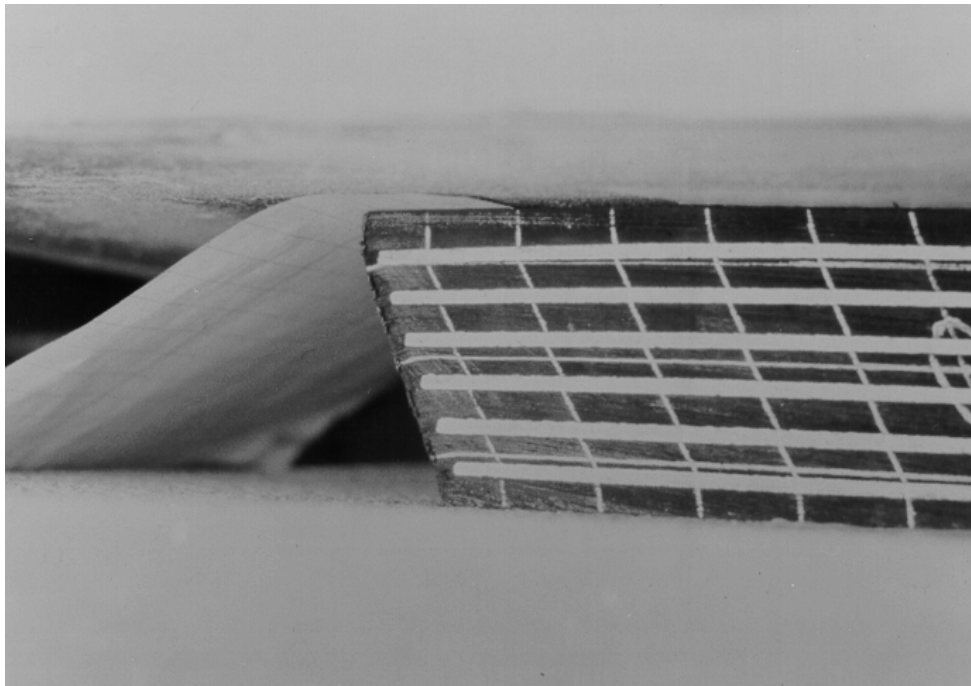


Figure 4- 6 *Flat bearing loaded non-uniformly at low compressive stress*

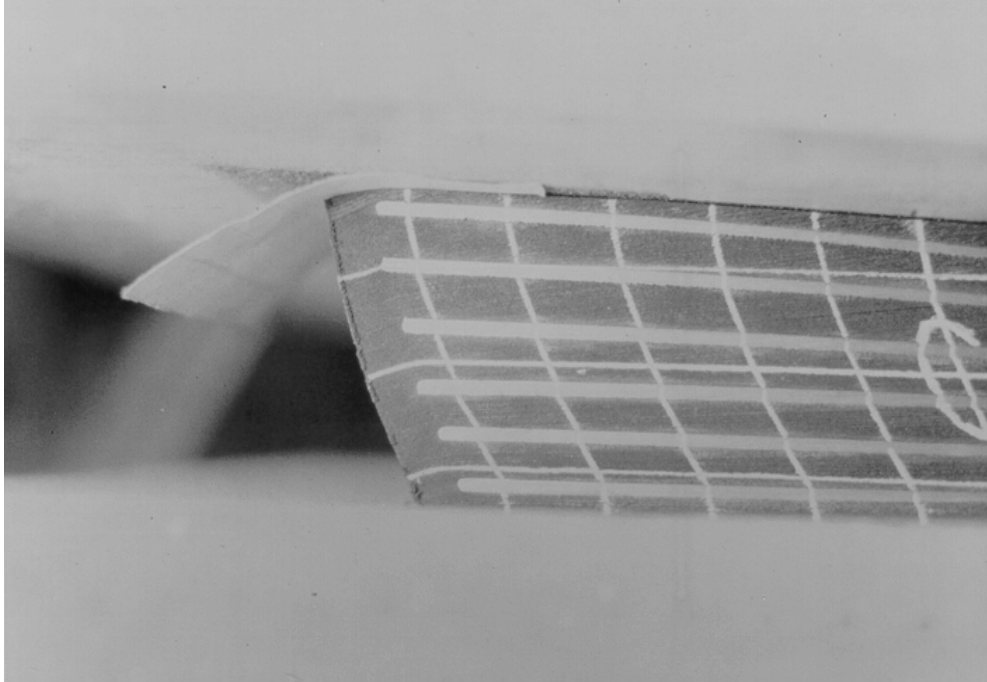


Figure 4-7 Tapered bearing loaded non-uniformly on the thin end

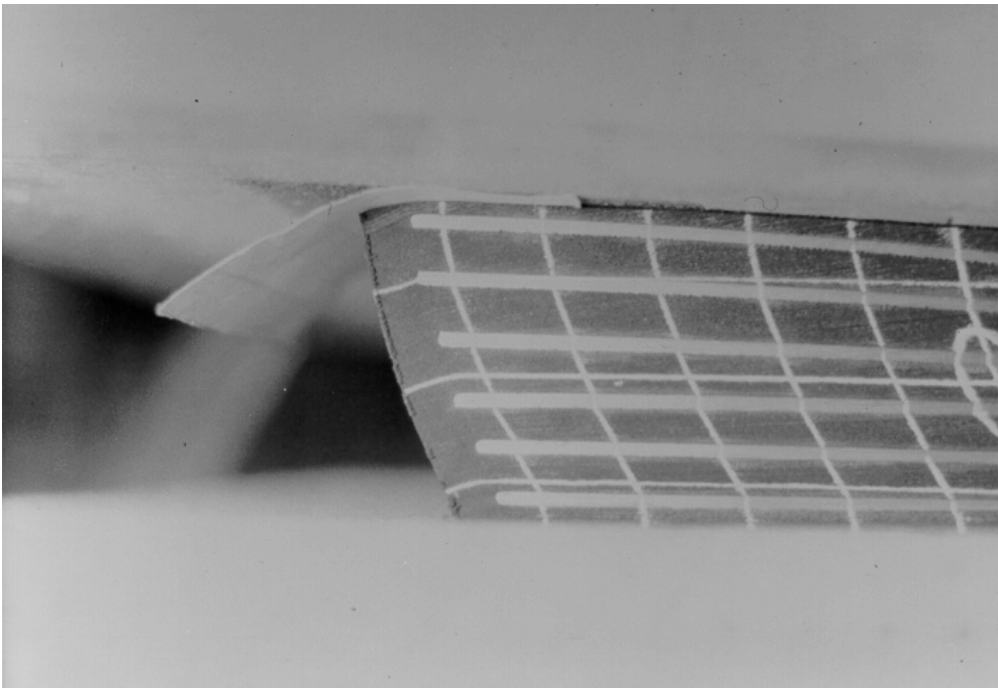


Figure 4-8 Bearing under non-uniform loading at 3.85 MPa (550 psi)

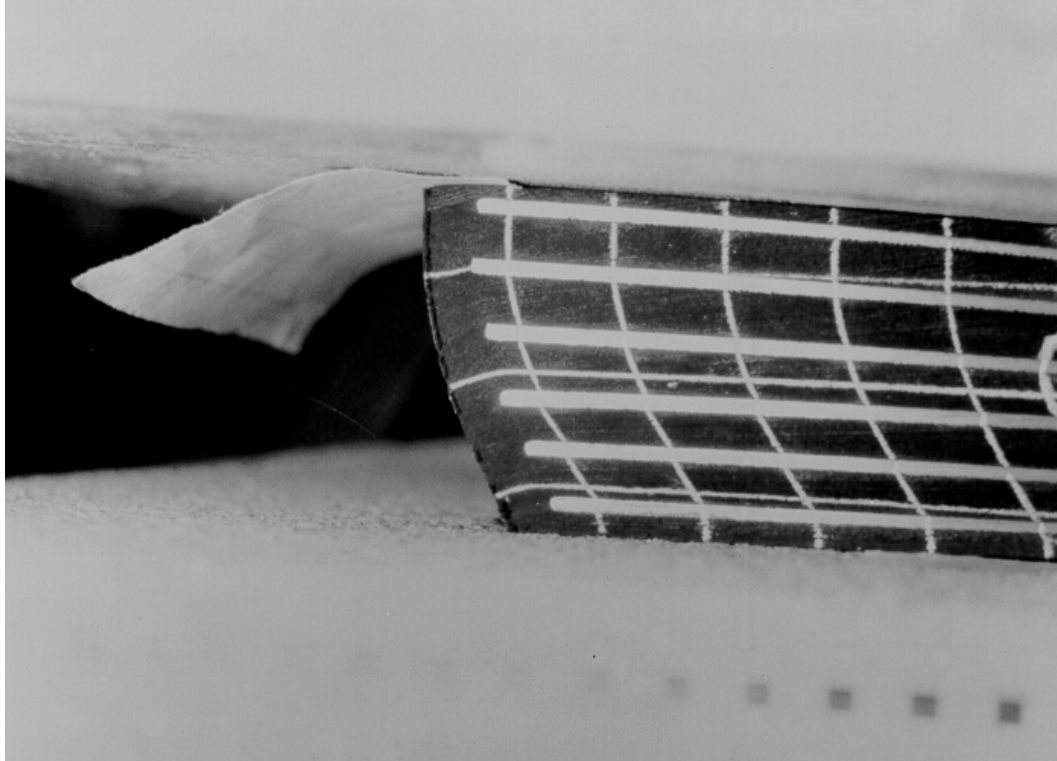


Figure 4- 9 Bearing under non-uniform loading at 7.69 MPa (1100 psi)

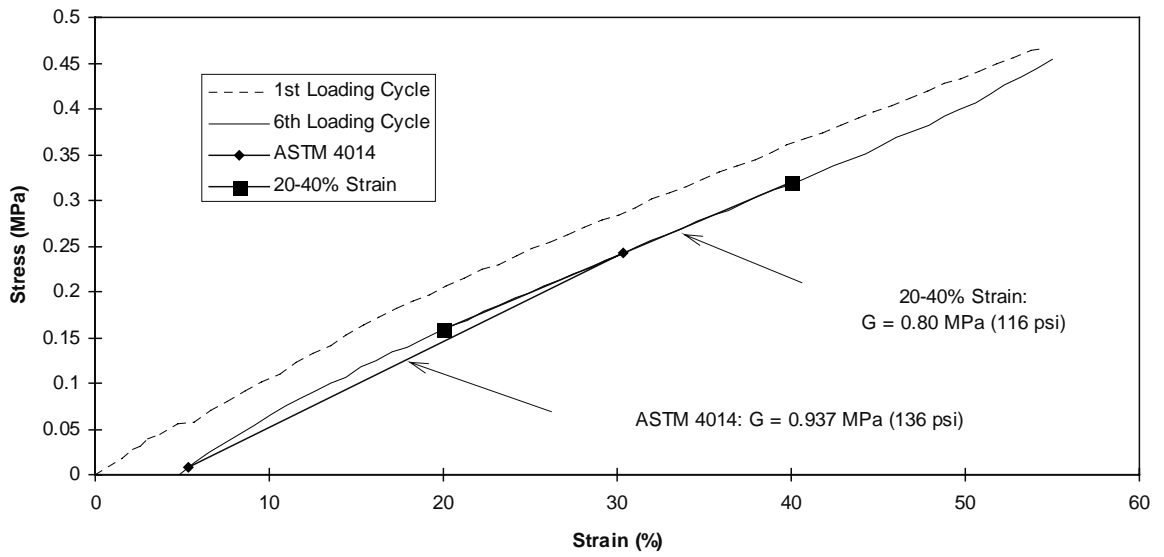


Figure 4- 10 Typical shear stress-strain curve from ASTM 4014 test

4.1.3 Comparison with Shear Modulus Tests on Plain Specimens

As part of this study, numerous shear modulus tests were performed on 50.8x50.8x12.7-mm (2"x2"x0.5") and 101.6x101.6x25.4-mm (4"x4"x1") plain rubber pads by Ardizoglou (1) according to the method prescribed by ASTM 4014. The specimens were provided by Manufacturer A as described in Chapter 2. A comparison of the shear moduli determined from 229x356-mm (9"x14") specimens versus the ASTM specimens is presented in Table 4.9. Although some material tests were performed with applied compressive stress, the values shown below were determined at zero compressive stress. The shear modulus values for the small-scale tests were arrived at by taking the slope of the load-displacement curve between 20 and 40% strain rather than as prescribed by ASTM 4014 as that method yields high values especially in the durometer ranges used in this study (1). Results show that the larger ASTM specimens give a value closer to that determined by the full-scale tests but still high in comparison. Additionally, the results of similar materials tests on plain specimens provided by Manufacturers B and C are shown in Table 4.10. Figure 4.10 shows a typical stress-strain curve from the ASTM 4014 shear modulus test. Note the difference between this relationship and that shown in Figure 4.3. Figure 4.10, which is from Reference (1), shows clearly why the modulus as determined by the standard ASTM test yields higher values.

Table 4- 10 Comparison of ASTM and full-scale shear modulus tests, Manufacturers B and C

Manufacturer	Nom. Shear Modulus MPa (psi)	Shear Modulus MPa (psi)		
		50.8x50.8 x25.4 mm (2"x2"x1")**	101.6x101.6 x25.4 mm (4"x4"x1")**	Full-Scale Specimens*
B	0.7 (100)	0.703 (102)	0.638 (92.5)	0.623 (90.4)
	1.4 (200)	1.08 (156)	1.04 (151)	0.935 (136)
C	0.7 (100)	0.758 (110)	0.738 (107)	0.623 (90.4)
	1.4 (200)	1.08 (155)	1.02 (148)	0.862 (125)

* Average of all matched slope tests (both 3 and 6 reinforcing shims, flat and tapered specimens) at 3.85 MPa (550 psi). Shear modulus between zero and 50% strain.

** Shear modulus between 20-40% strain

4.2 COMPRESSIVE STIFFNESS/MODULUS TESTS

4.2.1 TEST PROGRAM

Compressive stiffness tests were performed on one 229x356-mm (9"x14") specimen of each design from each manufacturer. Tests were conducted using a SATEC loading apparatus at a loading rate of approximately 11.1 kN (2.5 kips) per second for reinforced bearing and approximately 4.45 kN (1.0 kips) per second for plain bearings. Plain bearings were loaded to 7 MPa (1000 psi) and reinforced bearings were loaded to 14 MPa (2000 psi) for several cycles until the load-displacement curves showed good repeatability for each subsequent cycle. (The stiffness is greater during the first few cycles because the original molecular bonds are all still intact. The vast majority of these bonds that will eventually break have done so after only a few cycles and therefore subsequent cycles give a good indication of the long-term stiffness). A computer data acquisition system recorded load and displacement readings at a rate of one line per second. In tests on tapered bearings, an aluminum shim was bolted to the loading platen of the apparatus to ensure that the specimens bearings were compressed uniformly.

The compressive stiffness for reinforced bearings was determined by using a computer regression analysis on the data points between 3.45 and 10.35 MPa (500 and 1500 psi). These limits were chosen because they correspond to the most common working ranges for bearings typical of those in use. (There is no standard ASTM test for compressive modulus determination). Extrapolation of the slope appears to give a reasonable estimate of the load-displacement relationship at stresses lower than 3.45 MPa (500 psi) as well. The same stress limits were used for all reinforced bearing specimens although various reinforcing schemes would, of course, not realize the same strains at the same stresses. Additionally, these stress limits are the same as those used in the compression fatigue experiments performed in this study. Due to the behavior of plain bearings, (see section 4.2.2), the compressive stiffness determination was made at lower stress levels by a regression analysis between zero and 1.72 MPa (250 psi). At stresses above this level the curves are non-linear.

4.2.2 RESULTS

Before any tests were performed on reinforced bearings, plain rubber pads provided by Manufacturer A were tested for compressive stiffness. A stress-strain relationship for a nominal 0.7 MPa (100 psi) shear modulus pad is shown in Figure 4.11.

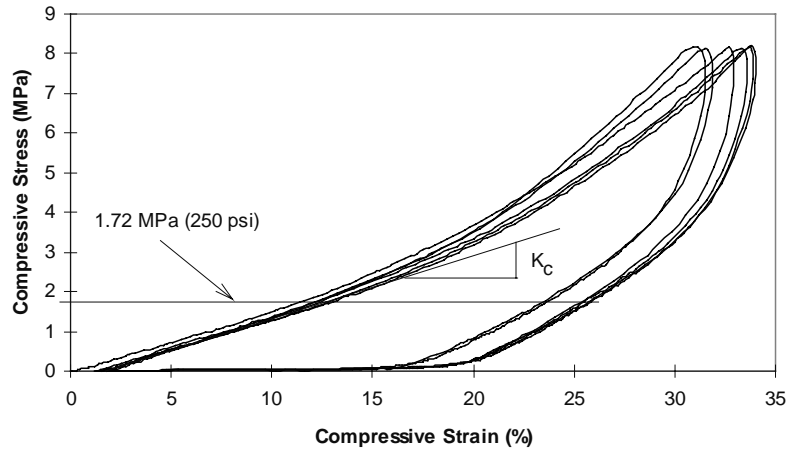


Figure 4- 11 Compressive stress-strain relationship for plain pad

The results show a decrease in stiffness for the first few cycles. The slope of the load displacement curve in Figure 4.11 above was found to be 27.6 kN/mm (157.7 kips/in) which, when converted to compressive modulus with $h_{rt} = 46.5 \text{ mm}$ (1.83") and $A = 0.0813 \text{ m}^2$ (126 in²) yields $E_c = 15.8 \text{ MPa}$ (2,291 psi). As soon as any reinforcing steel shims are added to the specimen, the stiffness increases dramatically. A nominal 0.7 MPa (100 psi) shear modulus reinforced (2 steel shims) bearing also from Manufacturer A yielded a load-displacement curve with a slope of 181 kN/mm (1033 k/in) between 3.45 and 10.35 MPa (500 and 1500 psi) and a compressive modulus of 101.2 MPa (14,675 psi), a significant increase over the unreinforced specimen. The results of the tests on specimens from Manufacturers B and C are shown Table 4.11, which gives the slopes of the load-displacement relationships between 3.45 and 10.35 MPa (500 and 1500psi). Although there is some scatter, when the data are averaged within general categories, clear trends can be observed.

Table 4- 11 Compressive stiffness test results

Nominal Taper (%)	Steel Shims	Stiffness kN/mm (kips/in) Manufacturer B Measured Durometer		Stiffness kN/mm (kips/in) Manufacturer C Measured Durometer	
		57	69	54	70
		Flat	3	203 (1163)	293 (1672)
	6	664 (3795)	741 (4237)	547 (3127)	747 (4268)
4	3	234 (1338)	244 (1396)	204 (1166)	232 (1328)
	6	623 (3564)	802 (4586)	415 (2370)	485 (2772)
6	3	220 (1260)	283 (1620)	259 (1481)	273 (1561)
	6	579 (3310)	823 (4705)	440 (2517)	618 (3534)
Average	3	219 (1253)	273 (1563)	224 (1280)	264 (1506)
	6	622 (3556)	789 (4509)	467 (2671)	617 (3525)

Table 4- 12 Effect of increasing shape factor on compressive modulus

Steel Shims (Shape Factor)	Nominal 0.7 MPa (100 psi)		Nominal 1.4 MPa (200 psi)		Percent Increase	
	Average Compressive Stiffness kN/mm (kips/in)	Average Shear Modulus MPa (psi)	Average Compressive Stiffness kN/mm (kips/in)	Average Shear Modulus MPa (psi)	Comp. Stiffness	Shear Modulus
3 (6.26)	222 (1266)	0.619 (88.5)	268 (1535)	0.867 (124)	21	40
6 (11.0)	545 (3114)	0.650 (93)	703 (4017)	0.944 (135)	29	45

Table 4- 13 Effect of increasing shape factor on compressive modulus

Steel Shims (Shape Factor)	Nominal (0.7 MPa) 100 psi	Nominal 1.4 MPa (200 psi)
	Average Compressive Stiffness kN/mm (kips/in)	Average Compressive Stiffness kN/mm (kips/in)
3 (6.26)	242 (1266)	268 (1535)
6 (11.0)	545 (3114)	703 (4017)
Percent Increase	145	162

The compressive stiffnesses of the unreinforced pads provided by Manufacturer A were 27.6 kN/mm (158 kips/in) for 65 durometer material and 28.7 kN/mm (164 kips/in) for 71 durometer material. The tests show that increasing the hardness of the elastomer has a much lesser effect upon the compressive stiffness than does increasing the shape factor by using more shims.

Effect of Increasing Hardness/Shear Modulus on Compressive Modulus

Table 4.12 shows the effect of increasing the elastomer hardness on the specimen’s compressive stiffness. Because the shear moduli as determined from the shear modulus tests showed that the nominal 50 and 55 durometer materials were very close in shear modulus and the nominal 60 and 70 durometer materials were also very close in shear modulus, the compressive stiffnesses from these two hardness ranges were averaged together and listed as nominal 0.7 and 1.4 MPa (100 and 200 psi) shear modulus respectively.

Effect of Increasing Shape Factor on Compressive Modulus

If the same averaging technique is used to compare increases in shape factor at the same hardness/shear modulus, the results show a much more dramatic increase in compressive stiffness as shown in Table 4.13. Clearly, increasing the number of reinforcing shims has a dramatic effect on the compressive stiffness in comparison to increasing the hardness of the elastomer.

Effect of Tapering on Compressive Modulus

Table 4.14 shows the average of all bearings tested in the categories listed. Table 4.14 shows that tapering the bearing has a very small effect upon the compressive stiffness of bearings with only 3 reinforcing shims. The effect on bearings with 6 shims however is to lower the compressive stiffness by 11.3% over a flat design. The reason for this disparity is that the lightly reinforced bearings have very thick elastomer layers in either flat or tapered designs. Once any initial compressive force is applied to them, they behave similarly, which is to bulge excessively and deflect significantly. The behavior of the 6 shim bearings is quite different. The flat 6 shim bearings show almost no sign of significant bulging or deformation when loaded even up to 14 MPa (2000psi). As shown in Figure 4.12, these bearings are very stiff axially.

When a tapered 6 shim bearing is loaded, although the bearing does not bulge very much between steel shims, the bearing as a whole bulges in the direction of the thick end. Figures 4.13 and 4.14 show this behavior.

The typical stress-strain relationships for a 3 shim flat bearing and a 3 shim 4 % tapered bearing (Figure 4.15) are very similar while those for a 6 shim flat bearing and a 6 shim 6% tapered bearing (Figure 4.16) clearly show that the tapered bearing is less axially stiff.

Table 4- 14 Influence of taper on compressive stiffness

Steel Shims (Shape Factor)	Stiffness kN/mm (kips/in)	
	Flat Bearings	Tapered Bearings
3 shims (6.26)	247 (1415)	244 (1394)
6 shims (11.0)	675 (3857)	599 (3420)

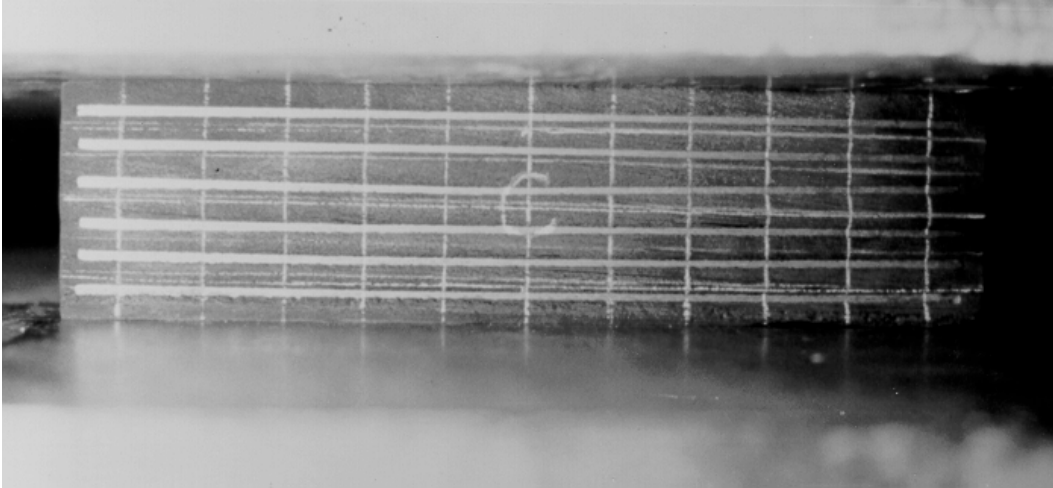


Figure 4- 12 Flat 6 shim bearing loaded to 14 MPa (2000 psi) in compression

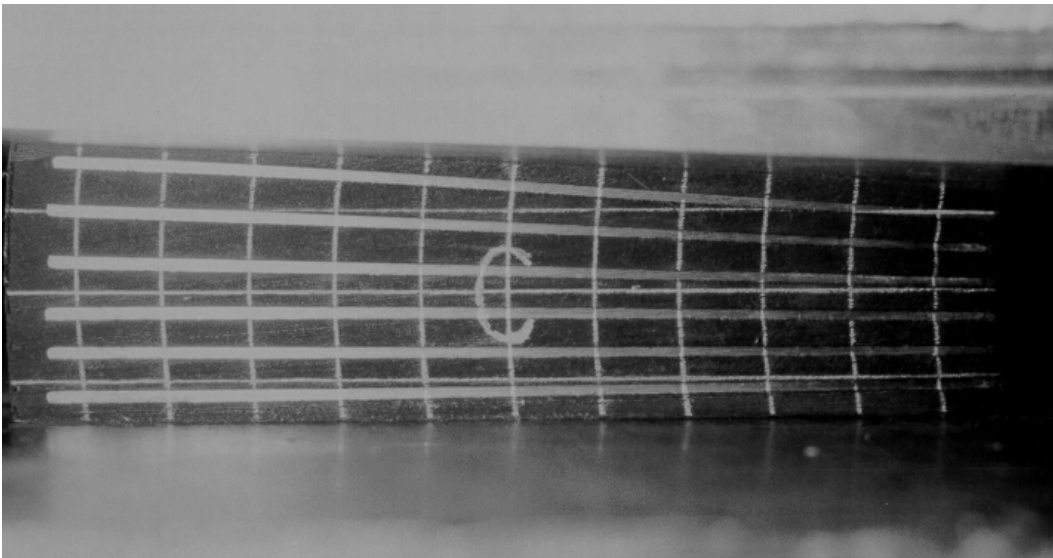


Figure 4- 13 Tapered 6 shim bearing loaded to 3.5 MPa (500 psi)

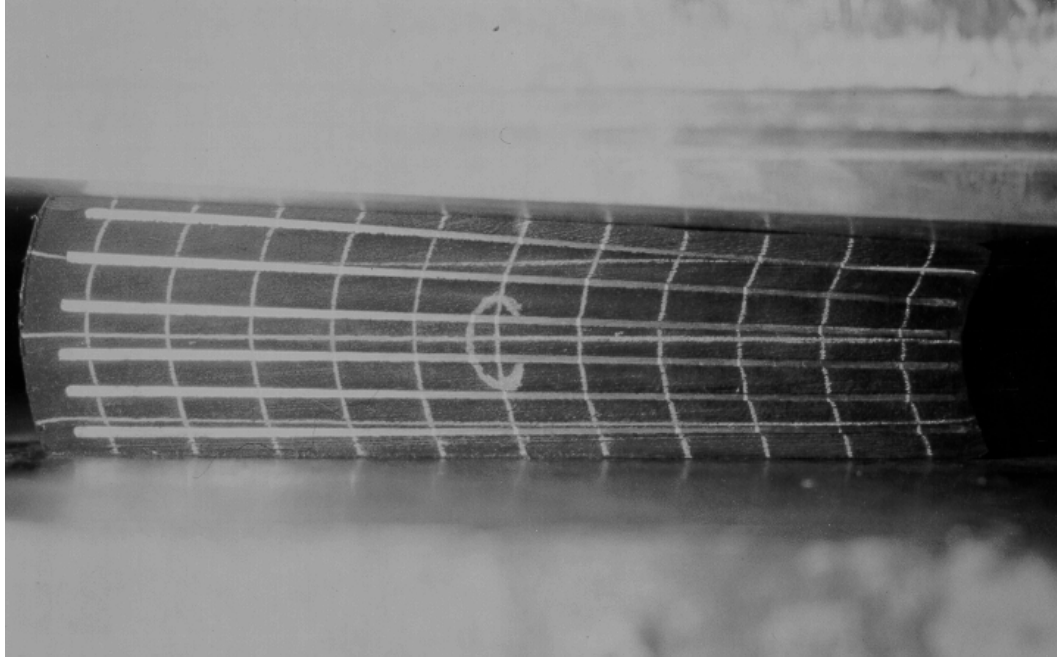


Figure 4- 14 Tapered 6 shim bearing loaded to 14 MPa (2000 psi)

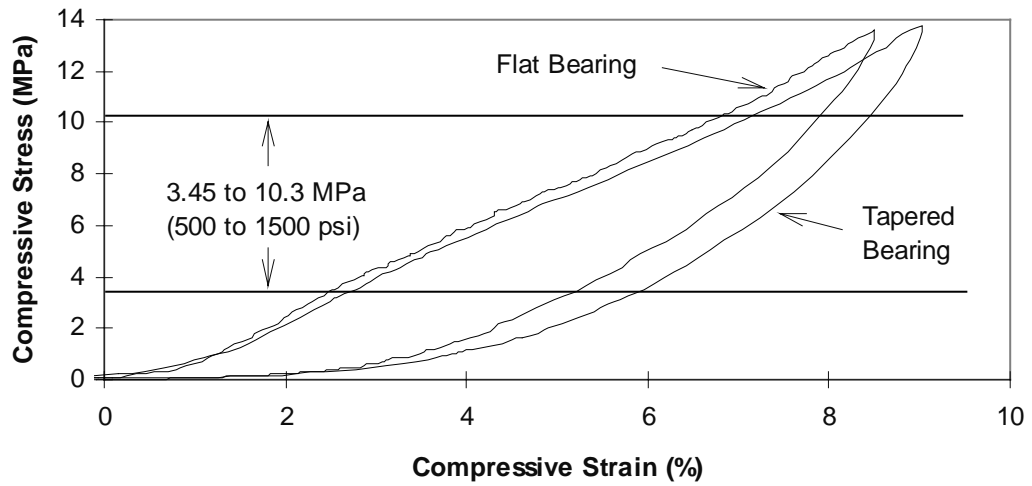


Figure 4- 15 Stress-strain curves for 70 durometer flat and tapered 3 shim bearings

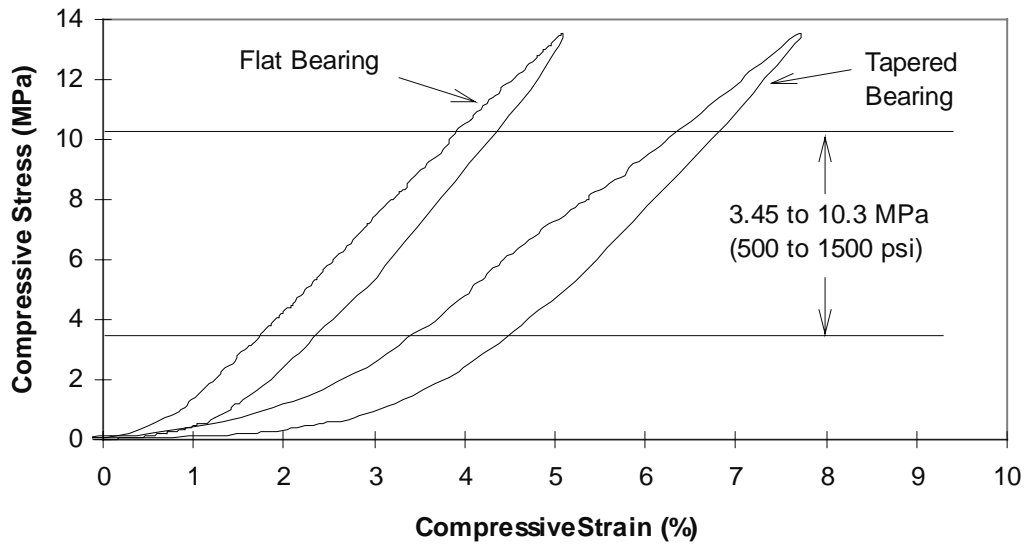


Figure 4-16 Stress-strain curves for 54 durometer flat and tapered 6 shim bearings

Influence of Reinforcing Shim Orientation on Compressive Modulus and Deformation

When the one 57 durometer, 6% taper, 3 shim specimen with steel shims oriented parallel to one another is compared to the 54 and 57 durometer, 6% taper 3 radially oriented steel shim specimens the compressive modulus and deformations were very similar. Results are shown in Table 4.15.

Table 4-15 Influence of reinforcing shim orientation on compressive modulus and deformation

	Parallel Shims	Radial Shims
Compressive Modulus MPa (ksi)	133.1 (19.30)	134.3 (19.48)
Compressive Strain (%)		
3.45 MPa (500 psi)	3.8	3.7
6.90 MPa (1000 psi)	6.5	6.1
10.35 MPa (1500 psi)	8.9	8.3

While the specimen with parallel steel shims appears to be less stiff axially as exhibited by both compressive modulus and deformations, the difference between the two designs is small which will produce little influence on compressive behavior.

The marginal increase in deformation in the parallel shim specimen may be due to the greater bulging of the large wedge of unreinforced elastomer.

4.2.3 EXPERIMENTAL VERSUS CALCULATED VALUES

As explained in Chapter 1, the most accepted method of determining compressive modulus, E_c , is from

$$E_c = 3G(1+2kS^2) \tag{4.4}$$

which is also given by AASHTO. A comparison of experimentally determined and calculated compressive moduli is presented in Table 4.16.

The comparison shows that Equation 4.4 yields increasingly more accurate results as the shape factor of the specimen increases. One reason for this disparity could be that Equation 4.4 includes a correction for material compressibility, k , which assumes that the harder the elastomer, the greater the deformation due to compression of the elastomer itself. (In calculations made for Table 4.16, $k=0.675, 0.575, \text{ and } 0.55$ for 55, 65, and 70 durometer material respectively). It has been suggested by Lindley (13) that this factor may not really be necessary. If k is set equal to 1.0 for the calculation for the plain and 2 shim bearings, the result is a much more

Table 4- 16 Experimental vs. calculated compressive modulus

Bearing Design	Compressive Modulus MPa (psi)		Ratio Calculated: Experimental
	Experimental	Calculated	
Plain 0.7 MPa (100 psi)	16.0 (2295)	7.42 (1061)	0.46 (0.71)*
Plain 1.4 MPa (200 psi)	16.6 (2369)	9.06 (1295)	0.55 (0.85)*
2 shim 0.7 MPa (100 psi)	102.6 (14675)	53.1 (7592)	0.52 (0.84)*
2 shim 1.4 MPa (200 psi)	100.8 (14421)	61.8 (8833)	0.61 (1.08)*
Mfr B 3 shim 0.7 MPa (100 psi)	122.9 (17577)	100.4 (14353)	0.82 (1.20)*
Mfr C 3 shim 0.7 MPa (100 psi)	125.5 (17951)	100.4 (14353)	0.80 (1.18)*
Mfr B 3 shim 1.4 MPa (200 psi)	159.0 (22737)	114.9 (16437)	0.72 (1.30)*
Mfr C 3 shim 1.4 MPa (200 psi)	150.7 (21474)	109.9 (15715)	0.73 (1.32)*
Mfr B 6 shim 0.7 MPa (100 psi)	340.8 (48734)	317.6 (45418)	0.93 (1.38)*
Mfr C 6 shim 0.7 MPa (100 psi)	260.4 (37243)	306.9 (43889)	1.18 (1.74)*
Mfr B 6 shim 1.4 MPa (200 psi)	458.8 (65611)	346.1 (49497)	0.75 (1.37)*
Mfr C 6 shim 1.4 MPa (200 psi)	350.2 (50072)	333.6 (47705)	0.95 (1.73)*

accurate estimate of the compression modulus at low shape factors but a poor estimate of the compressive modulus for higher shape factors (values shown in parentheses in column 4 above). Fortunately, the AASHTO formula (Equation 4.4) gives reasonable results for shape factors most commonly used for bridge bearings.

Analysis of experimental results also shows that the empirical formula (Equation. 4.4) gives a better prediction of the increase in compression modulus due to an increase in material hardness/shear modulus or shape factor. A comparison of experimental results and calculated predictions is shown in Table 4.17.

Table 4- 17 Actual and predicted changes in compression modulus

Change in Design 229x356 mm (9"x14") Specimens		Actual Increase in Modulus (%)	Predicted Increase in Modulus (%)
Increase Shear Modulus From 0.62 to 0.90 MPa (90 to 130 psi)	3 Shims	21	17
	6 Shims	29	21
Increase Shape Factor From 6.26 to 11.0	0.7 MPa (100 psi)	145	208
	1.4 MPa (200 psi)	162	208

Although AASHTO allows the use of Equation 4.4 to determine the compressive modulus for use in deformation calculations, the straight line modulus is not accurate for predicting the actual deformation at a given stress. For that reason, there are a number of stress-strain curves published in various references (AASHTO among them) that predict a strain for a bearing of a given shape factor and hardness at a range of stresses. The stress-strain data generated from this study for flat bearings agree reasonably well with those published by AASHTO (32) and other sources (6,7,13) but show some deviation from the stress-strain curves which assume a linear stress-strain relationship. As none of these curves consider tapered bearings, a series of such relationships was produced from the data recorded during this study and is presented in Figure 4.17.

The stress-strain data were averaged together for all tapered bearings within the durometer and hardness category as the 6% bearings deflected only slightly more than the 4% bearing at a given stress level. Again, the 3 shim bearings, whether tapered or not, behaved reasonably similarly. The dashed lines represent the stress-strain relationship based upon Equation 4.4.

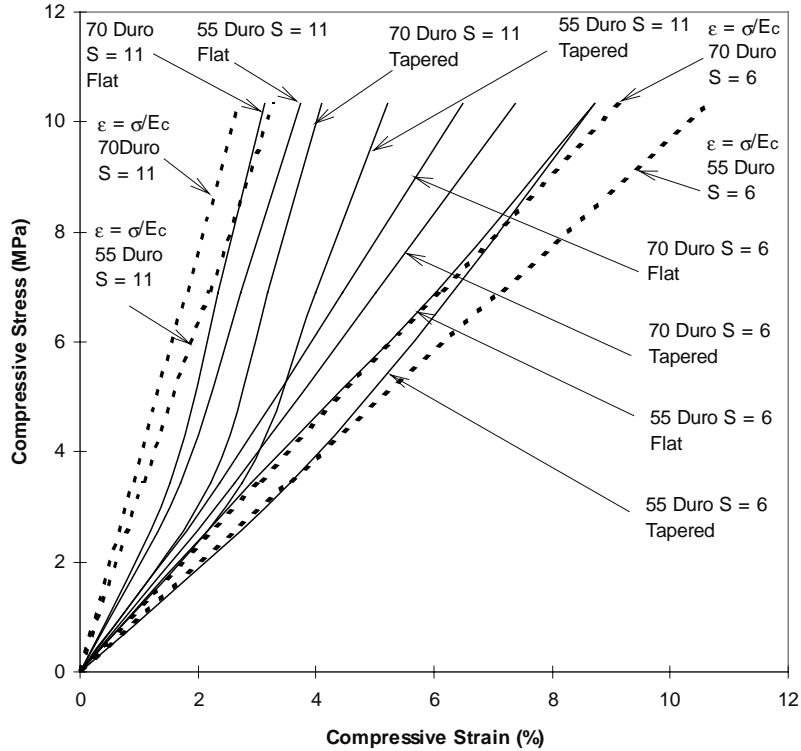


Figure 4- 17 Stress-strain curves for flat and tapered bearings of 55 and 70 durometer

4.3 ROTATIONAL STIFFNESS TESTS

Rotational stiffness tests were conducted to evaluate the ability of each bearing design to accommodate girder rotations. Tests were performed to establish a moment-rotation relationship for each bearing design as well as to determine the point at which the lever arm (girder) lifted-off from the bearing. Additionally, the bottom corners of the bearing's less compressed edge were observed for any sign of uplift, a term applied to describe a net upward movement of any point on the bearing during rotational loading (12,25,32,33).

4.3.1 TEST PROGRAM

The same pair of nominal 50- and 70-durometer (54 and 69 measured) bearings which were used for the shear modulus tests were rotated through 1.9 degrees in either direction using the test set up shown schematically in Figure 4.18. Comparisons of performance were made based on hardness/shear modulus, shape factor, and taper at compressive stresses of 3.85 MPa (550 psi) and 7.69 MPa (1100 psi).

Pressure was applied to the double acting ram via a hydraulic hand pump so that the bearings would be rotated as slowly as possible. Three cycles of rotation in either direction were completed. Linear potentiometers positioned 114 mm (4.5 inches) from the bearing center line were used to measure the rotation of the lever arm electronically. A digital inclinometer was employed to visually identify the point at which the desired rotation had been achieved as shown in Figure 4.19.

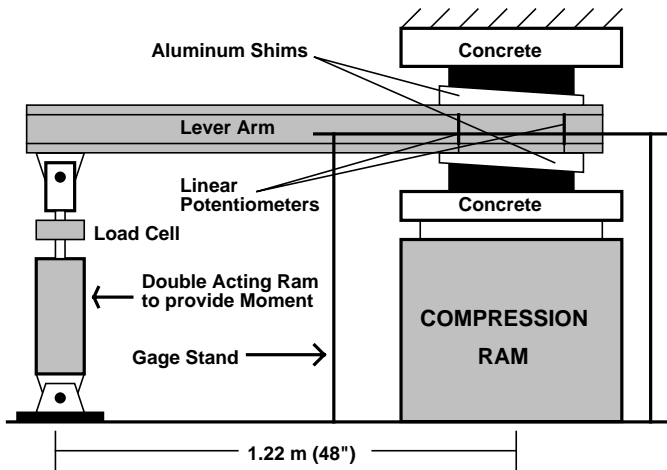


Figure 4- 18 Schematic diagram of rotational stiffness test setup

the moment-rotation relationship became non-linear was recorded for comparison. This was accomplished by computing the slope of the curve from the zero rotation point to every subsequent point on the line. The point at which the slope started to decrease was identified as the “rotation capacity”. This method was used because it was very difficult to visually observe the start of lift-off. However, photographic records were made of every bearing at the rotation where lift-off exceeded approximately 20 mm. Table 4.19 shows the average rotation capacities calculated from the tests. A zero indicates that the moment-rotation curve was non-linear from the origin.

4.3.2 TEST RESULTS

Analysis of the test results showed a significant difference in the moment-rotation relationships of the axially stiff and the axially flexible bearings especially when compared at the two different compressive stress levels. Figures 4.20 and 4.21 show the moment-rotation curves for the least stiff bearing - 54 durometer 3 reinforcing shim - at 7.69 MPa (1100 psi) and the stiffest bearing - 69 durometer 6 reinforcing shim - at 3.85 MPa (550 psi). Note the differences in linearity.

The slopes of the linear portions of the relationships were taken in each direction and averaged to compare the rotational stiffnesses of the various designs and are given in Table 4.18. In an attempt to calculate the rotation at which lift-off might be starting, the point where



Figure 4- 19 Rotational stiffness test instrumentation

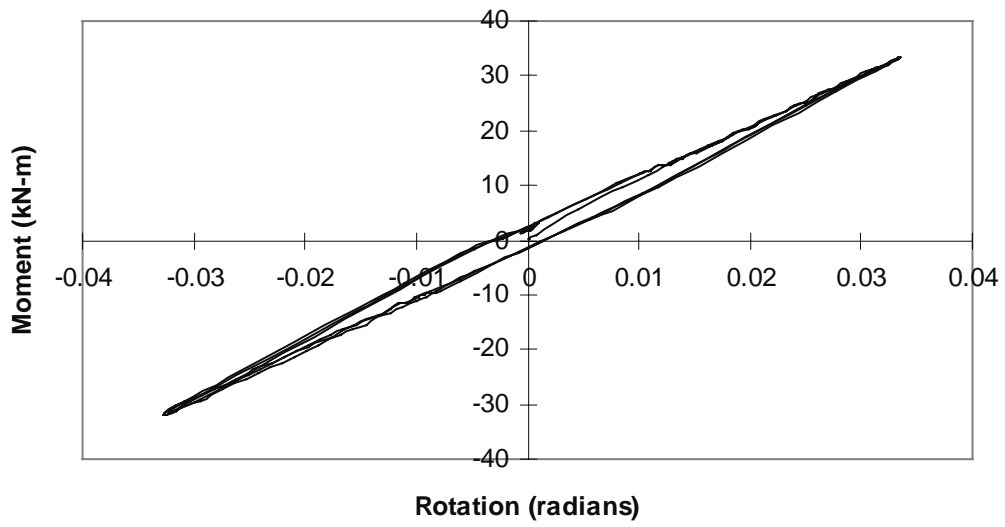


Figure 4- 20 Moment-rotation curve - flat 54 Durometer 3 shim bearing at 7.69 MPa

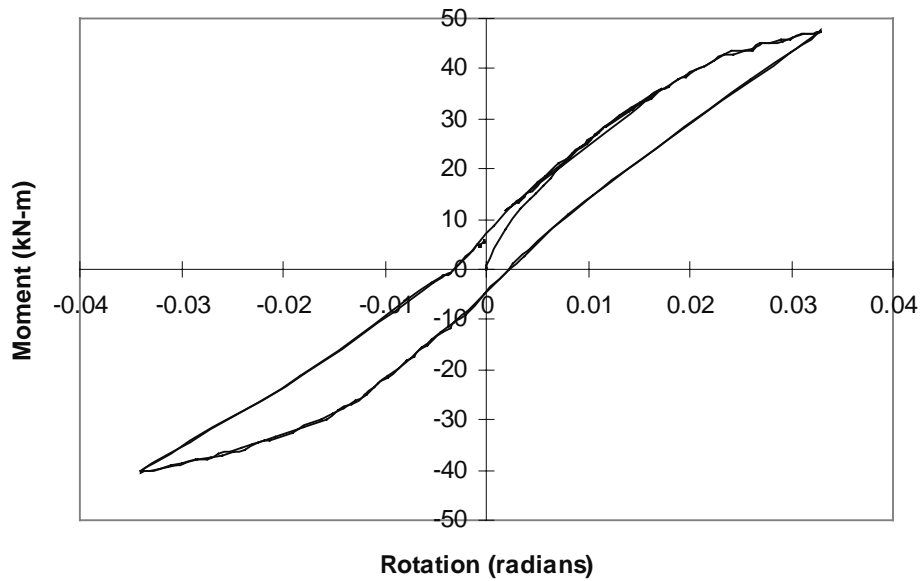


Figure 4- 21 Moment-rotation curve - flat 69 Durometer 6 shim bearing at 3.85 MPa

Table 4- 18 Average rotational stiffnesses

Bearing Design		Rotational Stiffness N-m/radian (K-in/degree)			
		54 Durometer		69 Durometer	
		3.85 MPa (550 psi)	7.69 MPa (1100 psi)	3.85 MPa (550 psi)	7.69 MPa (1100 psi)
Flat	3 shim	408 (63.1)	479 (74.0)	538 (83.2)	545 (84.2)
	6 shim	829 (128)	845 (131)	865 (134)	1132 (175)
4% Taper	3 shim	450 (69.5)	471 (72.7)	390 (60.2)	522 (80.6)
	6shim	780 (121)	830 (128)	962 (149)	1072 (166)
6% Taper	3shim	386 (59.6)	405 (62.6)	390 (60.3)	438 (67.7)
	6shim	856 (132)	856 (132)	975 (151)	1085 (168)

Table 4- 19 Average rotation capacities of bearings

Bearing Design		Rotation Capacity Radians (Degrees)			
		54 Durometer		69 Durometer	
		3.85 MPa (550 psi)	7.69 MPa (1100 psi)	3.85 MPa (550 psi)	7.69 MPa (1100 psi)
Flat	3 shim	0.013 (0.745)	0.0332 (1.9)	0.0066 (0.38)	0.0332 (1.9)
	6 shim	0 (0)	0.0192 (1.1)	0 (0)	0.00436 (0.25)
4% Taper	3 shim	0.0168 (0.96)	0.0332 (1.9)	0.0244 (1.4)	0.0332 (1.9)
	6shim	0.0107 (0.615)	0.0171 (0.98)	0.00585 (0.335)	0.0162 (0.93)
6% Taper	3shim	0.0227 (1.3)	0.0332 (1.9)	0.0244 (1.4)	0.0332 (1.9)
	6shim	0.0087 (0.5)	0.0185 (1.06)	0.00812 (0.465)	0.0112 (0.64)

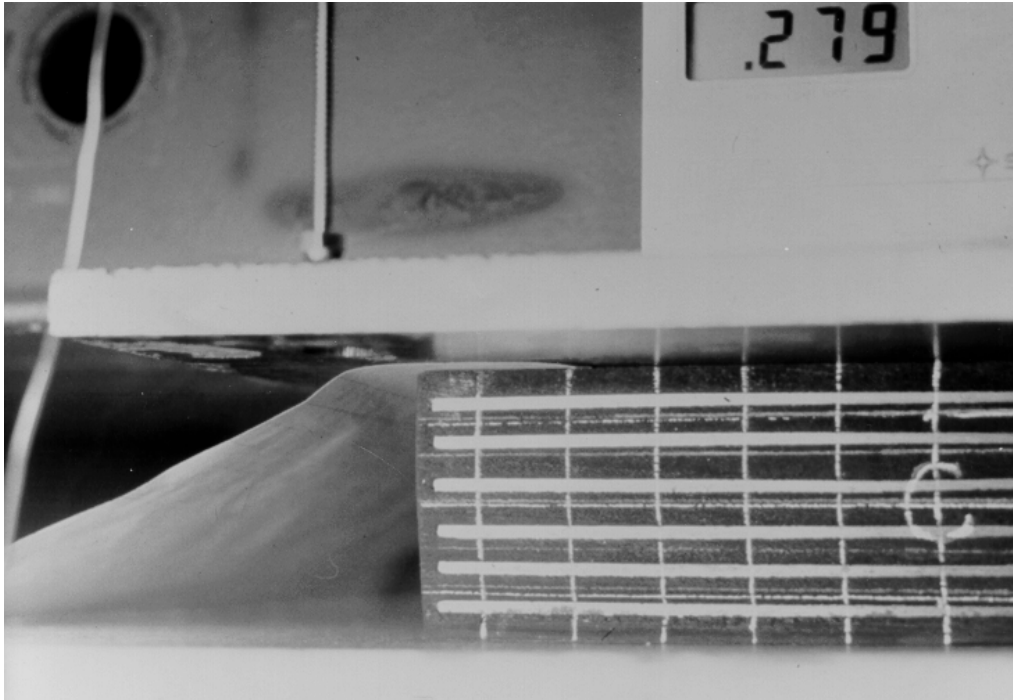


Figure 4- 22 Bearing exhibiting lift-off at 3.85 MPa (550 psi)



Figure 4- 23 Bearing exhibiting lift-off at 7.69 MPa (1100 psi)

The data presented was analyzed to determine the effect of compressive stress on rotational stiffness and rotation capacity. Figures 4.22 and 4.23 show the same bearing at the point where the lever arm has lifted off. In Figure 4.22 the bearing is being compressed at 3.85 MPa (550 psi) and in Figure 4.23 the compressive stress is 7.69 MPa (1100 psi). The slip of paper inserted between the top of the bearing and the lever arm shows the extent to the lever arm lift-off from the bearing. Note that there is no observable uplift of the bearing's less compressed corners. They are clearly still in contact with the concrete surface and are still in compression.

Table 4.20 summarizes the effect of a change in compressive stress from 3.85 MPa (550 psi) to 7.69 MPa (1100 psi) on rotation capacity and rotational stiffness. Overall, doubling the compressive stress resulted in an average 10.8% increase in rotational stiffness and a 120% increase in rotation capacity. These findings are significant in that the rotation capacity allowed in the current AASHTO specification (twice the compressive deformation divided by the length) can be shown to be overly conservative by the following example. Consider the case of a flat 54 durometer bearing under 7.69 MPa (1100 psi) compressive stress:

Table 4- 20 Influence of compressive stress on rotational stiffness and rotation capacity

Bearing Design	Rotational Stiffness Increase (%)	Rotation Capacity Increase (%)
3 Shim	11.6	84.5
6 Shim	10.0	155.2
50 Durometer	5.83	135.6
70 Durometer	15.7	104.0

Calculate compressive deformation: Use Figure 4.18 $\Delta_c = 1.27$ mm (0.050 inches)

Calculate allowable rotation by to AASHTO: $\theta = 2\Delta_c/L = 2 (1.27 \text{ mm})/229 \text{ mm} = 0.011$ radians

From Table 4.19, the average rotation capacity as defined in this study for this bearing at this compressive stress is 0.0192 radians (1.1 degrees). Photographic records show that even when rotated as far as 0.0293 radians, only approximately a 20-mm length of lift-off was observed. Furthermore, there is no experimental evidence that this small degree of lift-off is actually detrimental to the bearing. Results of the rotation capacity tests presented above will be considered in making recommendations for design specifications to be given later in this report.

Influence of Hardness/Shear Modulus on Rotation Capacity/Stiffness

Table 4.21 shows the effect of increasing the elastomer hardness from 54 durometer to 69 durometer (shear modulus 0.62 MPa (90 psi) to 0.90 MPa (130 psi)) upon rotational behavior. Results appear logical with the possible exception of a harder 3 shim bearing producing more rotation capacity, but a 2.0 % change should really be regarded as indicating no influence rather than being a sign of a clear trend. It does seem clear however, that the higher durometer 6 shim bearings have poor rotational behavior (greater rotational stiffness and lower rotation capacity.)

Table 4- 21 Effect of increasing hardness on rotational behavior

	Change in Rotational Stiffness (%)	Change in Rotation Capacity (%)
3 Shim	+ 8.63	+ 2.0
6 Shim	+ 21.9	- 38.2

Influence of Shape Factor on Rotational Behavior

Table 4.22 shows how increasing the shape factor of the specimens effected their rotational behavior. Once again, the 69 durometer hardness material shows a less desirable trend than does the softer material.

Table 4- 22 Effect of increasing shape factor on rotational behavior

Steel Shims (Shape Factor)	Rotational Stiffness kN-m/rad (K-in/deg)		Rotation Capacity Radians (Degrees)	
	54 Durometer	69 Durometer	54 Durometer	69 Durometer
3 Shim (6.26)	433.1 (66.9)	470.7 (72.7)	0.0253 (1.45)	0.0258 (1.48)
6 Shim (11.0)	832.6 (128.6)	1015 (156.8)	0.0124 (0.71)	0.00768 (0.44)
Change (%)	+92.3	+115.8	-51.1	-70.4

Effect of Tapering on Rotational Behavior

Figure 4.24 shows a typical moment-rotation relationship for a 54 durometer, 6 steel shim, 6% tapered bearing at 7.69 MPa (1100 psi) compressive stress. The shape of the curve is typical of all of the highly reinforced low durometer bearings at the higher compressive stress level. The only variation from the relationship observed for flat bearings is that there is an initial moment due to the lever arm restraining the bearings' natural tendency to rotate toward their thick end when compressed. Figures 4.25a and 4.25b show the same tapered bearing under 7.69 MPa (1100 psi) at the point where the lever arm has lifted off from the bearing.

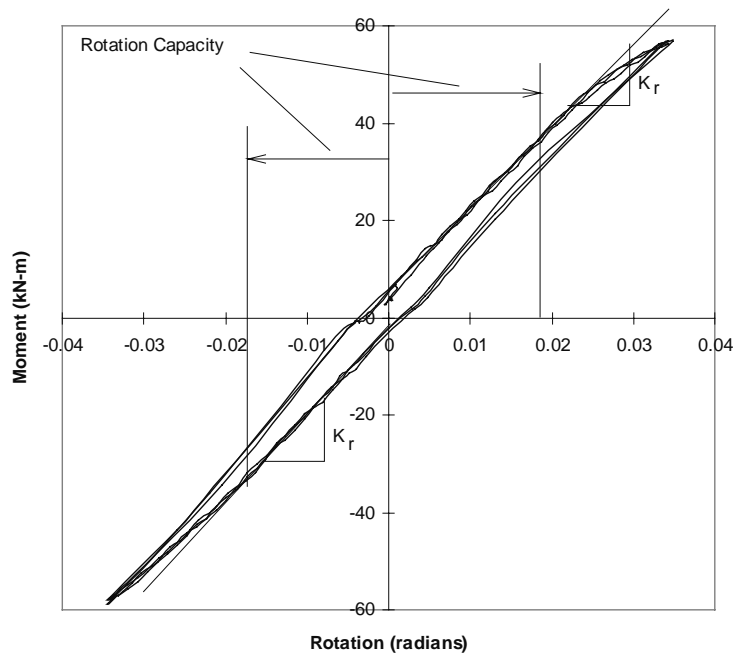
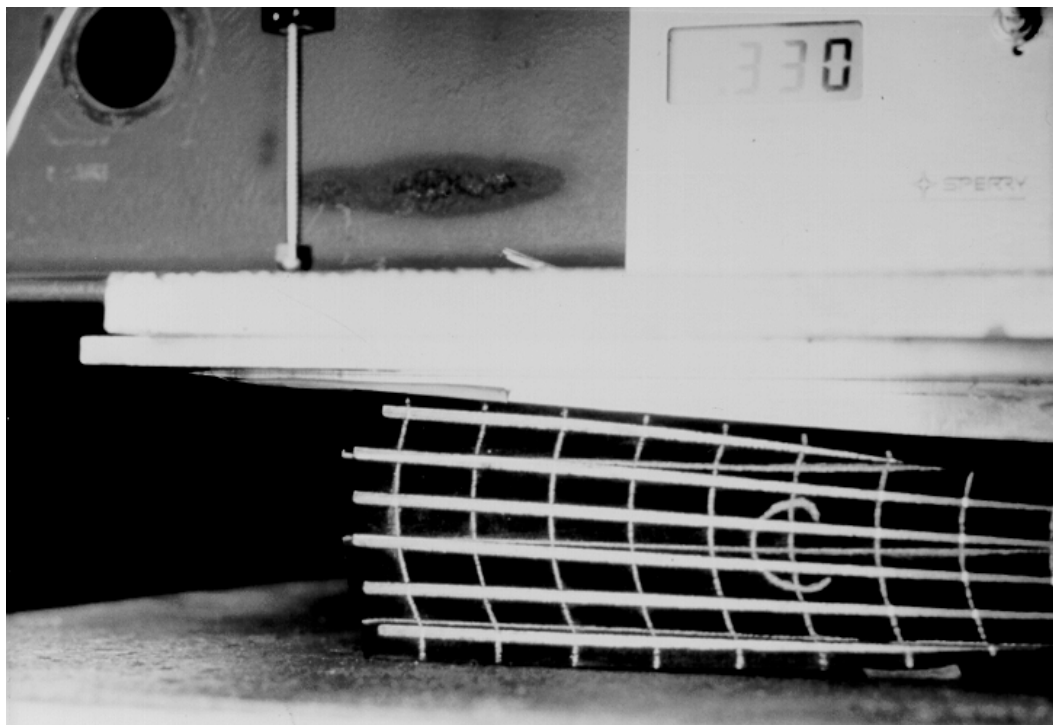


Figure 4- 24 Typical moment-rotation relationship for a tapered bearing



(a)



(b)

Figure 4- 25 Tapered bearing at lever arm lift-off

Table 4.23 gives the percentage change in rotational stiffness and rotation capacity for tapered bearings versus flat bearings of the same design. (Results for all tapered bearings are averaged together).

Table 4- 23 *Influence of taper on rotational behavior*

Bearing Design	Change in Rotational Stiffness (%)	Change in Rotation Capacity (%)
3 Shim	-12.4	+28.5
6 Shim	+1.0	+104.0
54 Durometer	-1.77	+23.0
69 Durometer	-5.29	+77.0

Although the trend is clear in change in rotation capacity, the average loss of rotational stiffness, which is less than 5% does not indicate any significant change. The change in rotation capacity may be less a reflection of the capacity of tapered bearings as it is the lack of capacity of flat bearings which appeared to show very low rotation capacity especially under 3.85 MPa (550 psi) compressive stress. In no way do the test results indicate any reason why the use of tapered bearings would not be recommended. In fact, as shown in Table 4.19 tapered bearings exhibited more rotation capacity than flat bearings with all other parameters the same.

Effect of Reinforcing Shim Orientation on Rotational Behavior

As described in Chapter 2, one 57 durometer, 3 shim, 6% taper specimen was fabricated with steel shims parallel to one another rather than radially oriented. This design was tested in the same manner as all others and a comparison to similar tapered bearing designs (54 durometer, 3shim) is made in Table 4.24. Although the measured hardness of this specimen is different from the 54 durometer specimens, recall from Section 4.1 that the actual shear modulus of the nominal 50 durometer and 55 durometer specimens was almost identical. For this reason a direct comparison can be made.

Table 4- 24 *Influence of steel shim orientation on rotational behavior*

Shim Orientation	Rotational Stiffness kN-m/rad (k-in/deg)		Rotation Capacity radians (degrees)	
	3.85 MPa (550 psi)	7.69 MPa (1100 psi)	3.85 MPa (550 psi)	7.69 MPa (1100 psi)
Radial Orientation	417 (64.5)	438 (67.7)	0.0197 (1.13)	0.0332 (1.90)
Parallel Orientation	335 (51.8)	385 (59.5)	0.0216 (1.24)	0.0267 (1.53)

The fact that the parallel orientation design produced a lower rotational stiffness is not surprising considering the thickness of the unreinforced wedge of elastomer that provides the taper to accommodate the girder slope. The reason for the rotation capacity at the higher compressive stress being lower than that of bearings with the radially oriented shims is not apparent and could be due to a test anomaly.

4.3.3 SUMMARY OF ROTATIONAL BEHAVIOR TESTS

Figure 4.26 shows a graphical display of the moment-rotation relationships of the flat bearings tested as part of this study. From this comparison, the increase in rotational stiffness due to increases in material hardness, shape factor, and compressive stress can be seen readily. Figure 4.27 shows a comparison of typical

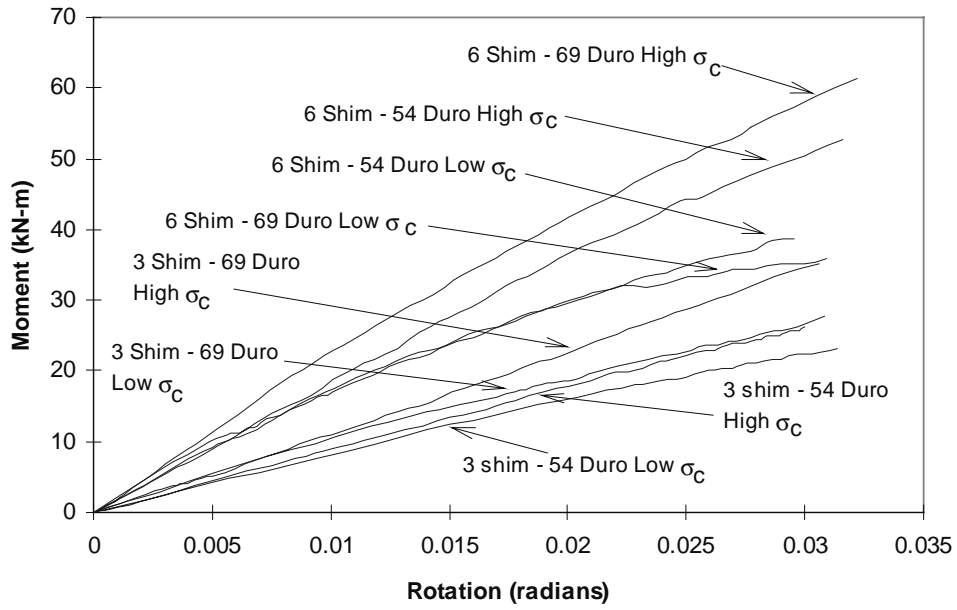


Figure 4- 26 Comparison of flat bearing designs

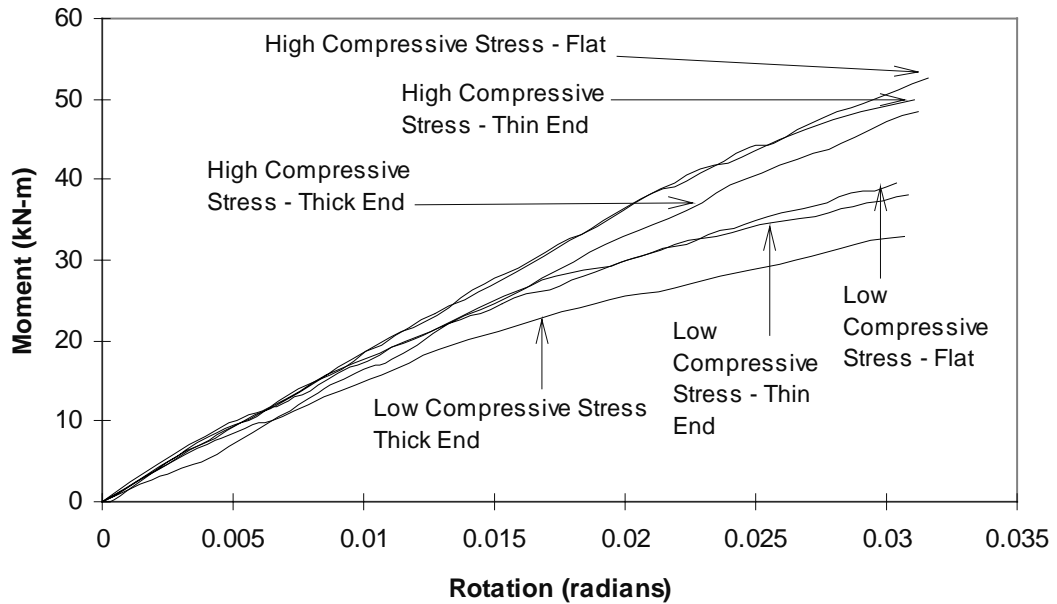


Figure 4- 27 Comparison of flat and tapered designs

relationships for 6 shim, 54 durometer tapered bearings versus a 6 shim, 54 durometer flat bearing at both compressive stress levels. Note the similarity in performance between the flat and tapered designs for this lower durometer material. Predictably, the thick end of the tapered bearing shows less stiffness than does the thin end and either end of a flat bearing.

Three sources were used to make comparisons of experimental results and theoretical predictions of the rotational stiffness for the specimens tested. Lindley (13) gives the “tilting stiffness” of a single elastomer layer as shown below:

$$K_t = 3Gk_r^2 \left(P + \frac{0.062L^2Q}{t^2} \right) \frac{A}{t} \quad (4.5)$$

where:

K_t = Tilting Stiffness, kN-m/radian

G = shear modulus, MPa

k_r = radius of gyration about tilting axis, mm

P = numerical factor based on plan shape ($P = 1$ if square, $P = 1.33$ if $W \gg L$), $P=1$ in Eq. 4.5

L = Length, mm

Q = numerical factor based on plan shape ($Q = 0.75$ if square, increases with W/L), $Q=0.859$ in Eq. 4.5

t = thickness of one elastomer layer, mm

A = Plan area, m^2

Rejcha (23) gives a “moment corresponding to a rotation” as shown below:

$$M_{\alpha_e} = C_M G \alpha_e \left(\frac{L^5 W}{t_e^3} \right) \quad (4.6)$$

where:

M_{α_e} = moment required to rotate one elastomer layer α_e radians, kN-m

C_M = a numerical factor based upon the L/W ratio

G = shear modulus, MPa

α_e = rotation of one elastomer layer, radians

L = length, mm

W = width, mm

t_e = thickness of one elastomer layer, mm

Also, section 14.6.2 of the current AASHTO specifications (32) give the “moment induced by bending of a rectangular bearing about an axis parallel to its long side” as

$$M = \frac{(0.5E_c)I\theta_{TL,x}}{h_{rt}} \quad (4.7)$$

where:

- I = moment of inertia about the x-axis, mm⁴
 E_c = compressive modulus from Equation 4.3, kN/mm²

Predictions of the rotational stiffness for the various designs are given in Table 4.25 below along with the average rotational stiffnesses for all tests performed including flat and tapered specimens.

Table 4- 25 Comparison of rotation test results and theoretical calculations

Bearing Design	Rotational Stiffness kN-m/radian (k-in/degrees)			
	Lindley*	Rejcha*	AASHTO*	Experimental
54 Durometer 3 shim	341 (52.6)	314 (48.4)	384 (59.3)	430 (66.9)
54 Durometer 6 shim	1032 (159)	984 (152)	1173 (181)	836 (130)
69 Durometer 3 shim	446 (68.8)	411 (63.4)	413 (63.7)	468 (72.7)
69 Durometer 6 shim	1413 (218)	1342 (207)	1329 (205)	1087 (169)

* Shear moduli used in Equations 4.4, 4.5 and 4.6 were as determined from full-scale shear modulus tests

Other than for the most axially stiff designs, all methods give a reasonably accurate estimate of the rotational stiffnesses determined in the laboratory. AASHTO's equation is no exception, giving good results for the lower shape factor but poor results for the higher shape factor. Overall however, there are significant differences between test and theory; generally, the theory overestimates the bearing stiffness for higher shape factors.

By current AASHTO Specifications, rotations for the 6 steel shim nominal 0.7 MPa (100 psi) bearings tested in this study would be restricted to approximately 0.010 radians. As shown in Section 4.3, these bearings were subjected to rotations of as much as 0.03 radians with no adverse effects noted. As described in Chapter 1, the basis for the current AASHTO limitations on shear, compression and rotation is given by the following relationship (25):

$$\gamma_s + \gamma_c + \gamma_r \leq 3.0 \quad (4.8)$$

This relationship requires that the total amount of shear strain from all sources be limited to 3.0. Since the current limitation on shear strain due to shear is 0.5, the strain due to compression and rotation combined must be limited to 2.5 (according to AASHTO). The shear strain due to compression can be expressed by the following relationship (25):

$$g_c = 6 S e_c \quad (4.9)$$

For the 6 shim bearings (S = 10.96) described above, the compressive strain at 6.9 MPa (1000 psi) is approximately 2.5 %, yielding a shear strain due to compression of 1.64. Assuming the maximum shear strain due to shear (0.5), the shear strain due to rotation would be required to be less than 0.856 to conform to basis for the AASHTO Specification. The shear strain due to rotation can be expressed as (25):

$$\gamma_r = C_r S \theta \frac{L}{2h_{rt}} \quad (4.10)$$

where C_r is a constant, the value of which is dependent upon the bearing's length to width ratio. For the bearings used in this study, the value of C_r is 3.13. Setting γ_r equal to 0.856 and solving for θ using $h_{rt}=44.5$ mm (1.75") and $L=229$ mm (9"), the allowable rotation for the bearing is 0.010 radians. If there were no shear strain due to shear (as in the rotational stiffness tests), the allowable rotation would have been 0.015 radians. Therefore, the bearings tested in rotation at 6.9 MPa (1000 psi) compressive stress were subjected to rotations 2 times that deemed allowable by AASHTO with no damage noted. A computation of the actual shear strain in a bearing of the same design as those tested here undergoing a rotation of 0.03 radians, a shear deformation of 50% h_{rt} and a compressive stress of 6.9 MPa (1000 psi) yields a magnitude of 4.73. Although this exceeds the current AASHTO limit, both British and European international codes have allowed this magnitude of shear strain (33).

4.4 DISCUSSION OF STIFFNESS TEST RESULTS

Shear Modulus/Stiffness Tests

Manufacturing - Although manufacturers appear to be more comfortable quoting hardness rather than shear modulus, they were capable of providing the requested shear modulus at the low value with a good degree of accuracy. It is interesting to note that three different manufacturers all were able to supply 0.7 MPa (100 psi) shear modulus material within about 13 percent at three different either nominal or actual hardness ratings. (Durometer/Shear Moduli averages were: Manufacturer A - 65 durometer/0.680 MPa (98.6 psi); Manufacturer B - 57 durometer/0.604 MPa (87.5 psi); Manufacturer C - 54 durometer/0.602 MPa (87.3 psi)). However, manufacturers were not capable of producing the requested higher shear modulus material with any degree of accuracy. The user should assume that even when the manufacturer is well practiced in producing bearings with a specific shear modulus, a variation of ± 5 % from bearing to bearing should be expected and is certainly not detrimental.

Effect of Tapering - Taper does not appear to have any effect on the shear modulus of the bearing at least at lower hardness ratings. In these tests, only the 69 durometer tapered bearings showed any measurably different performance from comparable flat bearings. In none of the tests under matched or mismatched slope conditions did any of the tapered bearings show any tendency whatsoever to slip.

Shape Factor - Although the literature claims that shape factor should have no influence on shear modulus, both the experimental and analytical studies showed an increase in shear modulus with an increase in shape factor. One reason for this might be that at 50% strain, the specimens with only 3 shims were not sheared to the point where the shims would start bending significantly and providing any measurable resistance to the horizontal force. This is not the case with the 6 shim specimens which displayed steel shim bending early in the shear strain cycle. Additionally, the elastomer layer between the steel shims is much thinner in the 6 shim specimens than in the 3 shim specimens. If the elastomer between the steel shims is considered bonded, from the materials properties tests performed by Ardizoglou (1), it would be predicted that the thinner layers would produce the higher shear modulus. In any case, although lower shear modulus is more desirable, the higher shape factor does not increase the stiffness more than about 7% which is not appreciable.

Non-Uniform Loading - Non-uniform loading tends to decrease the shear modulus of the bearing and produce a gap between the top of the bearing and the bottom of the girder. This effect is greater in bearings that have greater axial stiffness.

Effect of Compressive Stress - It appears that increased compressive stress would be beneficial insofar as it tends to lower the force produced by the same amount of shearing. Additionally, even though axially stiff bearings displayed difficulty accommodating non-uniform loading at low compressive stresses, when the compressive stress on these bearings is increased, they are less prone to exhibit any gap between the girder and the bearing than when they are loaded non-uniformly under low compressive stress.

Compressive Modulus/Stiffness Tests

Factors Effecting Compressive Stiffness - The greatest influence on compressive stiffness is the shape factor. Increasing elastomer hardness without increasing the shape factor has only a marginal effect on increasing axial stiffness. Although there is an additional cost to the user when shims are added to the design, it is not very large. The 6 shim bearings ordered for this study cost approximately 12% more than the 3 shim bearings.

Effect of Taper - Taper does not appear to have any discernible effect upon compressive stiffness in lower shape factor bearings. As the shape factor increases, the taper appears to cause a lower compressive stiffness and greater deformations. For bearings with a shape factor of 10.96, the loss of stiffness was in the range of 11%, and the additional deformation was in the range of 30 to 60% over the flat design with the 6% tapered bearings deflecting more than the 4% tapered bearings. However, the absolute magnitude of the deformations was only in the range of 1.27 mm (0.50") to 2.54 mm (0.10"), which is not very significant.

Empirical Formula for Compressive Modulus Determination - The most commonly employed formula for compressive modulus (Equation 4.4) gives better results at higher rather than lower shape factors. As the tendency within the past several years has been to design bearings with shape factors over 5, the formula can be used to predict compressive modulus with a reasonably high degree of certainty.

Deformations - The compressive modulus formula cannot precisely estimate the axial deformation at a given stress level because the stress-strain relationship is not linear, especially in bearings with higher shape factors. For this reason, a number of stress-strain relationships are given by various sources and should be used to estimate compressive deformations. Stress-strain relationships for tapered bearings by hardness and shape factor are presented in this chapter.

Rotational Stiffness Tests

Effect of Hardness/Shape Factor on Rotational Behavior - Increasing either of these parameters increases the rotational stiffness and decreases the rotation capacity (except in the case of rotation capacity of low shape factor bearings), a generally undesirable trend. The worst possible rotational behavior performance would be from a high shape factor, high hardness design.

Effect of Compressive Stress - Increasing the compressive stress causes an increase in rotational stiffness and rotation capacity. While increased rotational stiffness may not be desirable, the increase is only in the 10% range but the increase in rotation capacity, which is most definitely desirable, is in the range of 120%. This means that lift-off due to girder rotation is much less likely to occur. For high shape factor bearings made from low durometer material, the effect of increasing the compressive stress is to allow this design to achieve approximately 60% of the rotation capacity of the lower shape factor bearings.

Formulas for prediction of Rotational Stiffness - While not generally published in the most common literature on elastomeric bearings Equations 4.5 and 4.6 given by Lindley (13) and Rejcha (23) appear to give better agreement with the results from this study but the difference between test and theory is about 20%. The AASHTO equation (4.6) gives better results for lower shape factors than it does for higher shape factors.

Limits on Rotation Capacity - From the calculation of rotation capacity and photographic records of the tests, elastomeric bearings can absorb a significantly larger imposed rotation than is suggested by current guidelines. Calculations of the shear strains due to rotation sustained by the bearings tested in this study indicate that the bearings were subjected to 50% more strain than would be allowed by the current AASHTO Specification without observable damage. Furthermore, other codes (33) have allowed rotations and shear strains far in excess of those currently allowed by AASHTO.

Common Factors

Degree of taper - With the exception of compressive deformations, the degree of taper (up to the 5.5% used in this study), did not appear to influence bearing behavior. While there were some differences noted between flat

and tapered bearings overall, the only measurable differences in behavior between 4% nominal and 6% nominal designs was in compressive deformation.

High Hardness Not Desirable - In terms of forces transmitted to the girder and abutment, and in lower rotation capacity, especially at low compressive stress levels, higher hardness material appears to be undesirable.

Benefits of Higher Compressive Stress - Allowing bearings to be subjected to higher compressive stresses appears to have several benefits. The horizontal forces produced through shearing are reduced, the rotation capacity before lift-off is increased, the bearing can adapt to non-uniform loading more readily and a smaller bearing can be used (as long as the situation permits).

Shim Orientation - At least within the limits of this study, (low durometer, 3 steel shim, 6% bearing taper), shim orientation does not appear to have any significant effect upon stiffness behavior. Almost all differences noted between the designs with parallel shim orientation versus radial shim orientation are well within the 5% range and must be regarded as due to experimental margins of accuracy.

Cover Layer Thickness - According to the current AASHTO Specification, the cover layers of the 6 shim (S = 10.96) 0.7 MPa (100 psi) nominal bearings were too thick (6.35 mm (0.25 in)) to carry more than 6.80 MPa (986 psi) because they would bulge excessively and thereby become too highly stressed in shear. In both the shear modulus and rotational stiffness tests, bearings with this design were subjected to 7.59 MPa (1100 psi) routinely and their cover layers never showed any signs of excessive bulging (see Figures 4.9, 4.23, and 4.25). Additionally, the same bearings were subjected to 13.8 MPa (2000 psi) in the compression stiffness tests and the cover layers still did not show any excessive bulging (see Figures 4.12 and 4.14). In many cases, the cover layers were fabricated as much as 2.54 mm (0.10 in) thicker than specified yielding layers of 8.89 mm (0.35 in), but were not observed to bulge excessively.

CHAPTER 5

COMPRESSIVE CREEP BEHAVIOR

Compressive creep is an important consideration in bearings constructed of elastomers because of the well-recorded propensity for these materials to exhibit creep behavior and the long-term nature of the bearings' use. Although creep must be factored into the design, results from this study will show that compressive creep in reinforced bearings will not become a critical consideration.

5.1 TEST PROGRAM

One bearing of each design from each manufacturer was subjected to a constant compressive pressure of 5.17 MPa (750 psi) for two weeks to determine its long-term creep behavior. Pressure was applied by an 8900-kN (2000-kip) hydraulic ram shown in Figure 5.1 and was kept steady by the same type of constant pressure system used in the shear test apparatus (see Figure 2.3). An aluminum shim was used to match the slope of the bearing when tapered specimens were tested.

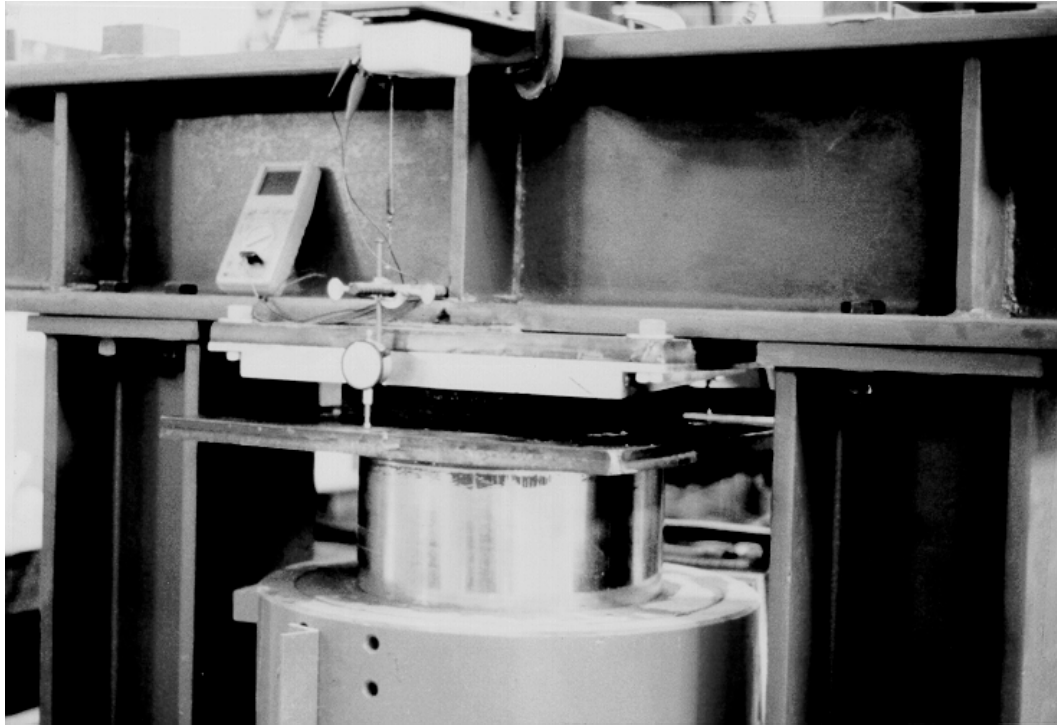


Figure 5-1 Compressive creep apparatus

The specimen was positioned in the apparatus and the platen was raised by a hydraulic pump until the bearing could not move freely. The hydraulic pump was then disconnected from the system and the long-term pressure was applied instantaneously by the dead weight system. The instantaneous deformation was measured with 3 dial gages and a electronic motion transducer and averaged to determine a final value. Deformation readings were taken each minute for the first ten minutes, then at 15, 20, 30, 45, 60 and 90 minutes. Additional readings were taken each hour for several hours during the first day and then once every 24 hours thereafter. Creep at any time was determined by dividing the change in deformation by the instantaneous deformation to obtain a value for creep in percent of initial deformation. Figures 5.2, 5.3, and 5.4 show various representations of creep behavior for a 55 durometer 6% tapered bearing with three reinforcing steel shims. Figure 5.2 is a standard creep plot while Figures 5.3 and 5.4 show the two methods which were used in this study to predict long-term creep. Those methods are described below:

Logarithmic Prediction

A plot of creep (percent of initial deformation) against time in hours on a logarithmic scale is shown in Figure 5.3. Although some sources (6,13) claim that creep deformation is linear when plotted against time on a log scale, this behavior was rarely observed beyond the one-hour reading in the vast majority of the tests. Therefore,

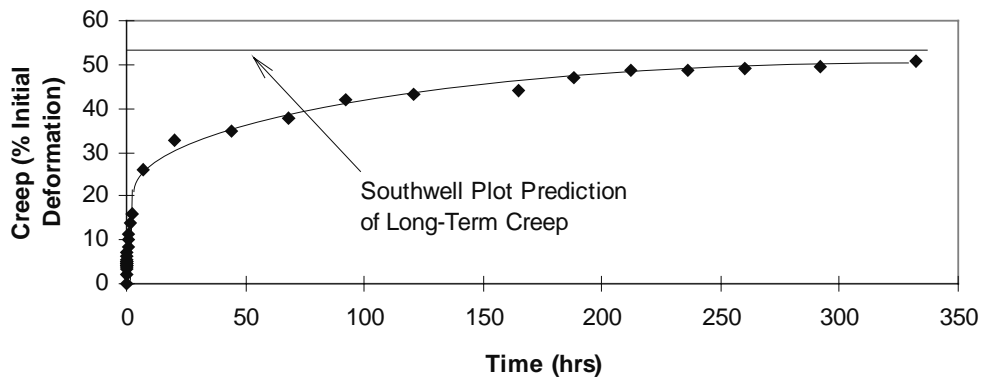


Figure 5- 2 Standard creep relationship

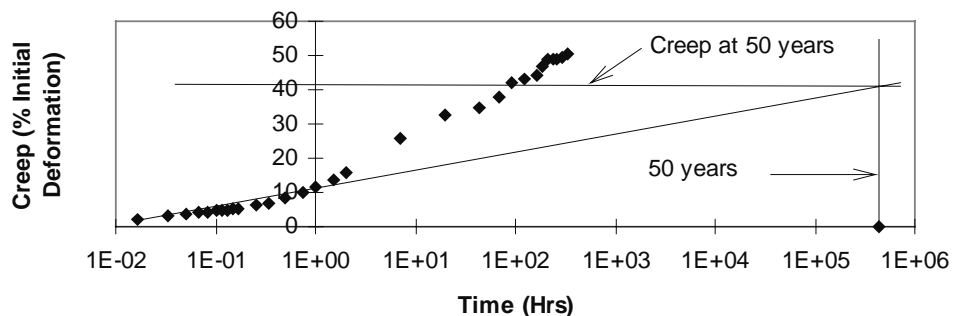


Figure 5- 3 Logarithmic prediction of long-term creep

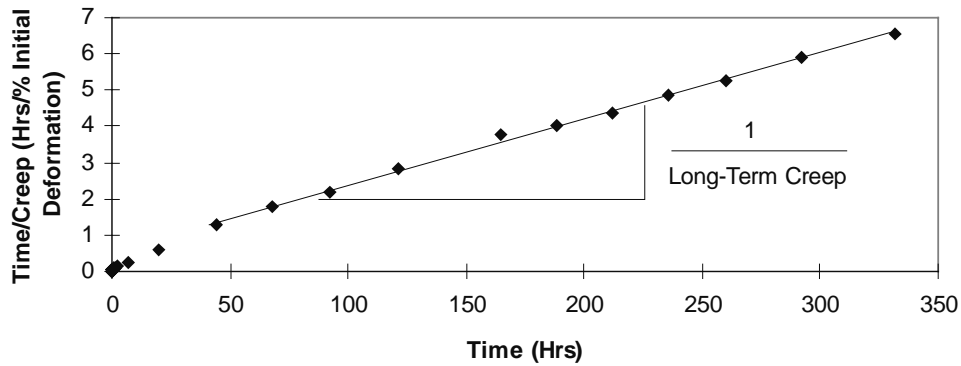


Figure 5-4 Southwell plot prediction of long-term creep

determination of the slope of the line used to predict 50-year creep deformation was limited to creep values between one minute and one hour only. The points between time equal to one minute and time equal to one hour were used to calculate the slope of the line and the creep value corresponding to one hour was used as the y-intercept for extrapolating the value of total creep at 50 years.

Southwell Plot Prediction

The Southwell plot, a method generally used to predict buckling loads, gives time divided by cumulative creep at that point plotted against time as shown in Figure 5.4. The inverse of the slope of this line was taken as the long-term creep prediction. For the vast majority of tests, this relationship showed excellent linearity from the 50-hour mark onward, varying only a few percentage points from day to day through the end of the test period.

According to theoretical analysis (39) the Southwell plot should be capable of predicting the true buckling load within 3% as long as the applied load is 80% of P_{cr} . In the case of long-term creep prediction, provided the test continues to the point where more than 80% of the total creep is realized, the Southwell plot should predict the true creep value within 3%. In tests performed by duPont over several years (7), it was concluded that 85% of the long-term creep in elastomeric pads is realized within two weeks of initial loading. Thus, the Southwell plot should provide a highly accurate method of predicting long-term creep behavior.

5.2 TEST RESULTS

Analysis of Creep Deformations

Table 5.1 gives a summation of the actual creep deformations recorded during the 2-week tests by category. (54-57-durometer and 69-70-durometer specimens are grouped into 55- and 70-durometer categories respectively). The results are reasonably consistent and the data show very little scatter.

The only major trend that is illustrated above is the difference between the 3 shim and the 6 shim bearings, the creep deformation of the former being approximately 3.5 times that of the later. Lower shape factor tapered specimens displayed 14% more creep deformation than comparable flat specimens while 55- durometer specimens deformed about 20% more than comparable 70-durometer specimens. Neither of these comparisons is significant in light of the actual magnitude of the deformations.

Table 5-1 Two-week creep deformations

Bearing Design	Total Creep Deformation After Instantaneous mm (inches)	
	3 Shim	6 Shim
All	1.242 (0.0454)	0.358 (0.0130)
Flat	1.135 (0.0421)	0.355 (0.0133)
Tapered	1.283 (0.0481)	0.361 (0.0128)
55 Durometer	1.275 (0.0502)	0.355 (0.0142)
70 Durometer	1.201 (0.0417)	0.363 (0.0120)

Influence of Shape Factor on Compressive Creep Behavior

Table 5.2 shows an average of compressive creep predictions in terms of percent of initial deformation predicted by both methods described above according to shape factor. Results reflect tests at all hardness values and without regard to degree of taper.

Table 5-2 Influence of shape factor on long-term compressive creep behavior

Number of Reinforcing Shims (Shape Factor)	Long-Term Creep Deformation (% Initial Deformation)	
	Logarithmic Prediction	Southwell Plot Prediction
2 (4.69)	52.0	46.0
3 (6.26)	34.8	44.8
6 (11.0)	10.9	16.2
Ratio 6 Shim:3 Shim	0.31	0.36

Figure 5.5 shows creep curves for a 3 and a 6 shim specimen on an absolute scale including initial deformations.

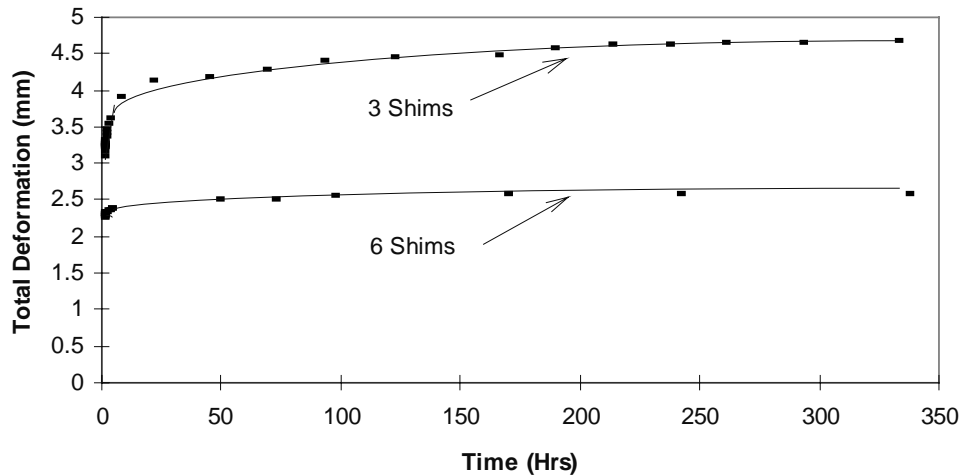


Figure 5-5 Comparison of total compressive deformation in 3 versus 6 shim specimens

The results show that shape factor has a clear effect upon long-term creep. The only reference to this behavior is that in the AASHTO Specification (32) where it is stated that plain bearings creep more than reinforced ones due to slip at the interface. However, Figure 5.5 illustrates very clearly that the absolute magnitude of the deformations for the two shape factors is still quite small. Considering that the magnitude of the initial deflection for these shape factors at 5.17 MPa (750 psi) is between 1.91 mm (0.075 inches) and 4.45 mm (0.175 inches), the difference in methods yields an extremely small variation on an absolute scale -- 0.267 mm (0.0105 inches) for the lowest shape factor and 0.109 mm (0.00420 inches) for the highest shape factor.

Influence of Hardness on Compressive Creep Behavior

Table 5.3 below shows test results according to hardness (3 and 6 reinforcing shim specimens have been averaged together within hardness ratings to achieve the greatest number of samples). As reported earlier in this study, because all of the specimens from Manufacturers B and C were delivered at approximately 55 or 70 durometer, results from the tests are averaged within those hardness values.

Table 5- 3 Influence of hardness on compressive creep behavior

Hardness	Long-Term Compressive Creep Deformation (% Initial Deformation)	
	Logarithmic Prediction	Southwell Plot Prediction
55 Durometer	28.2	30.5
70 Durometer	18.4	30.6

The results show good agreement between the two methods except in the 70-durometer category. The reason for this discrepancy is that the 70-durometer specimens displayed much less creep during the first hour of the test than did the 55-durometer specimens. When long-term creep was estimated by the Southwell plot method, the results showed that durometer had no clear effect on creep behavior with the both hardnesses creeping similarly in both 3 and 6 shim specimens. Other studies (6,7) have shown that creep is greater in harder elastomers because the initial deformation is lower and the actual long-term deformation is very similar. Thus, as a percentage of initial deformation, harder elastomers creep more.

Influence of Taper on Compressive Creep Behavior

Table 5.4 shows the results of the creep tests sorted by bearing cross-sectional geometry and by shape factor. No differences were noted in the creep behavior of the nominal 4% specimens versus the nominal 6% specimens, therefore these tests were averaged together into one “tapered” category.

Table 5- 4 Influence of bearing taper on compressive creep behavior

Cross-Section	Reinforcing Shims (Shape Factor)	Long-Term Compressive Creep Deformation (% Initial Deformation)	
		Logarithmic Prediction	Southwell Plot Prediction
Flat	3 shim (6.26)	38.2	40.0
	6 shim (11.0)	13.4	15.3
Tapered	3 shim (6.26)	32.9	48.2
	6 shim (11.0)	9.5	16.7

The two methods show good agreement when predicting the behavior of the flat bearings, but not in predicting the behavior of the tapered specimens. In Chapter 4, it was shown that tapered bearings deflect slightly more than flat bearings, with the 6 shim tapered specimens displaying a greater increase over their flat counterparts than did the 3 shim tapered specimens. When the creep deformation after the first hour (which is comparable for both flat and tapered specimens) is divided by the instantaneous deformation (which is greater for the tapered specimens), the logarithmic method predicts a lower long-term creep for tapered bearings. The Southwell plot method however takes into account the total creep deformation over the two week test period and shows that tapered specimens actually do creep slightly more than flat ones with the lower shape factor creeping more than the higher ones which is consistent with results previously discussed.

5.3 DISCUSSION OF CREEP TEST RESULTS

Overall, long-term creep predictions from the Southwell plot method as well as from simply calculating the two week creep deformation as a percentage of the instantaneous deformation and dividing that number by 0.85 gave reasonably consistent results and also good agreement with published data on creep behavior. Predictions from the logarithmic extrapolation method were generally reliable, but there was a great deal of scatter in the data. In some cases, the points taken between one minute and one hour were not linear, and in others they predicted either a very low or very high long-term value. For several tests, due to very slow creep during the first hour, this method predicted long-term creep deformations that were less than those which actually occurred after two weeks. When averaged, the results from the logarithmic predictions appear reasonable, but for any given test, they could differ from the Southwell plot method results by 100%. Therefore, if the logarithmic prediction method were to be used, it would be recommended that a number of tests be performed on similar specimens and that the results of those tests be averaged to achieve the most accurate estimate of the long-term value.

Test results were reasonably consistent with published data from other studies (6) as shown in Table 5.5. The results given measure creep as a percentage of instantaneous deformation.

Table 5- 5 Comparison of creep test results

Hardness	Experimental Test Results*		duPont (AASHTO) (Plain Pads Only)	CALTRANS (Reinforced Pads)
	3 shim	6 shim		
50			25	
55	45	16		25
60			35	
70	45	16	45	
* Southwell Plot results only, tapered and flat specimens averaged				

The reference (6) did not state the shape factor for the CALTRANS study which was performed on full-size specimens with both steel and fiberglass reinforcement, but the compressive stress of 6.9 MPa (1000 psi) was comparable to that used in this report -- 5.17 MPa (750 psi). No shape factors or compressive stresses were given for the duPont study which was performed in the 1950's and is used as the official AASHTO guideline for estimating long-term creep deformations according to the most current specification.

Design Implications

As shown by the test results presented above, compressive creep does not need to be a major consideration on the part of the bearing designer for shape factors comparable to those cited in this study. The magnitude of the long-term creep deformation represents an extremely small additional compressive deformation above that which occurs instantaneously. Higher shape factor bearings exhibit less long-term creep than do lower shape factor bearings, but there does not appear to be any significant difference in performance between similarly

reinforced bearings of different hardness ratings (although other sources give a greater creep deformation for elastomers of higher hardness) or between flat and tapered designs. Overall, creep must be considered in a thorough design but due to its very small magnitude will most likely not influence the outcome.

CHAPTER 6

FATIGUE TESTS

During its service life the typical bearing may be subjected to thousands of shear and compression fatigue cycles. Shear fatigue occurs primarily as a result of thermal expansion and contraction while compression fatigue is a result of traffic loading, particularly heavy truck traffic. Elastomeric bearing should be capable of resisting fatigue loading without excessive degradation of performance and without significant physical damage. Replacing “worn out” bearings is not a desirable task. To determine the optimum design for resistance to fatigue loadings, specimens were subjected to repeated shear and compression loadings that were designed to exceed those expected in the field. A total of 24 fatigue tests were conducted, 12 shear fatigue and 12 compression fatigue.

6.1 SHEAR FATIGUE TESTS

Although traffic loading also results in shear stress to the bearing when repeated stopping and starting is considered, the thermal expansion and contraction of the bridge girders which is of a much greater magnitude must be considered the major source of shear fatigue. While current specifications allow shear strains up to 50%, this limitation takes into consideration all expansion or contraction during the entire service life of the bridge including creep and shrinkage as well as yearly thermal extremes. Therefore, on a daily basis, it would be expected that bearings are sheared through a much lesser percent strain. In field studies associated with the project, daily shear strains in the range of less than 20% were typical. To ensure that specimens tested during this study were subjected to the most rigorous standards, however, a daily shear strain of 50% was presumed for the entire service life of the bearing.

6.1.1 TEST PROGRAM

One set of bearings representing each possible design (shear modulus, taper, shape factor) was subjected to 20,000 cycles—which corresponds to a 55-year service life—at 50% shear strain under 3.45 MPa (500 psi) compressive stress to observe their tendency to delaminate or crack. Load-displacement measurements were taken throughout the test to determine if the specimen lost shear stiffness during the course of the repeated cycling. Figure 6.1 shows the shear fatigue apparatus used in this study. The shear strain was imposed by a double-acting hydraulic ram regulated by an electronic load controller, which was adjusted to maintain a constant sinusoidal load at a rate of 0.2 cycles/second. Because the control unit was load sensitive, a motion transducer was connected to the middle platen and the maximum load setting was adjusted until the specimen strain was at 50% in either direction. Due the difficulty of maintaining a constant compressive stress while the bearings were shearing, pressure maintaining system similar to that described in Chapter 3 was employed and can be observed in Figure 6.1.

One 229-mm x 711-mm (9” x 28”) was cut into three 229-mm x 229-mm (9” x 9”) sections for fatigue testing. Steel shims were intentionally exposed so that any delamination would be readily observed. Two sections were tested simultaneously in shear fatigue and the third in compression

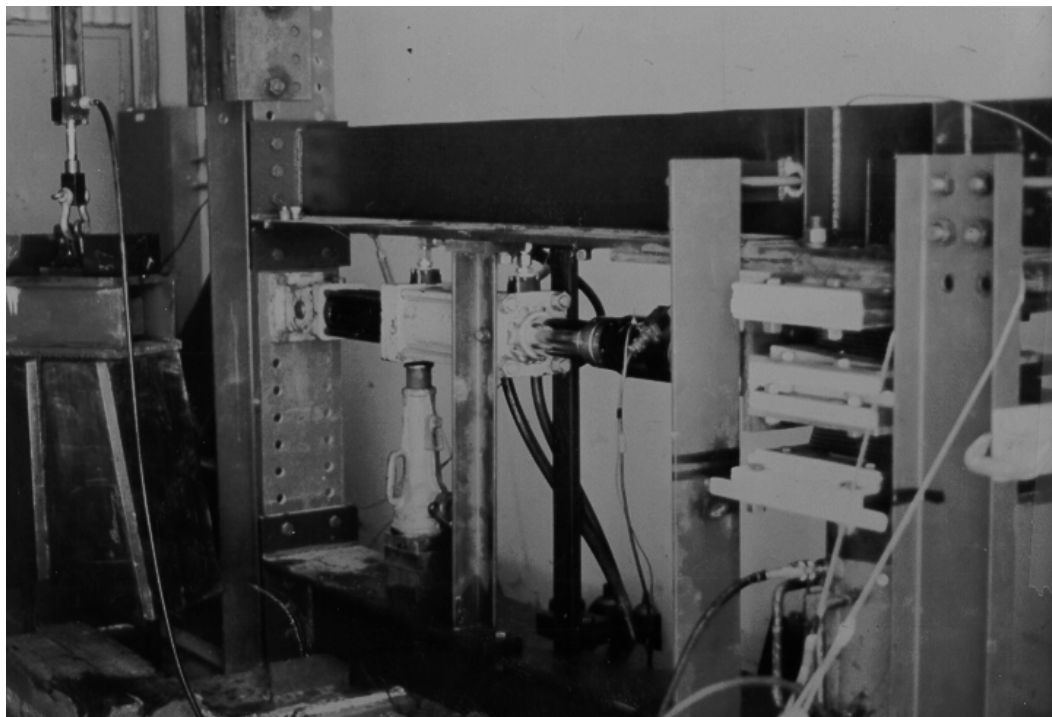


Figure 6-1 Shear fatigue apparatus

fatigue. Prior to testing, each specimen was thoroughly examined for pre-existing flaws which were noted so as not to be assumed as being caused by fatigue loading when the tests was completed. Specimens were bonded on their bottom surfaces with epoxy to 6.35-mm (0.25") steel plates to preclude their slipping during the test and then positioned in the test apparatus as shown in Figure 6.2. For tests on tapered specimens aluminum shims which matched the slope of the bearings were employed. The compressive force was then applied via the dead weight hydraulic system.

Immediately upon starting the test, the total load and actual displacements from -50% to +50% strain were recorded to obtain a starting shear stiffness for the specimen. These measurements were repeated throughout the test (which normally lasted approximately 28 hours) and recorded to keep track of shear stiffness loss.

6.1.2 TEST RESULTS

Fatigue damage

Throughout the testing, the specimens were visually examined for damage due to shear fatigue. No cracking of the elastomeric material itself was ever noted in any of the tests. In fact, one specimen, prior to the start of the test, was discovered to have an elliptical shaped flaw in the elastomer which was measured precisely during the inspection and was found not to have increased in size after being subjected to 20,000 shear cycles. The only physical damage to the bearings was "fretting" of the elastomeric material on the top and bottom surfaces due to the repeated rubbing against the platens. Figure 6.3 shows typical "fretting" damage on the surface of a test specimen.

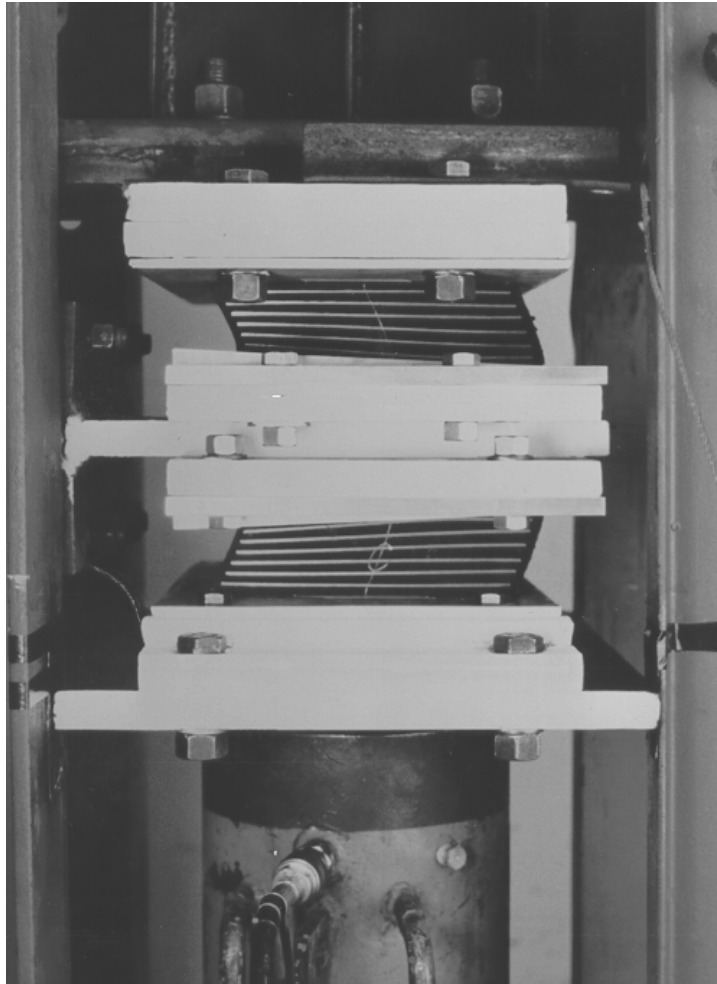


Figure 6- 2 Bearings in shear fatigue apparatus

Loss of Shear Stiffness

Shear stiffness loss was noted and is shown in Table 6.1.

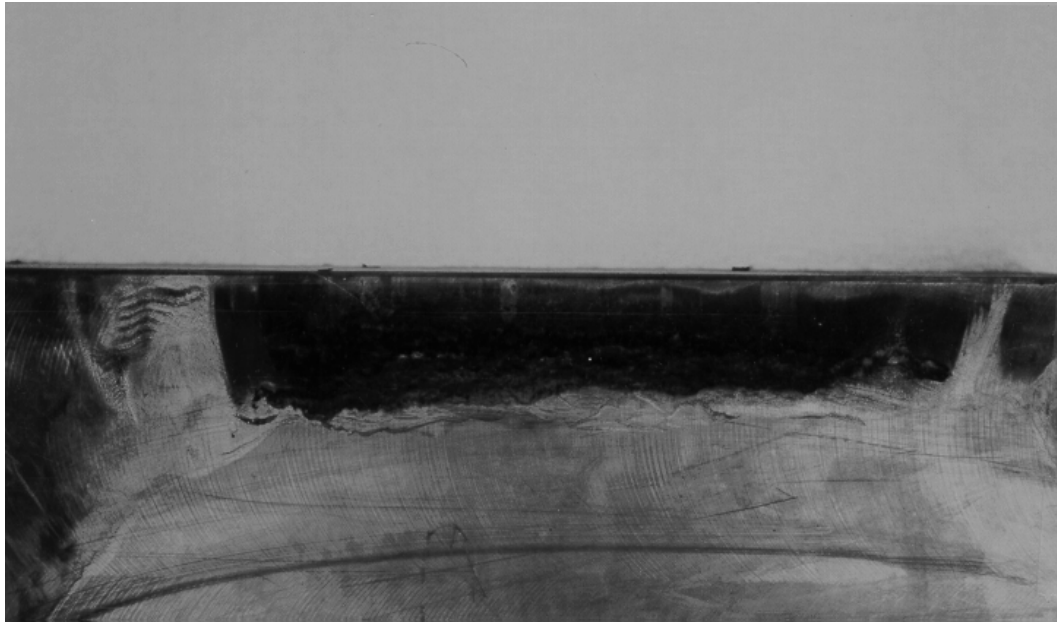


Figure 6-3 Fretting damage on bearing surface

Table 6-1 Loss of shear stiffness due to shear fatigue loading

Design Parameters	Loss of Shear Stiffness (%)
3 Steel Shims*	7.3
6 Steel Shims*	7.5
Flat	5.6
Tapered	8.1
55† Durometer*	3.4
70‡ Durometer*	10.8
Average	7.4
* all flat and tapered specimens, † all 54-57 durometer specimens, ‡ all 69-70 durometer specimens	

A degree of stiffness loss is expected as a result of repeated shearing due to the breaking of molecular bonds between polymers. The results show that the only obvious influence upon loss of shear stiffness during fatigue loading is hardness (shear modulus) which should not be surprising given that the harder specimens have a higher shear stiffness to start with and therefore can realize the greatest reduction. Although the results above show that tapered bearings lost more stiffness than flat bearings, the difference is not significant enough to show a real trend.

6.2 COMPRESSION FATIGUE TESTS

The source of compression fatigue loads is heavy truck traffic. During the service life of a bearing, millions of cycles of such loading may be realized. The magnitude of the stress above that which is caused by dead weight, assuming that the entire load from one half of a 142-kN (32-kip) axle is applied to one bearing which is 229 mm x 559 mm (9"x22"), is in the range of 0.557 MPa (80 psi). Therefore, a representative compression fatigue test would consist of several million interval loads at a low compressive stress range. Since this was not practical, tests performed in this study were designed to be as conservative as possible and subjected specimens to much greater stress ranges at higher frequencies for fewer cycles. Clear differences in performance between bearing designs were noted.

6.2.1 TEST PROGRAM

One bearing representing each possible design was subjected to 500,000 compression fatigue cycles at a frequency of one cycle per second with a mean stress 6.9 MPa (1000 psi) and a stress range of 6.9 MPa (1000 psi) to observe physical damage and to record loss of compressive stiffness. As in the shear fatigue tests, each 229x229-mm (9"x9") specimen was thoroughly inspected before testing so that damage due to fatigue would be properly catalogued. Specimens were bonded to a 6.35-mm (0.25") steel plate with epoxy cement and then bolted into position in the test apparatus. A compressive load-displacement curve from zero to 13.8 MPa (2000 psi) was recorded before the start of the test. The compressive force was applied via a 3115-kN (700-kip) hydraulic ram regulated by an electronic load controller adjusted for the mean and cyclic loads described above. At the end of each test another load-displacement curve was recorded so that the before and after stiffnesses might be compared. For tests on 4% tapered bearings, an aluminum shim machined to precisely match the bearing slope was employed. For tests on 6% tapered bearings however, rather than using a matched aluminum shim, the same 4% shim was employed to force a relative rotation between the top and bottom surfaces of the bearing in addition to the compressive displacement. As described in Section 4.3, shear strains due to compression and rotation can be calculated. By using Equations 4.9 and 4.10, it was determined that the lower durometer 3 and 6 shim 6% bearings were subjected to a maximum shear strain of 5.33 and 3.86 respectively for 500,000 cycles. The higher durometer 3 and 6 shim bearings realized shear strains of 5.42 and 3.65 respectively. These stresses are far in excess of the current AASHTO limitation.

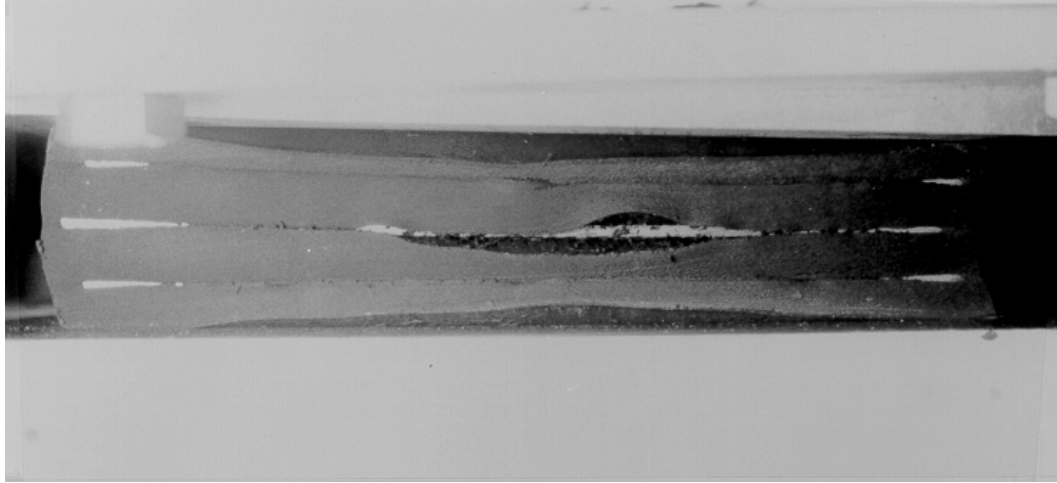


Figure 6- 4 Bearing with three reinforcing shims at 10.35 MPa (1500 psi)

6.2.2 TEST RESULTS

Fatigue Damage

Because all bearings were subjected to the same stresses, the deformations realized by the lower shape factor specimens were far greater than were those realized by the higher shape factor specimens which resulted in significant fatigue damage to bearings with 3 steel shims but no observable damage to those with 6 steel shims. Examples are shown in Figures 6.4 and 6.5.

Typically, extensive delamination was noted in the 3 shim specimens at approximately 250,000 cycles, but in some cases as early as 150,000 cycles. No delamination was ever noted in the 6 shim specimens.

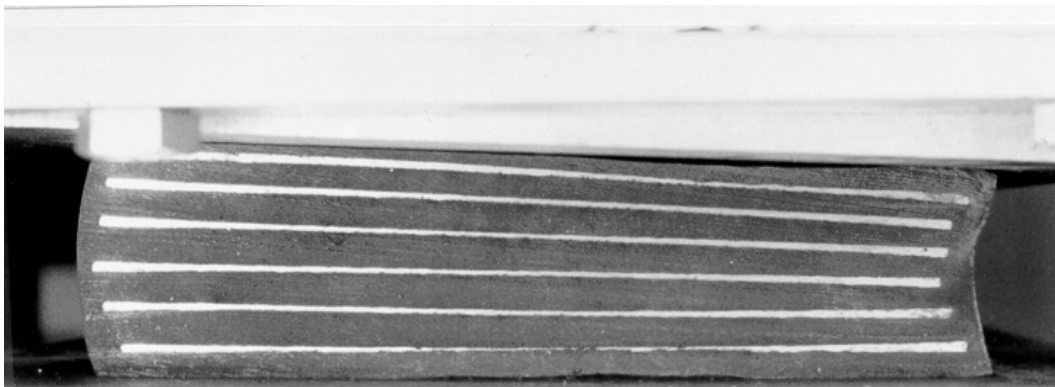


Figure 6- 5 Bearing with six reinforcing shims at 10.35 MPa (1500 psi)

Table 6-2 *Loss of compressive stiffness due to compression fatigue loading*

Design Parameters	Loss of Compressive Stiffness (%)
3 Steel Shims*	13.5
6 Steel Shims*	3.8
Flat	6.6
Tapered	9.7
55† Durometer*	8.2
70‡ Durometer*	9.1
Average All Specimens	8.65

* all flat and tapered specimens, † all 54-57 durometer specimens, ‡ all 69-70 durometer specimens

Loss of Compressive Stiffness

Results of stiffness tests reflect the behavior described above. Table 6.2 shows the loss of compressive stiffness after 500,000 cycles according to the various design parameters.

The results show that the only parameter that has a definite impact upon the loss of stiffness due to compression fatigue loading is the shape factor because of the greater shear strains in the less reinforced bearings. Hardness does not appear to influence the results nor does the reduction in stiffness due to taper appear to be significant enough to cause alarm. As far as the influence of repetitive non-uniform loading is concerned, when the results from the tests on the 4% tapered bearings (which were loaded uniformly) are compared to those of the 6% tapered bearings (which were loaded non-uniformly), the 4% specimens actually lost more stiffness than the 6% specimens. This is probably not the sign of a clear trend, but rather an indication that non-uniform loading has no impact upon loss of compressive stiffness due to fatigue. Following completion of all scheduled tests, a 55 durometer 6 shim 6% taper bearing was tested for an additional 1,500,000 cycles to determine the point at which the more highly reinforced specimens would begin to exhibit fatigue damage. This 6% bearing was loaded non-uniformly with a 4% platen as before so that it would be subjected to fatigue in rotation as well as in compression. For this specimen, at 649,000 cycles, rubber was noted to have started splitting from repeated bulging between the steel shims on one side. At 946,500 cycles, this splitting was noted to have increased and some delamination at the rubber/steel interface was also noted. At 1,373,000 cycles delamination was observed to have progressed to the point where the rubber was bulging 1-2 mm out from around the steel shims at mid-height and -length of the cross-section. From this point through 2,000,000 cycles, the surface area showing this delamination increased to about 50% on both exposed faces. A load-displacement curve was recorded at the completion of 2,000,000 cycles and a 9% loss of compressive stiffness was noted, which is still significantly less stiffness loss than the 3 shim bearings realized after only 500,000 cycles.

6.3 DISCUSSION OF FATIGUE TESTS

Shear Fatigue

Repetitive shear strain does not appear to result in any lasting damage to elastomeric bearings when tested under service stresses. In the worst case, higher hardness bearings lost an average of 10% of their original shear stiffness but there are no detrimental effects upon elastomeric bearing performance due to a small reduction in shear stiffness without delamination. Results of the tests performed as part of this study are consistent with tests performed at the Battelle Memorial Institute in 1970 (17) where neoprene and natural rubber specimens were subjected to 100,000 shear cycles at $\pm 50\%$ strain and research performed at the University of Washington (24) where neoprene and natural rubber bearings were subjected to 20,000 cycles at $\pm 50\%$ strain. Results are shown in Table 6.3. Because specimens in the other studies represented as a more continuous range of hardnesses and shear moduli, the data presented in those studies have been divided as best as possible according to hardness and shear modulus values used in this study so that a better comparison may be made with the results presented herein.

Table 6-3 Comparison of shear fatigue test results

Hardness or Shear Modulus MPa (psi)	Loss of Shear Stiffness (%)		
	Test Results	Battelle Memorial Institute	University of Washington
< 0.69 (100)	3.4	2.0	
50-57 Durometer	3.4		4.1
> 0.69 (100)	10.8	7.0	
58-70 Durometer	10.8		1.4

Compression Fatigue

Compression fatigue loading can result in damage to bearings based upon the tests described above. However, these tests were performed at stress levels that were far in excess of those found under service conditions. Based upon these tests, bearings with a higher shape factor are less likely to suffer fatigue damage because they do not bulge as much under load as do bearings with lower shape factors. This finding is consistent with the analytical study (10) which found that, in 3 shim bearings under pure compression, the elastomer shear stresses at the rubber/steel shim interface were more than twice the magnitude of those in 6 shim bearings. Repetitive non-uniform compressive loading has no adverse effect on elastomeric bearings out of proportion to the damage that would be realized had the bearing been loaded uniformly. Based upon the calculated shear strains due to compression and rotation, a total strain of as much as 3.86 for 500,000 cycles did not result in any observable

damage. In the test program at the University of Washington (24), a compressive fatigue study was performed on flat bearings with shape factors slightly lower than the 3 shim specimens used in this report, all of which had similar hardness ratings (approximately 52). The results of those tests showed that the average loss of compressive stiffness was 11.0% after an average of 1,000,000 cycles at similar mean stresses and stress ranges.

Common Factors

Bearings with tapered elastomeric layers do not realize fatigue damage or loss of stiffness at a rate significantly higher than do bearings with only uniform elastomeric layers.

CHAPTER 7

DETERMINATION OF FAILURE STRESSES

Although failure of elastomeric bearings is much more likely to be defined in terms of deterioration or slipping, the study would not be complete without a determination of the stresses at which failure in the more traditional senses (yield, fracture, etc.) occur. For this reason, a number of tests were performed to evaluate the behavior of the specimens under the greatest possible compressive and shear stresses. Even though tensile forces may be produced in elastomeric bearings due to compression and shear loading, unbonded bearings would never be placed in direct tension and therefore no tests of bearings in tension were performed.

7.1 COMPRESSION FAILURE TESTS

The most current AASHTO specifications allow reinforced elastomeric bearings to be subjected to a maximum compressive stress of 11.0 MPa (1600 psi). The design procedure calls for an analysis of the hydrostatic force produced by the elastomeric material bulging and thereby exerting tensile stresses on the reinforcing steel shims. As long as the shims are thick enough to resist this stress without yielding, the design is acceptable. Compressive failure tests which were intended to identify the stresses at which the reinforcing steel yielded and then fractured were performed on 37 specimens representing a cross-section of the numerous designs examined in this study. Due to the magnitude of the forces required to bring the most axially stiff specimens to fracture, not all of the specimens were taken to this level. The results do however provide a clear basis for comparison of the influence of various design parameters upon the bearings' ability to resist substantial compressive stresses. In addition to testing reinforced bearings, two plain specimens were also tested to observe the behavior of the elastomer itself when subjected to the most extreme compressive forces possible.

7.1.1 TEST PROGRAM

Figure 7.1 shows the compression failure test apparatus which consisted of an 8900-kN (2000- kip) hydraulic ram attached to a self-reacting steel frame capable of withstanding the maximum force that the ram could apply. A fixed steel upper platen was bolted to the ram piston and a steel lower platen was bolted to the heavily reinforced concrete pedestal as shown below.

One 229-mm x 711-mm (9" x 28") bearing was cut into three 229-mm x 229-mm (9" x 9") specimens, each of which was subjected to increasing compressive force until the reinforcing shims fractured, the elastomer debonded from the steel shims or split, or the capacity of the test machine was reached. For tests on tapered specimens, a machined aluminum shim was bolted to the upper platen. Tapered bearings were subjected to compression under matched slope and intentionally mismatched slope conditions to determine the effects of non-uniform loading (4% bearings against 6.25% platens and 6% bearings against 4.17% platens). Compressive force was determined by multiplying the ram area by the hydraulic line pressure measured by a pressure transducer. Vertical deflection was measured by a linear potentiometer. Data were recorded by computer data acquisition system.



Figure 7- 1 Compression failure test apparatus

7.1.2 TEST RESULTS

Unreinforced Bearings

The first tests were performed on unreinforced specimens to observe whether permanent material damage could be caused through excessive compressive loading. Figure 7.2 shows an unreinforced bearing loaded to approximately 31.0 MPa (4500 psi).

Figure 7.3 shows the accompanying stress-strain curve for the plain pad 229 mm x 356 mm x 46.5 mm (9"x14"x1.83"). The relationship shows that after the compressive stress reached 13.8 MPa (2000 psi), there was very little additional deflection despite a more than doubling of the stress.

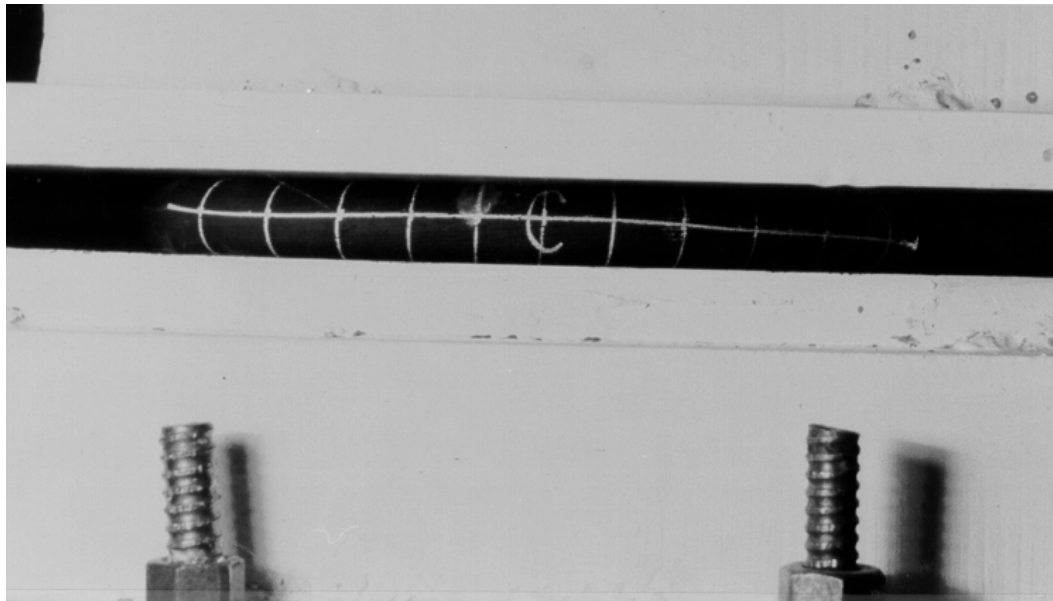


Figure 7-2 Unreinforced bearing under 31.0 MPa (4500 psi) compressive stress

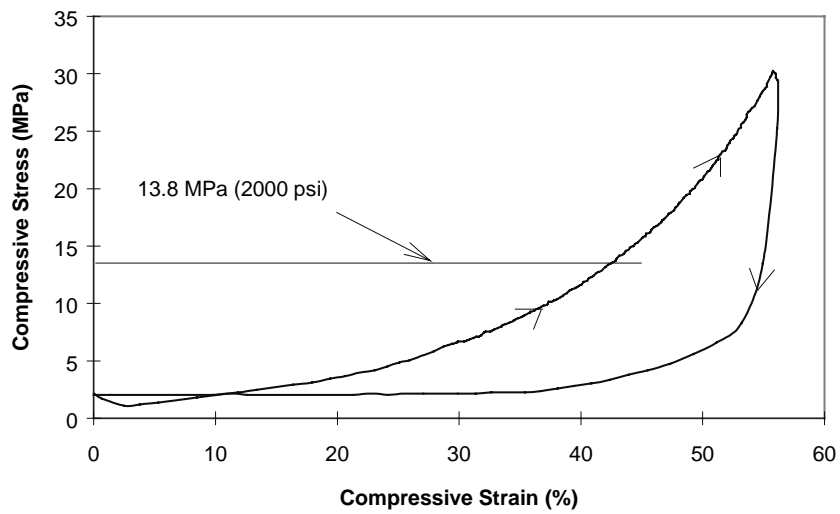


Figure 7-3 Stress-strain relationship for a plain pad loaded to 31.0 MPa (4500 psi)

At a certain point, the material appears to become practically incompressible. When unloaded, the specimen showed no sign of any damage or permanent deformation and appeared to regain its original shape immediately.

Reinforced Bearings

Subsequent tests on reinforced bearings gave a wide variety of results. The best conclusion which can be reached is that while one can expect comparable results from each specimen cut from the same original bearing, there need not be any similarity between bearings of similar designs, nor is there any predictable trend by which to predict the failure mechanism. Reinforcement yielding, and fracture, as well as delamination and elastomer tearing appear to be functions of the individual bearing at higher compressive stresses, but a reasonable conclusion can be made as to a minimum expected safe level of compressive loading. Figure 7.4 shows a reinforced bearing stress-strain relationship that includes a number of the failure mechanisms observed during these tests. At first, the bearing shows a reasonably linear stress-strain relationship. At approximately 55.2 MPa (8000 psi) the slope decreases. This was interpreted as the point where yielding of the steel shims became significant enough to cause a decrease in compressive stiffness. The same interpretation was made by researchers at The University of Washington (33). At 86.2 MPa (12,500 psi) and at 105 MPa (15,250 psi) sharp drop-offs in the stress with accompanying increases in strain occurred, which were interpreted as signifying elastomer tearing or debonding along the rubber/steel interface. In most cases, debonding was easily observed with specimens still in the test machine. At very high stress levels, even if debonding has occurred in some regions, where the elastomer/steel bond is still intact, the reinforcement approaches fracture. At 124 MPa (18,000 psi), when fracture finally occurs, a significant drop in the stress is observed, along with a substantial increase in strain.

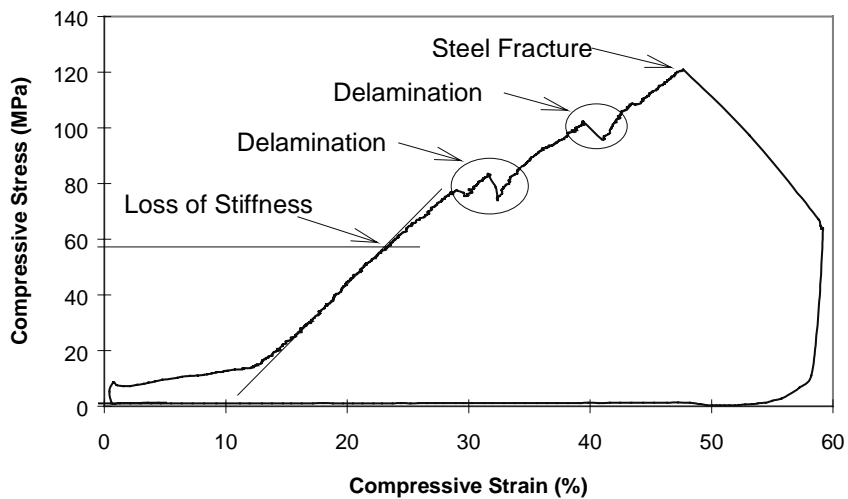


Figure 7- 4 Reinforced bearing compression test stress-strain relationship

Figures 7.5 and 7.6 show specimens with severe elastomer tearing/delamination and with fractured reinforcing steel shims.

A summation of the results from the compression tests on reinforced bearings is presented in Table 7.1. In most cases, specimens with 6 reinforcing steel shims could not be brought to the point of fracture before exceeding the capacity of the test apparatus. It seems reasonably clear that the only *flat and tapered specimens, **not included in ave or other categories, †54-57 durometer specimens discernible trend is that the 2 shim specimens lost stiffness and fractured much earlier than the 3 and 6 shim specimens. Additionally, because both 3 and 6 shim specimens lost stiffness at almost the same stress and fractured at almost the same stress, 6 shim specimens strain less at both levels of stress than do 3 shim specimens. It also appears clear that non-uniform loading does not effect the compression behavior of tapered bearings nor does orientation of reinforcing shims. No real conclusion can be reached concerning the influence of hardness. One reason for tapered bearings appearing to strain more than flat bearings at both stress levels is that the displacement recorded is most likely increased slightly due to the specimen slipping out somewhat during the test.

Comparison of Experimental and Theoretical Results

Equation 2.1 gave an expression for the minimum steel shim thickness required to preclude yielding based upon the design compressive stress for the bearing. Equation 7.1 shows Equation 2.1 rearranged to give the compressive stress required to cause the reinforcing shims to yield in a bearing with shims of a known yield strength and thickness (no factor of safety is included).

$$\sigma_c = \frac{4F_y h_s}{3(h_{r1} + h_{r2})} \quad (7.1)$$

Table 7-1 Results of reinforced bearing compression tests

Design Parameter	Stiffness Loss Stress MPa (psi)	Strain %	Fracture Stress MPa (psi)	Strain %
2 Steel Shim**	45.2 (6550)	35	67.4 (9770)	50
3 Steel Shim*	71.0 (10300)	36	117.2 (17000)	56
6 Steel Shim*	77.9 (11300)	22	128.3 (18600)	36
55† Durometer*	75.9 (11000)	32	118.6 (17200)	52
69 Durometer*	70.3 (10200)	27	122.1 (17700)	47
Flat	70.0 (10000)	25	123.4 (17900)	43
Tapered (all)	76.6 (11100)	33	117.9 (17100)	56
Tapered (non-uniform load)	77.2 (11200)	36	119.5 (17300)	56
Parallel Steel Shims**	82.7 (12000)	40	123.4 (17900)	55
Average	73.7 (10700)	30	120.4 (17500)	49



Figure 7-5 Elastomer tearing/delamination



Figure 7-6 Fractured reinforcing steel shims

where h_s is the thickness of the steel shim and h_{r1} and h_{r2} are the thicknesses of the elastomer layers around the steel. This equation is based upon theory which applies to bearings with $W \gg L$ (25). For bearings with $W < 2L$ (as were all specimens tested here), and also with no factor of safety applied, the theoretical compressive stress to cause first yield is presented by Rejcha (23) as

$$\sigma_c = \frac{F_y}{1.99} \left(\frac{h_s}{h_r} \right) \quad (7.2)$$

where h_r is the thickness of the elastomer layers above and below the steel plate (assuming that the elastomer layers are of equal thickness). Table 7.2 compares the experimental stress at which compressive stiffness loss was first observed and the theoretical value of compressive stress required to cause yield assuming a yield stress of 310 MPa (45 ksi), the average yield stress given in the Mill report from the manufacturer who fabricated the vast majority of the compression test specimens.

Table 7- 2 Comparison of theoretical yield stresses and experimental stiffness loss stress

Number of Reinforcing Steel Shims	Theoretical First Yield MPa (psi)	Experimental Stress MPa (psi)
2 Shim*	35.8 (5190)	45.9 (6650)
3 Shim	37.1 (5400)	71.0 (10300)
6 Shim	64.8 (9410)	77.9 (11300)

* 3.4-mm (10 gage) shims vs. 2.7-mm (12 gage) for 3 and 6 shim specimens

Obviously, the theoretical calculation suggests that yielding will occur much earlier than the observed compressive stiffness loss. This may be due to the fact that the theoretical calculation gives the point at which the stress in the steel plate(s) reaches yield at its center alone. For yielding to progress beyond this point, additional compressive stress would be required. Therefore, it is possible that yielding had begun at the theoretical value of compressive stress but stiffness loss was only noticeable on the stress-strain curve much later. This may account for the fact that several specimens were loaded beyond the theoretical stress values given above and unloaded without observing any permanent deformation. There does not appear to be any other clear explanation of the discrepancy between the values presented above.

7.2 SHEAR FAILURE TEST

Although failure by reinforcing steel yielding or by delamination caused by excessive shear strain is extremely unlikely in elastomeric bearings anchored by friction alone, one such test was performed to evaluate the conditions required to initiate this type of failure.

7.2.1 TEST PROCEDURE

One 70-durometer hardness ($G = 1.19 \text{ MPa}$ (172.5 psi)) 229-mm x 559-mm x 38-mm (9" x 22" x 1.5") natural rubber bearing pad with two 3.18-mm (0.125-inch) steel shims which was removed from service was cut in half and placed in the test apparatus described in Chapter 2. In order to prevent the specimens from slipping against the concrete surface, a compressive stress of approximately 24.1 MPa (3500 psi) was required. The middle platen of the apparatus was translated continuously until the steel reinforcing shims could be visibly observed to bend significantly. Once this occurred, the platen was reversed until the horizontal load was zero and the specimens were removed from the apparatus.

7.2.2 TEST RESULTS

The horizontal force increased linearly up to 111.6 kN (25.1 kips) which corresponded to 150% shear strain. From this point onward, the bearing did not shear any further, but its edges began to roll over severely. Additional horizontal force was applied up to 168 kN (37.8 kips) and the rollover continued to the point where the reinforcing steel had clearly yielded in bending. Figure 7.7 shows one of the specimens after it was removed from the test apparatus.

No elastomer splitting or delamination was noted. Under normal circumstances, assuming a 5.17-MPa (750-psi) compressive stress, a full-sized bearing 229 mm x 559 mm (9"x22"), and a friction coefficient of as much as 0.3, the horizontal force required to shear the bearing to 150%

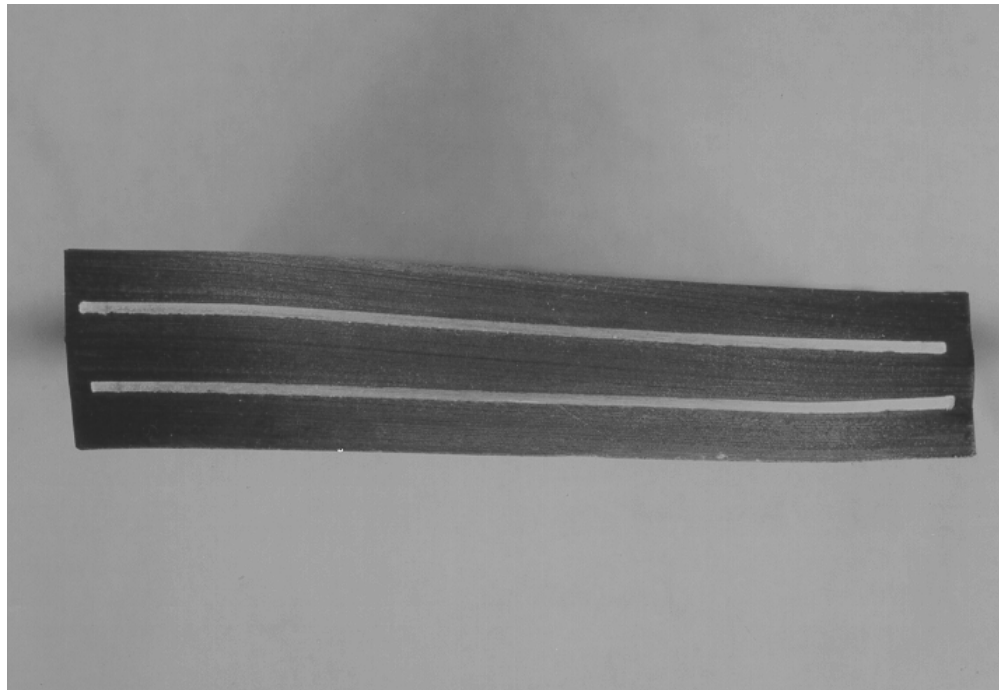


Figure 7- 7 Specimen with steel shims yielded in shear

strain would never have been realized as slipping would have occurred at a much lower strain making steel yield impossible.

7.3 DISCUSSION OF FAILURE TESTS

Compression Failure

Failure of elastomeric bearings in compression is very unlikely given the current compressive stress restrictions given by AASHTO. Tests performed in this study indicate that, as long as the elastomer is well constructed, there will be no delamination prior to yield of the reinforcing. Therefore, the theoretical calculations for the compressive stress required to produce steel yield represent the lowest stress level at which any damage to the bearing would be expected. This is good because it affords the designer the ability to preclude failure due to compressive stress with a reasonably conservative estimate. According to the most liberal design method allowed by AASHTO, the 55 durometer 6 shim bearings tested in this study could be subjected to a compressive stress of 9.31 MPa (1350 psi). During testing, the worst of these bearings did not show any loss of compressive stiffness until the compressive stress reached 59.6 MPa (8640 psi) which is reasonably comparable to the predicted stress level of 64.8 MPa (9410 psi) given in Table 7.2. This represents a factor of safety against compressive failure of more than 6. Clearly, allowable compressive stresses can be increased with very little concern.

Shear Failure

Shear strains much greater than 100% are required to fail a bearing by yielding the reinforcement in bending. Given that only a gross design miscalculation would result in a bearing realizing such strains, failure in shear is a very unlikely occurrence. It is much more likely that slipping will occur before shear failure.

CHAPTER 8

CONCLUSIONS AND RECOMMENDATIONS

8.1 CONCLUSIONS

Based upon the results from this study, the existing literature, and numerous discussions with bearing manufacturers a number of conclusions can be reached regarding the performance of elastomeric bearings under various conditions.

8.1.1 BEARING SLIP

Antiozonant Additives

Waxes used by manufacturers to ensure that natural rubber bearings satisfy the ozone degradation test migrate to the surfaces of the bearings and severely reduce the coefficient of friction against the bearing seat and the girder bottom. In numerous cases where excessive slip has been observed, the bearings concerned have been analyzed and been shown to be saturated with wax. Although waxes are occasionally included in neoprene compounds, neoprene does not require a wax additive to guard against ozone degradation and no neoprene bearings have been observed to walk out. Without the waxy coating, the coefficient of friction of natural rubber against typical concrete surfaces can be conservatively taken as 0.2 and an analysis can be performed to determine the normal force required to prevent slip from occurring. By current specifications covering the bearing manufacturing industry, it would be impossible for the engineer to differentiate between waxes that are the most aggressive in migrating to the bearings' surface and those that migrate less or more slowly.

Contact Surfaces

The nature of the contact surface is a factor that is closely associated with the slip analysis. In tests on both concrete and steel contact surfaces, the coefficient of friction was substantially higher when the surface was roughened and non-glossy. In concrete surfaces, a glossy finish even if rough caused a substantial decrease in the coefficient of friction. Roughened, non-glossy steel or concrete surfaces resulted in friction coefficients well in excess of 0.2.

8.1.2 COMMON DESIGN CONSIDERATIONS

Shear Modulus Determination

A reasonable assumption as to the shear modulus of the bearing can be made from the hardness rating. However, in no way should it be expected that a precise shear modulus can be determined without physical testing. In this study, durometer ratings from 53 to 65 produced shear moduli of 0.586 MPa (85 psi) to 0.70 MPa (100 psi) while durometer ratings of 68 to 72 produced shear moduli of 0.793 MPa (115 psi) to 1.00 MPa (145 psi). There are numerous published guidelines for shear modulus estimation based upon hardness, but the manufacturer is the best source for reliable shear modulus information. The ASTM 4014 shear modulus determination test on plain elastomer

specimens yields very high results compared to those given by direct shear tests of bearings under compressive stresses in the 3.45 MPa (500 psi) to 6.90 MPa (1000 psi) range. This is especially true when the specimens used in the ASTM procedure are small and thin. In this study, bearings made from nominal 0.70 MPa (100 psi) and 1.4 MPa (200 psi) elastomer tested at shear moduli of 0.680 MPa (98.6 psi) and 0.841 MPa (122 psi) respectively. ASTM 4014 tests on the plain elastomer yielded shear moduli of 0.959 MPa (139 psi) and 1.32 MPa (192 psi) respectively when 102 x 102 x 25.4-mm (4" x 4" x 1") specimens were used and 1.02 MPa (148 psi) and 1.45 MPa (210 psi) respectively when 51 x 51 x 12.7-mm (2" x 2" x 0.5") specimens were used. However, if the shear modulus is determined using the linear portion of the load-displacement curve from the ASTM test rather than by the secant modulus procedure, the results are closer to those determined from full scale tests. In this study, when the shear modulus was determined using the slope of the ASTM test load-displacement curve between 20 and 40% shear strain for the 102 x 102 x 25.4-mm (4" x 4" x 1") specimens, the shear moduli were 0.814 MPa (118 psi) and 1.12 MPa (162 psi) respectively. While still high in comparison to the full-scale tests, the results are much closer than those determined by the standard ASTM procedure.

Manufacturing Precision and Accuracy

Manufacturers were fully capable of supplying the requested shear modulus within 13% when asked for 0.7 MPa (100 psi) material. They were not, however, capable of providing material in the 1.4 MPa (200 psi) range as this level is rarely requested. Suppliers were also adept at reproducing the same compound over time so that each bearing produced could be expected to have the same shear modulus $\pm 5\%$. Overall, manufacturers supplied bearings at the correct plan dimensions almost exactly and the correct elastomer thickness within 3.5%, although one entire shipment was fabricated with an elastomer thickness almost 5% higher than requested. Due to the difficulty of positioning steel shims precisely in every bearing, the thicknesses of the various elastomer layers were prone to wider variations. Tapered bearings are generally produced at discrete slopes to limit the manufacturer's inventory of sloped molding platens. The manufacturer can quote the standard slopes available prior to fabrication. In this study, tapered bearings were provided at 4.17 and 5.5% slopes.

Elastomer Hardness

In this study, increasing hardness from 55 to 70 durometer resulted in increased shear stiffness, compressive stiffness and rotational stiffness. However, the percentage increase in compressive stiffness (25%) and rotational stiffness (15%) was less than the percentage increase in shear stiffness (43%). Harder bearings produce a greater horizontal force when sheared, resulting in greater forces being transferred to the bridge abutment and girder. The friction force required to restrain the bearing must be greater, thereby increasing the possibility of slipping. Harder bearings with high shape factors have limited ability to deform axially, and therefore have very little rotation capacity. Harder bearings also tended to lose more shear stiffness in fatigue after 20,000 cycles at 50% strain than did lower durometer bearings. Hardness did not appear to influence creep, loss of compressive stiffness, and fracture point in tests to compressive failure, or loss of compressive stiffness in fatigue after 500,000 cycles at a mean stress of 6.9 MPa (1000 psi) and a stress range of 6.9 MPa (1000 psi). However, there are some beneficial aspects to harder elastomers, which are discussed in Section 8.1.3.

Shape Factor

In this study, increasing the shape factor from 6.26 to 10.96 resulted in increased shear, compressive, and rotational stiffness. The greatest increase was in compressive stiffness (150%) followed by rotation (22%) and then shear (7%). As they were more axially stiff, bearings with higher shape factors showed an average 60% decrease in rotation capacity over those with lower shape factors. The more highly reinforced specimens showed better performance in compression fatigue tests as measured by delamination and loss of compressive stiffness. They tended to creep less under constant compressive load, and withstood more compressive stress before loss of compressive stiffness and fracture in compressive failure tests. Shape factor did not appear to influence loss of shear stiffness in fatigue.

Compressive Stress

During the shear and rotational stiffness portions of this study, specimens were tested at 3.85 and 7.69 MPa (550 and 1100 psi). The effect of increasing compressive stress was to lower the shear stiffness by 6%, increase rotational stiffness by 10%, and increase rotational capacity by 120%. Higher compressive stress also tended to reduce the effect of non-uniform loading. Additionally, greater compressive stress makes bearing slip less likely. (Although the friction coefficient of rubber decreases with increasing compressive stress, the net friction force is greater at higher stress levels than at lower stress levels). Compressive stress was not observed to damage even the most lightly reinforced specimens at levels below 34.5 MPa (5000 psi).

Rotation Capacity

Rotational stiffness tests showed that elastomeric bearings can be subjected to far greater rotations than allowed under the current AASHTO Specifications without sustaining any visible damage. In Chapter 1, Equation 1.7 gave the AASHTO limitation for allowable bearing rotations as twice the compressive deformation divided by the plan dimension perpendicular to the axis of rotation. The intent of this limitation is to ensure that the girder never lifts off from the bearing. Additionally, AASHTO limits the total shear strain in the elastomer from shear, compression and rotation to 3.0 as given in Equation 1.6. Based on the AASHTO Specifications, bearings of both hardness ratings with 6 shims would be allowed rotations of from 0.004 radians (0.235 degrees) at 3.85 MPa (550 psi) to 0.010 radians (0.573 degrees) at 7.7 MPa (1100 psi). During rotational stiffness tests in this study bearings were routinely subjected to rotations of 0.033 radians (1.9 degrees). In no case was there any observable sign of damage to the specimen. Lift-off to a 20-30-mm (0.79-1.2") depth of separation between the bearing surface and the lever arm was noted at a rotation of 0.0176 radians (1.01 degrees) under 3.85 MPa (550 psi) compressive stress for the 69 durometer bearings and 0.0293 radians (1.68 degrees) for the 54 durometer bearings at 7.7 MPa (1100 psi). In none of the tests was any uplift of the bearing from the bearing seat noted although this is cited as one of the key reasons for the restrictive specifications concerning rotations (32). If total shear strain of 3.0 is used as a criterion for limiting compressive stresses and rotations (as is the underlying AASHTO assumption), and lift-off is disregarded, the bearings described above would be allowed to sustain rotations of from 0.011 radians (0.653 degrees) for the 54 durometer bearings at 7.7 MPa (1100 psi) to 0.0212 radians (1.21 degrees) for the 69 durometer bearings at 3.85 MPa (550 psi). If, however, a total shear strain of 5.0 were allowed as in some foreign codes (33) the bearings would be allowed to sustain rotations of from 0.034 radians (1.95 degrees) for the 54 durometer bearings at 7.7 MPa (1100 psi) to 0.044 radians (2.52 degrees) for the 69 durometer bearings at 3.85 MPa (550 psi). There would be, of course, substantial lift-off, but whether or not this would actually cause an eventual

failure in the bearing is subject to interpretation. The magnitude of total shear strain to be allowed for bearings designed in the US can be set at a safe level based upon further testing, but in compression fatigue tests performed in this study, bearings were subjected to 500,000 cycles of combined compression and rotation fatigue at a maximum shear strain of 3.86 with no observable damage.

Steel Shims

Steel shims used in most of the specimens in this study were 2.7 mm (0.1046") thick Grade A570 with $F_y = 276$ MPa (40 ksi). This was the minimum thickness that manufacturers felt confident in using to preclude damage during vulcanization. None of the tests showed any results that would indicate a need to increase the thickness of the shims beyond this size.

Cover Layers

The β -factor, as currently specified by AASHTO, results in an overly conservative design for the cover layers of bearings with high shape factors. For the test specimens used in this study with $S = 10.96$, the elastomer cover layer was approximately 6.35 mm (0.25"). Observation of these specimens during shear modulus tests at 7.69 MPa (1100 psi) showed no indication of excessive bulging of the cover layer. Based on this shape factor, current specifications would have required a β -factor to be applied, reducing the thickness of this layer to 4.52 mm (0.18") to carry the compressive stress. Given the results of physical examinations of the bearings, it is unlikely that the smaller thickness could have been precisely maintained during the fabrication process.

8.1.3 DESIGN OF TAPERED BEARINGS

Maximum Taper

In this study, bearings with 4% and 6% nominal tapers were tested. With the exception of the magnitude of compressive deformations, none of the test results showed any difference in performance between the 4% and 6% specimens even in cases where a difference was observed between flat and tapered bearings. Although no specimens with greater than a 6% taper were tested, this slope is clearly significant and will result in a great deal of horizontal displacement under dead load alone (before thermal expansion or contraction) as explained in Chapter 3. Therefore, extreme care must be taken by the designer to calculate the expected bearing deformation due to taper.

Slope Mismatch

During shear modulus tests, bearings were intentionally compressed against platens that were 1.5% to 2% out of parallel with the bearing surface. Based upon observation of the test specimens subjected to shear strains at 50% elastomer thickness, this degree of mismatching had no obvious detrimental effect upon the bearings' performance. When the mismatch tended to compress the thin end of a tapered bearing or either end of a flat bearing, there was a resulting very thin gap between the platen and the bearing. In the worst case, the length of the gap was measured at approximately 45 mm (1.77") which represented only 20% of the bearing's surface area. This was most obvious in axially stiff bearings at 3.85 MPa (550 psi). When the compressive stress was increased to 7.69 MPa (1100 psi), the gap was almost completely closed.

Compressive Deformations

Tapered bearings deflected more than flat bearings of the same hardness and reinforcement scheme. The magnitude of the additional deformation ranged from 10 to 20% for the 6.26 shape factor specimens and 30 to 60% for the 10.96 shape factor specimens in the 3.45 MPa (500 psi) to 6.9 MPa (1000 psi) compressive stress range. The finite element study by Hamzeh (10) found a 25% increase in deformation for 55 durometer tapered bearings with a shape factor of 10.96. Additional deformations were influenced by degree of taper. For the lower shape factor tapered specimens a 4% bearing deformed approximately 10% more than a flat bearing and a 6% bearing deformed approximately 20% more than a flat design. At the higher shape factor, the 4% bearings deformed close to 30% more than their flat counterparts and the 6% tapered specimens deformed an average of 60% more.

Horizontal Deflections

Tapered bearings deflect horizontally under girder dead load alone. The magnitude of the horizontal deflection can be estimated by calculating the shear deformation which would occur given a shear force of $0.4\theta P$ where θ is the bridge slope and P is the compressive force on the bearing. Additionally, the bearing's critical buckling load must be calculated and the initial deflection magnified accordingly. Harder tapered bearings deform less under dead load than do comparable lower durometer bearings. This is an important design consideration especially when larger slopes are involved. In tests performed in this study, 70 durometer bearings of lower shape factor deflected horizontally 30% less and harder bearings of higher shape factor deflected horizontally 43% less under dead load than did comparably designed 55 durometer bearings.

Orientation of Steel Shims

In all cases but one, steel shims in tapered bearings were oriented radially, with equal spacing at each point along the length of the cross-section. One tapered specimen with shims oriented parallel to one another was tested for comparison to the others. The performance of the specimen with parallel shims was essentially identical to that of the specimens with radial shims with one important exception. As stated above, tapered bearings deflect horizontally under girder dead load in direct proportion to the magnitude of the girder slope and dead load. In tests designed to measure the horizontal displacement under dead load, the specimen with parallel shims displaced 40% less than did the comparable (same slope and shear modulus) specimen with radially spaced shims. This behavior is extremely significant because girders are typically unrestrained horizontally and are therefore free to displace with the bearing. Limiting this displacement to the smallest magnitude possible is highly desirable.

8.2 RECOMMENDATIONS

In light of the conclusions stated above, the following recommendations are made concerning the design and employment of elastomeric bearings.

8.2.1 RECOMMENDATIONS TO PRECLUDE BEARING SLIP

1. Elimination or Relaxation of the Ozone Resistance Specification — There is ample evidence that natural rubber bearings would not be adversely effected if the ozone

specification were relaxed or even eliminated. Previous studies have questioned the effect of ozone on bearings (17,33) and the accuracy of accelerated aging tests (9) and others have shown that ozone damage even after one hundred years of exposure is restricted to only a few millimeters of surface penetration (13). A relaxation of the specification would allow bearing manufacturers to eliminate wax antiozonants and to pass the specification by using chemical antiozonants alone, which do not result in a viscous surface coating and reduction of the friction coefficient.

2. No Surface Coating — Whether the ozone specification is relaxed or not, a simple performance specification stating that no material may accumulate on the surface of the bearing is absolutely essential. As there is almost no way of telling what is actually in the bearing, the designer must require that the surface remain free from any material which could cause a slipping problem to occur. Although the problem has been associated with natural rubber bearings, some manufacturers have stated that it is common practice to include waxes in neoprene even though that material should be able to pass the specification without them. Therefore, banning the use of natural rubber is not a panacea.
3. Bearing Contact Surfaces — Bearing seat concrete surfaces must be rough (wood screed finish) and must not have a glossy finish. Although it would be advisable to roughen the bottom of the girder as well, this may be difficult and not cost effective. Ensuring that the bearing seat is properly finished will at least guarantee that one surface will be slip-resistant.

8.2.2 RECOMMENDATIONS COMMON TO ALL ELASTOMERIC BEARINGS

4. Shear Modulus Determination — The shear modulus of the bearings must be known during the design process. The best way to determine the shear modulus is to test full-scale reinforced specimens in direct shear under the design compressive stress. If this is not possible, the ASTM 4014 test can be performed on the plain elastomer using 102x102x25.4-mm (4"x4"x1") specimens and the slope of the linear portion of the load-displacement curve used to determine the shear modulus. This will give a shear modulus, which exceeds, but is much closer to, that determined in full-scale testing.
5. Hardness/Shear Modulus — From analysis of the results of hundreds of tests and of numerous previous studies, it is recommended that bearing material be of 50 to 55 durometer hardness which commonly results in a shear modulus of 0.55 to 0.66 MPa (80 to 95 psi) at normal temperatures -- 23°C (73°F). The reasons for this recommendation are given below:

Lower Shear Forces Produced - Regardless of the shear stiffness of the bearing, it will strain depending upon the expansion and contraction of the girder. The lower the shear stiffness, the lower the shear forces produced and transmitted to the abutment and girder and the less likely that these forces will overcome those of friction keeping the bearing from slipping.

More Capable of Accommodating Non-Uniform Loading and Rotations - As shown by the results of tests performed in this study, lower hardness specimens were much more capable of distorting to accommodate the irregularities of the loading medium than were harder

specimens. The rotational stiffness is generally lower, a desirable trait, and the ability to absorb girder rotations, especially at higher shape factors is significantly greater.

Less Loss of Stiffness in Shear Fatigue - Although lower shear stiffness is desirable, the designer would like to know that the bearing will exhibit the same properties after 20 years in service as it did when it was new.

Less Low-Temperature Stiffening - Other studies (17,23) have shown that lower hardness materials have a much lesser tendency to stiffen at low temperatures. This is an extremely desirable trait considering the consequences of creating greater shear forces as described above. Additionally, natural rubber has been found to be more resistant to low temperature stiffening than other materials (5,24)

Lesser Effect of Aging - Elastomeric materials of all hardness ratings stiffen equally with age. Therefore it is better to start with the lowest possible hardness to keep the effects of stiffening with age to a minimum.

6. **Shape Factor** — From the tests results, bearings with a higher shape factor appear to out-perform those with a lower shape factor. Therefore, it is recommended that the shape factor fall within the range of 8 to 11 in bearings designed for use in most typical applications. Reasons for this recommendation are given below:

Resistance to Compression Fatigue - In compression fatigue tests, the specimens with the higher shape factor withstood fatigue loading far in excess of that expected during typical service life without physical damage or loss of stiffness. Lower shape factor bearings sustained substantial physical damage and loss of compressive stiffness. The reason for this behavior is that the higher shape factor bearings are subjected to much less shear strain at the steel shim elastomer interface than are the lower shape factor bearings.

Significantly Lower Axial Deformations - Higher shape factor bearings even of low hardness material can withstand compressive stresses on the order of 6.9 MPa (1000 psi) with axial deformations on the order of 4.5% strain.

Lower Compressive Creep - While compressive creep is not a major design consideration, the more highly reinforced bearings exhibited such low creep that the initial deformation can, for all intents and purposes, be considered the long-term deformation.

7. **Compressive Stress Level** — Based upon the test results, it is recommended that bearings be designed to accommodate the greatest compressive stress possible up to 6.9 MPa (1000 psi) under dead load alone and that, unless the engineer foresees a significant live load, the effects of live load need not be considered. A shape factor within the range of 8 to 11 will ensure that this level of compressive stress can be sustained. Additionally, the design should ensure a minimum compressive stress of 3.45 MPa (500 psi) under dead load. The reasons for these recommendations are given below:

Better Slip Resistance - The greater normal force will result in a lesser tendency for the bearing to ever slip. Additionally, the higher compressive stress results in a lower shear stiffness thus creating a lesser horizontal force during shear.

Better Accommodation of Rotations and Mismatched Loading - Test results clearly show that at 7.69 MPa (1100 psi), even the highly reinforced bearings of low hardness show

excellent ability to accommodate rotations and mismatched loading and even equal the performance of the lower shape factor bearings of low hardness at 3.85 MPa (550 psi). If minimizing the effects of mismatched loading or significant rotations are of greatest concern to the designer, proportioning the bearing so that the compressive stress is maximized is the best course of action.

Live Load Not a Factor - Compression fatigue tests have shown that the higher shape factor bearings are almost unaffected by cyclic loading at a mean stress of 6.9 MPa (1000 psi) and a stress range of 6.9 MPa (1000 psi). Additionally, as described in Chapter 6, even in the worst case, a live load from a truck wheel would increase the stress on a single bearing by less than 0.69 MPa (100 psi). Assuming a total load equal to the dead load should result in a conservative design.

Significant Factor of Safety - On the basis of compression failure tests for higher shape factor specimens, the worst specimen exhibited loss of compressive stiffness at 59.6 MPa (8640 psi). If the maximum compressive stress allowed by the AASHTO method were applied, the factor of safety against steel yielding would be more than 6. Obviously, there will be little danger of compression failure.

8. Non-Uniform Loading/Bridge End Rotations — Given the standard design of a bearing with a shape factor of 10 and 50 to 55 durometer hardness, it is recommended that that the current AASHTO rotation restrictions to prevent lift-off be removed and that total shear strain be used as a criterion to limit the stresses from all sources. Based upon tests performed in this study, bearings like those described above can be subjected to rotations of 0.024 radians at 3.85 MPa (550 psi) and 0.030 radians at 7.7 MPa (1100 psi) with only minimal lift off (15-20%). If bridge end rotations are expected to exceed these magnitudes, the designer should ensure that the area of the bearing remaining loaded is not subjected to more compressive stress than could be safely accommodated.
9. Elastomer Cover Layer — Based upon observations of performance during shear modulus tests and physical examination of tests specimens, it is recommended that no β -factor be applied to elastomer cover layers 9.5 mm ($\frac{3}{8}$ ") thick or less. In most cases, the thickness of elastomer layers can be determined by dividing the total elastomer thickness (as dictated by shear strain limitations) by the number of steel shims plus one (as determined by the shape factor = 10). Considering a 229-mmx559-mm (9"x22") bearing with 63.5 mm (2.5") of elastomer and a shape factor of 10, the cover layer would be only 2.32 mm (0.091") thicker than if the β -factor were applied. Test results show that cover layers less than 8.89 mm (0.35") do not bulge excessively and that manufacturing tolerances may not permit such precision in any case.

8.2.3 RECOMMENDATIONS FOR TAPERED BEARINGS

10. Maximum Taper — It is recommended that tapered bearings be allowed with the provision that the engineer calculate the horizontal displacement of the bearing/girder system and deem them acceptable for his design. In this study, bearings with tapers up to 5.5% were tested and performed satisfactorily. There is no indication that this is actually an upper bound.

11. Slope Mismatch — As described in Chapter 2, manufacturers typically produce tapered bearings in discrete increments to limit their inventory of sloped mold platens. For this reason, there will always be a slight mismatch between the taper of the bearing and the slope of the bridge girder. For a 229-mm (9”) long bearing, a length commonly used, tapered pads are available in 1.39% increments. The amount of non-uniform loading (mismatch) need never be greater than half this amount as long as the slope of the bridge is correctly calculated. As the current AASHTO specification allows 0.01 radians of girder/flat bearing mismatch, it is recommended that the mismatch between tapered bearing top surfaces and girders be allowed up to 0.01 radians. Based upon test results, this degree of mismatch will not result in a significant separation between the bearing and the girder as long as compressive stresses above 3.45 MPa (500 psi) are maintained.
12. Compressive Deformations — Based upon test results and the finite element study by Hamzeh (10), it is recommended that for the standard bearing design suggested in this report (50-55 durometer, Shape Factor = 10) that the compressive deformation of the tapered bearing should be determined by using the stress-strain relationships given by AASHTO for flat bearings and increasing the strain by 10% for each 0.01 radian of taper. In the absence of a precise theoretical analysis, this will yield a reasonable estimate of the compressive deformation for tapered bearings conforming to the standard design given above.
13. Controlling Horizontal Deflections — If tapered bearings are being designed to accommodate a significant bridge slope (4.5 to 5.5%), it is recommended that the designer use a harder elastomer (with a higher shear modulus) to reduce horizontal deflections under the bridge dead load alone. Additionally, horizontal deflections can be reduced by orienting reinforcing shims parallel to one another as described in recommendation 14.
14. Steel Shim Orientation — It is recommended that tapered bearings be designed so that steel reinforcing shims are oriented parallel to one another and that the taper be created by using a solid cover layer of elastomeric material. In both the experimental and analytical study, there was no significant difference in performance between bearings with radially oriented and parallel shims. Bearings with parallel shims are easier to fabricate and the shims are less likely to be bent or misoriented during vulcanization. Most significantly, tapered bearings with parallel shims deflect horizontally under dead load significantly less than do those with radially spaced shims. As long as parallel shims are specified, the horizontal deflection under dead load (P) can be estimated using an equivalent horizontal force of 0.40P without magnification for P- Δ effects, because the initial deflection will actually be less than would result from $H = 0.40P$. The thickness of the cover layer of tapered elastomeric material will be taken at mid-bearing length to determine if the β -factor should be applied to that layer.

8.3 SUGGESTED FUTURE RESEARCH

Performance at Higher Compressive Stresses

This study showed that highly reinforced bearings have no difficulty performing well at compressive stresses of 7.69 MPa (1100 psi) and, in fact, benefit in several ways from the higher stress. Additional research could show that acceptable performance may be possible at compressive stresses much greater than 7.69 MPa (1100 psi) with the appropriate shape factor.

Ozone Degradation Testing

Several sources have suggested that ozone attack on bearings is insignificant. To justify eliminating or relaxing the ozone degradation specification, ozone exposure tests should be performed on full-scale bearings rather than on elastomer samples to determine whether ozone attack actually damages more than just the surface of the pad.

CHAPTER 9

RECOMMENDED DESIGN PROCEDURE

The purpose of this section is to describe a simple design procedure based upon a collation of experimental test results, comparisons with the finite element study and information from previous research. Emphasis has been placed on standardizing as many of the design parameters as possible to facilitate the procedure and ensure excellent performance as described earlier. The method is applicable to steel reinforced flat and tapered rectangular bearings.

Standard Design Parameters

As recommended in Chapter 8, the standard design parameters shall be as given below:

- Elastomer hardness: 50 to 55 durometer
- Shape factor: $9.5 < S < 10.5$
- Steel reinforcing shims: 2.7 mm (12 gage), Grade A570 steel, $F_y = 276 \text{ MPa}$ (40 ksi)
- Compressive stress level: 3.45 MPa (500 psi) $\leq \sigma_c \leq 6.9 \text{ MPa}$ (1000 psi)
- Total Height $\leq L/3$ and $W/3$ (Ensures Stability according to AASHTO specification)

The expected shear modulus for 50-55 durometer hardness material with $S \approx 10$ is 0.64 MPa (93 psi) at 3.45 MPa (500 psi) compressive stress and 0.6 MPa (87 psi) at 6.9 MPa (1000 psi) compressive stress. Considering that any particular bearing could be delivered at $\pm 5\%$ of these values, an average shear modulus of 0.62 MPa (90 psi) shall be used.

1. Determine Plan Dimensions/Calculate Compressive Stress

The goal of the bearing design is to arrive at plan dimensions that will result in a dead load compressive stress of 6.9 MPa (1000 psi). Although this will result in excellent performance, the girder geometry and reaction may not permit the designer to attain this compressive stress level. For example, if a girder with a 610-mm (24") wide flange has a dead load reaction of 445 kN (100 kips), the designer may want to specify a bearing width of at least 457 mm (18") and a length of 229 mm (9") so that the girders will be well-supported during construction. This would result in a compressive stress of 4.31 MPa (625 psi) rather than 6.9 MPa (1000 psi). In all cases however, a minimum compressive stress of 3.45 MPa (500 psi) shall be maintained to ensure anchorage by friction and minimize lift-off due to rotation and non-uniform loading.

2. Determine Required Elastomer Thickness

No change is recommended from the current standard of 50% elastomer shear strain from expansion/contraction over the life of the bridge. Therefore, the minimum required elastomer thickness shall still be twice the anticipated total expansion or contraction of the bridge considering the yearly thermal cycle. For many short to medium span bridges, the minimum required thickness would result in a very thin bearing pod. Since bearings are relatively cheap, a

thicker bearing, say 38 mm (1.5 in) may be a more practical solution. For tapered bearings, the designer shall include in the estimate of girder displacement the amount of horizontal movement that the girder will experience due to the bearing shearing under dead load. This condition was described in Chapter 3 where it was shown that the actual shear deformation of the bearing could be estimated by using the experimentally determined “equivalent” horizontal force, $H = 0.4\theta P$, where θ is the slope of the bridge and P is the compressive load. The shear deformation of the bearing under dead load alone shall be determined by using the relationship

$$\Delta_s = \frac{Hh_{rt}}{GA} \quad (9.1)$$

The bearing elastomer thickness shall be increased by the value of $2\Delta_s$ to ensure that $h_{rt} \geq 2\Delta_s$ in the final design. This will result in a tapered bearing which will have a greater elastomer thickness and more steel reinforcing shims than one which supports the same girder with no slope. For a typical application, a tapered bearing designed as outlined in this chapter would cost approximately 15% most than a flat bearing. In a tapered bearing, h_{rt} shall be taken as the elastomer thickness at mid-length of the bearing.

3. Calculate Compressive Deformation Including Creep

Using Figures 14.4.1.2A and B from the 1992 AASHTO Specifications for Highway Bridges, the compressive deformation for 55 durometer elastomeric bearings with a shape factor of 10 is as given in Table 9.1. For bearings designed according to the standard parameters given above the additional deformation due to long-term creep can be taken as 15% of the instantaneous deformation given in Table 9.1.

Table 9- 1 Compressive deformation for 55 durometer bearings of $S = 10$

Compressive Stress MPa (psi)	Compressive Strain (%)
3.45 (500)	2.2
4.14 (600)	2.6
4.82 (700)	3.0
5.52 (800)	3.4
6.21 (900)	3.7
6.90 (1000)	3.9

As long as $S \approx 10$ is maintained, there is no need to do any additional calculations of compressive deformation. An additional 10% deformation must be added for each 0.01 radians of bearing taper.

4. Check Bridge End Rotations

Although there is no formal limit on the amount of rotation that the bearing may accommodate, the designer shall check that, if the bridge end rotations are expected to be significant and result in lift-off, the portion of the bearing still in contact with the girder is not subjected to a compressive stress exceeding the maximum allowed under this design procedure (6.9 MPa (1000 psi)). For bearings conforming to the standard design parameters, the designer shall anticipate that approximately 80% of the bearing will remain loaded at an end rotation of 0.024 radians under 3.45 MPa (500 psi) or 0.03 radians at 6.9 MPa (1000 psi) compressive stress

5. Specify Bearing Taper — The correct bearing taper to request from the manufacturer shall be based upon the bridge slope as shown in Table 9.2, which gives a recommended range of use for specific bearing tapers assuming a 229-mm (9") length and 3.175-mm (0.125") increments in taper across the length. These standard tapers are based upon information provided by one of the manufacturers of test specimens used in this study. Test results indicating acceptable mismatches between bearings and girders are taken into account.

Table 9- 2 Standard tapered bearing ranges

Bridge Slope	Bearing Taper (%)
0 - 1.0%	Zero (Flat)
1.0 - 2.08 %	1.39
2.09 - 3.47 %	2.78
3.48 - 4.86 %	4.17
4.87 - 6.25 %	5.56

The intention of these guidelines is to allow maximum use of flat bearings and then to limit the unavoidable mismatch as much as possible. If a bearing length other than 229 mm (9") is used, the standard tapers will vary. The manufacturer shall be required to quote to the designer the precise tapers that are fabricated.

6. Specify Steel Reinforcement/Elastomer Layer Thickness

The required number of reinforcing steel shims shall be determined according to the following relationship:

$$n = \frac{2Sh_{rt}(L + W)}{LW} - 1 \quad (9.2)$$

where S = 10 for the standard design. The result will be rounded up or down to the closest whole number, which will change the shape factor slightly. A subsequent calculation of the shape factor shall be performed to ensure that it is between 9.5 and 10.5. As stated above, the standard reinforcing steel shim shall be 2.7-mm (12 gage), A570 steel with $F_y = 276 \text{ MPa}$ (40 ksi). The elastomer layer thickness shall be determined by dividing the total elastomer thickness required by the number of steel layers plus one (n+1). Generally the layer thickness should be rounded to the nearest $\frac{1}{8}$ " (3.18 mm) because the bulk material used to manufacture the bearings is approximately $\frac{1}{8}$ " (3.18 mm) thick. If the cover layer is 9.5 mm ($\frac{3}{8}$ " or less, no β - factor need be applied. From the relationship between shim thickness, yield strength and elastomer layer thickness given in Equation 2.1 (which includes a factor of safety of 2), the designer shall assume that if S = 10 and the compressive stress is 6.9 MPa (1000 psi) or less, the steel will not yield unless the elastomer layer thickness is greater than 35.3 mm (1.39"), a very unlikely occurrence. The manufacturer may recommend increasing the thickness of the shims for bearings with very large plan dimensions to prevent bending during vulcanization. For tapered bearings, the steel reinforcing shims shall be oriented parallel to one another and the taper shall be created by using a solid cover layer of elastomeric material. The total elastomer thickness h_{rt} to be used in Equation 9.2 shall be taken at mid-length. The thickness of the cover layer of tapered elastomeric material shall be taken at mid-bearing length to determine if the β -factor must be applied to that layer.

7. Ensure No Slip

The designer shall assume a friction coefficient of 0.2 and calculate the horizontal force produced by the bearing shearing through 50% strain according to the relationship $\mathbf{H} = \mathbf{GA}\gamma$, where A is the plan area of the bearing. For the standard design described in this section, G, the shear modulus shall be assumed to be 0.62 MPa (90 psi), and the horizontal force produced by the bearing shearing through 50% strain is $H = 0.00155A$ kN (0.225A kips). To ensure that $N\mu > \mathbf{H}$, the designer must check that

$$\mathbf{N} > \mathbf{0.00155A \text{ kN (0.225A kips)}} \quad \mathbf{(9.3)}$$

N shall include only dead load and not be factored. For a girder with a typical 445 kN (100 kip) dead load reaction, as long as A is less than 0.286 m² (444 in²) slip will not occur.

APPENDIX A

PROPOSED SPECIFICATIONS

This Appendix gives proposed specifications based upon the results of tests performed in this study. In many cases, the existing specifications can be broadened without risk to the safety of elastomeric bearing design. Division I - Design specifications are reproduced in their entirety with proposed revisions noted and commentary included to explain the rationale behind the change. For Division II - Construction specifications only paragraphs where changes are proposed are shown along with their corresponding commentary.

DIVISION I - DESIGN

14.1 GENERAL

An elastomeric bridge bearing is a device constructed partially or wholly from elastomer, the purpose of which is to transmit loads and accommodate movements between a bridge and its supporting structure. This section of the Specification covers the design of plain pads (consisting of elastomer only) and reinforced bearings (consisting of alternate layers of steel or fabric reinforcement and elastomer, bonded together). ~~Tapered elastomer layers in reinforced bearings are not permitted.~~ *Span slopes greater than 0.01 radians may be accommodated with bearings with a built in taper. Such taper shall be limited to 0.055 radians.* In addition to any internal reinforcement, bearings may have external steel load plates bonded to the upper or lower elastomer layers or both.

~~Two~~ *Three* design procedures are provided in this section. Bearings reinforced with steel may be designed either by the procedures defined in 14.4.1, 14.4.2 or the one in *14.4.3*. Bearings with fabric reinforcement or unreinforced pads shall be designed by 14.4.1 ~~Both~~ *All of the* design procedures are based

on service loads and require that no impact fraction be added to the live load. The materials, fabrication, and installation of the bearings shall be in accordance with the requirements of Section 18.2 of Division II of the Specification.

C14.1 GENERAL

~~Two~~ *Three* design methods are included. Method A is generally simpler but results in more conservative designs. Bearings designed according to Method B will generally be more highly stressed but are subject to more stringent test requirements. *Method C applies to flat and tapered rectangular bearings which meet specific criteria as outlined in paragraph 14.4.3.*

Tapered layers in reinforced bearings are expressly prohibited because they cause large shear strains, and bearings made with them fail prematurely because of delamination or rupture of reinforcement.

14.2 DEFINITIONS

Longitudinal Axis	=	The axis of the bearings parallel to the longitudinal axis of the bridge girder(s)
Lot	=	A group of bearings

		made from the same batch of materials			=	of a bearing
Transverse Axis	=	The axis of the bearing perpendicular to the longitudinal axis			=	$\frac{\text{Plan Area}}{\text{Area of Perimeter Free to Bulge}}$
A	=	Gross plan area of the bearing			=	$LW / 2h_{ri} (L + W)$ for rectangular without holes
b _f	=	Width of flange of steel girder (in.)	t _f	=		Thickness of steel girder flange (in.)
D	=	Gross diameter of a circular bearing (in.)	W	=		Gross dimension of rectangular bearing parallel to the transverse axis
E _c	=	Effective compressive modulus of the elastomer, taking account of restraint of bulging = $3G(1+2kS^2)$ (psi)	β	=		Modifying factor having a value of 1.0 for internal layers of reinforced bearings, 1.4 for cover layers, and 1.8 for plan pads. If slip is prevented from occurring at the surface of plain pads or outer layers of reinforced bearings under all circumstances, or if the cover layer of reinforced bearings is $\frac{3}{8}$ in. or less , β factors smaller than those defined above may be used at the discretion of the Engineer. β shall never be taken as less than 1.0
F _y	=	Yield strength of the steel reinforcement (psi)				
F _{yg}	=	Yield strength of the steel girder (psi)				
G	=	Shear modulus of the elastomer (psi) at 73°F				
H	=	Design shear force on bear (lb) = $G A \Delta_h / h_{rt}$				
h _{rt}	=	Total elastomer thickness of the bearing (in.) = $\sum h_{ri}$ (measured at mid-length for bearings with built-in tapers)				
h _{ri}	=	Thickness of elastomer layer number i (in.)				
h _s	=	Thickness of one steel reinforcement layer (in.)	Δ _c	=		Instantaneous compressive deflection of bearing (in.)
k	=	Constant dependent on elastomer hardness (see Table 14.3.1 for values)	Δ _h	=		Total horizontal movement of superstructure, measured from state at which bearing is undeformed (in.)
L	=	Gross dimension of rectangular bearing parallel to the longitudinal axis (in.)				
n	=	Number of reinforcing layers	Δ _s	=		Shear deformation of the bearing in one direction from the undeformed state, accounting for
P	=	Compressive load on the bearing (lb)				
S	=	Shape factor of one layer				

ϵ_{ci}	=	support flexibility (in.) Instantaneous compressive strain in elastomer layer number i (change in thickness divided by the unstressed thickness)
θ	=	Relative rotation of top and bottom surfaces of bearing (in.)
θ_b	=	Built-in bearing taper (radians)

Subscripts:

DL	=	dead load
TL	=	total load
LL	=	live load
x	=	about transverse axis
z	=	about longitudinal axis
σ_c	=	P/A = average compressive stress on the bearing caused by the dead and live load, excluding impact

C14.2 DEFINITIONS

The compressive stress allowed by design Method A (Article 14.4.1) is now expressed as a single function of S/β for all bearings, but use of the appropriate value of β causes the allowable stress on a plain pad to be 56 percent of that of a reinforced bearing layer of the same dimensions if it is limited by GS/β . Cover layers of reinforced bearings are treated similarly except that $\beta = 1.4$. ***In cases where the cover layer of a reinforced bearing is less than 0.333 inches, the β -factor need not be applied because cover layers this thin do not show any propensity to bulge excessively.*** Design Methods B and C (Articles 14.4.2 and 14.4.3) covers only steel reinforced bearings, for which $\beta = 1.0$ or $\beta = 1.4$ (outer cover layers ***greater than 0.333 inches thick***).

14.3 MATERIAL PROPERTIES

The shear modulus at 73°F shall be used as the basis for design. If the material is specified explicitly by its shear modulus, that value shall be used in the design and the other properties shall be obtained from Table 14.3.1. If the material is specified by its hardness, the shear modulus shall be taken as the value from the range for that hardness given in Table 14.3.1, which is most conservative for each part of the design. Intermediate values shall in all cases be obtained by interpolation.

Material with a shear modulus greater than 200 psi or a nominal hardness greater than 60 shall not be used for reinforced bearings. Under no circumstances shall the nominal hardness exceed 70 or the shear modulus exceed 300 psi.

For the purposes of bearing design, all bridge sites shall be classified as being in temperature zone A, B, C, D, or E. The zones are defined by their extreme low temperatures or the largest number of consecutive days for which the temperature has ever remained below 32°F, whichever gives the more severe condition. Values are given in Table 14.3.2. In the absence of more precise information, Figure 14.3.1 may be used as a guide in selecting the zone required for a given region.

Table 14.3.1 Elastomer properties at different hardnesses

Hardness (Shore 'A')	50	60	70
Shear Modulus (psi)	95-130	130-	200-
at 73 degrees F (MPa)	0.68-	200	300
	0.93	0.93-	1.43-
		1.43	2.14
Creep deflection - 25 yr	25%	35%	45%
Instantaneous Defl.			
k	0.75	0.6	0.55

Table 14.3.2 Low Temperature zones and elastomer grades

Low Temperature Zone	A	B	C	D	E
50 Year Low Temperature (°F)	0	-20	-30	-45	All Others
Maximum number of consecutive days when the temperature does not rise above 32 °F	3	7	14	N/A	N/A
Minimum Low Temperature Elastomer Grade Without Special Provisions	0	2	3	4	5
Minimum Low Temperature Elastomer Grade With Special Provisions	0	0	2	3	5

Bearings shall be made from AASHTO low temperature grades of elastomer required for each low temperature zone as defined in Section 18.2 of Division II. The minimum grade of elastomer required for each low temperature zone is specified in Table 14.3.2. The special provisions required in Table 14.3.2 are that either a positive slip apparatus be installed and the bridge components shall be able to withstand forces arising from a bearing force equal to twice the design shear force or that the components of the bridge be

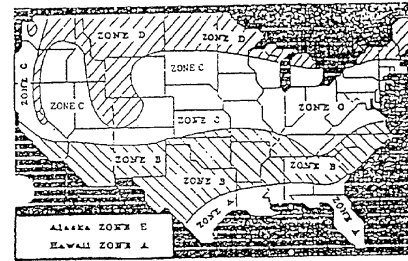


Figure 14.3.1 Map of low temperature zones

able to resist forces arising from a bearing force four times the design shear force as defined in Section 14.6

14.4 BEARING DESIGN METHODS

14.4.1 Method A - Design Procedure for Steel Reinforced, Fabric Reinforced or Plain Bearings

14.4.1.1 Compressive Stress

Unless shear deformation is prevented, the average compressive stress σ_c in any layer shall satisfy:

$$\sigma_{c,TL} \leq GS/\beta$$

and $\sigma_{c,TL} \leq 1,000$ psi for steel-reinforced bearings

or $\sigma_{c,TL} \leq 800$ psi, for plain pads or fabric reinforced bearings

These stress limits may be increased by 10 percent where shear deformation is prevented. In bearings consisting of layers of different thickness, the value of S used shall be that which produces the smallest S/β .

14.4.1.2 Compressive Deflection

The compressive deflection, Δ_c , of the bearing shall be so limited as to ensure the serviceability of the bridge. Deflections due to total load and to live load alone shall be considered separately.

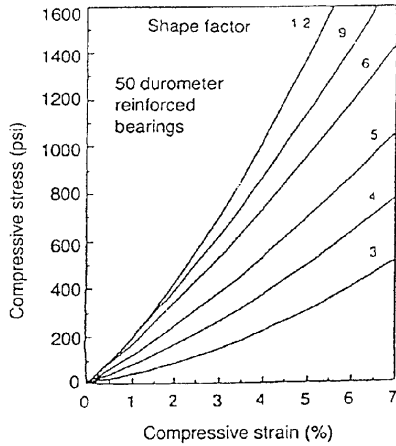


Figure 14.4.1.2A Compressive stress vs. strain for 50 durometer steel-reinforced bearings

Instantaneous deflection shall be calculated as

$$\Delta_c = \sum \epsilon_{ci} h_{ri}$$

Values for ϵ_{ci} shall be obtained from design aids based on tests such as presented in Figures 14.4.1.2A and 14.4.1.2B, by testing or by an approved analysis method. Figures 14.4.1.2A and 14.4.1.2B are for internal layers of reinforced pads or cover layers of reinforced bearings if S is replaced by S/β .

The effects of creep of the elastomer shall be added to the instantaneous deflection when considering long-term deflections. They shall be computed from information relevant to the elastomeric compound used if it is available. If not, the values given in Article 14.3 shall be used.

14.4.1.3 Shear

The horizontal bridge movement shall be taken as the maximum possible deformation caused by creep, shrinkage, and post-tensioning, combined with thermal effects computed in accordance with Section 3.16. The maximum shear deformation of the bearing, Δ_s , shall be taken as the horizontal bridge movement, modified to account for the pier flexibility and construction procedures.

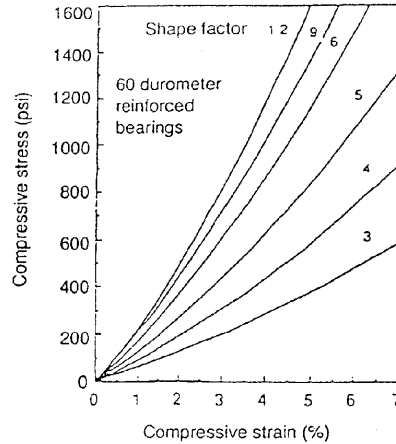


Figure 14.4.1.2B Compressive stress vs. strain for 60 durometer steel-reinforced bearings

If a positive slip apparatus is installed, Δ_s need not be taken larger than the deformation corresponding to first slip.

The bearing shall be designed so that $h \geq 2\Delta_s$.

14.4.1.4 Rotation

The rotational deformations about each axis shall be taken as the maximum possible rotation between the top and bottom of the bearing caused by initial lack of parallelism and the girder rotation. They shall be limited by:

$$\theta_{TL, x} \leq 2\Delta_c/L$$

and $\theta_{TL, z} \leq 2\Delta_c/W$, for rectangular bearings

or $(\theta_{TL, x}^2 + \theta_{TL, z}^2)^{1/2} \leq 2\Delta_c$ for circular bearings

14.4.1.5 Stability

To ensure stability, the total thickness of the bearing shall not exceed the smallest of:

$L/5$, $W/5$ or $D/6$ for plain pads $L/3$, $W/3$, or $D/4$ for reinforced bearings

14.4.1.6 Reinforcement

The reinforcement shall be fabric or steel and its resistance in pounds per linear inch at working stress levels in each direction shall not be less than

$$1,400 h_{ri} \quad \text{for fabric}$$

$$1,700 h_{ri} \quad \text{for steel}$$

For these purposes h_{ri} shall be taken as the mean thickness of the two layers of the elastomer bonded to the reinforcement if they are of different thicknesses. The resistance per linear inch is given by the product of the material thickness of the reinforcement and the allowable stress. The allowable stress shall be calculated taking into account fatigue loading but ignoring holes in the reinforcement. Holes shall be prohibited in fabric reinforcement. They are not recommended in steel reinforcement; but, if they exist, the steel thickness shall be increased by a factor $(2 \times \text{gross width})/(\text{net width})$.

14.4.2 Method B - Optional Design Procedure for Steel Reinforced Bearings

Bearings shall not be designed by the provisions of Section 14.4.2 unless they are subsequently tested in accordance with the requirements of Section 18.2.7 of Division II of this specification.

14.4.2.1 Compressive Stress

In any layer, the average compressive stress shall satisfy

$$\sigma_{c,TL} \leq 1,600 \text{ psi}$$

$$\sigma_{c,TL} \leq 1.66 \text{ GS}/\beta$$

$$\sigma_{c,LL} \leq 0.66 \text{ GS}/\beta$$

for bearings fixed against shear deformations

$$\sigma_{c,TL} \leq 1,600 \text{ psi}$$

$$\sigma_{c,TL} \leq 2.00 \text{ GS}/\beta$$

$$\sigma_{c,LL} \leq 1.00 \text{ GS}/\beta$$

where $\beta = 1.0$ for internal layers and 1.4 for cover layers *greater than $\frac{3}{8}$ inches thick*.

14.4.2.2 Compressive Deflection

Same as 14.4.1.2

14.4.2.3 Shear

Same as 14.4.1.3

14.4.2.4 Rotation and Combined Rotation and Compression

The rotational deformations about each axis shall be taken as the maximum possible rotation between the top and bottom of the bearing caused by initial lack of parallelism and girder end rotation. They shall be limited by:

$$\theta_{TL,x} \leq 2\Delta_c/L$$

and $\theta_{TL,z} \leq 2\Delta_c/W$, for rectangular bearings

or $(\theta_{TL,x}^2 + \theta_{TL,z}^2)^{1/2} \leq 2\Delta_c/D$ for circular bearings

In bearings subjected to both compression and rotation about the transverse axis of the bearing, the average compressive stress shall satisfy, for bearings subject to shear deformations

$$\sigma_{c,TL} \leq \frac{1.66GS/\beta}{1 + \frac{L\theta_{TL,x}}{4\Delta_c}}$$

or, for bearings fixed against shear deformations

$$\sigma_{c,TL} \leq \frac{2.0GS/\beta}{1 + \frac{L\theta_{TL,x}}{4\Delta_c}}$$

where $\theta_{TL,x}$ is the total rotation about the transverse axis of the bearing, including the effects of initial lack of parallelism, creep, shrinkage, and temperature.

Reduced stress levels for rotations about the longitudinal axis of the bearing shall be computed by a rational method.

14.4.2.5 Stability

The bearing shall be proportioned to prevent stability failure. The average compressive stress due to total dead load and live load on rectangular bearings shall satisfy:

if the bridge deck is free to translate horizontally

$$\sigma_{c,TL} \leq G / \left\{ \frac{3.84(h_r/L)}{S\sqrt{1+2L/W}} - \frac{2.67}{S(S+2)(1+L/4W)} \right\}$$

or, if the bridge deck is not free to translate horizontally

$$\sigma_{c,TL} \leq G / \left\{ \frac{1.92(h_r/L)}{S\sqrt{1+2L/W}} - \frac{2.67}{S(S+2)(1+L/4W)} \right\}$$

If L is greater than W for a rectangular bearing, stability shall be checked by the above formula with L and W interchanged.

The stability of circular bearings may be evaluated by using the equations for a square bearing with $W = L = 0.8D$.

14.4.2.6 Reinforcement

The thickness of the reinforcement h_s shall satisfy

$$h_s \geq \frac{1.5(h_{r1} + h_{r2})\sigma_{c,TL}}{F_y}, \text{ for total load}$$

$$h_s \geq \frac{1.5(h_{r1} + h_{r2})\sigma_{c,LL}}{F_{sr}}, \text{ for live load}$$

where F_{sr} is the allowable stress range based on fatigue loading. F_{sr} shall be taken from Table 10.3.1A of Division I of this specification using category A for a Nonredundant Load Path Structure. If holes exist, the minimum thickness shall be increased by a factor

$$\frac{2 \times \text{gross width}}{\text{net width}}$$

14.4.3 Method C - Simplified Design Procedure for Standard Flat and Tapered Steel Reinforced Bearings

This procedure shall apply only to rectangular steel reinforced bearings without holes which meet the following criteria:

Hardness: 50-55 durometer

$$85 \leq G \leq 95 \text{ psi}$$

$$9.5 < S < 10.5$$

$$\sigma_{c,DL} \geq 500 \text{ psi}$$

For bearings with built in taper, S shall be calculated based on the thickness of the internal elastomer layers.

14.4.3.1 Compressive Stress

The average compressive stress in any layer shall satisfy:

$$\sigma_{c,DL} \leq 1,000 \text{ psi}$$

A β -factor need not be applied to cover layers providing that such layers are no greater than $\frac{3}{8}$ inches thick.

14.4.3.2 Compressive Deflection

The compressive deflection, Δ_c , of the bearing shall be so limited as to ensure the serviceability of the bridge. Deflections due to total load and to live load alone shall be considered separately.

Instantaneous deflection shall be calculated as

$$\Delta_c = \sum \epsilon_{ci} h_{ri}$$

Values for ϵ_{ci} shall be obtained from design aids based on tests such as presented in Figures 14.4.1.2A and 14.4.1.2B, by testing or by an approved analysis method. Figures 14.4.1.2A and 14.4.1.2B are for internal layers of reinforced pads or cover layers of reinforced bearings if S is replaced by S/ β when required..

Instantaneous deflections for bearings with built in tapers shall be assumed to be 10 percent greater per 0.01 radians of taper than instantaneous deflections for flat bearings

The effects of creep of the elastomer shall be added to the instantaneous deflection when considering long-term deflections. For reinforced bearings which satisfy the

requirements of this design procedure, the value of the long-term deflection may be taken as 15 percent of the instantaneous deflection.

C 14.4.3.2 Compressive Deflection

Tests and analyses of bearings with built in tapers show that these bearings deflect on the average 10 percent more than flat bearings for every 0.01 radians of taper. This is due to the entire bearing bulging in the direction of the thick end of the pads. For bearings meeting the criteria of this design method, this additional deflection is not significant.

Creep tests show that for highly reinforced bearings of low hardness/shear modulus, the value of long-term creep is approximately 15 percent of initial deflection.

14.4.3.3 Shear

The horizontal bridge movement shall be taken as the maximum possible deformation caused by creep, shrinkage, and post-tensioning, combined with thermal effects computed in accordance with Section 3.16 for bearings with mounting plates permanently attached to the top and bottom elastomeric layers. For bearings without mounting plates, only thermal effects need be considered. The maximum shear deformation of the bearing, Δ_s , shall be taken as the horizontal bridge movement, modified to account for the pier flexibility and construction procedures. If a positive slip apparatus is installed, Δ_s need not be taken larger than the deformation corresponding to first slip.

The bearing shall be designed so that
$$h_{rt} \geq 2\Delta_s$$

For bearings with built in tapers, the horizontal deflection due to the girder dead weight acting on the sloped surface shall be calculated as

$$\Delta_s = 0.4\theta_b P h_{rt} / GA$$

and shall be included in the horizontal bridge movement used to determine the required h_{rt} .

C14.4.3.3 Shear

Tests and analyses of tapered bearings show that a horizontal deflection is produced in bearings with a built in taper under the dead load of the girder alone. The magnitude of the horizontal deflection has been empirically determined as shown above.

The engineer must first calculate h_{rt} based upon shortening and then use this value to determine Δ_h due to the dead weight based upon G and A . The value of this deflection should be added to Δ_s so that the bearing will satisfy the $2\Delta_s \leq h_{rt}$ limitation.

14.4.3.4 Rotation

The rotational deformations about each axis shall be taken as the maximum possible rotation between the top and bottom of the bearing caused by initial lack of parallelism and the girder rotation. Permissible rotations are not formally limited, however the designer shall ensure that if bridge end rotations greater than 0.024 radians at 500 psi or 0.030 radians at 1000 psi compressive stress are anticipated, that the compressive stress on the bearing be assumed to act on only 80% of the plan area due to lift off.

For bearings with a built in taper, such taper shall not exceed 0.055 radians. In cases where the bearing taper does not precisely match the bridge slope, such mismatch shall

not exceed 0.01 radians and the value of the mismatch shall be subtracted from the maximum allowable bearing rotation given above.

C14.4.3.4 Rotation

Due to the axial flexibility of bearings meeting the criteria of this design method, the rotation capacity can be assumed to be as given in Article 14.4.3.4.

Because bearings with built in tapers are normally fabricated in discrete increments by manufacturers, some small lack of parallelism between the girder bottom and the bearing top surface is to be expected, but will not adversely effect the bearing's performance if the guidelines in Article 14.4.3.4 are followed.

14.4.3.5 Stability

Same as Paragraph 14.4.1.5

14.4.3.6 Reinforcement

The reinforcement shall be steel and its resistance in pounds per linear inch at working stress levels in each direction shall not be less than $1,700 h_{ri}$.

For these purposes h_{ri} shall be taken as the mean thickness of the two layers of the elastomer bonded to the reinforcement if they are of different thicknesses. If bearings with a built in taper are used, reinforcing steel shims shall be oriented parallel to one another and the taper created by using a solid cover layer of elastomeric material. The thickness of the cover layer of tapered elastomeric material shall be taken at mid-bearing length to determine if the β -factor must be applied. The resistance per linear inch is given by the product of the material thickness of the reinforcement and the allowable stress. The allowable stress shall

be calculated taking into account fatigue loading.

C14.4.3.6 Reinforcement

In bearings with a built in taper, orienting reinforcing shims parallel to one another facilitates fabrication, reduces the likelihood of shim misorientation or bending during vulcanization, and reduces horizontal deflection under dead load.

14.5 ANCHORAGE

If the design shear force, H, due to bearing deformation exceeds one-fifth of the compressive force P due to dead load alone, the bearing shall be secured against horizontal movement. The bearing shall not be permitted to sustain uplift force.

14.6 DESIGN FORCES FOR SUPPORTING STRUCTURE

The forces imposed by the bearing on the substructure are a function of the stiffness of the bearing and the flexibility of the substructure. Maximum forces to be applied by the bearing (for a rigid substructure) may be computed in accordance with Section 14.6.1 for shear and in accordance with 14.6.2 for moment.

14.6.1 Shear Force

If a positive slip apparatus is installed, H shall be taken as the largest force which can be transmitted by the apparatus. If no positive slip apparatus is installed, the design shear force shall be taken as not less than $H = G A \Delta_h / h_{rt}$, where Δ_h is the horizontal movement of the bridge superstructure relative to conditions when the bearing is undeformed and G is the shear modulus of the elastomer at 73°F.

14.6.2 Moment

The moment induced by bending of a rectangular bearing about an axis parallel to its long side shall be taken as not less than $M = (0.5 E_c) I \theta_{TL,x} / h_{rt}$, where $I = WL^3/12$.

14.7 STIFFENERS FOR STEEL BEAMS AND GIRDERS

The flanges of steel members seated on elastomeric bearings must be flexurally stiff enough not to risk damage to the bearing. Any necessary stiffening may be accomplished by means of a sole plate or a vertical stiffener. The stiffening requirements of this section do not replace any others in this specification, but should be read in conjunction with them.

Single-webbed beams and girders symmetric about their minor axis and placed symmetrically on the bearing need no additional stiffening if

$$\frac{b_f}{2t_f} < \sqrt{\frac{F_{yg}}{3.4\sigma_c}}$$

where b_f = total flange width, t_f = thickness of flange or combined flange and sole plate, and F_{yg} = yield stress of the girder steel.

14.8 PROVISIONS FOR INSTALLATION EFFECTS

Allowance shall be made during design for misalignment in bridge girders due to fabrication and erection tolerance, camber, and other sources. The bearings shall be located and installed in such a way as to permit subsequent replacement.

DIVISION II - CONSTRUCTION

18.2 ELASTOMERIC BEARINGS

18.2.3 Materials

18.2.3.1 Properties of the Elastomer

Add to the existing specification:

Under no circumstances will any residual foreign matter accumulate on the bearing surface due to secretion from within the elastomer. Antiozonant waxes which migrate to the surface of the bearing for the purpose of guarding against ozone degradation are expressly prohibited as an ingredient in the elastomer compound.

TABLE 18.2.3.1A and TABLE 18.2.3.1B

Delete:

OZONE

D 1149

C18.2.3.1 Properties of the Elastomer

Add to the current commentary:

Recent research has proven that accumulation of viscous materials on bearings surfaces due to secretion of additives in the elastomer compound have caused severe slipping and required replacement of the bearings. The source of this secretion is antiozonant waxes which are used by manufacturers to ensure that the compound will pass the ozone specification. There is no known satisfactory level of this substance and, according to manufacturers, during the service life of the bearing, all of

the wax will eventually migrate to the bearing surface. For this reason, waxes must be categorically prohibited as an ingredient in elastomer compounds.

There is no evidence that ozone attack damages any part of the bearing other than the surface to a depth of approximately one millimeter. For this reason, the ozone specification has been deleted.

18.2.5 Fabrication Tolerances

Plain pads and laminated bearings shall be built to the specified dimension within the following tolerances:

4. Parallelism with Opposite Face
*Parallelism with Opposite Face /
Deviation from Design Taper Top
and Bottom Sides*
0.005 radians
0.02 radians

C18.2.5 Fabrication Tolerances

Some of the tolerances have been changed to relative values, because an absolute value such as 1/16 in. may be overly large for a small bearing and unrealistically small for a large bearing. Parallelism of the two faces of a single layer is controlled by the limitation on thickness at any point.

18.2.7.3 Ambient Temperature Tests on the Elastomer

The elastomer used shall at least satisfy the limits in the appropriate Table 18.2.3.1A or B for durometer hardness, tensile strength, ultimate elongation, heat resistance, and compression set. ~~and ozone resistance.~~

C18.2.7 Testing

Add to the existing specification:

The ozone resistance test is no longer required.

18.2.8 Installation

Bearings shall be placed on surfaces that are plane to within 1/16 in. and, unless the bearings are placed in opposing pairs, horizontal to within 0.01 radians. Any lack of parallelism between the top and bottom of the bearing and the underside of the girder that exceeds 0.01 radians shall ***be accommodated by employing a bearing with a built in taper***, or corrected by grouting or as otherwise directed by the Engineer.

C18.2.8 Installation

If the bearing seat is not horizontal, gravity loads will cause shear in the elastomer. The underside of the girder and the top surfaces of the bearing must also be parallel to avoid excessive rotation and the stresses it causes in the bearing. ***Employing elastomeric bearings with a built in taper (up to 0.055 radians) that matches the girder slope within 0.01 radians is an acceptable method of accommodating bridge grades.***

APPENDIX B

DESIGN EXAMPLES USING METHOD C SPECIFICATIONS

The purpose of the section is to give design examples based upon the procedure proposed in Chapter 9 of this report. The examples are intended to illustrate the simplicity of the method due to the standardization of a number of design parameters. Example 1 shows the design of a bearing for a bridge with no grade. Example 2 shows how the bearing design would be modified if the same bridge were on a 3.5% grade. The bearings do not have mounting plates. Horizontal displacement due to shrinkage and creep are not considered in the bearing design because these permanent deformations can be accommodated by one-time slip between girder and bearing.

B. 1 STANDARD PARAMETERS

The standard design parameters as recommended in Chapters 8 and 9 are as follows:

HARDNESS: 50-55 DUROMETER

Shear Modulus: $0.586 \text{ MPa (85 psi)} < G < 0.655 \text{ MPa (95 psi)}$ (use $0.62 \text{ MPa -- 90 psi}$ for calculations)

SHAPE FACTOR: $8.5 < S < 11$

Compressive Stress due to Dead Load: $\sigma_c \geq 3.45 \text{ MPa (500 psi)}$

Reinforcing steel shims: A570 steel $F_y = 276 \text{ MPa (40 ksi)}$, $h_s = 2.7 \text{ mm (12 gage)}$

B.2 EXAMPLE 1: BRIDGE WITHOUT GRADE

Bridge: Prestressed Concrete Girder, $\alpha = 9.9 \times 10^{-6} \text{ mm/mm}^\circ\text{C}$ ($5.5 \times 10^{-6} \text{ in/in}^\circ\text{F}$)

Span Length: 36.6 m (120')

Dead load reaction: $P = 534 \text{ kN (120 kips)}$

Bridge Grade: None

Yearly high temperature: $49^\circ\text{C (120}^\circ\text{F)}$

Yearly low temperature: $-6.7^\circ\text{C (20}^\circ\text{F)}$

Girder flange width: 610 mm (24")

Maximum rotation due to live load and thermal effects: 0.003 radians

1. Determine Plan Dimensions/Calculate Compressive Stress:

Assume $L = 229 \text{ mm (9")}$

Use $W = 458 \text{ mm (18")}$ to ensure stability of girders during erection

$A = 0.105 \text{ m}^2$ (162 in^2)

$\sigma_c = 5.11 \text{ MPa (741 psi)} \therefore \text{OK}$

2. Determine Required Elastomer Thickness:

$$\Delta_{ts} = (9.9 \times 10^{-6} \text{ mm/mm}^\circ\text{C})(36600 \text{ mm})(56^\circ\text{C}) = 20.3 \text{ mm (0.80")}$$

$$\Delta_h = \text{Thermal contraction} = 20.3 \text{ mm (0.80")}$$

Assume half of contraction/expansion occurs at each bearing: $\Delta_s = 10.2 \text{ mm (0.40")}$

$$\text{Minimum required } h_{rt} = 2(10.2 \text{ mm}) = 20.3 \text{ mm (0.80 in)}$$

Specify $h_{rt} = 38 \text{ mm (1.5")}$ for practical reasons (lower shear stress, better ability to handle slope mismatches due to camber and sweep)

3. Calculate Compressive Deformation Including Creep

Based on $\sigma_c = 5.11 \text{ MPa (741 psi)}$:

From Table 9.1, $\epsilon_c = 3.2\%$

$$\therefore \Delta_c = (0.032)(38 \text{ mm}) = 1.22 \text{ mm (0.048")}$$

$$\text{Long-term Deformation} = 1.15(\Delta_c) = 1.40 \text{ mm (0.055")}$$

4. Check Bridge End Rotation

Rotation = 0.003 radians \therefore upward displacement = $0.003 (229/2) = 0.34 \text{ mm} < 1.4 \text{ mm}$ so no uplift expected for $\sigma_c = 5.11 \text{ Mpa (741 psi)}$

5. Specify Steel Reinforcement/Elastomer Layer Thickness

Start with $S = 10$, use Equation 9.2 to calculate n , number of reinforcing shims

$$n = ((2 S h_{rt} (L+W))/LW) - 1 = 4$$

Use 4, Grade A570 steel shims, 2.67 mm (12 gage)

Calculate h_{ri} : $h_{ri} = 38 \text{ mm}/5 \text{ layers} = 7.6 \text{ mm (0.3")}$ Use 6.4 mm ($\frac{1}{4}$ ") cover layers and 9.5 mm ($\frac{3}{8}$ ") for the three interior layers

Recalculate S : $S = 8 \therefore$ OK since it is within the target range. If values less than 8 are used, then check that $\sigma_c \leq 1.66GS$

6. Ensure No Slip

Check for $N > 0.00155 A \text{ (kN)}$:

$$0.00155 A = 0.00155(457 \text{ mm})(229 \text{ mm}) = 162.2 \text{ kN (36.5 kips)} < 534 \text{ kN (120 kips)} \therefore \text{OK}$$

Final Design

G = 90 psi (50-55 durometer)

S = 8

L = 229 mm (9") W = 457 mm (18")

$h_{rt} = 41.3 \text{ mm (1.625")}$ $h_{r_{cover}} = 6.4 \text{ mm (1/4")}$, $h_{ri} = 9.5 \text{ mm (3/8")}$

4 Grade A570 2.67 mm (12 gage) steel shims

Total height = 52 mm (2.05")

B.3 EXAMPLE 2: BRIDGE ON 3.5% GRADE

ALL SPECIFICATIONS ARE THE SAME EXCEPT THAT THE BRIDGE IS ON A 3.5% GRADE

1. Determine Plan Dimensions/Calculate Compressive Stress:

Use same dimensions as Example 1:

L = 229 mm (9"), W = 457 mm (18")

A = 0.105 m² (162 in²)

$\sigma_c = 5.11 \text{ MPa (741 psi)}$

2. Determine Required Elastomer Thickness:

$\Delta_{ts} = (9.9 \times 10^{-6} \text{ mm/mm}^\circ\text{C})(36600\text{mm})(56^\circ\text{C}) = 20.3 \text{ mm (0.80")}$

$\Delta_h = 20.3 \text{ mm} = (0.80\text{"})$

Assume half of contraction/expansion occurs at each bearing: $\Delta_s = 10.2 \text{ mm (0.40")}$

Determine $\Delta_{s,DL}$ from girder dead due to 3.5% slope load assuming $h_{rt} = 38 \text{ mm (1.5")}$

$\Delta_{s,DL} = 0.4\theta_b P h_{rt} / GA = 0.4(0.035)(534 \text{ kN})(38 \text{ mm}) / (0.621 \text{ MPa})(0.105 \text{ m}^2)$
 $= 4.36 \text{ mm (0.172")}$

Min $h_{rt} = 2(10.2 \text{ mm} + 4.4 \text{ mm}) = 29.2 \text{ mm (1.15")} < 38 \text{ mm (1.5")} \therefore \text{OK}$

3. Calculate Compressive Deformation Including Creep

Based on $\sigma_c = 5.11$ MPa (741 psi):

From TABLE 9.1, $\epsilon_c = 3.2\%$

$$\therefore \Delta_c = (0.032)(38 \text{ mm}) = 1.22 \text{ mm (0.048")}$$

Additional deformation due to taper (use bridge slope as taper), $\theta_b = 0.035$ radians:

$$\therefore \Delta_c = (1.35)(1.22 \text{ mm}) = 1.65 \text{ mm (0.065")}$$

$$\text{Long-term Deformation} = 1.15(\Delta_c) = 1.89 \text{ mm (0.075")}$$

4. Check Bridge End Rotation

Rotation = 0.003 radians + 0.01 radian (maximum mismatch between girder and bearing)

= 0.013 radians \therefore upward displacement = $0.013 \left(\frac{229}{3}\right) = 1.49 \text{ mm} < 1.89 \text{ mm}$ so no uplift expected for $\sigma_c = 5.11$ MPa (741 psi)

5. Specify Bearing Taper

From TABLE 9.2:

If bridge slope is 3.5%, most likely bearing taper is 4.17% (0.0417 radians)

Permanent mismatch = $0.0417 - 0.0350 = 0.0067$ radians < 0.01 radians assumed

6. Specify Steel Reinforcement/Elastomer Layer Thickness

Start with $S = 10$, use Equation 9.2 to calculate n , number of reinforcing shims

$$n = ((2 S h_{rt} (L+W))/LW) - 1 = 4.0$$

Use 4, Grade A570 steel shims, 2.7 (12 gage)

Calculate h_{rt} : $h_{rt} = 38 \text{ mm}/5 \text{ layers} = 7.6 \text{ mm (0.3")} < 8.46 \text{ mm (0.333")}$

Use 6.4 mm ($\frac{1}{4}$ ") cover layers and 9.5 mm ($\frac{3}{8}$ ") for the three interior layers. $h_{rt} = 41.3 \text{ mm (1 } \frac{5}{8} \text{ ")}$

Recalculate S : $S = 8 \therefore$ OK since it is within the target range

Check total height at mid length for compliance with AASHTO stability specification:

$$h_{rt} + 4h_s = 41.3 \text{ mm} + 4(2.67 \text{ mm}) = 52.0 \text{ mm (2.05")} > \frac{L}{3} \text{ OK}$$

7. Ensure No Slip

Check for $N > 0.00155 A$ (kN):

$$0.00155 A = 0.00155(457 \text{ mm})(229 \text{ mm}) = 162 \text{ kN (36.5 kips)} < 534 \text{ kN (120 kips)} \therefore \text{OK}$$

Final Design

$G = 0.090 \text{ ksi (50-55 durometer)}$

$S = 8$

$L = 229 \text{ mm (9")}$ $W = 457 \text{ mm (18")}$

$h_{rt} = 41.3 \text{ mm (1 5/8")}$ $h_{ri} = \text{top and bottom layers, 6.4 mm (1/4") interior layers, 9.5 mm (3/8")}$

4 Grade A570 2.7 mm (12 gage) steel shims oriented parallel to one another

Total height at mid length = 52.0 mm (2.05")

Height at thin end = $52.0 + (0.0278)(229/2) = 55.2 \text{ mm (2 3/16")}$

Height at thick end = $52.0 - (0.0278)(229/2) = 48.8 \text{ mm (1 15/16")}$

See Figure B.1 for cross-section of final tapered bearing design.

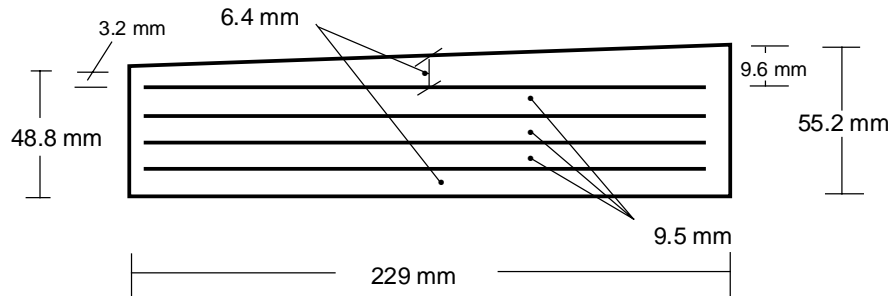


Figure B.1 Dimensions of Final Tapered Bearing Design

The flat and tapered designs are very similar. The same amount of elastomer and steel is used in both designs.

APPENDIX C

SELECTED PROPERTIES OF NATURAL RUBBER

The mechanical properties given are those of filled rubber vulcanizates and not are confined to bearing applications alone.

C.1 MECHANICAL PROPERTIES

Hardness (International Rubber Hardness Degrees scale range 0-100): 45 - 80

Density: 1.15 Mg/m^3 (71.6 lbs/ft³)

Poisson's Ratio: 0.4997

Bulk Modulus: 2000 - 2200 MPa (290-319 ksi) directly proportional to hardness

Compressive Qualities:

Compressive Modulus - a function of (directly proportional) to hardness and shape factor
Compressive Strength (approximate): 1000 MPa (145 Ksi)

Tensile Qualities:

Tensile Modulus - a function of (directly proportional to) hardness and shape factor
- at low strains, equal to the compressive modulus

Tensile Strength: 15-30 MPa (2175 - 4350 psi) indirectly proportional to hardness
(A = original cross section)

Elongation at Break: 200-600% directly proportional to hardness

Shear Qualities:

For 45-80 durometer hardness

Shear Modulus at 2% strain: 0.5-4.0 MPa (72.5 - 580 psi) directly proportional to hardness

Shear Modulus at 50% strain: 0.5-1.6 MPa (72.5 - 232 psi) directly prportional to hardness

C.2 THERMAL PROPERTIES

Specific Heat: $1.5 \text{ kJ/kg/}^\circ \text{C}$

Coefficient of volume expansion: $53 \times 10^{-5}/^\circ \text{C}$

Temperature at which stiffening begins to occur: -20°C

Low-temperature crystallization point: -25°C

Glass transition temperature: -60°C

Vulcanization temperature: $120\text{-}220^\circ \text{C}$

Temperature at which molecular breakdown occurs: 300°C

APPENDIX D

NOTATION

This Appendix gives the notation used throughout this report.

Longitudinal Axis	=	The axis of the bearings parallel to the longitudinal axis of the bridge girder(s)
Lot	=	A group of bearings made from the same batch of materials
Transverse Axis	=	The axis of the bearing perpendicular to the longitudinal axis
A	=	Gross plan area of the bearing
D	=	Gross diameter of a circular bearing
E_c	=	Effective compressive modulus of the elastomer, taking account of restraint of bulging = $3G(I + 2kS^2)$ (MPa, psi)
F_y	=	Yield strength of the steel reinforcement (MPa, psi)
G	=	Shear modulus of the elastomer (MPa, psi) at 73°F
H	=	Design shear force on bearing = $G A \Delta_h/h_r$
h_r	=	Total elastomer thickness of the bearing = $\sum h_{ri}$ (measured at mid-length in a tapered bearing)
h_{ri}	=	Thickness of elastomer layer number I
h_s	=	Thickness of one steel reinforcement layer
k	=	Constant dependent on elastomer hardness = 0.75, 0.60, and 0.55 for 50, 60, and 70 durometer elastomeric material, respectively
L	=	Gross dimension of rectangular bearing parallel to the longitudinal axis
n	=	Number of reinforcing layers
P	=	Compressive load on the bearing
S	=	Shape factor of one layer of a bearing (non-dimensional)
	=	$\frac{\text{Plan Area}}{\text{Area of Perimeter Free to Bulge}}$
	=	$\frac{LW}{2h_{ri}(L+W)}$ for rectangular without holes
W	=	Gross dimension of rectangular bearing parallel to the transverse axis
β	=	Modifying factor having a value of 1.0 for internal layers of reinforced bearings, 1.4 for cover layers, and 1.8 for plain pads
Δ_c	=	Instantaneous compressive deformation of bearing
Δ_h	=	total horizontal movement of superstructure, measured from state at which bearing is undeformed
Δ_s	=	Shear deformation of the bearing in one direction from the undeformed state, accounting for support flexibility
ϵ_{ci}	=	Instantaneous compressive strain in elastomer layer I (change in thickness divided by the unstressed thickness)
θ	=	Relative rotation of top and bottom surfaces of bearing (radians)
θ_b	=	Built in bearing taper (radians)

Subscripts:

DL	=	dead load
TL	=	total load
LL	=	live load
x	=	about transverse axis
z	=	about longitudinal axis
σ_c	=	P/A = average compressive stress on the bearing caused by the dead and live load, excluding impact

APPENDIX E

INDIVIDUAL TEST RESULTS

This Appendix gives the results of individual shear modulus, compressive stiffness, rotational stiffness, compressive creep, shear and compression fatigue, and compression failure tests by specimen.

NOTES:

- Specimen Code: First Letter - Manufacturer
 100,200 - Specified Shear Modulus - 0.7 MPa (100 psi), 1.4 MPa (200 psi)
 2,3,6 - Number of reinforcing steel shims
 0,4,6 - Requested Taper, Flat, 4%, 6%
 ** - denotes replicate test (on different specimen of same design)
- Manufacturer A provided only a limited number of specimens which were tested for shear and compressive stiffness, compressive creep and compression failure.
- Manufacturers B & C provided 3 each 229x711-mm (9"x28") bearings which were tested as follows:

TABLE E.1 DISTRIBUTION OF TEST SPECIMENS FROM MANUFACTURERS B AND C

Test	Manufacturer B	Manufacturer C
Shear Modulus	Bearing #1 cut in half	Bearing #1 cut in half
Compressive Stiffness	One half of Bearing #2	One half of Bearing #2
Rotational Stiffness	Bearing #1 (Shear Modulus Specimen)	Bearing #1 (Shear Modulus Specimen)
Compressive Creep	Other half of Bearing #2	Other half of Bearing #2
Compression Fatigue	only two tested	One third of Bearing #3
Shear Fatigue	only one tested	Other two thirds of Bearing #3 cut in half
Compression Failure	Bearing #3 cut in thirds	only one tested

E.1 SHEAR MODULUS TESTS

NOTES:

- Shear area (A) = 0.0813 m^2 (126 in^2) for all specimens
- Shear moduli listed are an average of simultaneous tests on two specimens (See Figure 2.2)
- Shear modulus is based on the slope of the load-displacement relationship from 0-50% strain

TABLE E.2 SHEAR MODULUS TESTS ON SPECIMENS FROM MANUFACTURER A

Specimen	Shore A Durometer Hardness	Total Elastomer Thickness mm(in)	Measured Taper (%)	Shear Modulus MPa (psi) $G = Hh_{rt} / \Delta_s A$ At $\sigma_c = 4.39 \text{ MPa}$ (637 psi)
A100-0-0	65	47.5 (1.87)	0	0.703 (102)
A100-2-0	62	45.5 (1.79)	0	0.658 (95.5)
A200-2-0	68	46.0 (1.81)	0	0.841 (122)
	70	45.5 (1.79)		0.825 (118)**
	69	45.7 (1.80)		0.869 (126)**

TABLE E.3 SHEAR MODULUS TESTS ON 0.7 MPa (100 PSI) SPECIMENS FROM MANUFACTURER B

Specimen	Shore A Durometer Hardness	Total Elastomer Thickness mm (in)	Measured Taper (%)	Calculated Shear Modulus $G = Hh_{rt} / \Delta_s A$ MPa (psi)	
				At $\sigma_c =$ 3.8 MPa (550 psi)	At $\sigma_c =$ 7.6 MPa (1100 psi)
B100-3-0	56	45.0 (1.77)	0	0.596 (86.4)	0.539 (78.2)
				0.574 (83.3)	0.506 (73.3)
B100-3-4	56	44.2 (1.74)	4.27	0.517 (74.9)	0.510 (73.9)
				0.537 (77.8)	0.535 (77.6)
B100-3-6	55	45.7 (1.80)	5.95	0.599 (86.9)	0.558 (81.0)
				0.563 (81.6)	0.548 (79.4)
B100-3-6*	56	45.0 (1.77)	5.59	0.606 (88.0)	0.574 (83.3)
				0.526 (76.3)	0.548 (79.4)
B100-6-0	58	44.5 (1.75)	0	0.645 (93.6)	0.615 (89.2)
				0.604 (87.6)	0.600 (87.1)
B100-6-4	59	43.7 (1.72)	4.18	0.657 (95.4)	0.631 (91.5)
				0.597 (86.6)	0.582 (84.5)
B100-6-6	59	44.7 (1.76)	5.56	0.643 (93.2)	0.592 (85.8)
				0.606 (88.0)	0.593 (86.0)

NOTES:

- Results in the first row for each specimen are from tests under matched slope conditions.
 - Results in the second row are from mismatched slope tests: Flat bearings against a 1.5% sloped platen, 4% bearings against a 6.25% sloped platen, and 6% bearings against a 3.8% sloped platen.
- * - denotes the one specimen with reinforcing shims oriented parallel to one another

TABLE E.4 SHEAR MODULUS TESTS ON 1.4 MPa (200 PSI) SPECIMENS FROM MANUFACTURER B

Specimen	Shore A Durometer Hardness	Total Elastomer Thickness mm (in)	Measured Taper (%)	Calculated Shear Modulus $G = Hh_{rt}/\Delta_s A$ MPa (psi)	
				At $\sigma_c =$ 3.8 MPa (550 psi)	At $\sigma_c =$ 7.6 MPa (1100 psi)
B200-3-0	72	46.0 (1.81)	0	0.986 (143)	0.876 (127)
				0.903 (131)	0.931 (135)
B200-3-4	69	46.2 (1.82)	4.78	0.848 (123)	0.834 (121)
				0.862 (125)	0.841 (122)
B200-3-6	69	47.8 (1.88)	5.41	0.876 (127)	0.855 (124)
				0.848 (123)	0.876 (127)
B200-6-0	72	46.2 (1.82)	0	1.02 (148)	0.979 (142)
				0.882 (128)	0.931 (135)
B200-6-4	70	46.2 (1.82)	4.89	0.924 (134)	0.876 (127)
				0.882 (128)	0.848 (123)
B200-6-6	71	46.5 (1.83)	5.75	0.959 (139)	0.890 (129)
				0.869 (126)	0.855 (124)

TABLE E.5 SHEAR MODULUS TESTS ON 0.7 MPa (100 psi) SPECIMENS FROM MANUFACTURER C

Specimen	Shore A Durometer Hardness	Total Elastomer Thickness mm(in)	Measured Taper (%)	Calculated Shear Modulus $G = Hh_{rt}/\Delta_s A$ MPa (psi)	
				At $\sigma_c =$ 3.79 MPa (550 psi)	At $\sigma_c =$ 7.59 MPa (1100 psi)
C100-3-0	55	44.5 (1.75)	0	0.630 (91.4)	0.570 (82.6)
				0.615 (89.3)	0.575 (83.4)
C100-3-4	55	45.0 (1.77)	4.10	0.640 (92.9)	0.592 (85.8)
				0.602 (87.3)	0.562 (81.5)
C100-3-6	54	45.0 (1.77)	5.80	0.589 (85.5)	0.557 (80.8)
				0.613 (88.9)	0.569 (82.5)
C100-6-0	55	44.5 (1.75)	0	0.658 (95.4)	0.605 (87.7)
				0.637 (92.3)	0.617 (89.4)
C100-6-4	54	44.5 (1.75)	4.00	0.637 (92.3)	0.583 (84.5)
				0.519 (75.3)	0.537 (77.9)
C100-6-6	55	44.7 (1.76)	5.70	0.630 (91.4)	0.591 (85.7)
				0.637 (92.4)	0.609 (88.3)

TABLE E.6 SHEAR MODULUS TESTS ON 1.4 MPa (200 PSI) SPECIMENS FROM MANUFACTURER C

Specimen	Shore A Durometer Hardness	Total Elastomer Thickness mm(in)	Measured Taper (%)	Calculated Shear Modulus $G = Hh_{rt} / \Delta_s A$ MPa (psi)	
				At $\sigma_c =$ 3.79 MPa (550 psi)	At $\sigma_c =$ 7.59 MPa (1100 psi)
C200-3-0	65	46.5 (1.83)	0	0.786 (114)	0.786 (114)
				0.786 (114)	0.786 (114)
C200-3-4	66	45.5 (1.79)	3.68	0.841 (122)	0.821 (119)
				0.703 (102)	0.772 (112)
C200-3-6	68	45.7 (1.80)	6.02	0.800 (116)	0.779 (113)
				0.807 (117)	0.807 (117)
C200-6-0	68	45.0 (1.77)	0	0.876 (127)	0.834 (121)
				0.786 (114)	0.807 (117)
C200-6-4	68	45.0 (1.77)	3.93	0.924 (134)	0.883 (128)
				0.731 (106)	0.793 (115)
C200-6-6	67	45.2 (1.78)	5.65	0.876 (127)	0.841 (122)
				0.903 (131)	0.869 (126)

E.2 HORIZONTAL FORCES AND DISPLACEMENTS FROM COMPRESSION LOADS ALONE

NOTES:

- All specimens were those used for shear modulus tests. Plan area= 0.0813 m² (126 in²)
- Horizontal displacement tests were performed only on tapered bearings at matched slopes
- Horizontal forces were determined by preventing horizontal displacements. See Chapter 3, Section 3.1.

TABLE E. 7 HORIZONTAL FORCE & DISPLACEMENT TESTS - 0.7 MPa (100 PSI) SPECIMENS - MANUFACTURER B

Specimen	Shore A Durometer Hardness	Total Elast. Thick. mm(in)	Meas. Taper (%)	Middle Platen Slope (%)	Horizontal Force, H kN (kips)	
					Horizontal Displ., Δ _s mm(in) †	
					At σ _c =3.8 MPa (550 psi)	At σ _c =7.6 MPa (1100 psi)
B100-3-0	56	45.0 (1.77)	0	1.5	1.73 (0.391)	3.37 (0.758)
B100-3-4	56	44.2 (1.74)	4.27	3.8	4.32 (0.971)	5.79 (1.30)
				6.25	2.74 (0.108) †	6.55 (0.258) †
B100-3-6	55	45.7 (1.80)	5.95	6.25	5.53 (1.24)	11.6 (2.60)
				3.8	6.81 (1.53)	15.3 (3.41)
B100-3-6*	56	45.0 (1.77)	5.59	6.25	7.87 (0.310) †	19.2 (0.754) †
				3.8	5.07 (1.14)	10.4 (2.33)
B100-6-0	58	44.5 (1.75)	0	1.5	4.75 (0.187) †	11.4 (0.450) †
				3.8	1.84 (0.414)	2.84 (0.639)
B100-6-4	59	43.7 (1.72)	4.18	3.8	1.32 (0.296)	1.69 (0.379)
				6.25	1.08 (0.0424) †	2.35 (0.0927) †
B100-6-6	59	44.7 (1.76)	5.56	6.25	4.27 (0.958)	8.48 (1.91)
				3.8	5.43 (1.22)	10.4 (2.34)
					5.49 (0.216) †	11.4 (0.450) †
					1.79 (0.403)	3.63 (0.817)

* denotes the one specimen with reinforcing shims oriented parallel to one another

† horizontal displacement data are given in the shaded cells

TABLE E.8 HORIZONTAL FORCE & DISPLACEMENT TESTS - 1.4 MPa (200 PSI) SPECIMENS - MANUFACTURER B

Specimen	Shore A	Total Elast.	Meas.	Middle Platen	Horizontal Force kN (kips)	
					Horizontal Displ. mm(in) †	
	Durometer Hardness	Thick. mm(in)	Taper (%)	Slope (%)	At $\sigma_c=3.8$ MPa (550 psi)	At $\sigma_c=7.6$ MPa (1100 psi)
B200-3-0	72	46.0 (1.81)	0	1.5	1.40 (0.313)	3.00 (0.675)
B200-3-4	69	46.2 (1.82)	4.78	3.8	4.00 (0.900)	8.85 (1.99)
				6.25	2.62 (0.103) †	6.43 (0.253) †
B200-3-6	69	47.8 (1.88)	5.41	6.25	6.48 (1.46)	14.5 (3.27)
				3.8	6.48 (1.46)	15.3 (3.43)
B200-6-0	72	46.2 (1.82)	0	1.5	1.16 (0.260)	2.77 (0.621)
B200-6-4	70	46.2 (1.82)	4.89	3.8	3.48 (0.781)	9.80 (2.20)
				6.25	1.78 (0.070) †	4.67 (0.184) †
B200-6-6	71	46.5 (1.83)	5.75	6.25	6.48 (1.46)	14.8 (3.32)
				3.8	5.64 (1.27)	14.0 (3.15)
					4.06 (0.160) †	8.05 (0.317) †
					3.42 (0.769)	8.64 (1.94)

† horizontal displacement data are given in the shaded cells

TABLE E.9 HORIZONTAL FORCE & DISPLACEMENT TESTS - 0.7 MPa (100 PSI) SPECIMENS - MANUFACTURER C

Specimen	Shore A Durometer Hardness	Total Elast. Thick. mm(in)	Meas. Taper (%)	Middle Platen Slope (%)	Horizontal Force kN (kips)	
					Horizontal Displ. mm(in) †	
					At $\sigma_c=3.8$ MPa (550 psi)	At $\sigma_c=7.6$ MPa (1100 psi)
C100-3-0	55	44.5 (1.75)	0	1.5	1.79 (0.402)	2.97 (0.669)
C100-3-4	55	45.0 (1.77)	4.10	3.8	4.48 (1.01)	9.48 (2.13)
					5.03 (0.198) †	10.6 (0.416) †
				6.25	7.88 (1.77)	16.4 (3.69)
C100-3-6	54	45.0 (1.77)	5.80	6.25	6.58 (1.48)	14.6 (3.29)
					8.41 (0.331) †	17.5 (0.688) †
				3.8	4.00 (0.900)	8.64 (1.94)
C100-6-0	55	44.5 (1.75)	0	1.5	1.53 (0.343)	4.00 (0.900)
C100-6-4	54	44.5 (1.75)	4.00	3.8	4.00 (0.900)	9.16 (2.06)
					6.38 (0.251) †	13.6 (0.535) †
				6.25	6.48 (1.46)	14.4 (3.24)
C100-6-6	55	44.7 (1.76)	5.70	6.25	10.1 (2.27)	19.2 (4.32)
					10.8 (0.425) †	21.3 (0.837) †
				3.8	5.65 (1.27)	12.6 (2.83)

† horizontal displacement data are given in the shaded cells

TABLE E.10 HORIZONTAL FORCE & DISPLACEMENT TESTS - 1.4 MPa(200 PSI) SPECIMENS - MANUFACTURER C

Specimen	Shore A Durometer Hardness	Total Elast. Thick. mm(in)	Meas. Taper (%)	Middle Platen Slope (%)	Horizontal Force kN (kips)	
					Horizontal Displ. mm(in) †	
					At $\sigma_c=3.8$ MPa (550 psi)	At $\sigma_c=7.6$ MPa (1100 psi)
C200-3-0	65	46.5 (1.83)	0	1.5	1.53 (0.343)	1.92 (0.432)
C200-3-4	66	45.5 (1.79)	3.68	3.8	4.79 (1.08)	10.3 (2.32)
				6.25	3.91 (0.154) †	7.97 (0.314) †
C200-3-6	68	45.7 (1.80)	6.02	6.25	7.53 (1.69)	17.5 (3.93)
				3.8	6.37 (1.43)	15.2 (3.41)
C200-6-0	68	45.0 (1.77)	0	1.5	5.00 (0.197) †	10.7 (0.423) †
C200-6-4	68	45.0 (1.77)	3.93	3.8	3.37 (0.758)	8.43 (1.89)
				6.25	1.84 (0.414)	3.11 (0.698)
C200-6-6	67	45.2 (1.78)	5.65	6.25	5.58 (1.25)	13.2 (2.96)
				3.8	4.72 (0.186) †	9.04 (0.356) †
					9.53 (2.14)	20.9 (4.69)
					8.23 (1.85)	19.1 (4.30)
					6.65 (0.262) †	13.6 (0.534) †
					3.63 (0.817)	10.5 (2.37)

† horizontal displacement data are given in the shaded cells

E.3 COMPRESSIVE STIFFNESS TESTS

NOTES:

- Plan Area (A) = 0.0813 m² (126 in²) for all specimens
- Stiffness reported is the slope of the load-displacement relationship from 3.45 MPa (500 psi) to 10.35 MPa (1500 psi) compressive stress

TABLE E.11 COMPRESSIVE STIFFNESS TEST RESULTS ON SPECIMENS FROM MANUFACTURERS A AND B

Specimen	Shore A Hardness	Total Elastomer Thickness- mm(in)	Measured Taper (%)	Compressive Stiffness kN/mm (kips/in)
A100-0-0	65	46.5 (1.83)	0	27.5 (158)
A100-2-0	62	45.5 (1.79)	0	180 (1033)
A200-0-0	68	46.2 (1.82)	0	28.6 (164)
A200-2-0	68	45.5 (1.79)	0	178 (1019)
	70	46.0 (1.81)	0	175 (1000)**
B100-3-0	58	45.0 (1.77)	0	203 (1163)
B100-3-4	59	44.2 (1.74)	4.21	234 (1338)
B100-3-6	56	45.5 (1.79)	5.96	220 (1260)
B100-3-6*	58	45.0 (1.77)	5.46	240 (1376)
B100-6-0	59	44.2 (1.74)	0	664 (3795)
B100-6-4	59	43.2 (1.70)	4.17	623 (3564)
B100-6-6	60	44.2 (1.74)	5.54	579 (3310)
B200-3-0	71	46.0 (1.81)	0	293 (1672)
B200-3-4	70	46.5 (1.83)	4.79	244 (1396)
B200-3-6	69	47.2 (1.86)	5.40	283 (1620)
B200-6-0	72	46.5 (1.83)	0	741 (4237)
B200-6-4	72	46.7 (1.84)	4.89	802 (4586)
B200-6-6	70	46.5 (1.83)	5.77	823 (4705)

* - denotes the one specimen with reinforcing shims oriented parallel to one another

TABLE E.12 COMPRESSIVE STIFFNESS TEST RESULTS ON SPECIMENS FROM MANUFACTURER C

Specimen	Shore A Durometer Hardness	Total Elastomer Thickness mm (in)	Measured Taper (%)	Compressive Stiffness kN/mm (kips/in)
C100-3-0	54	44.5 (1.75)	0	209 (1194)
C100-3-4	55	44.7 (1.76)	4.50	204 (1166)
C100-3-6	55	45.5 (1.79)	5.80	259 (1481)
C100-6-0	55	44.5 (1.75)	0	547 (3127)
C100-6-4	55	44.5 (1.75)	4.10	415 (2370)
C100-6-6	54	45.0 (1.77)	5.80	440 (2517)
C200-3-0	68	45.5(1.79)	0	285 (1629)
C200-3-4	68	45.5(1.79)	4.00	232 (1328)
C200-3-6	68	46.0(1.81)	6.08	273 (1561)
C200-6-0	70	45.5(1.79)	0	747 (4268)
C200-6-4	69	45.7(1.80)	3.82	485 (2772)
C200-6-6	68	45.2(1.78)	5.65	618 (3534)

E.4 ROTATIONAL STIFFNESS TESTS

NOTES:

- Rotational stiffness reported is the slope of the linear portion of the moment rotation curve.
- Shear area (A) = 0.0813 m² (126 in²) for all specimens

TABLE E.13 ROTATIONAL STIFFNESS TESTS ON SPECIMENS FROM MANUFACTURERS B AND C

Specimen	Shore A Durometer Hardness	Total Elastomer Thickness mm (in)	Measured Taper (%)	Rotational Stiffness N-m/radian (K-in/degree)	
				At $\sigma_c = 3.8$ MPa (550 psi)	At $\sigma_c = 7.6$ MPa (1100 psi)
C100-3-0	55	44.5 (1.75)	0	408 (63.1)	479 (74.0)
C100-3-4	55	45.0 (1.77)	4.10	450 (69.5)	471 (72.7)
C100-3-6	54	45.0 (1.77)	5.80	386 (59.6)	405 (62.6)
B100-3-6*	56	45.0 (1.77)	5.59	335 (51.8)	385 (59.5)
C100-6-0	55	44.5 (1.75)	0	829 (128)	845 (131)
C100-6-4	54	44.5 (1.75)	4.00	780 (121)	830 (128)
C100-6-6	55	44.7 (1.76)	5.70	856 (132)	856 (132)
B200-3-0	72	46.0 (1.81)	0	538 (83.2)	545 (84.2)
B200-3-4	69	46.2 (1.82)	4.78	390 (60.2)	522 (80.6)
B200-3-6	69	47.8 (1.88)	5.41	390 (60.2)	438 (67.7)
B200-6-0	72	46.2 (1.82)	0	865 (134)	1132 (175)
B200-6-4	70	46.2 (1.82)	4.89	962 (149)	1072 (166)
B200-6-6	71	46.5 (1.83)	5.75	975 (151)	1085 (168)

* - denotes the one specimen with reinforcing shims oriented parallel to one another

E.5 COMPRESSIVE CREEP TESTS

TABLE E.14 COMPRESSIVE CREEP TESTS ON SPECIMENS FROM MANUFACTURERS A, AND B

Specimen	Shore A Durometer Hardness	Total Elastomer Thickness mm (in)	Measured Taper (%)	Creep Percent Initial Deflection	
				Southwell Prediction	Logarithmic Prediction
A100-2-0	62	46.5 (1.83)	0	43.0	46.2
A200-2-0	68	45.5 (1.79)	0	49.5	58.0
B100-3-0	58	45.0 (1.77)	0	45.0	34.5
B100-3-4	59	44.2 (1.74)	4.21	41.5	44.2
B100-3-6	56	45.5 (1.79)	5.96	55.5	37.1
B100-3-6*	58	45.0 (1.77)	5.46	50.5	67.5
B100-6-0	59	44.2 (1.74)	0	12.0	17.5
B100-6-4	59	43.2 (1.70)	4.17	17.5	16.4
B100-6-6	60	44.2 (1.74)	5.54	15.5	15.3
B200-3-0	71	46.0 (1.81)	0	40.4	32.5
B200-3-4	70	46.5 (1.83)	4.79	42.7	21.4
B200-3-6	69	47.2 (1.86)	5.40	47.0	24.1
B200-6-0	72	46.5 (1.83)	0	11.3	5.25
B200-6-4	72	46.7 (1.84)	4.89	14.0	6.47
B200-6-6	70	46.5 (1.83)	5.77	15.3	6.78

* - denotes the one specimen with reinforcing shims oriented parallel to one another

TABLE E.15 COMPRESSIVE CREEP TESTS ON SPECIMENS FROM MANUFACTURER C

Specimen	Shore A Durometer Hardness	Total Elastomer Thickness mm (in)	Measured Taper (%)	Creep	
				Percent Initial Deflection Logarithmic Prediction	Southwell Prediction
C100-3-0	54	44.5 (1.75)	0	35.0	47.0
C100-3-4	55	44.7 (1.76)	4.50	47.5	46.0
C100-3-6	55	45.5 (1.79)	5.80	X	X
C100-6-0	55	44.5 (1.75)	0	17.0	15.5
C100-6-4	55	44.5 (1.75)	4.10	18.0	8.00
C100-6-6	54	45.0 (1.77)	5.80	X	X
C200-3-0	68	45.5(1.79)	0	35.5	38.8
C200-3-4	68	45.5(1.79)	4.00	42.5	23.4
C200-3-6	68	46.0(1.81)	6.08	60.5	34.0
C200-6-0	70	45.5(1.79)	0	21.0	15.2
C200-6-4	69	45.7(1.80)	3.82	16.5	5.60
C200-6-6	68	45.2(1.78)	5.65	20.0	7.60

X - Bearings slipped out during creep test yielding additional deformations above creep amount

E.6 FATIGUE TESTS

NOTES:

- Plan area on all fatigue specimens = 0.0523 m² (81 in²)

TABLE E.16 SHEAR FATIGUE TESTS ON SPECIMENS FROM MANUFACTURERS B AND C

Specimen	Shore A Durometer Hardness	Total Elastomer Thickness mm(in)	Measured Taper (%)	Shear Stiffness kN/mm (kips/in)	
				Starting	Ending
C100-3-0	53	44.5 (1.75)	0	0.895 (5.10)	0.857 (4.89)
C100-3-4	53	45.0 (1.77)	4.19	0.885 (5.05)	0.842 (4.81)
C100-3-6	53	45.5 (1.79)	5.99	0.875 (4.99)	0.863 (4.93)
B100-6-0	60	44.5 (1.75)	0	Lost Data	Lost Data
C100-6-4	67	44.7 (1.76)	4.16	0.937 (5.35)	0.930 (5.30)
C100-6-6	68	45.2 (1.78)	5.73	0.972 (5.55)	0.930 (5.30)
C200-3-0	67	45.2 (1.78)	0	1.24 (7.05)	1.15 (6.55)
C200-3-4	68	45.7 (1.80)	4.18	1.35 (7.70)	1.17 (6.65)
C200-3-6	67	48.0 (1.89)	5.93	1.31 (7.45)	1.14 (6.50)
C200-6-0	69	45.5 (1.79)	0	1.33 (7.55)	1.26 (7.15)
C200-6-4	69	45.2 (1.78)	4.06	1.42 (8.10)	1.22 (6.95)
C200-6-6	67	45.7 (1.80)	5.83	1.31 (7.45)	1.14 (6.50)

TABLE E.17 COMPRESSION FATIGUE TESTS ON SPECIMENS FROM MANUFACTURERS B AND C

Specimen	Shore A Durometer Hardness	Total Elastomer Thickness mm(in)	Measured Taper (%)	Compressive Stiffness kN/mm (kips/in)	
				Starting	Ending
B100-3-0	58	44.5 (1.75)	0	111 (636)	102 (583)
C100-3-4	53	45.0 (1.77)	4.19	114 (650)	98.1 (560)
C100-3-6	53	45.5 (1.79)	5.99	102 (580)	90.2 (515)
B100-6-0	60	44.5 (1.75)	0	214 (1223)	207 (1179)
C100-6-4	54	44.7 (1.76)	4.16	202 (1155)	177 (1010)
C100-6-6	55	45.2 (1.78)	5.73	173 (990)	173 (990)
C200-3-0	67	45.2 (1.78)	0	132 (755)	113 (645)
C200-3-4	68	45.7 (1.80)	4.18	143 (816)	114 (650)
C200-3-6	67	48.0 (1.89)	5.93	117 (669)	102 (584)
C200-6-0	69	45.5 (1.79)	0	234 (1334)	234 (1334)
C200-6-4	69	45.2 (1.78)	4.06	251 (1432)	234 (1333)
C200-6-6	67	45.7 (1.80)	5.83	242 (1383)	242 (1383)

E.7 COMPRESSION FAILURE TESTS

NOTES:

- Plan area on all specimens from Manufacturers B and C = 0.0523 m² (81 in²)

TABLE E. 18 COMPRESSION FAILURE TESTS ON 3 STEEL SHIM SPECIMENS FROM MANUFACTURER B

Specimen	Shore A Durometer Hardness	Total Elast. Thick. mm(in)	Meas. Taper (%)	Stress at Loss of Stiffness MPa (psi)	Strain (%)	Fracture Stress MPa (psi)	Strain (%)
B100-3-0a	57	1.78	0	76.6 (11100)	35	140 (20300)	56
b				84.8 (12300)	40	140 (20300)	59
B100-3-4a	56	1.87	4.16	72.4 (10500)	42	121 (17500)	60
b				72.4 (10500)	41	117 (16900)	57
c				68.1 (9870)	44	117 (17000)	66
B100-3-6a	55	1.80	6.00	72.4 (10500)	43	112 (16200)	60
b				73.8 (10700)	43	103 (14900)	57
c				76.6 (11100)	44	121 (17600)	59
B100-3-6*	56	1.76	5.59	86.9 (12600)	41	121 (17600)	56
b				80.7 (11700)	41	112 (16200)	55
c				85.5 (12400)	37	130 (18900)	52
B200-3-0a	71	1.81	0	55.3 (8020)	23	108 (15700)	41
b				54.5 (7900)	23	121 (17600)	49
c				53.2 (7720)	25	112 (16200)	68
B200-3-4a	69	1.82	5.08	59.6 (8640)	26	105 (15200)	
b				78.6 (11400)	34	129 (18700)	53
c				78.6 (11400)	35	129 (18700)	54
B200-3-6a	70	1.83	5.53	75.2 (10900)	39	106 (15400)	56
b				63.9 (9260)	33	102 (14800)	50
c				86.2 (12500)	34	111 (16100)	44

TABLE E. 19 COMPRESSION FAILURE TESTS ON 6 STEEL SHIM SPECIMENS - MANUFACTURERS B AND C

Specimen	Shore A Durometer Hardness	Total Elast. Thick. mm(in)	Meas. Taper (%)	Stress at Loss of Stiffness MPa (psi)	Strain (%)	Fracture Stress MPa (psi)	Strain (%)
B200-6-0a	71	1.81	0	82.3 (12000)	18	144 (20900)	32
b				76.6 (11100)	18	155 (22500)	34
c				78.6 (11400)	17	146 (21200)	36
B100-6-4a	57	1.71	4.11	80.9 (11700)	20	No Fracture	
b				80.9 (11700)	20	No Fracture	
c				76.6 (11100)	25	No Fracture	
B100-6-6a	56	1.74	5.53	85.5 (12400)	26	No Fracture	
b				97.9 (14200)	30	161 (23400)	51
c				80.9 (11700)	21	No Fracture	
C100-6-0a	55	1.79	0	63.9 (9260)	20	81.4 (11800)	26
b				73.8 (10700)	23	117 (17000)	41
c				59.6 (8640)	19	92.4 (13400)	29

NOTES:

- Specimens “a”, “b”, and “c” were all 229x229 mm (9”x9”) sections from one 229x711 mm (9”x28”) bearing
- Tests on specimens “a” and “b” for tapered bearings were performed at matched slopes
- Tests on specimens “c” for tapered bearings were performed at mismatched slopes: 4% bearings were compressed to failure against 6.25% platens and 6% bearings were compressed to failure against 4.17% platens.
- Tests marked “No Fracture” were discontinued when the compressive stress reached 155 MPa (22500 psi)

TABLE E.20 COMPRESSION FAILURE TESTS ON 2 STEEL SHIM SPECIMENS FROM MANUFACTURER A

Specimen	Shore A Durometer Hardness	Total Elast. Thick. mm(in)	Meas. Taper (%)	Stress at Loss of Stiffness MPa (psi)	Strain (%)	Fracture Stress MPa (psi)	Strain (%)
A100-2-0	63	1.81	0	52.0 (7540)	39	75.2 (10900)	53
A200-0-0	71	1.80	0	38.3 (5560)	31	59.7 (8659)	46

NOTE:

- Plan area on all specimens from Manufacturer A = 0.0813 m² (126 in²)

GLOSSARY

The sources of the definitions given below are primarily References (13) and (33).

Antioxidant—chemicals added to an elastomeric compound to reduce physical changes caused by chemical reaction with oxygen.

Antiozonant—chemicals added to an elastomeric compound to reduce changes in physical properties caused by chemical reaction with ozone.

Antiozonant Waxes—waxes added to an elastomeric compound for the purpose of migrating to the rubber surface and blocking ozone attack.

β -factor—a factor intended to account for the fact that unbonded elastomer layers (plain pads and cover layers of reinforced bearings) bulge more than internal layers of reinforced bearings. The shape factor of the pad or layer is divided by β to reflect the additional bulging. Equal to 1.8 for plain pads and 1.4 for cover layers of reinforced pads.

Bearing seat—the surface on the bridge abutment, normally concrete, upon which the bearing is positioned.

Bulk Modulus—a measurement of compressibility
$$\frac{\text{hydrostatic compression}}{\text{change in volume}}$$

Chloroprene—monomer compound formed by the reaction of vinylacetylene with hydrogen chloride. Generally polymerized to form polychloroprene (neoprene).

Compound—substance whose constituent elements are chemically bonded together. Also a term used by manufacturers when referring to a particular mix of ingredients.

Compressive Modulus— $E_c = \sigma_c / \epsilon_c = 3G(1 + 2kS^2)$

Creep—continued deformation under constant load

Crystallization—phase change of elastomer during which segments of the long-chain molecules gradually become reoriented with reference to each other resulting in an increase in stiffness and hardness.

Delamination—separation of elastomer and reinforcement.

Durometer—instrument for measuring the hardness of an elastomer.

Elastomer—any member of a class of polymeric substances possessing rubberlike qualities, especially the ability to regain shape almost completely after large deformation. Generally applied only to vulcanized materials. See Polymer.

Filler—material, not possessing rubberlike qualities, included in the elastomer compound. Carbon black is most commonly used and its addition tends to increase hardness, shear stiffness, and bulk modulus. It delays slightly the onset of low-temperature crystallization, and, because it is cheaper than raw polymer, it reduces the cost of the compounded elastomer.

Glass transition temperature—temperature at which natural rubber experiences a rapid increase in stiffness and becomes glass-like and brittle. Approximately -60°C .

Gum Rubber—unfilled, vulcanized rubber.

Hardness—mechanical property of a material which describes its resistance to indentation of a standard device (e.g., a durometer). Measured in degrees on several scales (International Rubber Hardness, Shore ‘A’, Shore ‘B’), each of which is based on the use of a different-shaped indenter. Measurements show considerable scatter, and numerical values on all scales are about the same for materials suitable for bridge bearings (i.e., 45-65)

Hydrostatic stress—direct stress having the same value in all directions.

IHRD - International Rubber Hardness Degrees (see hardness).

Laminate—layer of reinforcing material bonded to rubber in order to prevent its lateral expansion.

Low-temperature crystallization—crystallization caused by temperatures below -25 degrees C.

Natural Rubber (polyisoprene) -- polymer occurring naturally in the sap of plants, particularly *Hevea brasiliensis*.

Neoprene—any class of elastomers made by polymerization of chloroprene. Notable properties are good resistance to abrasion, oxidation and chemical attack. Neoprene (capitalized) has been used by the duPont company for many years to describe a particular product of the company.

Ozone resistance test—standard test (e.g., ASTM D1149) to determine the ability of a material to retain its original properties when subjected to high concentrations of ozone for a given period of time.

Polychloroprene—polymerized form of the monomer chloroprene. Chemical name for neoprene.

Polyisoprene—chemical name for natural rubber.

Polymer—a material made of long-chains of molecules consisting of linked smaller molecules or monomers. Rubbers are a class of polymer which have the potential for large elastic deformations under load. (i.e., those)

Polymerization—the process of forming long chains of molecules by joining a number of smaller molecules or monomers.

Relaxation—decrease of stress with time under constant deformation.

Rollover—local deformation other than due to simple shear at corners of an elastomer subjected to shear deformation.

Rubber—natural or synthetic organic polymer able to undergo very large deformations and then return to its original shape on removal of the load. The term is applied both to the raw polymer and to the compounded and vulcanized elastomer.

Set (or permanent set) - deformation not recovered after a load is removed

Shape Factor—dimensionless geometric factor defined as
$$\frac{\text{area of one loaded surface}}{\text{total area free to bulge}}$$

It gives an indication of the compressive stiffness of an elastomeric bearing, regardless of the shape in plan.

Shore Hardness -- (see hardness)

Vulcanizate—polymer which has been vulcanized

Vulcanization—process of inducing cross-links in a polymer by chemical reaction. Requires heat, pressure, and often a vulcanizing agent that varies with the polymer used.

REFERENCES

1. Arditoglou, Yorgho, "Tests on Rubber," Master's Thesis, University of Texas at Austin, May 1994. 84 pp.
2. Bell, L. W., Shloss, A. L. and Subramanian, N. S., "Additional Design Data on Full-Size Bridge Bearing Pads of Neoprene," *Special Publication SP-70, American Concrete Institute*. Detroit, Michigan, 1982, pp. 1087-1099.
3. "Bridge Bearings," *National Cooperative Highway Research Program Synthesis of Highway Practice #41*, National Research Council, Washington, D.C., 1977, 53 pp.
4. "Bridge Bearings," *Memo to Designers 7-1*, California Department of Transportation, June 1994, 69 pp.
5. Clark, Earl V. and Moulthrop, Kendall, "Load-Deformation Characteristics of Elastomeric Bridge Bearing Pads," *Highway Research Record #34*, Highway Research Board, Washington, D.C., 1963, pp. 90-116.
6. "Design of Neoprene Bearing Pads," E. I. duPont de Nemours and Company (Inc.), Elastomers Division, Wilmington, Delaware, August 1983, 13 pp.
7. "Engineering Properties of Neoprene Bridge Bearings," E. I. duPont de Nemours and Company (Inc.), Elastomer Chemicals Department, Wilmington, Delaware, 1959, 26 pp.
8. Fairbanks, Hardy E., "The Use of Elastomeric Pads as Bearings for Steel Beams," Master's Thesis, Agricultural and Mechanical College of Texas, August 1960, 114 pp.
9. Grote, Jupp, "Over 20 Years of Elastomeric Bearings Without Trouble: A Scheme for Safety and Reliability," *Special Publication SP-70, American Concrete Institute*, Detroit, 1982, pp. 865-886.
10. Hamzeh, Osama, "Finite Element Analysis of Elastomeric Bridge Bearings," Ph.D. Dissertation, The University of Texas at Austin, August 1995.
11. Iverson, James K. and Pfeifer, Donald W., "New PCI Bearing Pad Design Recommendations," *Special Publication SP94-14, American Concrete Institute*, Detroit, 1982, pp. 233-246.
12. Lee, David J., *The Theory and Practice of Bearings and Expansion Joints*, Cement and Concrete Association, UK, 1971, 65 pp.
13. Lindley, Peter B., *Engineering Design with Natural Rubber*, Malaysian Rubber Producers' Research Association, Hertford, England, 1992, 33 pp.
14. Lindley, Peter B., "Natural Rubber Structural Bearings," *Special Publication SP-70, American Concrete Institute*, Detroit, 1982, pp. 353-379.
15. Long, J. E., *Bearings in Structural Engineering*, Newnes-Butterworths Publishing, London, 1974. 161 pp.
16. Manning, D. and Bassi, K., "Bridge Bearing Performance in Ontario," *Special Publication SP94-59, American Concrete Institute*, Detroit, 1982, pp. 1017-1036.
17. Minor, John C. and Egen, Richard A., "Elastomeric Bearing Research," *National Cooperative Highway Research Program Report #109*, Transportation Research Board, National Research Council, Washington, D.C., 1970, 62 pp.
18. Ozell, A. M. and Diniz, J. F., "Report on Tests of Neoprene Pads Under Repeated Shear Loads," *Highway Research Board Bulletin #242*, National Research Council, Washington, D.C., 1960, pp. 20-27.
19. Pare, R. L. and Keiner, E. P., "Elastomeric Bridge Bearings," *Highway Research Board Bulletin #242*, National Research Council, Washington, D.C., 1960, pp. 1-19.
20. Pare, Robert Lee, "Neoprene Elastomer Bearings - Ten years Experience Proves Their Importance," *Civil Engineering*, November 1967, pp. 37-39.

21. Porter, L. S. and Meinecke, E. A., "Influence of Compression Upon the Shear Properties of Bonded Rubber Blocks," *Rubber Chemistry and Technology*, V. 53. pp. 1133-1144.
22. Purkiss, C. W., "New Design Parameters for Elastomeric Bridge Bearings: What They Mean in Terms of Performance," *Special Publication SP-70, American Concrete Institute*, Detroit, 1982, pp. 379-387.
23. Rejcha, Charles, "Design of Elastomer Bearings," *PCI Journal*, October 1964, pp. 62-78.
24. Roeder, C. W., Stanton, J. F. and Feller, T., "Low-Temperature Behavior and Acceptance Criteria for Elastomeric Bridge Bearings," *National Cooperative Highway Research Program Report #325*, Transportation Research Board, National Research Council, Washington, D.C., December 1989, 69 pp.
25. Roeder, C. W., Stanton, J. F. and Taylor, A. W., "Performance of Elastomeric Bearings," *National Cooperative Highway Research Program Report #298*, Transportation Research Board, National Research Council, Washington, D.C., October 1987, 100 pp.
26. Roeder, Charles W., Stanton, John F. and Taylor, Andrew W., "Failure Modes of Elastomeric Bearings and the Influence of Manufacturing Methods," *Special Publication SP94-17, American Concrete Institute*, Detroit, 1986, pp. 279-295.
27. Roeder, Charles W., Stanton, John F., "State-of-the-Art Elastomeric Bridge Bearing Design," *ACI Structural Journal* 88-S5, January-February 1991, pp. 31-41.
28. Schrage, I., "Anchorage of Bearing Pads by Friction," *Special Publication SP-70, American Concrete Institute*, Detroit, 1981, pp. 197-213.
29. Sestak, J. J., Aldridge, W. W. and Fears, F. K., "A Comparative Study of Elastomeric Materials for Bridge Bearing Pads," *The University of Oklahoma Research Institute*, Norman, Oklahoma, March 1967, 111 pp.
30. Standard Specifications for Highway Bridges, 8th Edition, AASHTO, Washington D.C., 1961.
31. Standard Specifications for Highway Bridges, 13th Edition, AASHTO, Washington D.C., 1985.
32. Standard Specifications for Highway Bridges, 15th Edition, AASHTO, Washington D.C., 1992.
33. Stanton, J. F. and Roeder, C. W., "Elastomeric Bearings Design, Construction, and Materials," *National Cooperative Highway Research Program Report #248*, Transportation Research Board, National Research Council, Washington, D.C., August 1982, 82 pp.
34. Stanton, John F. and Roeder, Charles W., "Elastomeric Bridge Bearings Specifications: Review of the Present and Proposals for the Future," *ACI Journal*, Nov-Dec 1983, pg. 514.
35. Stanton, John F. and Roeder, Charles W., "Elastomeric Bearings: An Overview," *Concrete International: Design and Construction*, V.14, No 1, January 1992, pp. 41-46.
36. Stevenson, A. and Price, A. R., "A Case Study of Elastomeric Bridge Bearings After 20 Years of Service," *Special Publication SP94-6, American Concrete Institute*, Detroit, 1986, pp. 113-136.
37. Suter, G. T. and Collins, R. A., "Static and Dynamic Elastomeric Bridge Bearing Tests at Normal and Low Temperatures," *Ontario Joint Highway Research Program Report #24*, Department of Civil Engineering, University of Toronto, September 1964. 101 pp.
38. Taylor, Andrew W., Lin, Albert N. and Martin, Jonathan W., "Performance of Elastomers in Isolation Bearings: A Literature Review," *Earthquake Spectra*, Vol. 8, No. 2, 1992, pp. 279-303.
39. Yura, Joseph A., personal communication.